MIT Project Apophis: The SET Mission Design Document

12.43/16.83 Space Systems Engineering

May 18th, 2017

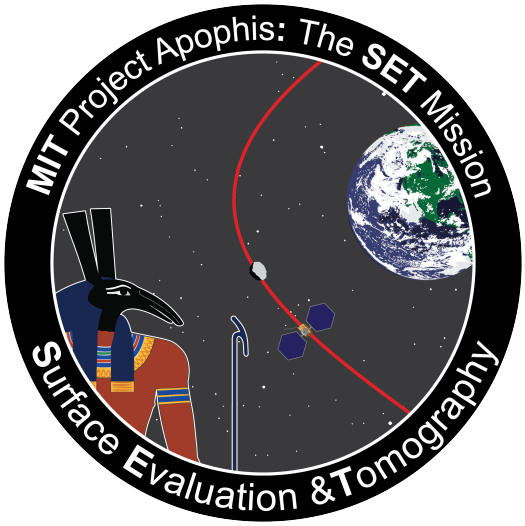

Asteroid Apophis is named after the Egyptian god of chaos and evil (left), and in Egyptian mythology, Set is the name of the god sent to intercept Apophis (right).

SET Mission Study Participants

Students

Andrew Adams
Dylan Cohen
Carlos Cruz
Alissa Earle
David Fellows
Joseph Figura
Roman Geykhman
Justin Gong
Jonas Gonzalez
Paulo Heredia
Nicholas James
Diego Mundo
Ellie Simonson
Jeremy Stroming
Max Vanatta
Amy Vanderhout
Emily Widder
Tori Wuthrich
Jim Clark

Instructors

Richard P. Binzel
David Miller
Jennifer Craig
Jane Connor
Christopher Jewison

We would like to thank the many consultants who have patiently answered questions and provided valuable input and feedback over the semester:

Farah Alibay (JPL)
Thomas Burbine (UMass)
Dennis Burianek (MIT/LL)
Mark Chodas (MIT)
Paul Chodas (JPL)
Emily Clements (MIT)
Mitch Ingham (JPL)
Lindley Johnson (NASA)
Laura Kerber (JPL)
Javier de Luis (Aurora)
Cateline Lantz (MIT)
Rebecca Masterson (MIT)
Jeff Mendenhall (MIT/LL)
Ryan Park (JPL)
Tom Roberts (JPL)
Christopher Semisch (MIT/LL)
Ellen Stofan (NASA)
Scott Uebelhart (MIT)
Ryan Webb (JPL)
Dirk Zwemer (Intercax)

Contents

List of Figures

List of Tables

Foreword

Back in 1967, when the world was first learning that asteroids can pose a hazard to the Earth, MIT students were challenged with a fictitious "what if" scenario of an asteroid named Icarus on a collision course with Earth. The outcome of their study, called **Project Icarus**, became a book and a movie titled "Meteor" starring Sean Connery and Natalie wood. The movie didn't do so well.

On April 13th, 2029, a Friday, an actual asteroid close encounter is going to happen. The object is 350 meters across, the size of an aircraft carrier, with a mass of 20 million metric tons. This 2029 asteroid close encounter is science fact, not science fiction.

We can say for certain the asteroid **will miss the Earth** as it passes by less than 6 Earth radii away. That's less than 1/10th the distance to the Moon, and passing inside the belt of our geosynchronous satellites. An object this size passes this close about once per 1000 years. As the asteroid passes by, it will be visible to the naked eye in the nighttime sky.

So we do know the asteroid is going to miss. What we don't know is what the outcome will be of Earth's gravitational forces and tidal stresses on the asteroid. This will depend on the composition and internal construction of the asteroid, something that has never yet been measured for such a potentially hazardous object. Thus this close encounter provides a once-per-thousand year natural experiment to reveal the internal structure of a hazardous asteroid. Scientifically this is fascinating, but this is also something that might be essential to understand in the unlikely but not impossible event that an actual asteroid impact someday appears in the forecast.

The point we emphasize is that this 2029 asteroid encounter is real. Nature is doing this once-per-thousand year experiment for us. All we have to do is figure out how to watch. Thus, the real challenge and the Charge given to MIT students in *12.43 / 16.83 Space Systems Engineering* is to figure out how to do it, and show the spacefaring world the path forward that it can be done.

The asteroid's name is Apophis. This is MIT Project Apophis.

Richard P. Binzel
Professor of Planetary Science
Joint Professor of Aerospace Engineering

David W. Miller
Professor of Aerospace Engineering

Massachusetts Institute of Technology
Cambridge, Massachusetts
May 2017

Executive Summary

MIT Project Apophis: The SET Mission

Alissa M. Earle, Andrew Adams, Max Vanatta,
Dylan Cohen, Carlos Cruz, David Fellows, Joseph Figura, Roman Geykhman,
Justin Gong, Jonas Gonzalez, Paulo Heredia, Nicholas James, Diego Mundo, Ellie Simonson,
Jeremy Stroming, Amy Vanderhout, Emily Widder, Tori Wuthrich, Jim Clark

0.1 Scientific Motivation

Achieving an understanding of asteroids and their impact hazard is one of the great responsibilities and grand challenges of our era. Natures is cooperating by providing a once-per-thousand year opportunity to study the outcome of an extremely close passage by an unprecedentedly large 350 meter (aircraft carrier-size) 20 million metric ton asteroid name Apophis on (Friday) April 13, 2029. Apophis' close encounter will be *inside* Earth's geosynchronous satellite ring at a near-miss distance of 5.6 Earth radii, less than one-tenth the lunar distance. While previous spacecraft missions have studied asteroids, none has ever had the opportunity to study "live" the outcome of planetary tidal forces on their shapes, spin states, surface geology, and internal structure. All of these physical parameters, and their changing response to induced stresses, represent an incredible opportunity to gain vital knowledge for addressing the eventuality of a known asteroid on an actual impact trajectory. In response to the imperative for knowledge and the once-per-many generations extraordinary "experiment" that nature itself is providing, we propose and outline a mission concept sending a spacecraft to orbit Apophis with the objectives of surveying its surface and interior structure before, during, and after its 2029 near-Earth encounter. The asteroid Apophis is named after the Egyptian god of chaos and evil. The proposed spacecraft is named SET, for the Egyptian god (Set) sent on his solar boat to thwart Apophis.

In recent decades, understanding of asteroids has been transformed from points of light to geological worlds owing to modern spacecraft exploration and state-of-the-art radar and telescopic investigations. Yet internal geophysical structures remain largely unknown. Understanding the strength and internal integrity of asteroids is not just a matter of scientific curiosity, it is a practical imperative for advancing knowledge for planetary defense against the eventuality of an asteroid impact.

The April 13, 2029 near-Earth flyby of Apophis will provide the opportunity for internal geophysical study as well as a chance to test current hypothesis on the effects of tidal forces on asteroids. Mounting theoretical studies [37, 69, 84, 89, 88, 98, 113] and physical evidence [13, 63], for tidal forces altering the shapes, spins, and surfaces of near-Earth asteroids all point to these Earth-asteroid interactions being as fundamental to the asteroid hazard problem as impact studies themselves.

The SET mission is motivated by additional factors and science objectives beyond the unique natural experiment opportunity. By including a thermal instrument and continuing to orbit Apophis after the Earth encounter, SET will be able to monitor and decode the coupling of rotation and thermal cycling resulting in Yarkovsky drift. Direct correlation of thermal properties with the resulting Yarkovsky drift is important for both future orbit predictions of Apophis as well as improving general understanding of asteroid dynamics. The SETs orbiter will also be able to map Apophis' global geology and composition and study its interior structure, increasing knowledge of mid-sized (100s of meter diameter) asteroids. Spacecraft studies of asteroids can provide insight into the geologic and dynamic history of the

Table 1: Science Traceability Matrix for the SET mission

Top Level Mission Requirements	Science Goal	Science Measurement Requirement	Payload Requirement	Primary Instrument	Secondary instrument
M.O.1 - Characterize Apophis's shape, size, density, surface topography and composition, rotation rate, and spin state.	Surface Mapping (before, during, and after Earth encounter)	Survey Apophis' surface structure and shape to learn about geology of mid-sized (100's of meters diameter) asteroids	PLD.2	LORRI	Ralph-MVIC (pan)
		Survey Apophis' shape before and after encounter to determine the impact of tidal torques on an asteroid's shape	PLD.2	Ralph-MVIC (pan)	LORRI/Ralph-LEISA
		Measure Apophis' spin state and rotation rate before and after encounter to understand how tidal torques impact the dynamics of a potentially hazardous asteroid	PLD.2	Ralph-MVIC (pan)	LORRI/Ralph-LEISA
		Image Apophis' surface before, during, and after the encounter at sufficent resolution to observe possible land slides and other surface responses to tidal torques	PLD.3	LORRI	Ralph-MVIC (pan)
	Surface Composition Mapping (before, during, and after Earth encounter)	Map Apophis' surface with filters to allow for color imaging and broad band spectroscopy	PLD.4	Ralph-MVIC (color)	Ralph-LEISA
		Spectral mapping of Apophis' surface to look at compositional heterogeneities and better refine Apophis' spectral class with higher resolution and broader wavelength coverage than achievable with ground-based observations	PLD.1	Ralph-LEISA	Ralph-MVIC (color)
		Perform surface composition and color surveys both before and after encounter to look tidally induced resurfacing	PLD.1 & 4	Ralph	
		During encounter observe Apophis' surface with color filters at sufficient time and spatial resolution to observe tidally induced resurfacing	PLD.4	Ralph-MVIC (color)	Ralph-LEISA
M.O.2 - Characterize internal structure of Apophis before and after near-Earth event.	Internal Sturcture	Map Apophis' interior (before and after encounter) to interpret the strength and internal structure of a potentially hazardous asteroid	PLD.5	RRT	
			PLD.6	RRT	
M.O.3 - Characterize Apophis's orbit, accounting for the influencing factors of the Yarkovsky Effect.	Yarkovsky Effect	Post-encounter monitoring to decode the coupling of rotation and thermal cycling resulting in Yarkovsky drift	PLD.7	TES	LORRI/Ralph
Science Measurement Obective higlighted in blue are significent for understanding how a potentially hazardous asteroid responds to tidal torques					

objects they study and not only improves our understanding of these individual objects but also has important implications for understanding solar system formation [54].

0.2 Mission Objectives

The SET mission achieves its science and hazard assessment goals through three key Mission Objectives (Table 1.2).

M.O.1 General Characteristics

The first mission objective focuses on the characterization of Apophis' bulk properties, including: shape, size, mass, volume, bulk density, surface topography and composition, rotation rate, and spin state and encompasses the surface geology and composition mapping goals. Surveying Apophis' surface geology and composition will help with understanding Apophis' geologic and dynamical history. Observations of these properties from throughout the encounter can be used to look for signs of tidal deformation and seismic resurfacing, as well as changes in spin state or rotation rate.

M.O.2 Internal Structure

The second mission objective is to characterize the internal structure before and after encounter. The strength and cohesion of Apophis' interior can be determined from observations of Apophis' interior structure and how it responds to the tidal torques from the Earth encounter event. This is useful information for both general asteroid studies and has implications for impact scenario modeling and planetary defense.

M.O.3 Orbit Characterization

The final mission objective studies the process of Yarkovsky drift. Post-encounter the spacecraft will continue to monitor Apophis until the next ground tracking opportunity in 2036. These synoptic measurements of position, rotation, and thermal emission will help decode the coupling of rotation and thermal cycling resulting in Yarkovsky drift. This will improve future orbit determination for Apophis and all potentially hazardous asteroids.

0.3 Science Payload

SET's science goals and mission objectives are accomplished with four instruments. The mission leverages heritage (with instruments based on those flown on the New Horizons, OSIRIS-REx, Mars Reconnaissance Orbiter, and Lucy missions) to provide a capable, robust instrument suite while keeping cost and risk low.

0.3.1 LOng Range Reconnaissance Imager (LORRI)

LORRI is a 20.8 cm Ritchey-Chrétien telescope with a 1024x1024 pixel panchromastic CCD imager (with a $0.29° \times 0.29°$ field of view) [21]. It will be the first instrument to be able to resolve Apophis during the spacecraft's approach. During this time it will work on improving upon ground-based measurements of Apophis' rotation rate, spin state, and shape, while also looking for potential hazards. Once the spacecraft is orbiting Apophis, LORRI will be responsible for high-resolution imaging of Apophis' surface, with $0.0099m/pixel$ resolution at a distance of $2km$ from the asteroid's surface.

0.3.2 Ralph

Ralph consists of a panchromatic and color imaging camera (MVIC) and a special imager (LEISA).

Multi-spectral Visible Imaging Camera (MVIC) consists of 7 independent CCD arrays on a single substrate to produce panchromatic and colored images. Each CCD has a field of view of $5.7° \times 0.037°$, but works in time delay integration (TDI) mode to produce images with a much wider view [83]. MVIC will be responsible for broad panchromatic mapping of Apophis' surface once SET is in orbit, as well as color and broad band spectroscopy mapping, to look for signs of seismic resurfacing during Apophis' flyby of Earth.

Linear Etalon Imaging Spectral Array (LEISA) is a wedged filter infra-red spectral imager that creates spatially resolved spectral maps. LEISA is a scanning, imaging instrument, that makes use of a special filter over which the wavelength varies in one direction. With wavelength coverage from 0.45 to $4.0\mu m$, spatial resolution of $60.8\mu rad$, and a $0.9° \times 0.9°$ field of view [83], LEISA will reveal compositional heterogeneities and any changes in surface composition that may be triggered by Apophis' tidal interaction with the Earth.

0.3.3 Radio Reflection Tomography Instrument (RRT)

The RRT instrument for SET will be based on the SHARAD instrument used on the Mars Reconnaissance Orbiter, and will consist of a $10m$ dipole antenna that can be folded for launch, and deployed solely with the elastic properties of the encasing tube, as well as an electronics box for signal generation and power amplification [81]. This method measures the differences in dielectric properties of materials in the asteroid by recording the echoes of transmitted low-frequency radio waves, thus providing a way of imaging the internal structure. The RRT instrument will have a transmission frequency of $20MHz$ and a bandwidth of $5MHz$. Assuming a refractive index similar to Itokawa, this bandwidth will provide a spatial resolution of approximately $20m$, a similar size to the Chelyabinsk meteoroid and thus significant from a planetary protection perspective.

0.3.4 Thermal Emission Spectrometer (TES)

TES will consist of a telescope, interferometer assembly, electronics, and support structure and achieves its spectral range by implementing an interferometer, beam splitter, and moving mirror assembly [26]. TES will map mineralogical and thermophysical properties of Apophis with a spectral range of 6 to $100\mu m$. TES uses a single detector with a field of view of $8mrad$, so at a distance of $2km$ it will have a field of view on Apophis' surface of roughly $16m \times 16m$. TES can provide insight into Apophis' mineralogy, globally map the material distribution, and determine regolith physical properties based on diurnal temperature measurements [26]. Most importantly, the thermal measurements from TES, combined with imaging and ground-based radar tracking, will help decode the coupling of thermal cycling and rotation which results in Yarkovsky drift, which will aid in not only refining future predictions of Apophis' orbit, but also the orbits of other potentially hazardous asteroids.

0.4 Spacecraft

SET will utilize a LEOStar-3 bus, manufactured by Orbital ATK, which has heritage on the Dawn and Deep Space 1 missions (Figure 0.3.4).

Spacecraft Specifications:

- Length: $1.8m$ ($10m$ w/ RRT antenna deployed)
- Width: $1.8m$ ($18.6m$ w/ solar panels deployed)
- Height: $2m$
- Dry Mass: $633.5kg$
- Wet Mass: $1024.5kg$
- Power: two Orbital ATK Ultraflex solar panels

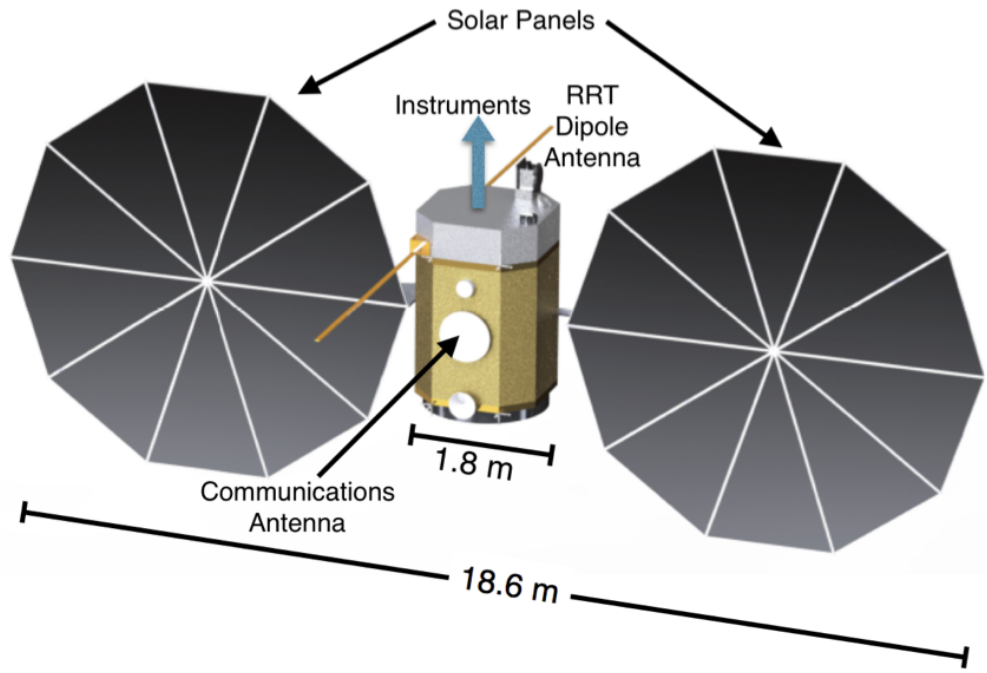

Figure 1: CAD Model of SET spacecraft layout. The instruments are all located at the top of the spacecraft to allow them to be used simultaneously. The RRT antenna and solar panels fold and are deployed after launch. (CAD Model by: Amy Vanderhout)

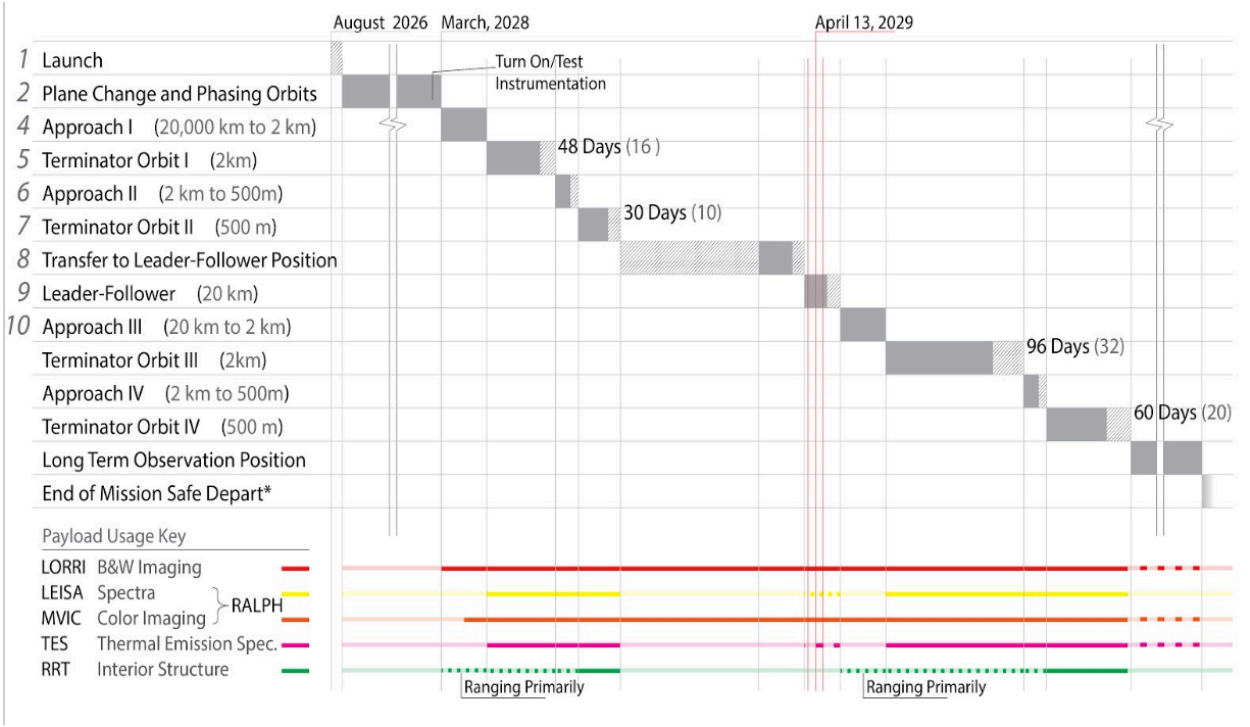

Figure 2: Proposed timeline of operations for the SET mission.

0.5 Concept of Operations

The SET Mission will **launch** in August 2026 within a 6 week launch window, with a back up launch window in August of 2027 (Figure 2). The spacecraft will calibrate its instruments as it exits the Earth's Sphere of Influence and will use Solar Electric Propulsion (SEP), to gradually match its orbit with Apophis' during the **plane change and phasing orbit phase**. In March 2028, the spacecraft will rendezvous with Apophis at its aphelion and begin the **Approach I phase**. During the Approach I phase the spacecraft will begin imaging with LORRI and then MVIC. This slow approach allows time for initial science observations and progressively maps the gravity field as SET enter Apophis' sphere of influence.

Once the spacecraft is $2km$ from the center of Apophis, it will enter a terminator orbit, beginning the **Terminator I phase**. This phase will consist of 15 orbits at $2km$, which are estimated to last for $48days$, and will serve as the initial characterization campaign of Apophis' surface for Mission Objective 1. Next, SET will enter **Approach II** and spiral down from the $2km$ orbit to a $500m$ orbit. For **Terminator II**, SET will orbit apophis in a $500m$ terminator for 30 days, ideal for the RRT instrument to study Apophis' internal structure for Mission Objective 2.

The spacecraft will then **transfer to leader-follower position** to prepare for Apophis' near-Earth flyby. For the **Leader-Follower phase**, SET will move to a position $20km$ ahead of Apophis, in order to observe Apophis from a safe distance and favorable viewing geometry during it's near-Earth flyby.

After the Earth Flyby Event, the spacecraft will complete a second set of **Approach** and **Terminator phases** to complete a second characterization campaign. Ideally, these phases would use the same orbital characteristics as before: using the imagers in the 2km orbit, then the RRT instrument in the 500m orbit. However, since there is uncertainty in the effect of Earth's tidal forces on Apophis during the event, these details cannot be set for sure until after the encounter.

Once the second full characterization campaign is complete, the spacecraft enters the **Long-Term observation phase**, and will stay in formation with Apophis while using TES and the imaging instrument to decode and evaluate the Yarkovsky effect. The plan is to stay in formation with Apophis for at least 7 years. Finally, for the **End of Mission phase**, SET will perform an exit burn to leave Apophis' sphere of influence, entering its own heliocentric orbit, compliant with all constraints for planetary protection.

0.6 Conclusions

The SET mission will take advantage of the incredible opportunity nature is providing to study the impact of tidal interactions on potentially hazardous asteroids. The mission will launch August of 2026 and arrive at Apophis in March of 2028, allowing for thirteen months of initial characterization before the April 13, 2029 Earth encounter event. The SET spacecraft leverages heritage to provide a robust, capable instrument suite that will improve knowledge of potentially hazardous asteroids from both a scientific and planetary defense perspective.

Acknowledgments

We would like to thank the 12.43/16.83 faculty, Prof. Richard P. Binzel, Prof. David Miller, Jennifer Craig, Jane Connor, and Christopher Jewison, for presenting us with this problem and helping us along the way.

We would also like to thank the many consultants who have patiently answered questions and provided valuable input and feedback over the semester: Farah Alibay (JPL), Thomas Burbine (UMass), Dennis Burianek (MIT/LL), Mark Chodas (MIT), Paul Chodas (JPL), Emily Clements (MIT), Mitch Ingham (JPL), Lindley Johnson (NASA), Laura Kerber (JPL), Javier de Luis (Aurora), Cateline Lantz (MIT), Rebecca Masterson (MIT), Jeff Mendenhall (MIT/LL), Ryan Park (JPL), Tom Roberts (JPL), Christopher Semisch(MIT/LL), Ellen Stofan (NASA), Scott Uebelhart (MIT), Ryan Webb (JPL), Dirk Zwemer (Intercax).

Chapter 1

Introduction & Systems Overview

1.1 Introduction

This document compiles the work of the MIT 16.83/12.43 Space Systems Engineering class during the spring semester of the 2016-2017 academic year. The goal of the class was to create a mission to observe the asteroid Apophis before, during and after its Earth flyby on April 13, 2029. Given this prompt, the class came up with the Surface Evaluation and Tomography (SET) mission.

1.1.1 Scientific Motivation

In recent decades, our understanding of asteroids has been transformed from points of light to geological worlds owing to modern spacecraft exploration and state-of-the-art radar and telescopic investigations. Yet their internal geophysical structures remain largely unknown. Understanding the strength and internal integrity of asteroids is not just a matter of scientific curiosity, it is a practical imperative for advancing knowledge for planetary defense against the eventuality of an asteroid impact.

Nature is providing a once-per-thousand year opportunity for internal geophysical study with the (Friday) April 13, 2029 near-miss of the potentially hazardous asteroid Apophis passing within the geosynchronous satellite ring: the predicted close approach distance is 5.6 Earth radii, less than one-tenth the lunar distance. Mounting theoretical studies [84, 89, 88, 69, 98, 113, 37] and physical evidence [13, 63], for tidal forces altering the shapes, spins, and surfaces of near-Earth asteroids all point to these Earth-asteroid interactions being as fundamental to the asteroid hazard problem as impact studies themselves.

Within the context of it being incredible that our spacefaring civilization would not mount an effort to take advantage of measuring and monitoring this extraordinary "natural experiment" that nature itself is providing, in this report we propose and outline a mission concept to send a spacecraft to orbit Apophis with the objectives of surveying its surface and interior structure before, during, and after its 2029 approach to Earth.

The SET Mission concept is motivated by additional factors and science objectives beyond the unique natural experiment opportunity.

The Yarkovsky effect results from the way the asteroid rotation affects the surface temperature distribution and anisotropic thermal reemission, and is the main non-gravitational orbit perturbation [23]. By including a thermal instrument and continuing to orbit Apophis after the encounter SET will be able to monitor and decode the coupling of rotation and thermal cycling resulting in Yarkovsky drift. This is important for both future orbit predictions of Apophis as well as improving general understanding of asteroid dynamics.

The SET orbiter will also be able to map Apophis' global geology and composition and study its interior structure, increasing knowledge of mid-sized (100's of meter diameter) asteroids. Roughly 10,000 objects of Apophis' size exist in the asteroid belt [41], of which very few have been studied in detail by spacecraft. Spacecraft studies of asteroids can provide insight into the geologic and dynamic history of the objects they study [54]. This not only improves understanding of these individual objects but also has important implications for solar system formation. Ground based observations of Apophis suggest an elongated shape

and cohesionless structure, which has implications for formation as well as impact scenario studies and long-term orbit predictions. These predictions can be refined by spacecraft observations. Imaging and radio reflectance tomography from an orbiting spacecraft can map the interior, precisely measure Apophis' shape, spin state, and rotation rate.

1.1.2 Mission Objectives and Rationale

We have grouped our science goals into three broad mission objectives. Our Mission Objectives are summarized in Table 1.1. An overview of the relationship between our science goals, measurement objectives, requirements, instruments, and mission objectives is presented in the Science Traceability Matrix (Table 1.2).

Table 1.1: Mission Objectives for the SET Mission

ID	Title	Requirement	Rationale	Techniques
M.O.1	Bulk Physical Properties	Characterize Apophis's shape, size, density, surface topography and composition, rotation rate, and spin state	To inform planetary defense initiatives and the scientific community	Panchromatic, color, and spectral imaging
M.O.2	Internal Structure	Characterize internal structure of Apophis before and after Earth Flyby event	To improve knowledge of tidal stresses on asteroids' internal structure	Radio Reflectance Tomography
M.O.3	Orbit Characterization	Characterize Apophis's orbit, accounting for the influencing factors of the Yarkovsky Effect	To improve knowledge of Apophis's orbit, the Yarkovsky Effect, and NEO orbital dynamics	Thermal Imaging

M.O.1 General Characteristics The first mission objective focuses on the characterization of Apophis' shape, size, density, surface topography and composition, rotation rate, and spin state. This objective will be lead by the Ralph and LORRI instruments (described in detail in subsections 3.3.2 and 3.3.1, respectively) and encompasses our surface geology and composition mapping goals. The measurements included within this objective accomplish a broad range of the scientific goals of the mission. Surveying Apophis' surface geology and composition will help us understand Apophis' geologic and dynamical history. By continuing to observe these properties throughout the encounter we can look for signs of tidal deformation and seismic resurfacing, as well as changes in spin state or rotation rate. From these, we can gain insights into the object's internal structure, supporting our second mission objective.

M.O.2 Internal Structure The second mission objective is to characterize the internal structure before and after encounter. These measurements will enable us to study the interior structure of Apophis as well as see how it responds to the tidal torques from the encounter with Earth, which will aid in determining the strength and cohesion of its interior. This is useful information for both general asteroid studies and has implications for impact scenario modeling and planetary defense. These efforts will be lead by the RRT instrument described in subsection 3.3.3.

M.O.3 Orbit Characterization The final mission objective studies the process of Yarkovsky drift. Post-encounter we will continue to monitor Apophis until the next radar ground tracking opportunity in 2036. During this phase observations will be focused on thermal measurements taken with TES (described in subsection 3.3.4) paired with imaging data to track Apophis' spin state and rotation rate. These measurements help us decode the coupling of rotation and thermal cycling resulting in Yarkovsky drift. This will improve future orbit determination and our understanding of asteroid dynamics.

Table 1.2: Science Traceability Matrix for the SET mission

Top Level Mission Requirements	Science Goal	Science Measurement Requirement	Payload Requirement	Primary Instrument	Secondary instrument
M.O.1 - Characterize Apophis's shape, size, density, surface topography and composition, rotation rate, and spin state.	Surface Mapping (before, during, and after Earth encounter)	Survey Apophis' surface structure and shape to learn about geology of mid-sized (100's of meters diameter) asteroids	PLD.2	LORRI	Ralph-MVIC (pan)
		Survey Apophis' shape before and after encounter to determine the impact of tidal torques on an asteroid's shape	PLD.2	Ralph-MVIC (pan)	LORRI/Ralph-LEISA
		Measure Apophis' spin state and rotation rate before and after encounter to understand how tidal torques impact the dynamics of a potentially hazardous asteroid	PLD.2	Ralph-MVIC (pan)	LORRI/Ralph-LEISA
		Image Apophis' surface before, during, and after the encounter at sufficent resolution to observe possible land slides and other surface responses to tidal torques	PLD.3	LORRI	Ralph-MVIC (pan)
	Surface Composition Mapping (before, during, and after Earth encounter)	Map Apophis' surface with filters to allow for color imaging and broad band spectroscopy	PLD.4	Ralph-MVIC (color)	Ralph-LEISA
		Spectral mapping of Apophis' surface to look at compositional heterogeneities and better refine Apophis' spectral class with higher resolution and broader wavelength coverage than achievable with ground-based observations	PLD.1	Ralph-LEISA	Ralph-MVIC (color)
		Perform surface composition and color surveys both before and after encounter to look tidally induced resurfacing	PLD.1 & 4	Ralph	
		During encounter observe Apophis' surface with color filters at sufficient time and spatial resolution to observe tidally induced resurfacing	PLD.4	Ralph-MVIC (color)	Ralph-LEISA
M.O.2 - Characterize internal structure of Apophis before and after near-Earth event.	Internal Sturcture	Map Apophis' interior (before and after encounter) to interpret the strength and internal structure of a potentially hazardous asteroid	PLD.5	RRT	
			PLD.6	RRT	
M.O.3 - Characterize Apophis's orbit, accounting for the influencing factors of the Yarkovsky Effect.	Yarkovsky Effect	Post-encounter monitoring to decode the coupling of rotation and thermal cycling resulting in Yarkovsky drift	PLD.7	TES	LORRI/Ralph
Science Measurement Obective higlighted in blue are significent for understanding how a potentially hazardous asteroid responds to tidal torques					

1.1.3 Concept of Operations (CONOPS)

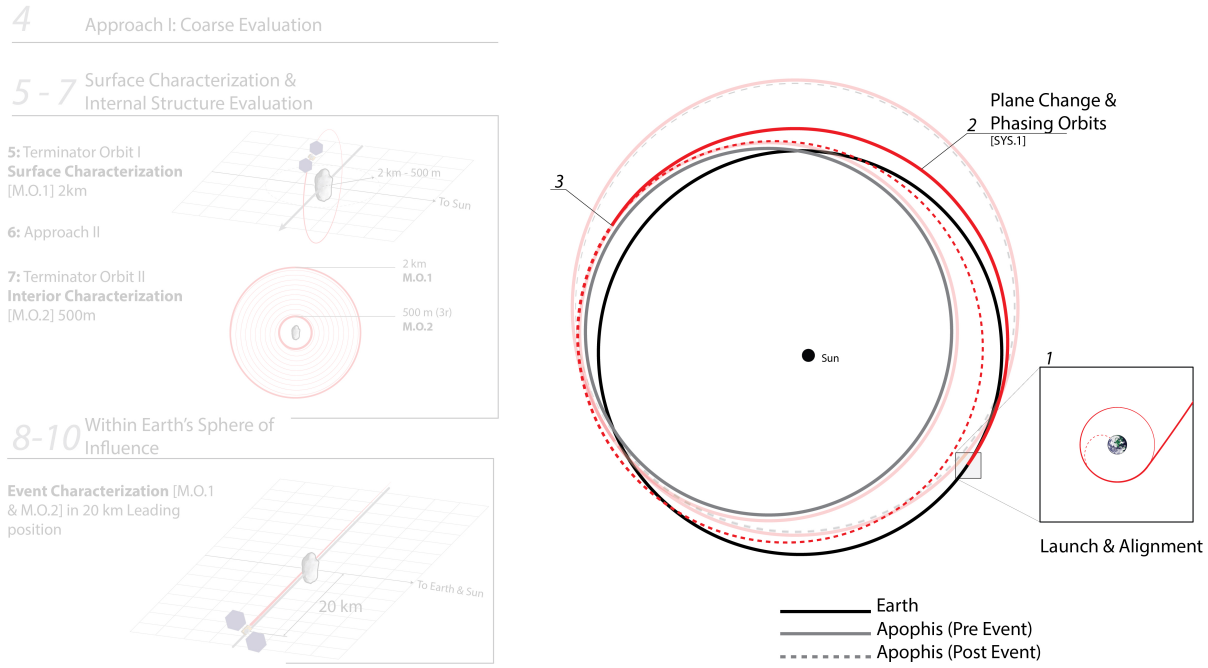

Figure 1.1: Launch and Cruise Phases

Launch and Cruise

The SET Mission will launch from Kennedy Space Center in August 2026 after which the spacecraft will

make alignment maneuvers and exit Earth orbit. The spacecraft will use Solar Electric Propulsion (SEP) to complete its bi-elliptic split plane trajectory to enter into Apophis' orbit.

Approach I

On March 21, 2028, the SET spacecraft will enter into Apophis' orbit at its aphelion. At this point, the spacecraft will still be over $10,000km$ from the asteroid. During the approach from this distance to Terminator I, the spacecraft will begin imaging using LORRI and MVIC to roughly characterize the asteroid and its dynamic behavior. The rotation rate, obliquity, precession will be extremely significant given the close proximity to Apophis during the later phases. Before proceeding to the next phase, these will be confirmed during this slow, long distance approach.

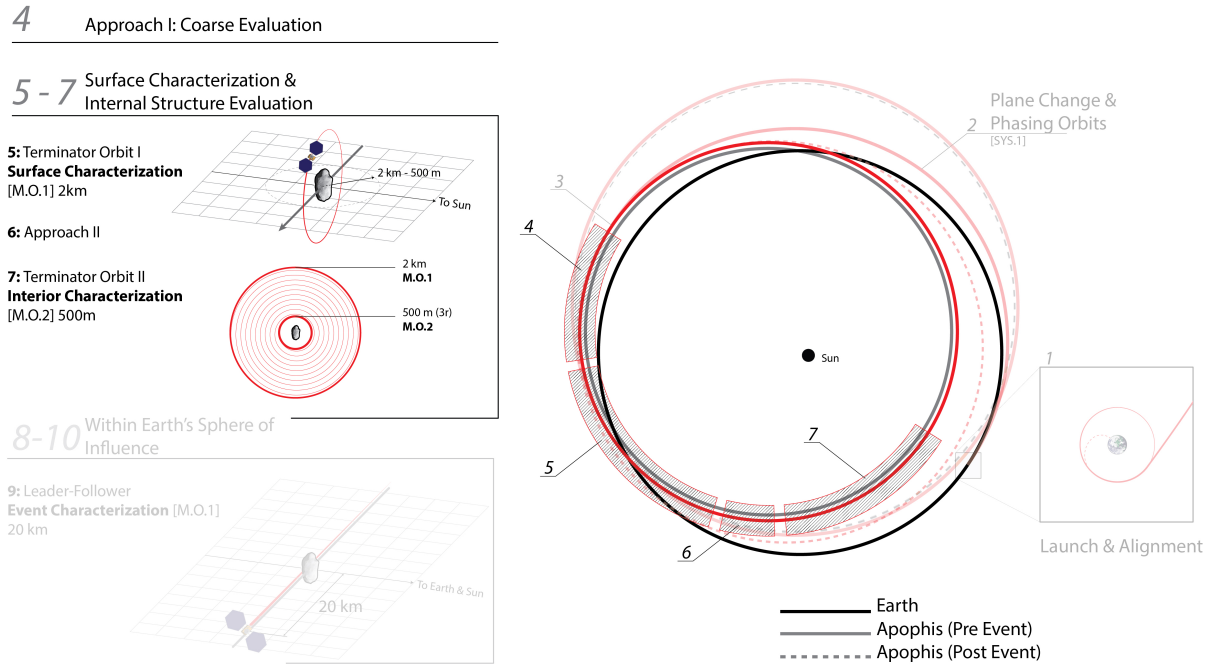

Figure 1.2: Terminator I, Approach II, and Terminator II

Terminator I, Approach II, and Terminator II

The spacecraft will enter into Apophis' sphere of influence and stay in a terminator orbit of approximately $2km$ for 48 days completing 15 orbits. This orbit will be focused on Mission Objective 1, bulk physical properties.

Terminator orbits will be used because of the low station-keeping energy and low chance of collision due to drifting from solar pressure. It is important to note that the estimated obliquity of the asteroid is 165 degrees with a rapid precession rate, meaning the spacecraft will not be in a true polar orbit, but will be close, within 15 degrees.

Following Terminator I at 2 km, the spacecraft will spiral down slowly during the Approach II phase into a tight terminator orbit of $500m$ from center. This $500m$ distance will require refinement and verification once the spacecraft is observing the orbital characteristics and the true gravitational field. In Terminator II orbit, the spacecraft will be performing the RRT, Radio Reflective Tomography, experiments primarily. Imagers will still be running as well, but are not the driving factor for the proximity. This phase will last a total of 30 days, 70 orbits, allowing for fine coverage of the surface.

For a more comprehensive view of the terminator orbit coverage for the two distances, please refer to Appendix E.

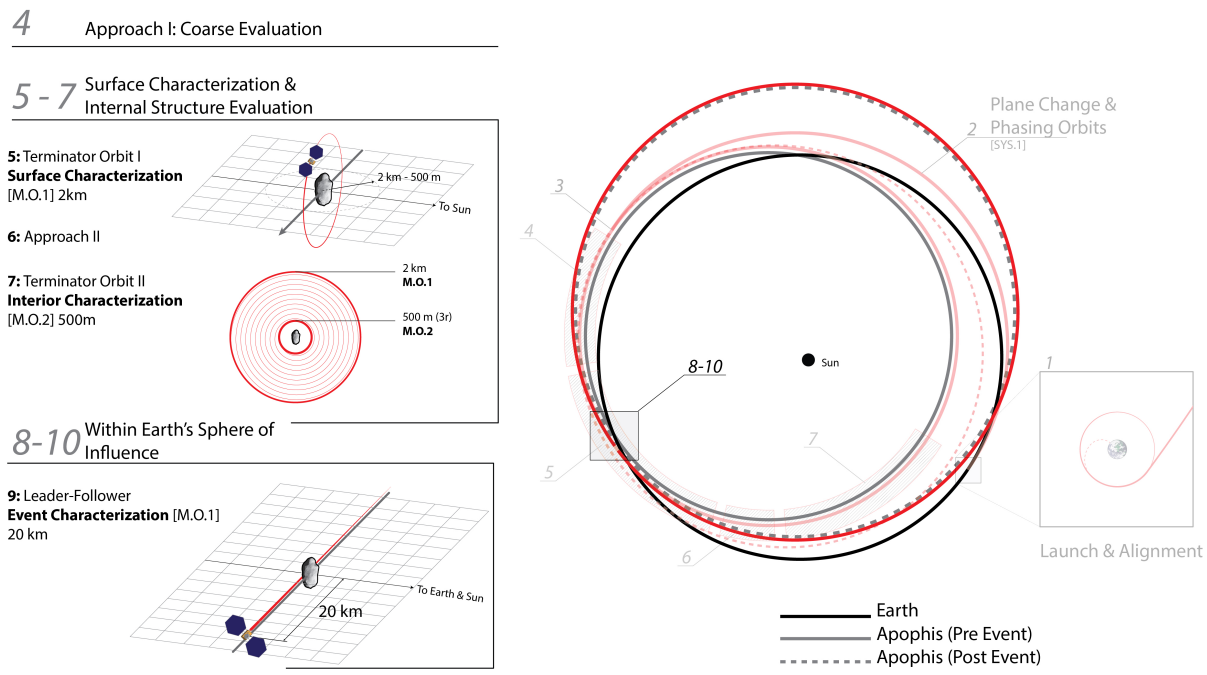

Figure 1.3: Leader-Follower

Leader-Follower

Approximately two weeks before the Earth flyby event, the spacecraft will exit the terminator orbit and enter into a heliocentric leader position $20km$ from Apophis. This distance will be refined based on the expected cohesion of the asteroid as determined from the initial characterization. If the risk of debris being ejected from the surface is high, the spacecraft will be further from the asteroid during the event, but if this risk is deemed unlikely, the distance can be reduced far lower, to ranges of single digit kilometers.

During the Earth flyby event, the imaging suite will be the primary function. LORRI and MVIC will be used the most out of the full suite, looking for small scale landslides, shifting debris, and resurfacing due to the tidal forces.

The spacecraft will maintain a high phase angle in respect to the asteroid with the Sun illuminating and exaggerating even small features.

Approach III, Terminator III, and Terminator IV

Following the Earth flyby event, the spacecraft will return begin a second barrage of surface and interior characterizations. This characterization will be nearly identical to the pre-event characterization (Terminator I, Approach II, and Terminator II), but since Apophis's orbital characteristics and dynamics are expected to change, the exact orbital characteristics of the spacecraft will be determined after the event.

This unknown variable of the obliquity and precession will be accounted for by both a large margin on the fuel and an extremely large margin on post-event lifetime.

Long-term Tracking

Following the second characterization campaign, the SET spacecraft will stay in formation with Apophis for an extended period after the Earth flyby event. For this study, we baseline a continuation for two full orbits, approximately three years, post-event to characterize and decode the rotation and thermal behaviors in relation to the Yarkovsky Effect. While the overall impact of the Yarkovsky Effect will be known through future radar measurements of Apophis, close observation with TES gives us the opportunity to monitor and decode the coupling of rotation and thermal cycling resulting in Yarkovsky drift. This satisfies our third Mission Objective.

End of Mission Plan and Potential Future Operations

After completing its mission, the SET spacecraft will leave Apophis and enter an elliptic orbit about the sun. This option was selected to first and foremost mitigate potential planetary protection risks presented by attempting to land the spacecraft on Apophis. However, this risk is extremely small due to the difference in speed of SET and Apophis being on the order of cm/s. Furthermore, there is little more scientific information to be gained from attempting a landing with the onboard instruments. Finally, there may be potential targets in SET's path after leaving Apophis that could be studied with SET's onboard instruments. Such a mission extension would be an added bonus to the scientific data gathered at Apophis.

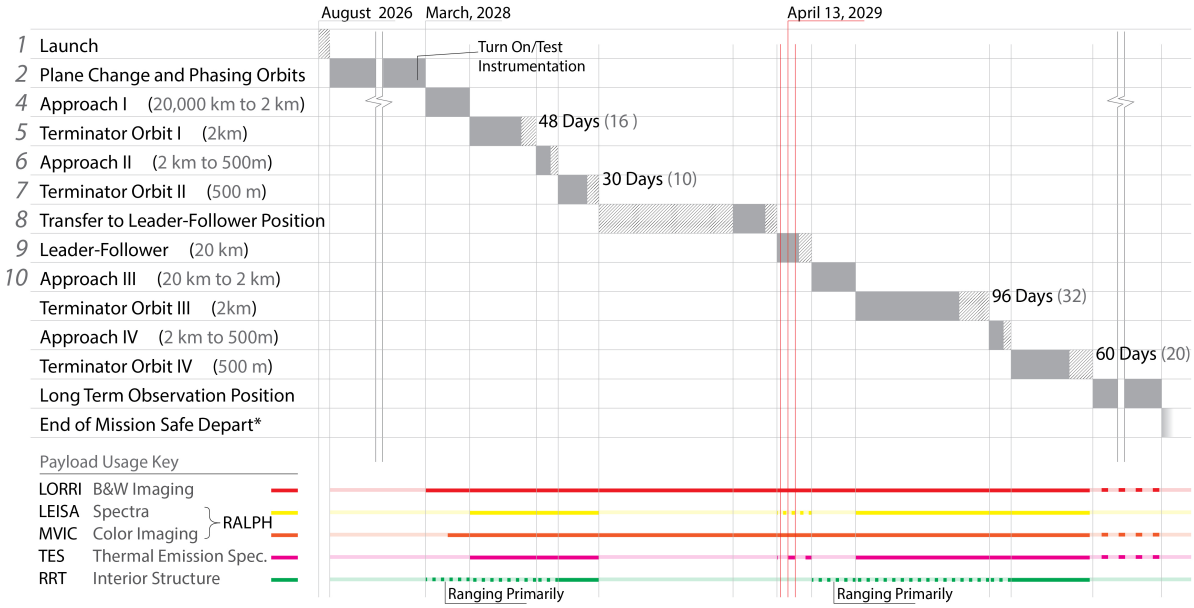

Figure 1.4: Mission Operation Timeline. The grey regions are allotted time while the hatched regions are margin

1.2 Systems Overview

1.2.1 System Requirements

The mission CONOPS and design stem from high-level system requirements developed to ensure SET achieves its scientific objectives. These requirements derive directly from the mission objectives, and inform subsystem-level requirements. The system requirements are organized as follows: (i) pre-requisites to data collection; (ii) requirements to characterize Apophis's general properties (M.O. 1); (iii) requirements to characterize Apophis's internal structure (M.O. 2); and (iv) requirements to characterize the Yarkovsky effect on Apophis. Table 1.3 below states the requirements and their respective rationales.

1.2.2 Model Based Systems Engineering (MBSE) Effort

Throughout the design process, the team undertook an effort to digitize the system design into a centralized model incorporating requirements, equipment, and operations. This initiative (herein, MBSE) ran in conjunction with traditional systems engineering and enabled an alternate perspective with which to consolidate a design.

The MBSE effort produced a Cameo Systems Modeler (SysML) model of the SET mission, and brought attention to oversights in initial systems-level assessments, particularly in relation to requirements. An appendix details discussion of the MBSE model and its contributions to the design process.

Table 1.3: System Requirements

ID	System Requirement	Parent	Rationale
SYS.1	**Getting There:** System shall achieve sufficient proximity to Apophis to conduct measurements.	M.O.1; M.O.2; M.O.3	System must be close enough to Apophis to conduct measurements.
SYS.2	**Staying There:** System shall maintain appropriate conditions to conduct measurements before, during, and after the 2029 Earth Flyby event*.	M.O.1; M.O.2; M.O.3	System must enable data collection
SYS.3	**Communication:** System shall be capable of sending and receiving data and instructions to and from the ground.	M.O.1; M.O.2; M.O.3	Operations and troubleshooting require exchange of system information and instructions. Data is only useful on the ground.
SYS.4	**Geometry:** System shall measure size and overall geometric characteristics of Apophis before, during, and after Earth Flyby event.	M.O.1	Required to inform future operations of this system, scientific communities, and planetary defense.
SYS.5	**Dynamics:** System shall measure rotation and spin state of Apophis before, during, and after Earth Flyby event.	M.O.1	Required to inform future operations of this system, scientific communities, and planetary defense.
SYS.6	**Surface:** System shall measure surface composition and distribution of surface features from the scale of boulders to regolith patches on Apophis before, during, and after Earth Flyby event.	M.O.1	Required to inform scientific communities, and planetary defense.
SYS.7	**Internal Structure:** System shall characterize the internal structure of Apophis, including detecting major fracture boundaries, voids, and internal rock variations before and after the Earth Flyby event.	M.O.2	Required to inform scientific communities, and planetary defense.
SYS.8	**Tracking:** System shall enable long-term, precision tracking of Apophis after Earth Flyby event until 2036 and then safely depart.	M.O.3	Required to gain understanding of the Yarkovsky/YORP effect. Track until next ground-based radar ranging measurements can be made in 2036.
SYS.9	**Thermal:** System shall measure Apophis's thermal emissions before and after Earth Flyby event.	M.O.3	Required to gain understanding of the Yarkovsky/YORP effect.

1.2.3 Block Diagrams

The MBSE team produced two block diagrams within the model that provide an overview of the SET mission design. These diagrams are the functional block diagram (Figure 1.5) and the structural block diagram (Figure 1.6). The functional block diagram (Figure 1.5) includes the physical components of the system and and the functional relationships between these physical components. These functional connections include power and data flow. The structural diagram is shown in Figure 1.6. The connections in this diagram represent physical relations, and the diagram depicts the structural layout of the system.

Both of these block diagrams are separated into three main components:

1. The spacecraft, SET, which represents the entire spacecraft and contains the bus and payload.
2. The bus, LEOStar-3, which contains the components required for the bus to complete maneuvers, transmit and receive data, provide power to the system, and provide thermal management.
3. The payload, which contains the instrumentation components required for the science component of the mission.

The following paragraph will briefly explain the setup of these diagrams. In the functional diagram, subcomponents are expressed by placing a subcomponent block within the parent component block. So for example, the SET spacecraft block, (the salmon, outermost block), represents the entire spacecraft and contains the bus (violet, inner block) and payload (teal, inner block) sub-diagrams. The structural block diagram represents subcomponents with arrows rather than sub-diagrams.

In both diagrams, 'Data Output', 'Mass', 'Power', and/or 'Price' is represented. In the functional block diagram, this is represented by the subcomponent blocks labelled 'Data Output', 'Mass', 'Power', and/or 'Price'. In the structural block diagram, these are represented under the value category of components and include default values. These values were used in the Parametric model of the system will be further explained in the Instances and Parametric section of the appendix.

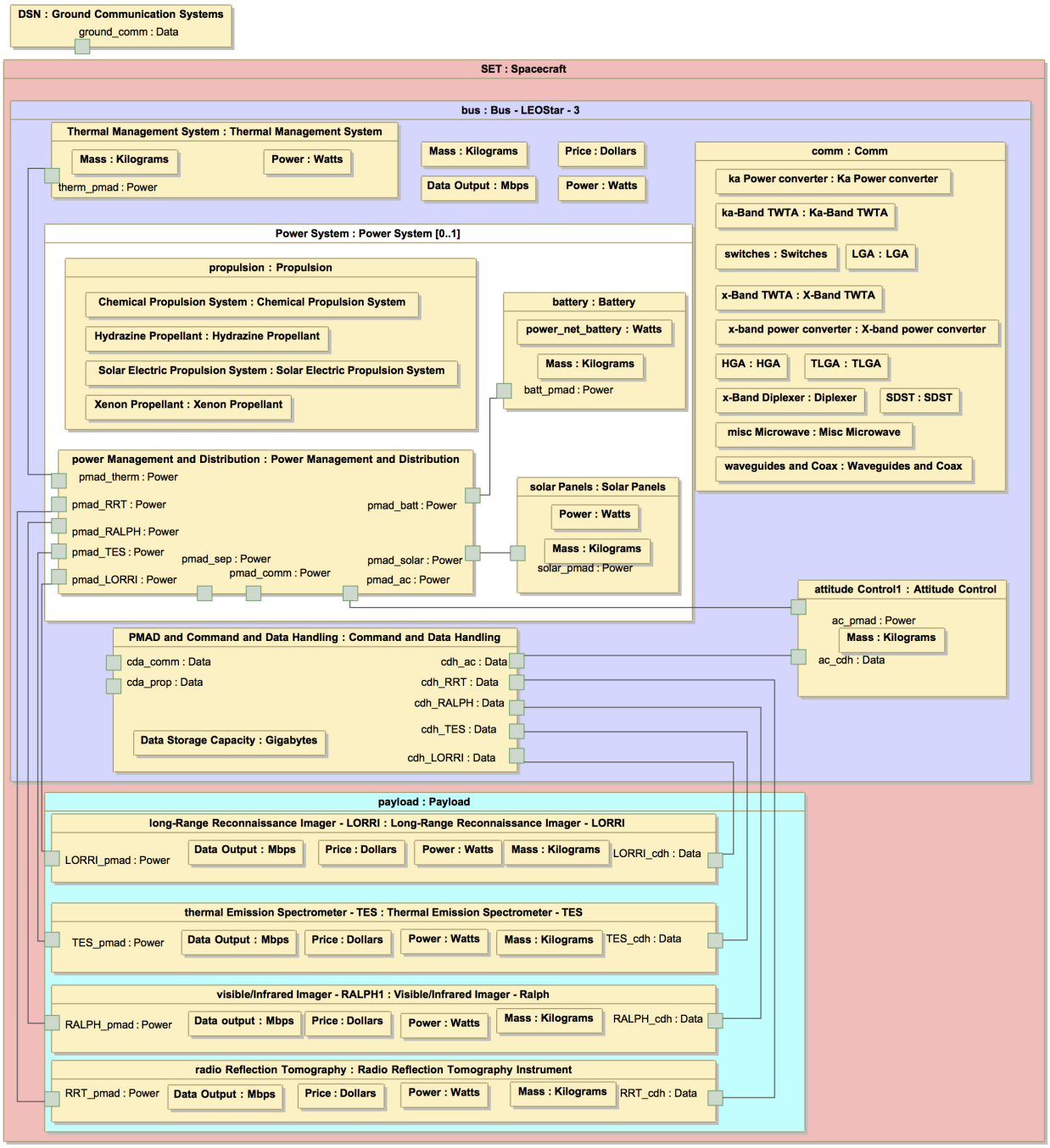

Figure 1.5: Functional Block Diagram

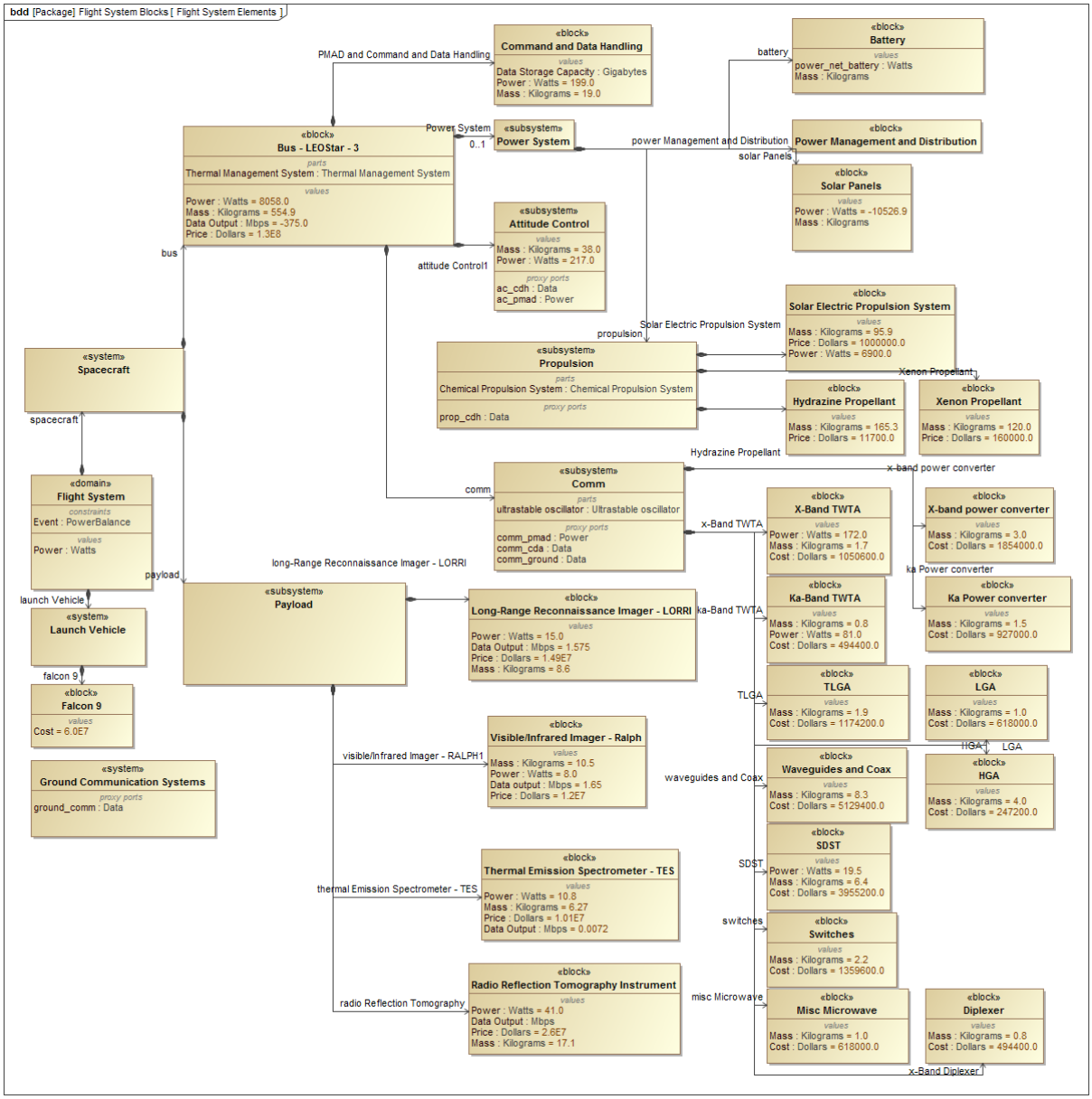

Figure 1.6: Structural Block Diagram

Chapter 2

Launch, Navigation, and Attitude Control

2.1 Subsystem Requirements

The Launch, Navigation, and Attitude Control (LNAC) subsystem team has developed requirements to support spacecraft launch, orbital trajectories, safe rendezvous with Apophis, science observations at Apophis, and post-mission disposal.

Table 2.1: LNAC Subsystem Requirements

ID	Derived Requirements	Parent	Verification
LNAC.1	**Trajectories.** LNAC shall compute launch windows and trajectories to intercept and rendezvous with Apophis before 2029 Earth flyby event. Trajectory options will quantify trades between launch opportunity, flight duration, and payload mass delivered.	SYS.2	Analysis
LNAC.2	**Rendezvous & Divert Hazard.** Intercept trajectories shall be quantified in terms of closing velocity and worst-case effect on long-term orbit of Apophis. Worst-case impact shall not perturb Apophis at 2029 near-Earth event by more than Yarkovsky drift effect.	SYS.1-2	Analysis
LNAC.3	**Launch Vehicle/Propulsion.** Launch vehicle shall be capable of meeting criteria developed in LNAC.1 within mission budget; propulsion shall execute all trajectory correction maneuvers with 50% margin.	SYS.1	Analysis
LNAC.4	**Science Operations.** System shall circumnavigate Apophis at an altitude of no higher than 2 km and no lower than 0.5 km in multiple planes; attitude control systems and propulsion hardware shall provide attitude control to 1 arcsec and 5 arcsec/sec during science observations.	SYS.1-2 PLD.2-4,6	Analysis
LNAC.5	**End of Mission Orbit.** System shall depart Apophis at the conclusion of science operations into an orbit that will not encounter Apophis or Earth, or contaminate other bodies.	SYS.8	Analysis

LNAC.1 relates to the the intercept and rendezvous stages of this mission. Intercepting and rendezvous

with Apophis prior to the 2029 near-Earth event fulfills an essential mission objective of taking measurements before Apophis' interaction with Earth (MO.2). Shorter Earth-Apophis transit times require higher delta-V costs, but longer transit times increase the risk of hardware failure, and decrease mission time at Apophis, so it is necessary to balance cost with time. This requirement is derived from SYS.1, which dictates that the spacecraft must achieve sufficient proximity to Apophis to take measurements.

LNAC.2 further expands on LNAC.1 and specifically addresses the effect of potential spacecraft impact on the orbit of Apophis by expressing closing velocity at rendezvous with Apophis in terms of planetary defense implications. This requirement dictates that the system will stay far enough away from Apophis that fail-miss trajectories are ensured. The choice of the Yarkovsky effect as the upper bound for acceptable impact perturbation reflects maximum known natural perturbations to asteroid orbits and was selected on the advice of Dr. Lindley Johnson.

LNAC.3 necessitates the selection of a launch vehicle that will support the mass of the spacecraft, enable the selected Earth-Apophis trajectory, and fall within a reasonable budget.

LNAC.4 pertains to the science operations that will be obtained during the station-keeping phase of this mission. The circumnavigation altitude values reflect the required resolution and pointing accuracy dictated by onboard imagers and other sensors (SYS.1).

LNAC.5 requires that the spacecraft depart Apophis after completing all observations and data collection in such a way that it does not endanger Earth from a planetary defense perspective by impacting Earth or Apophis. Additionally, the spacecraft shall not contaminate other bodies or violate any planetary protection requirements.

2.2 Launch Vehicle

In this design, SET is recommended for launch as the primary payload of SpaceX's Falcon 9 reusable rocket. This vehicle is shown in Figure 2.1. The Falcon 9 was chosen above comparable launch vehicles including the Atlas V and Delta IV families due to a number of considerations including payload capacity, cost, reliability, availability, and heritage. The Falcon 9 reusable meets Project SET's payload and delta-v requirements with a sizeable margin, and is also the lowest priced launch vehicle currently on the market that meets these requirements. The recoverable first stage booster offers additional cost savings over the full thrust version of the Falcon 9.

Figure 2.1: The SpaceX Falcon 9 Rocket takes off from Launch Pad 39A at the Kennedy Space Center in Cape Canaveral, FL on March 30, 2017.[104]

The launch vehicle must provide enough velocity to escape earth orbit and impart an additional 50 m/s of hyperbolic escape velocity (V_∞). Launch providers publicly publish payload delivery capabilities to Low Earth Orbit (LEO), an altitude of about 160-300 km. The orbital velocity in LEO can be approximated using Equation 2.1:

$$V_c = \sqrt{\frac{GM_E}{R + R_E}} \tag{2.1}$$

Where G is the Gravitational Constant, M_E is Earth's mass, and R is the orbital altitude, and R_E is the Earth's radius. An altitude of 200 km corresponds to a speed of about 7.78 km/s. Escape velocity from an orbit is calculated as:

$$V_{escape} = \sqrt{2}V_c \tag{2.2}$$

The total delta-v needed from LEO is then:

$$\Delta V_{total} = \sqrt{V_{escape}^2 + V_\infty^2} - V_c \tag{2.3}$$

A certain percentage of the mass delivered to LEO (m_{LEO}) must be propellant to achieve this delta-v. The final "throw mass"capability (the payload mass delivered at a certain final velocity) for a given V_∞ can be calculated using a rearrangement of the rocket equation given here:

$$m_f = m_{LEO} \times e^{\frac{-\Delta V_{total}}{gI_{sp}}} \tag{2.4}$$

Where g is Earth's gravitational acceleration and I_{sp} is the specific impulse of the rocket. Using this equation, it is possible to compare the performance capabilities of a variety of launch vehicles. The Falcon 9 resuable provides a payload margin of about 2000 kg for the required final velocity. This is shown in Figure 2.2.

In Figure 2.2, the dashed line indicates a vehicle still in development at the time of this report. The **X** marks the Project SET mass and velocity requirements. The recommended vehicle, the Falcon 9 reusable is plotted in bold blue with star markers. All commercially available launch vehicles listed in the key meet mission demands with a considerable margin.

Although exact costs are not provided publicly, cost estimates for several different launch vehicles are summarized in Table 2.2. At about $48 million, the reusable Falcon 9 is significantly lower cost than comparable vehicles.

Table 2.2: Launch Vehicle Estimated Cost

Launch Vehicle	**Approximate Cost**
Atlas V 401[5]	$109 million
Atlas V 431[5]	$130 million
Atlas V 551[5]	$153 million
Ariane 5[7]	$160-$175 million
Delta IV Medium[6]	$325-$375 million
Delta IV Heavy[6]	$109 million
Falcon 9[102]	$62 million
Falcon 9 (Reusable)[102]	$48 million
Falcon Heavy[102]	$90 million

Additionally, the Falcon 9 is compatible with the chosen LEOStar-3 spacecraft bus and has a history of successful orbital payload deliveries. Despite several high profile accidents, the Falcon 9 has successfully carried out 37 successful missions since 2009[103]. In comparison, the Atlas V family currently faces some uncertainty as it seeks to replace its Russian-built RD-180 first stage engine with an American-made variant. A successor has yet to be selected and flown [39]. This uncertainty also contributed to the selection of the Falcon 9.

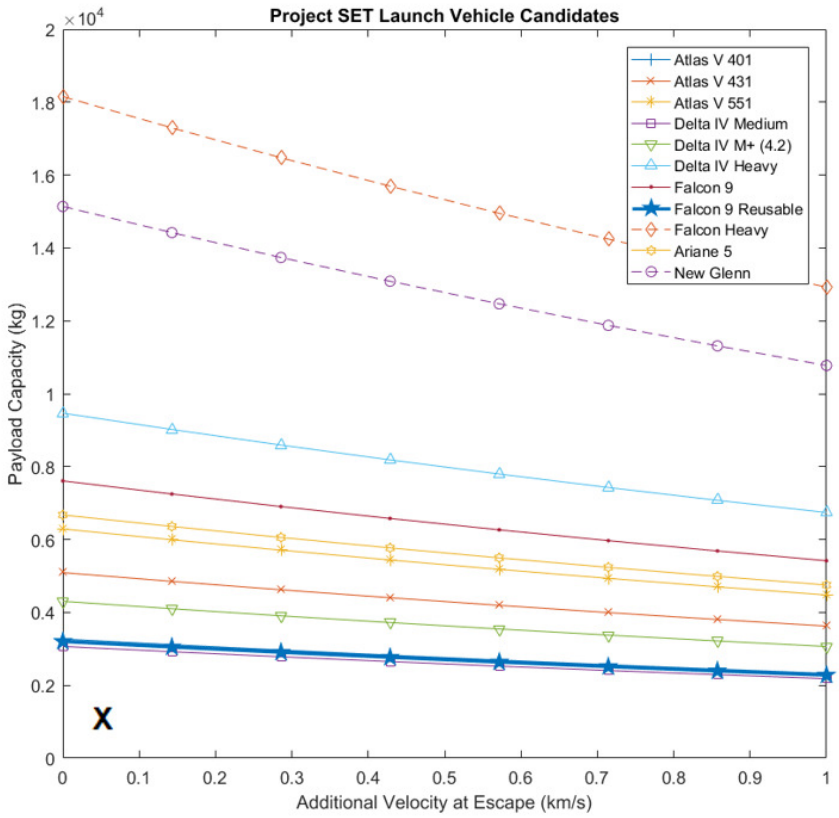

Figure 2.2: Payload delivery mass is plotted against additional velocity beyond escape for a range of launch vehicles.[5][6][7][102]

2.2.1 Launch Time and Location

The suggested launch location is the Kennedy Space Center (KSC) in Cape Canaveral, FL. KSC has substantial infrastructure in place to support payload integration and launch. Its low latitude is also advantageous for an approximately equatorial orbit desired for SET. This is in contrast to Vandenberg Air Force Base in California which is better suited for polar-inclined orbits. SpaceX also has a lease of several launch pads at Cape Canaveral and an advanced on-site missions operation center already in place. The Guiana Space Centre in French Guiana does offer the advantage of launching directly into the ecliptic plane since its latitude of 5.2° is less than the inclination of the ecliptic (23.5°). It also opens up the possibility of international collaboration with the European Space Agency (ESA). However, as seen in Table 7, the launch cost of the Ariane 5 rocket used by the ESA is over $100 million more than the Falcon 9 Reusable. This price discrepancy led to the final recommendation of Cape Canaveral.

Launch windows center on late August of every year with a margin of four weeks prior and two weeks after the optimal date. We baseline a launch date of August 24, 2026 at 4:00 AM EST. The Falcon 9 will take off with a flight azimuth of 90° (due east).

Since Kennedy Space Center is located at a latitude of 28.3°N and plane of the ecliptic is at an inclination of 23.5°, the vehicle cannot launch directly into the ecliptic and must execute a inclination changing burn. At the launch time selected, this angle is approximately 5°. Since both orbits are approximately circular with a constant altitude, the delta-v required is given by Equation 2.5:

$$\Delta V_i = 2V_c \times \sin(\frac{\Delta i}{2}) \tag{2.5}$$

Where i denotes the inclination angle. Given our orbital speed of 7.78 km/s, this maneuver requires that

the second stage of the launch vehicle provide a delta-v of 679 m/s in the cross track direction approximately 22 minutes after takeoff. This maneuver is diagrammed in 2.3 A delay of one hour to the launch time requires about 1.21 km/s delta-v, an increase of 531 m/s above the optimal value. This is still within the capabilities of the Falcon 9. A delay of up to six hours is allowable as long as the SET spacecraft is the sole payload–though this comes with considerable fuel waste.

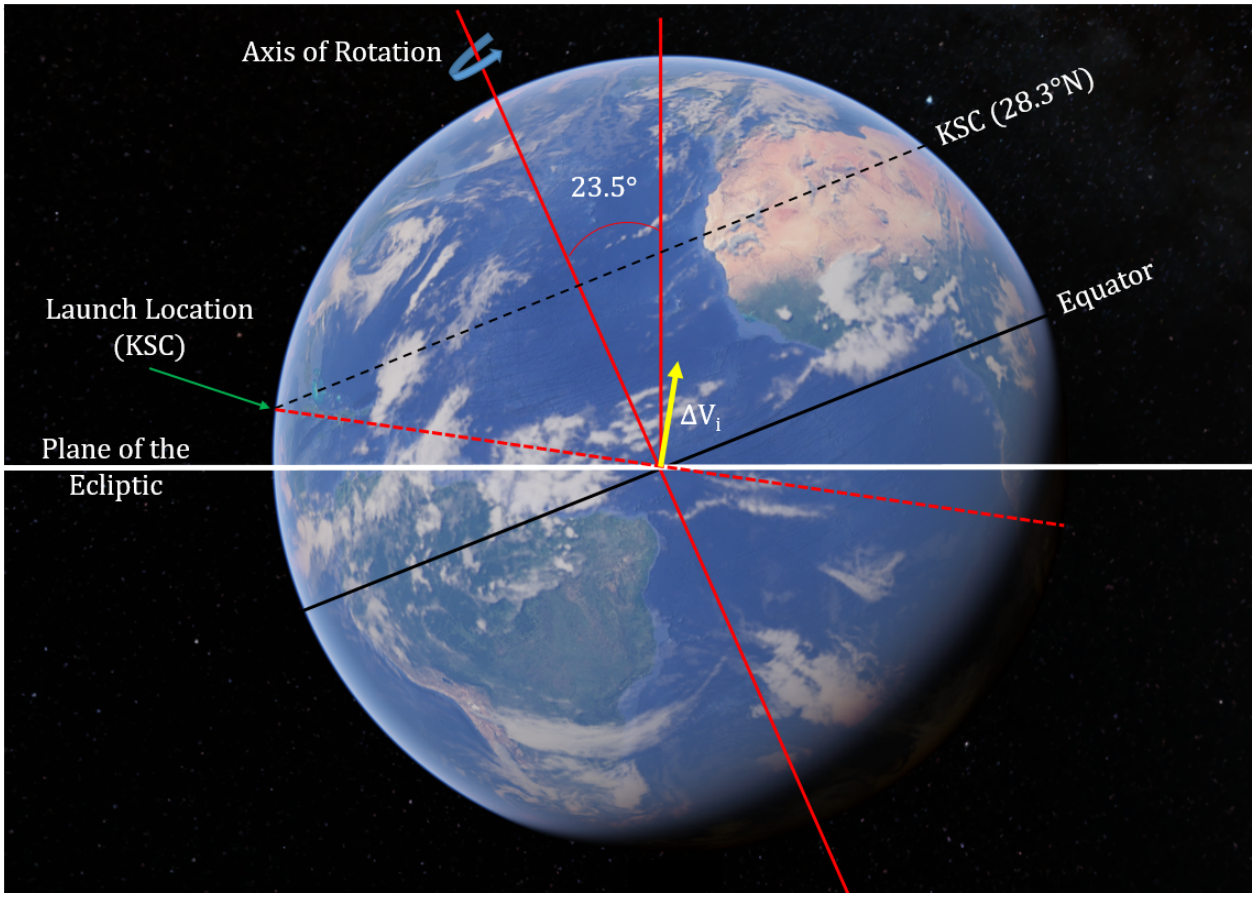

Figure 2.3: A visualization of the inclination change required to move from the initial orbital plane to the plane of the ecliptic.

Table 2.3 below breaks down the velocity requirements that must be provided by the launch vehicle for the suggested launch date and time of August 24, 2026 at 4:00 AM EST.

Launch Vehicle Burn	ΔV Required
LEO	7.8 km/s (altitude of 185 km) +~2 km/s due to drag
Inclination Change	**0.68 km/s**
Escape Velocity	11.0 km/s (LEO + **3.2 km/s**)
V_∞	0.78 km/s (Escape + **0.05 km/sec**)
Total From Parking Orbit	**3.32 km/s**

Table 2.3: Launch Vehicle ΔV Budget

2.3 Propulsion System

2.3.1 Trades, Downselect, and Rationale

The SET spacecraft will utilize a hybrid chemical and Solar Electric Propulsion (SEP) system to perform the required split-plane bi-elliptic trajectory. SEP offers much greater mass savings than a purely chemical-based propulsion system and is compatible with the two year approach timeline. Specifically, SET will utilize the new NASA Evolutionary Xenon Thruster (NEXT-C), and twenty four small hydrazine thrusters. Only one NEXT-C thruster will be carried, but redundant plumbing and propellant management system (PMS) will be installed in case of failure of the primary system. PMS failure is much more likely than thruster or power processing unit (PPU) failure. Implementing two thrusters also makes torque balance on the spacecraft more difficult because the thrust force is no longer on the line of center of gravity.

The trajectory has a delta-v budget as shown in Table 2.3.1.

Spacecraft Burn	**ΔV**	**Actual ΔV (waste due to SEP)**	**Propulsion Type**	**Duration**
Plane Change	1.72 km/s	1.74 km/s	SEP	76 days
Period Change	0.43 km/s	0.39 km/s	SEP	17 days
Final Velocity Match Maneuver	1.90 km/s	2.51 km/s	SEP	104 days
Attitude Adjustment, Station Keeping, Safety Margin	0.5 km/s	0.5 km/s	Hydrazine	N/A
Total	4.55 km/s	**5.14 km/s**	N/A	N/A

Table 2.4: Spacecraft ΔV Budget

As evident in the table, the spacecraft propulsion system must provide a minimum of 4.55 km/s of delta-v. This immediately dispels a purely chemical based system. Even using an I_{sp} of 220 seconds, the theoretical limit of hydrazine efficiency, this requires a mass fraction of 6.9. A spacecraft with 690% of the mass dedicated to propellant is not feasible. SEP provides a solution (see Figure 2.4), but hydrazine is still required for safety margin in addition to less time-lenient burns such as station keeping at Apophis.

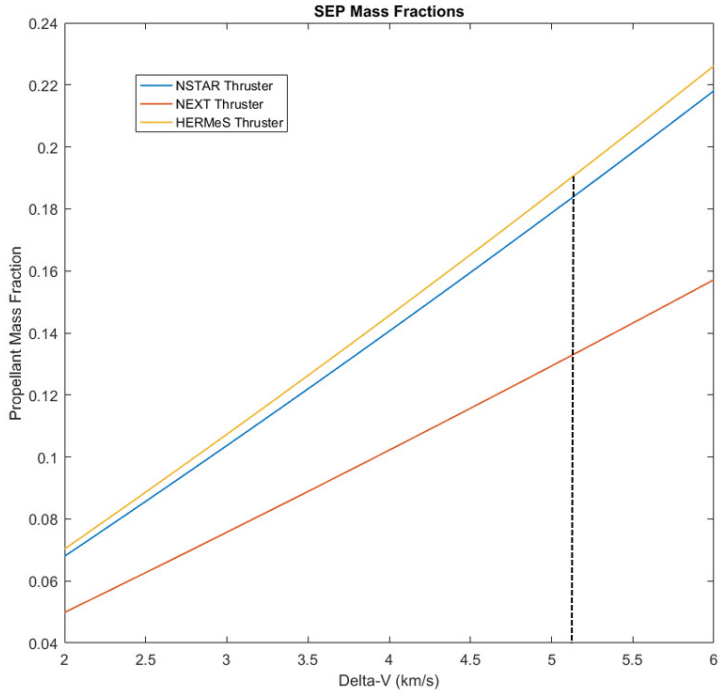

Figure 2.4: Delta-v vs. propellant mass fraction plotted for several different electric propulsion systems. The dashed line marks the delta-v required for the selected mission timeline. Mass fractions on the order of 10% are required for this mission.[43] [46][99]

Solar Electric Propulsion SEP works by using energy generated from solar panels to create a strong magnetic field that can be used to accelerate the ionized propellant (typically xenon) at great speeds out of the nozzle. Compared to chemical thrusters, electric propulsion systems provide low thrust (only several hundred milliNewtons) but are much more mass efficient. This allows a spacecraft to accelerate to high velocities over an extended time period. NASA first demonstrated this technology with the NASA Solar

Technology Application Readiness (NSTAR) used aboard the Deep Space 1 mission in 1998. Three such units were used on the Dawn spacecraft in 2007. Testing is currently underway on the NEXT and Hall-Effect Rocket with Magnetic Shielding (HERMeS) at NASA's Glenn Research Center with expected flight hardware delivery in 2019[91]. These thrusters offer more advanced capabilities than NSTAR.

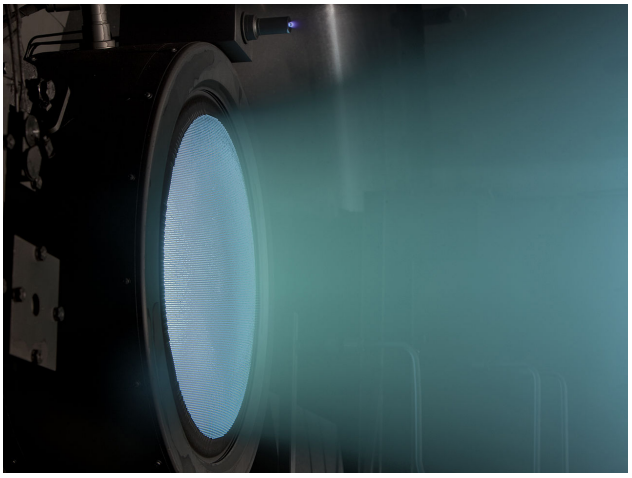

Figure 2.5: The NEXT thruster undergoing a long duration test in a vacuum chamber. Prototypes have completed sustained test burns of up to 5.5 years. [43]

As outlined previously, the trajectory has several components including a plane change, period change, and final velocity match. An analysis of completing these burns using SEP is provided below. This analysis provided initial estimates. Final numbers were computed using General Mission Analysis Tool (GMAT).

After the launch vehicle has provided the necessary escape plus hyperbolic velocity, SET will rely on SEP to conduct a plane change over one and a half revolutions to shift its orbit from the plane of the ecliptic to the plane of Apophis–a difference of 3.3°. This requires a delta-v of 1.72 km/s. Due to the nature of a low-thrust, distributed burn, there is a waste factor associated with using SEP. This waste factor is no more than two. Overall, the delta-v can be calculated using the equation below:

$$\Delta V_{Plane,actual} = \Delta V + \Delta V \sin(\frac{1}{2}\theta) \tag{2.6}$$

where θ is the burn-duration-angle as shown in Figure 2.6.

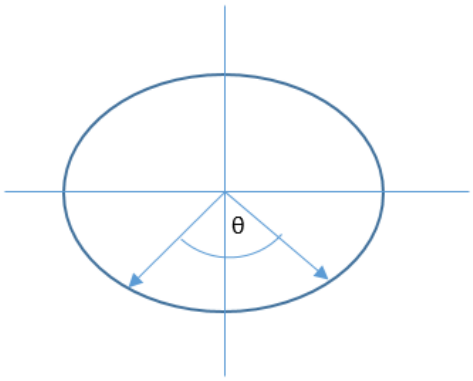

Figure 2.6: Geometry of a distributed burn centered on the semi-minor axis of the orbital ellipse.

The angle needed to complete the plane change delta-v is a function of the thrust of the engine used. Figure 2.7 displays the angle required to complete the plane change in one and a half revolutions for several different SEP system configurations.

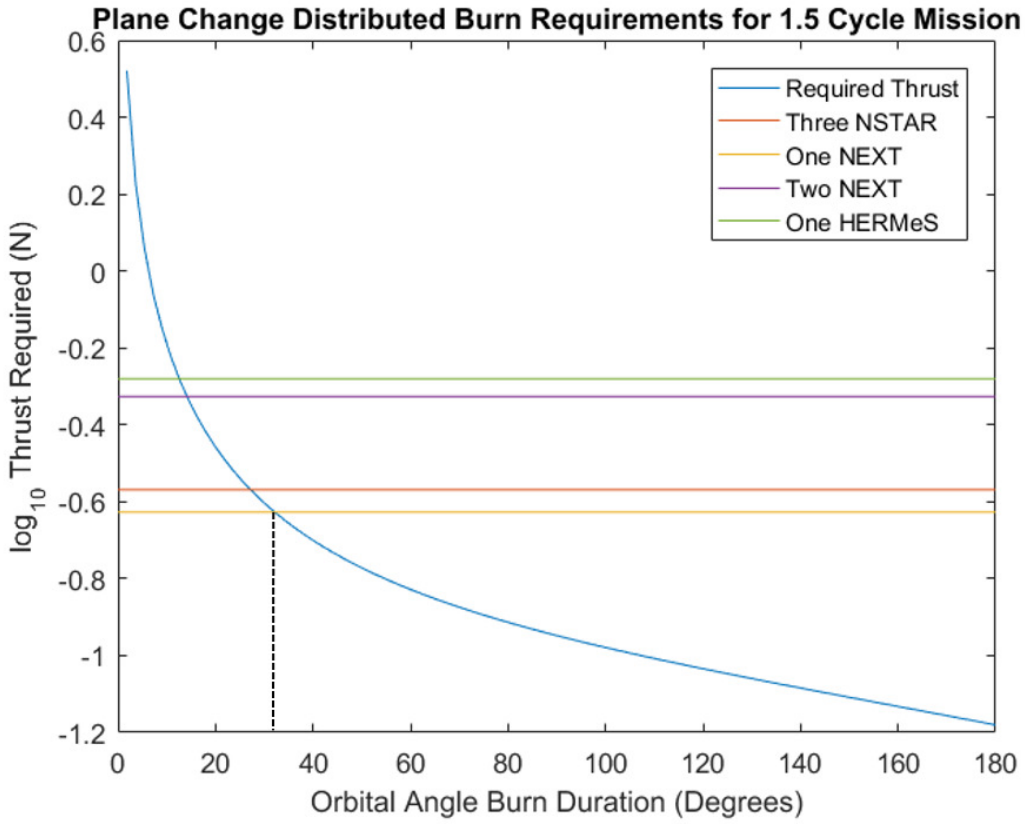

Figure 2.7: Thrust required to complete the plane change in 1.5 solar revolutions as a function of the orbital angle of a distributed burn. The capabilities of the assembly used for the Dawn mission (Three NSTAR), the NEXT thruster, and the HERMeS thruster are plotted for reference.

Using a single operational NEXT-C thruster, SET will complete the plane change with a burn over about 32◦ for each half revolution. This corresponds to an actual delta-v of 2.19 km/s for the plane change for a 633.7 kg spacecraft and 165.3 kg of hydrazine (for a total of 799 kg). An optimized plane change over only half of a revolution simulated in GMAT reduced this waste factor.

Next, there is a period change burn requirement. As an example from an alternate 2027 launch date, the required delta-v is 1.8 km/s. This can also be completed using SEP. In a worst case scenario, the phasing burn can be conducted with about a 10% waste factor, centered on aphelion. A 10% waste factor corresponds to a ΔV_{Actual}, phasing of about 2 km/s. In Figure 2.8, an example of the latter calculation is shown where we compare a 1.857 km/sec impulsive burn at aphelion with a distributed burn over a 90° arc. The resulting trajectory is several million kilometers off nominal during the burn, but that can be corrected down to under a few tens of thousands of kilometers with a small aphelion boost at the subsequent perihelion. The final velocity match maneuver is also amenable to SEP and is conducted in much the same way. Again, the final trajectory computed in GMAT minimizes the period change and analyzes the 2026 launch window.

Given this information, a trade space of different SEP thrusters can be built. This is done in 2.5. As can be seen, a single NEXT-C thruster with redundant plumbing accomplishes the mission requirements with the lowest total mass. The addition of a redundant plumbing brings the system mass to about 63.2 kg, while maintaining a xenon propellant mass of 103.8 kg. The xenon propellant mass was increased to 120 kg to provide an additional fuel margin. The 120 kg of xenon propellant falls well within the NASA qualification

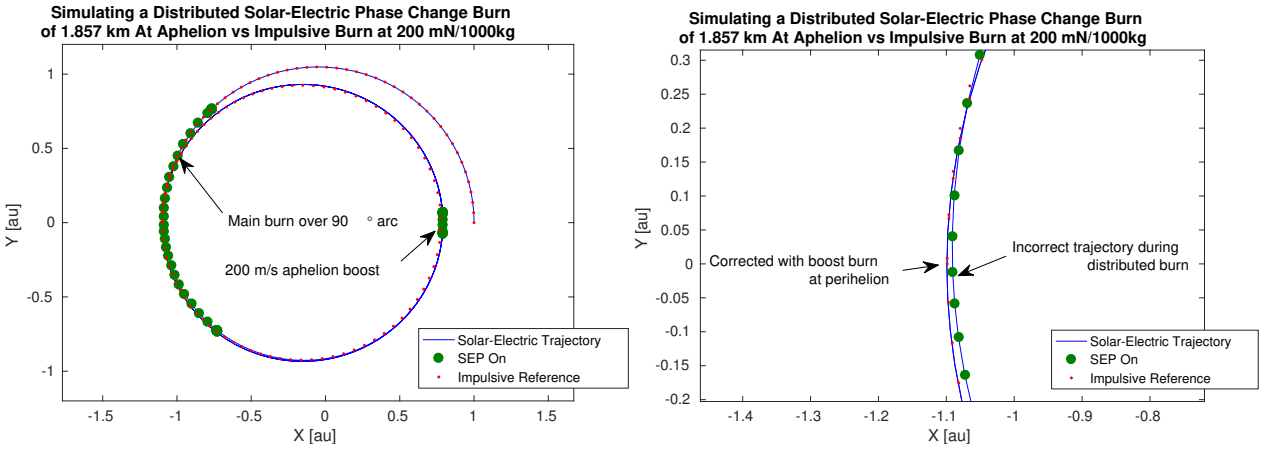

Figure 2.8: Period change burn maneuver and correction executed within one revolution.

of 450 kg of throughput mass. The NEXT has been tested to 750 kg throughput and has an estimated failure of 800 kg [43].

A spacecraft dry mass of 633.7 kg, 165.3 kg of hydrazine, and 120 kg of xenon put the wet mass at launch at 919 kg. For reference, the Dawn spacecraft had a dry mass of 747.1 kg, 45.6 kg of hydrazine (0.1 km/s), and 425 kg of xenon (13 km/s) for a total wet mass of 1217.7 kg at launch [85].

	3 NSTAR (Dawn)	1 NEXT-C	1 NEXT-C (with redundant plumbing)	2 NEXT-C	1 HERMeS
I_{sp}	3100 s	4190 s	4190 s	4190 s	3000 s
Thrust	0.276 N	0.236 N	0.236 N	0.472 N	0.525 N
Power	6.9 kW	6.9 kW	6.9 kW	13.9 kW	12.5 kW
Mass Fraction	0.18	0.13	0.13	0.12	0.19
*Xenon Mass**	143.5 kg	103.8 kg	103.8 kg	96.5 kg	148.7 kg
System Mass	103.6 kg	58.2 kg	63.2 kg	116.4 kg	157.0 kg
Total Mass*	**247.1 kg**	**162.0 kg**	**167.0 kg**	**212.9 kg**	**305.7 kg**

Table 2.5: Trade Space for SEP Systems [43] [46] [77] [90][99]

2.4 Trajectory

2.4.1 Planetary Safety Considerations

After SRR, it was pointed out that there are possible political ramifications of a collision between our spacecraft and Apophis. In the future, if Apophis is ever on a collision course with Earth, the SET mission could potentially be deemed responsible if it appears that the spacecraft may have altered the asteroid's trajectory. Thus, an analysis was conducted to determine the implications of the worst-case collision scenario for the spacecraft into Apophis. This analysis, which is described in detail below, demonstrated that the distance from Earth to Apophis at close approach could change by as much as several kilometers in the worst case.

This result led the collective group to the decision that a collision with Apophis must be avoided. This decision placed additional constraints on the choice of scientific instrument since high-speed impacts, which would be required for instruments such as a penetrator, were no longer possible. It further constrained the trajectory design as well, since a fail-miss trajectory, one that avoids Apophis in the event of a propulsion system failure, had to be used.

The calculations ruling out a direct transfer orbit were done as follows:

We use conservation of momentum to determine the approximate change in velocity of the asteroid resulting from the collision with the spacecraft.

$$\Sigma m\mathbf{v}_{\text{before}} = \Sigma m\mathbf{v}_{\text{after}} \tag{2.7}$$

In the frame of reference of the asteroid, the initial velocity of the asteroid is zero and the initial velocity of the spacecraft is the closing velocity. The asteroid is orders of magnitude more massive than the spacecraft. Further, assuming a worst case of a perfectly inelastic collision where spacecraft embeds itself into asteroid at impact, we simplify

$$m_{\text{spacecraft}} v_{\text{spacecraft,closing}} = m_{\text{asteroid}} \Delta v_{\text{worst case}} \tag{2.8}$$

For actual numbers, we assume a spacecraft mass the order of 1000kg and a worst-case closing velocity of 1000 m/sec. For the worst-case asteroid mass, we skew on the lower mass estimates and assume 10^{10} kg. Thus,

$$10^3 kg \times 10^3 m/s = 10^{10} kg \times \Delta v_{\text{maximum}} \tag{2.9}$$

and $\Delta v_{\text{maximum}} = 10^{-4}$ m/s

To calculate the effect that this much change in velocity would have on the position of Apophis, we assume a worst-case geometry where all of the momentum exchange occurs in-track. The change in eccentricity and period of Apophis's orbit will be negligible. However, the semi-major axis will be maximally affected by this geometry and the consequent change in period will build up over several years. The new period is calculated using the following equations:

$$\frac{1}{a_{\text{new}}} = \frac{2}{r_{\text{original}}} - \frac{v_{\text{new}}^2}{\mu_{\text{sun}}} \tag{2.10}$$

$$= \frac{2}{r_{\text{original}}} - \frac{(v_{\text{new}} + \Delta v_{\text{maximum}})^2}{\mu_{\text{sun}}} \tag{2.11}$$

$$T_{\text{new}} = 2\pi\sqrt{\frac{a_{\text{new}}^3}{\mu_{\text{sun}}}} \tag{2.12}$$

The distance that Apophis will be ahead of its originally predicted position will increase every revolution. The worst case is assumed- that Apophis will have 10 Apophis-years' worth of accumulated position change. This information is then used to determine how far Apophis is ahead of schedule by multiplying the accumulated in-track error by ten years and looking up the heliocentric ephemeris offset of the asteroid in the Horizons system. On 4/13/2029 the angle and closing velocity between Earth and Apophis's velocity vectors are as follows: $v_{\text{Earth Intercept}} = 29707$ m/s, $v_{\text{Apophis Intercept}} = 28309$ m/s, $\theta_{\text{Earth, Apophis}} = 12.3°$.

Using these values, the amount by which the distance from Earth to Apophis would change at the close approach is calculated:

$$\Delta x_{cross} = -1647m,$$

$$\Delta x_{along} = -6410m,$$

Under the worst case collision scenario, the asteroid could be as much as several kilometers closer to Earth at its closest approach. This is equal to or greater than the accumulated Yarkovsky drift over a comparable time period, meaning that rendezvous trajectories with high in-track closing velocities are not appropriate for this mission.

2.4.2 Trajectory Trade Space

The LNAC subsystem team considered two classes of intercept trajectories: direct and bi-elliptic transfers. The direct transfers involve launches and rendezvous locations generally near where the Earth's orbit and Apophis' orbit intersect and involve long coast periods on transfer orbits with often-high energies, necessitating high launch vehicle injection velocities and high rendezvous velocities that intercept the asteroid in its orbital plane. The launch opportunities for direct transfers are also infrequent. Example trajectories computed from first principles and extracted out of the NASA Ames Trajectory Browser tended to have launch vehicle V_∞ in excess of 2 km/sec, and rendezvous velocities in excess of 2 km/sec, and launch opportunities for the lower end of the total delta-Vs that occur either too early or too late, as presented at SRR.

The bi-elliptic options are a class of sub-optimal trajectories that have the following properties:

1. Annual launch opportunities. Every April for a transfer in the orbital plane of Apophis, every August for a split-plane transfer.
2. A coasting orbit close to that of Apophis, with intercept near its aphelion, with coast time and arrival date determined by the particular launch time.
3. Cost to transfer into coasting orbit + cost for Apophis velocity match maneuver = constant = 2.26 km/sec.
4. he transfer between the initial ellipse and the coasting orbit can be accomplished with Solar-Electric with about a 15% waste penalty.
5. The final velocity match maneuver must be done chemically if time is a factor.

In deciding between an in-plane bi-elliptic trajectory and a split-plane bi-elliptic trajectory, the two determining factors were the asteroid divert hazard and the launch vehicle penalty vs on-board propulsion benefit. The penalty of performing a plane-change of 3.3 degrees with solar-electric propulsion is minimal. Plane changes are naturally suited to distributed maneuvers and can be shown to waste no more than 50% propellant worst-case. The launch vehicle penalty of injecting directly into the orbital plane of Apophis rather than into the initial transfer ellipse is significant. Rather than requiring a V_∞ of 800 m/s launched in the plane of the ecliptic, the spacecraft will require 1700 m/sec launched straight down out of the plane of the ecliptic, reducing launch site availability and/or requiring a larger dog-leg maneuver, as well as a higher injection velocity rather. This compares against an 800 m/sec on-board delta-V reduction.

The safety case for the bi-elliptic orbit is even more compelling in that it can be structured as an inherently a fail-miss orbit with a rendezvous velocity mainly out of the plane of Apophis's orbit by scheduling the plane change maneuvers in a distributed fashion with only the final plane change maneuver (occurring either just before or just after the velocity match maneuver) bringing the two orbits into the same plane. This also enables structuring the approach so that a worst-case crash occurs at a velocity lower than the velocity match magnitude and out of plane, meaning that instead of changing the orbital period of Apophis by an amount that can accumulate to several kilometers in-track by the time of the 2029 Earth encounter, the worst-case perturbation is near zero at Earth encounter and no more than a small fraction of a kilometer elsewhere.

A table providing further breakdown of the selection of this bi-elliptic split-plane trajectory can be found in Table 2.6.

Trajectory Option	Launch Opportunity	Flight Time	Closing Speed/ Divert Hazard	Propellant Mass Fraction
Direct Transfer	Infrequent, High V_∞	>12-18 mo Minimum	>1km/sec in-track	> 2
Bi-elliptic Chemical	Annual (Apr) High V_∞	11-22 mo Variable Range	>0.5km/sec in-track	> 4
Bi-elliptic, Split-Plane Chemical	Annual (Aug) Low V_∞	7-18 mo	<1km/sec cross-track	> 7
Bi-Elliptic, Split-Plane SEP-only	Annual (Aug) Low V_∞	>30 mo	<1km/sec cross-track	< 1.5
Bi-elliptic, Split-Plane, Chemical/SEP Hybrid	Annual (Aug) Low V_∞	18-30 mo	<1km/sec cross-track	< 2

Table 2.6: Trajectory Trades

Direct Transfer

The direct-burn option requires two burns- the first to escape the Earth's orbit, entering the transfer orbit, and the second to exit the transfer orbit, matching the orbit of Apophis. In the figures below, the delta-v requirements are plotted as a function of launch date and length of time to reach Apophis. Figure 2.9 the total delta-v requirement, accounting for both burns, and Figures 2.10 and 2.11 show the requirements broken down by the escape burn and the rendezvous burn respectively. For this preliminary analysis, the need for a plane-change burn was neglected.

To create these plots, position and velocity data for the Earth and for Apophis were obtained from the Jet Propulsion Laboratory HORIZONS database [48]. For every ten days between February 2017 and April 2029, six trajectories were calculated- one for each travel time between one to six months. Using the desired rendezvous date and travel time, the corresponding departure date was determined. The required delta-v was then calculated using freely available MATLAB code to solve Lambert's problem [20].

As shown in Figure 2.9, there are two windows during which the required delta-v is significantly lower than at any other time. These two minimums correspond to the Hohmann transfer windows. It is advantageous to launch during these windows since the amount of delta-v required dictates the amount of fuel that the spacecraft will have to carry, and hence, the cost to launch the spacecraft.

It is also clear from this analysis that the slower trajectories require less delta-v, so from a cost perspective, it is advantageous to choose a slower trajectory. However, for the reasons mentioned above, direct-transfer trajectories were ruled out.

Bi-Elliptic Transfer

A preliminary analysis of the worst-case hazard of flying a 1000 kg-class mission to Apophis indicated that the effect of a SET-Apophis collision prior to the April 2029 event could at worst result in about 10 km in-track error, which translates to a few kilometers of radial error during the event. As detailed previously, this calculation is based on maximum in-track position change at the 2029 Earth flyby caused by a worst-case in-track collision with a 1000 kg spacecraft at 1 km/s relative velocity into a 1010 kg asteroid if allowed to

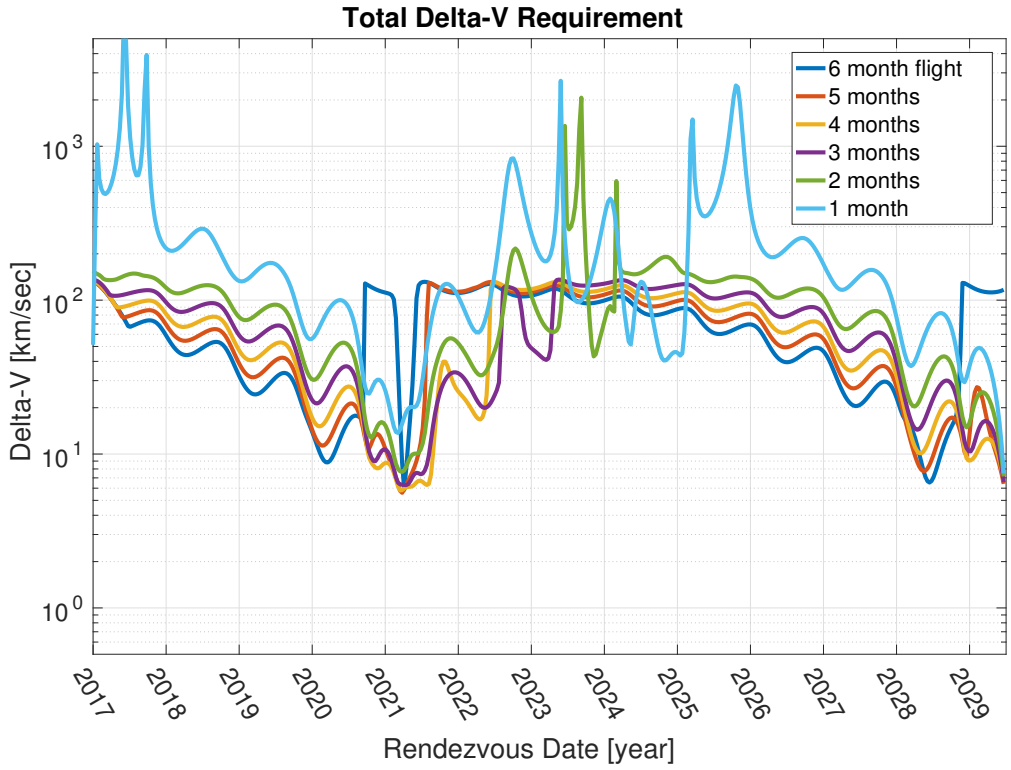

Figure 2.9: Direct Burn Total Delta-Requirements

accumulate for ten years. Though an extreme scenario, as the LNAC subsystem team cannot guarantee that "no matter what, it's only millimeters," we have elected to use an indirect approach trajectory, as follows, to mitigate Earth impact hazard.

A bi-elliptic split-plane intercept trajectory was therefore selected for this mission. This is a launch into a Hohmann-like transfer ellipse with aphelion directly under Apophis aphelion. A phase change burn is made on the first aphelion and a velocity-match burn occurs one revolution later. To account for the 3.3° angle of inclination between Earth's and Apophis' orbital planes, a plane change burn is executed with solar-electric propulsion along the line of nodes. This burn is executed independently of the phase change burn and the velocity match burn. Launch opportunities for bi-elliptic split-plane trajectories are every August from now until 2027, at which time a spacecraft would not arrive at Apophis in time to collect data prior to the April 2029 event.

The selection of a bi-elliptic split-plane trajectory has three implications for the subsystem requirement LNAC.2: Rendezvous and Divert Hazard. First, at all points until the final velocity match burn, the spacecraft is on a fail-miss trajectory. This means that there is no danger of intercepting Apophis before the desired rendezvous. Second, the intercept comes from above or below, not ahead or behind, Apophis, meaning the period of Apophis' orbit will be unaffected by any unintended perturbations. Indeed, a cross-orbit impact will have nominally zero effect on Apophis's location if it occurs near the point of the April 2029 event. Finally, the plane change burns may be split so that the last one is the rendezvous burn. This allows us to select an almost arbitrarily slow closing velocity.

This trajectory is also very forgiving from a launch perspective. The initial transfer ellipse may be launched into for about one month prior to the nominal window and up to two weeks after with minimal penalty on the V_∞ and minimal penalty on the phasing burn, where the latter penalty is defined as 100 m/sec of solar electric burn. These launch window margins were computed through application of Lambert's algorithm from Earth's location at nominal launch time plus/minus margin and the target point under Apophis aphelion.

A pictorial representation of the bi-elliptic split-plane transfer is shown in 2.12: As denoted in Figure

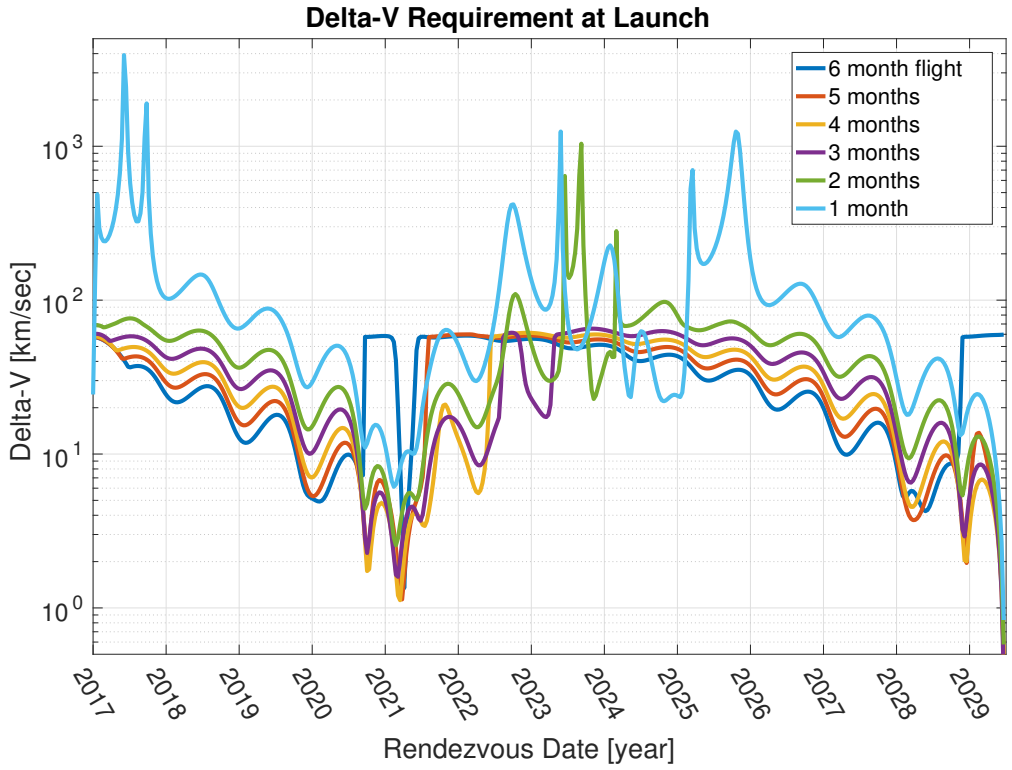

Figure 2.10: Direct Burn Launch Delta-V Requirements

2.12, Earth's orbit is shown in blue, and Apophis' orbit is shown in red. The spacecraft will launch into a Hohmann transfer ellipse to a point directly below Apophis aphelion. This transfer ellipse is shown in black in the diagram above. The spacecraft will then perform a phase change burn so that it arrives at Apophis' aphelion at the same time as Apophis arrives at its aphelion after one revolution; this orbit is shown in gray in the diagram above. Once the spacecraft and Apophis arrive at Apophis aphelion, the spacecraft will then execute a velocity match burn and begin the station-keeping phase of the mission. At the points denoted in orange in the diagram above, the spacecraft will perform plane change burns using solar-electric propulsion. Each of these burns will occur either along the line of nodes or at Apophis aphelion–the latter will constitute the rendezvous burn, as described previously. An orthogonal view of these maneuvers is shown in Figure 2.13: To select a viable launch date for this mission, MATLAB was used to calculate delta-V costs for launch dates in late August for each year up to 2027. Late August was selected because Earth is directly opposite Apophis aphelion at that time of year and thus facilitates a Hohmann transfer orbit. For each launch date, delta-V costs were calculated for the Hohmann transfer burn, the plane change burn, the phase change burn, and the final velocity match burn.

The ΔV costs for the Hohmann burn and the plane change burn are essentially equal for all launch opportunities, but the phase change burn and the velocity match burns depend on the location of Apophis when the spacecraft completes the Hohmann transfer phase of the mission. Taking into account the delta-V costs shown above and allowing for a reasonable program development timeline, the proposed launch date for Project SET is August 24, 2026. If for some reason this launch date is unachievable, an August, 2027 launch date will be used.

A table that outlines delta-V requirements for all stages of the trajectory from Earth to Apophis is shown in Table 2.3.1.

2.4.3 End-to-End Solar-Electric Trajectory

To confirm the intuition developed in the previous sections, a high-fidelity simulation was constructed using GMAT 2016 to determine the feasibility of executing the 2026 launch/2028 rendezvous with realistic solar-

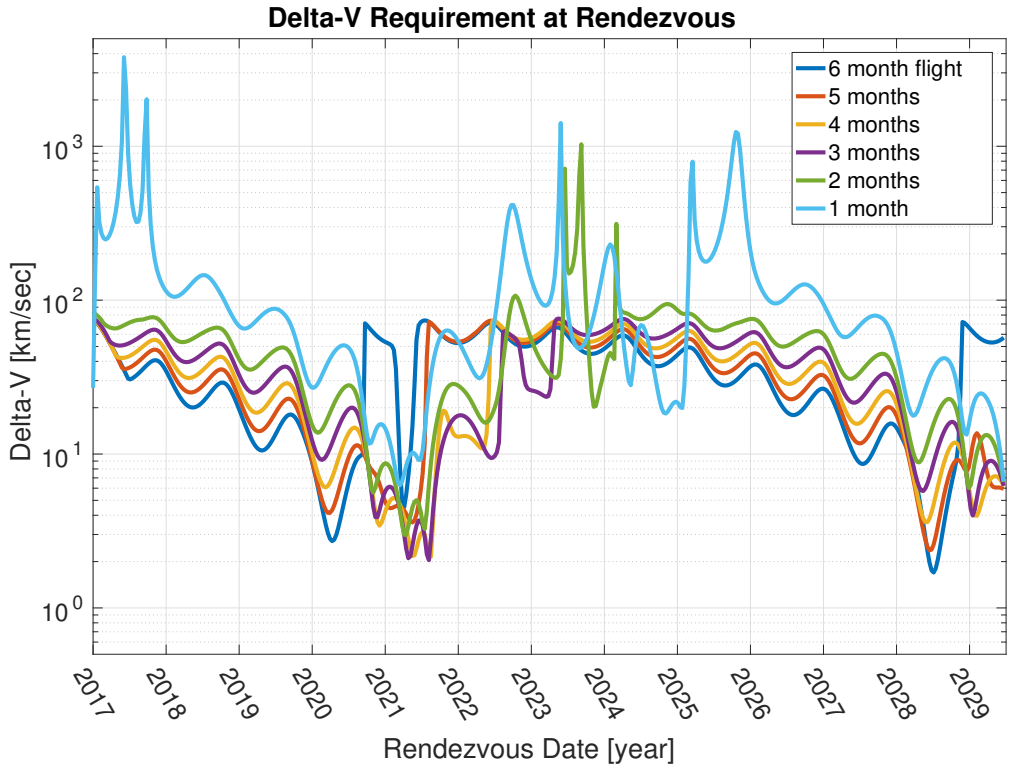

Figure 2.11: Direct Burn Rendezvous Delta-V Requirements

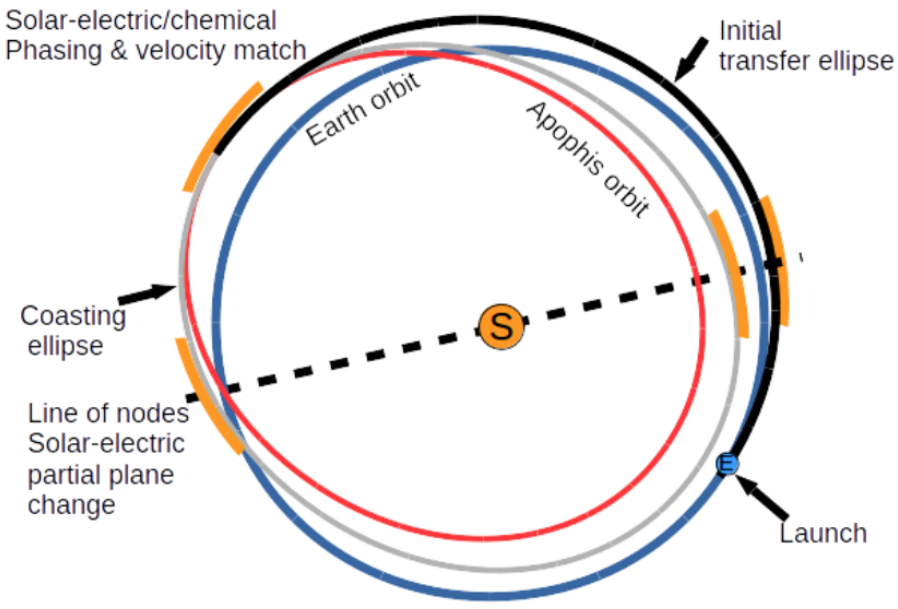

Figure 2.12: Bi-elliptic Transfer Schematic

electric propulsion. The force model consisted of all solar system major bodies and sixteen largest minor bodies. The positions and masses of the major bodies are sourced from the DE430 ephemeris. The positions of the minor bodies and of Apophis are sourced from binary SPICE kernels generated by the Horizons

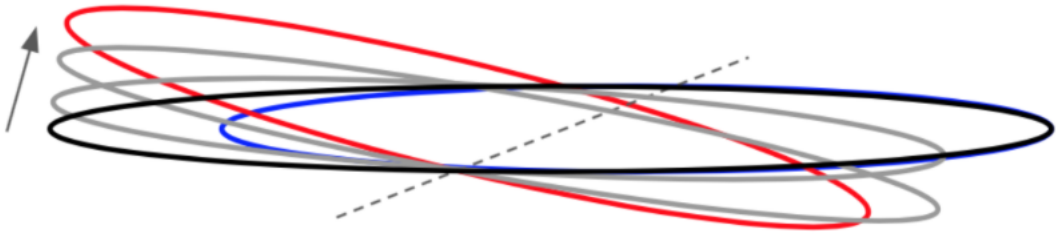

Figure 2.13: Plane Change Detail

Information System and masses are sourced from [38].

The initial condition of the simulation begins in a 185km x 218km parking orbit around the Earth in a plane near the ecliptic on August 24, 2026. The procedure to solve for the solar-electric trajectory is to first exactly target an all-impulsive trajectory and then (with manual intervention) to solve for distributed solar-electric burns corresponding to combinations of individual impulses.

All-Impulsive Seed Trajectory

The first **Target** block solves for the Earth-departure burn out of that parking orbit. A 3.25 km/sec escape burn is targeted to achieve a C3 energy of about 0.64 km^2/sec^2, corresponding to a V_∞ of approximately 800 m/sec with an outgoing asymptote along the heliocentric velocity vector of the Earth. The timing and magnitude of the escape burn are free parameters in the simulation and are solved for only once in the beginning of the run.

The escape burn is followed by an in-track trajectory correction maneuver ("TCM_Launch") approximately 12 hours later. The spacecraft is then propagated heliocentrically until it crosses the Earth/Apophis line of nodes, at which point a cross-track burn is executed to match planes. At nominal aphelion time a pure in-track period change burn is executed and one orbit later the velocity match burn is executed.

The magnitude of TCM_Launch, the magnitude of the plane change burn and its timing relative to the first crossing of the line of nodes, and the magnitude of the period change burn are all free parameters that are solved for concurrently in one **Target** block of the simulation. The **Achieve** objectives of the **Target** block are constraints on the relative offset of the spacecraft from Apophis at the end of the simulation. For this portion of the simulation, a point exactly 200 km "under" Apophis in the ecliptic plane is targeted.

The magnitude of the final velocity match burn is computed as the ecliptic plane component of the XY velocity difference between the spacecraft and the asteroid at the time of second aphelion. This is essentially an open-loop burn. To close the rendezvous loop, the velocity match burn is immediately followed with a Target block that varies all three components of a small trajectory correction maneuver to achieve a 10 km standoff distance from the asteroid at the nominal passage through the line of nodes. A second burn of 1 m/sec toward the asteroid places the simulation into an Apophis-centric incoming hyperbolic orbit and a final rendezvous burn is executed to enter orbit of Apophis at an altitude of 1 km.

The final solution for the impulsive trajectory is given in Table 2.7 and the locations of the burns are shown schematically in Figure 2.14.

Computation of the Solar-Electric Trajectory

The solar-electric trajectory was computed using the impulsive trajectory as an initial seed. Solar-electric burns were assumed to be fixed-thrust and parametrized by their total duration, start time or mid-point time, and for the final velocity match maneuver, by their orientation with respect to the nominal velocity vector. Rather than computing the entire set of maneuvers simultaneously inside a single Target block, the solution for the plane and period change burns was computed separately from the solution for the final

Table 2.7: Computed GMAT Impulsive Trajectory Burn Parameters

Maneuver	**Time**	**Magnitude [km/sec]**
Initial Condition	T0 = 2026 Aug 27 00:00:00 UTC	
Escape Burn In-track	TE = T0 + 9011.22 sec	3.25515
TCM_Launch In-track	TE + 36hr	-0.05965
TCM_PlaneChange Cross-orbit (-Z)	Node crossing - 1.6 days	-1.72077
TCM_PeriodChange In-track	Aphelion	-0.43709
TCM_VelocityMatch Open-loop match of Apophis velocity in ecliptic plane	Next aphelion 2028 Mar 26 11:32:12 UTC	-1.90192
TCM_R1 Target to rendezvous at node, direction solved-for in block	Same 2028 Mar 26 11:32:12 UTC	0.00016
TCM_R2 Burn toward Apophis. Open-loop burn	Node crossing 2028 May 27 06:28:40 UTC	0.01000
TCM_R3 Correction to R3 to achieve 1.2 km flyby height. Direction solved-for in block	Same	0.00238
TCM_R4 Enter circular orbit at 1.2km In-track in Apophis-centric coordinates	Node crossing + 820 sec	-0.01209

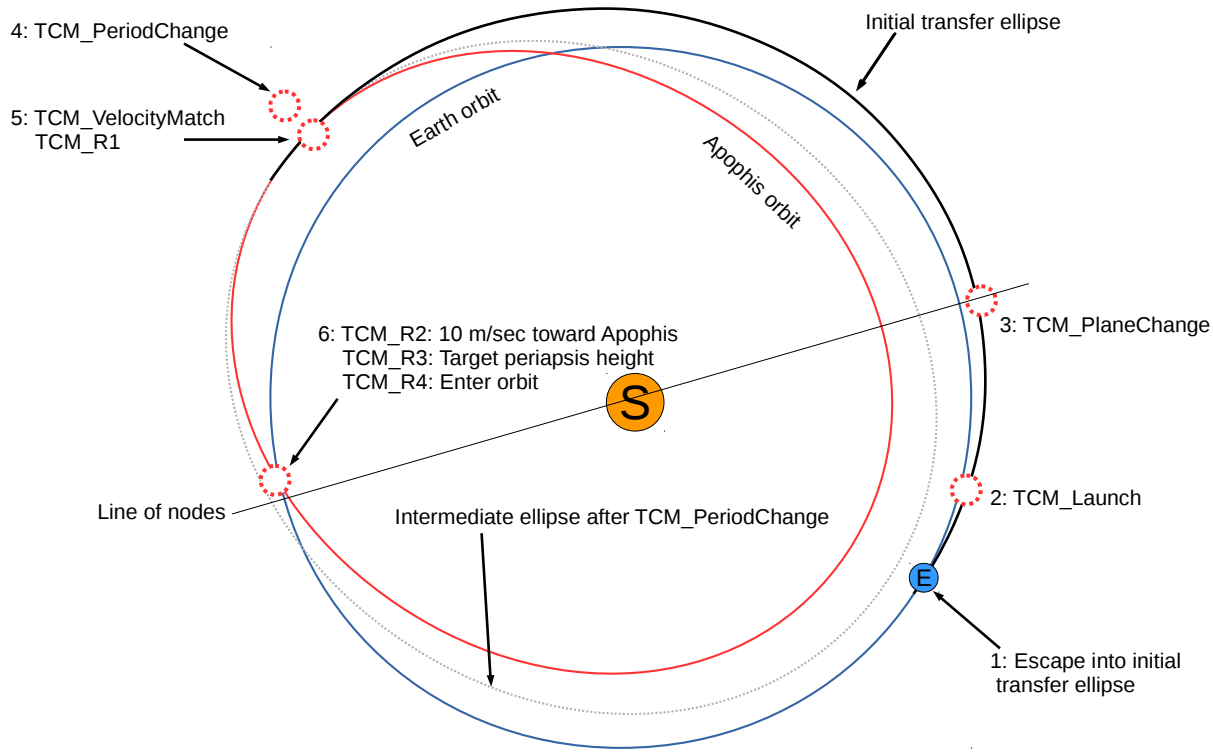

Figure 2.14: Location of Impulsive Burns. Not to scale.

velocity match burn. The solution was first run assuming a constant mass. With this approximate set of burns, a final solution using decreasing propellant mass was run.

The initial conditions of the spacecraft for the final trajectory are 634 kg dry mass, 165kg hydrazine mass, and 120 kg xenon propellant. The spacecraft is started immediately after the completion of the TCM_Launch maneuver as computed in the all-impulsive trajectory. All maneuvers assume a 236mN thruster.

The plane change and period change maneuvers are solved for concurrently in one Target block. The plane change is distributed over two locations as shown in Figure 2.12. Unlike the impulsive case, the distributed period change is composed of one burn at aphelion and a shorter burn at the subsequent perihelion as shown in Figure 2.16.

The free parameters of this first Target block are

1. Duration of plane change burn at first nodal crossing (Burn 1 in Figure 2.15)
2. Time offset of Burn 1 with respect to nodal crossing time
3. Duration of period change burn centered at aphelion passage (Burn 2 in Figure 2.15)
4. Duration of second half of plane change burn centered on second nodal crossing (Burn 3 in Figure 2.15)
5. Duration of aphelion raise burn centered on perihelion crossing (Burn 4 in Figure 2.15)

To solve for the plane change and period change burns, the spacecraft is propagated ballistically to its aphelion after completion of the perihelion burn. The Achieve lines in the block target the position and Z velocity of the spacecraft to a location 200 km under Apophis at its aphelion.

With values of the period and plane change burn parameters solved for, the spacecraft state is rewound back to the end of the plane change burn to solve for the velocity match burn. The final velocity match burn is composed of two phases:

1. An additional aphelion-boost burn occuring at perihelion immediately after Burn 4 with a fixed duration of 3.6 hours (Burn 5 in Figure 2.16)

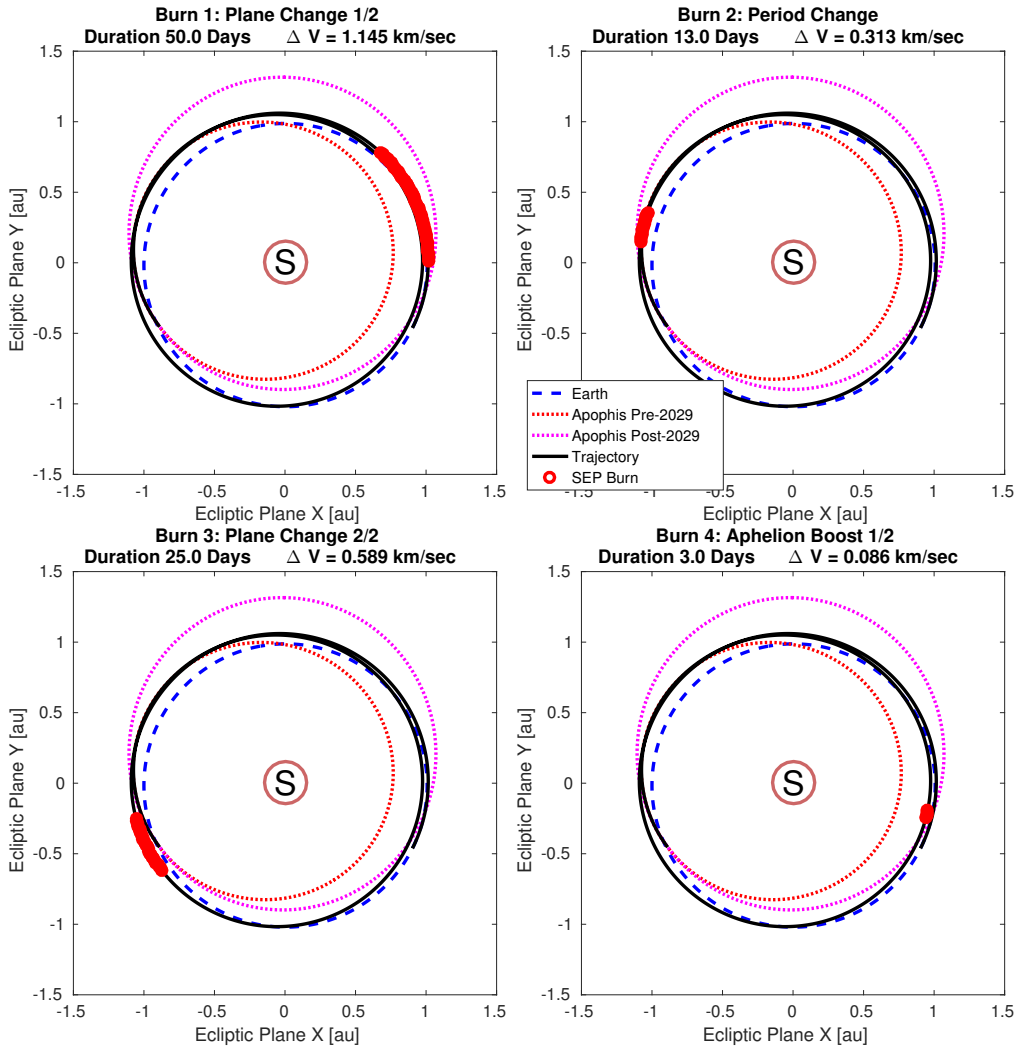

Figure 2.15: Solar-Electric Plane Change and Period Change Burns

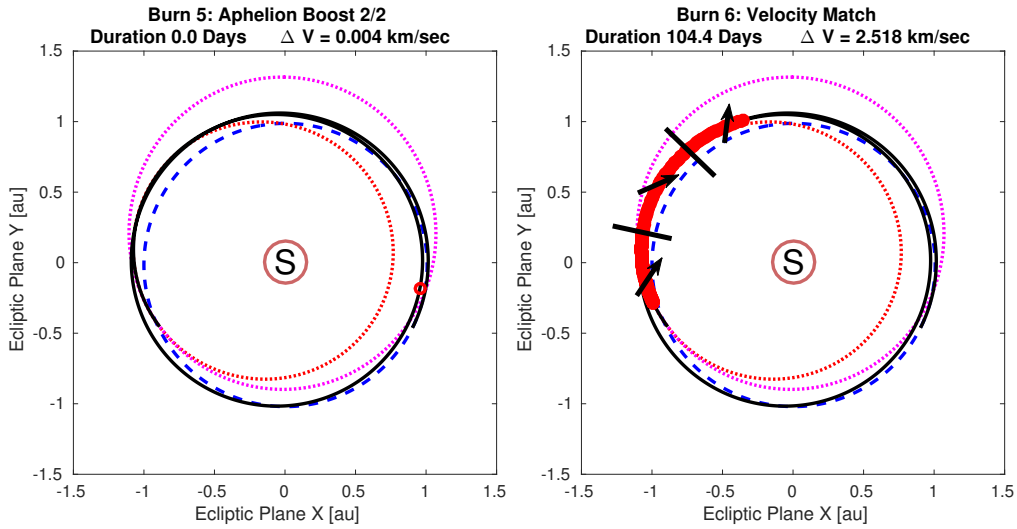

Figure 2.16: Solar-Electric Velocity Match Burn

2. A long duration burn near aphelion composed of three equal segments, each with different orientations with respect to the heliocentric LVLH frame (Burn 6 in Figure 2.16).

This burn concludes ten days before the nominal Apophis node crossing time on 27 May 2028

The fixed duration perihelion burn is required to kick the optimization out of a local saddle point that prevents convergence to the Achieve lines described below. The astute observer will note that we have already solved for an aphelion boost bust in the first half of this computation. However, that aphelion raise was targeted toward achieving an aphelion identical to that of Apophis. Because the distributed velocity match burn slows down, the spacecraft will begin losing aphelion altitude early with respect to the ballistic orbit that was rewound to solve for the velocity match burn. It is thus necessary to provide a small prophylactic aphelion boost.

Note that while it may be possible to combine the solution of the total duration and timing of the perihelion burn for a computation of a more fuel-optimal plan, this method provides an existence proof for a solar-electric trajectory and is deemed sufficient for the purpose of this early stage of mission planning. A similarly ad-hoc decision is made in the choice to split the velocity match burn into three segments, and to pin the end of the velocity match burn at ten days before the nominal nodal crossing time.

The free parameters of this Target block are

1. Total duration of the velocity match burn
2. The three azimuths with respect to in-track direction in the ecliptic plane of all three segments of the velocity match burn
3. The out-of-plane elevation angles of the last two of the three segments of the velocity match burn

The **Achieve** lines, corresponding to desired state 10 days before the nodal crossing on 17 May 2028 consist of spatial coordinates exactly 50 km under Apophis in the Ecliptic plane with velocities exactly matched to Apophis in all three dimensions.

Figure shows the final rendezvous geometry at the end of the velocity match maneuver decomposed into phase space of in-plane and out-of-plane components of closing velocity versus slant range. Final maneuvers to rendezvous with Apophis from this standoff position may be initiated at any time. The small amount of drift in standoff range and velocity for up to fifty days after the end of the solar-electric portion of the trajectory enable considerable latitude in selecting the time and speed of a final rendezvous burn.

Table 2.8 gives the final solved-for parameters of the solar-electric trajectory and fuel usage is shown in Figure 2.18. There is ample margin on both xenon fuel and (depending on final mission requirements) the amount of hydrazine carried. This implies that this particular trajectory is not necessarily optimal from a

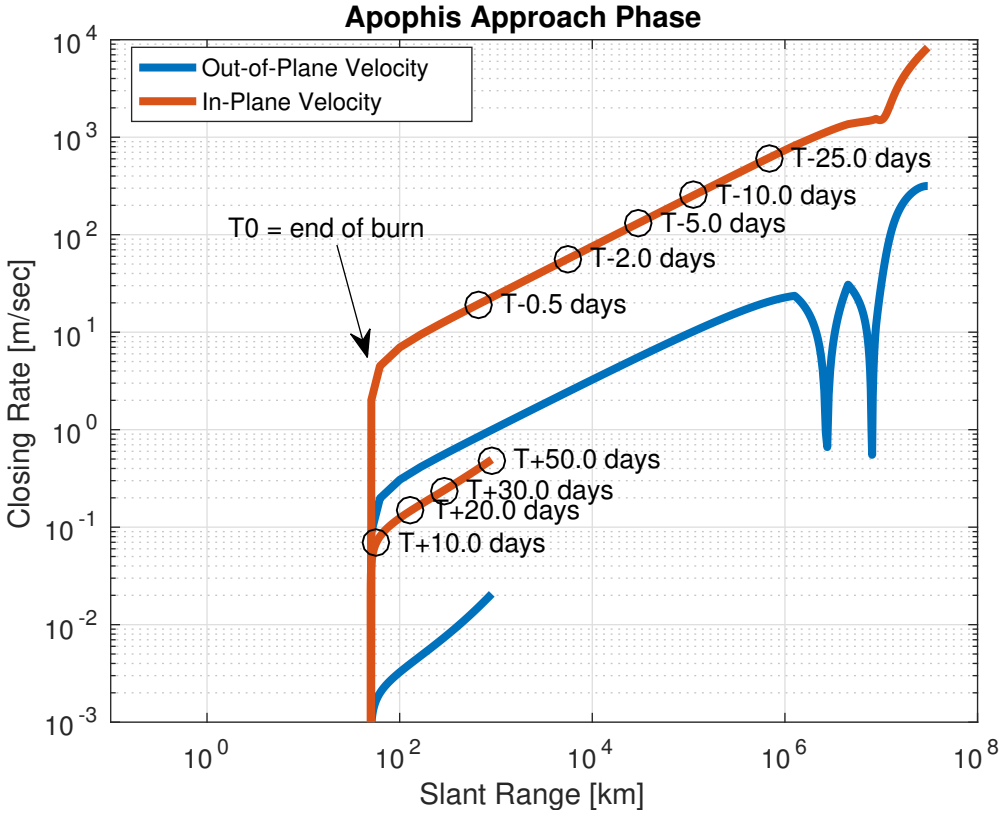

Figure 2.17: Phase Space Decomposition of Apophis Rendezvous. Time markers are with respect to the end of the velocity match maneuver on 17 May 2028. Maximum slant range of 50km "under" Apophis is targeted in this trajectory.

Table 2.8: Computed GMAT Solar-Electric Trajectory Burn Parameters

Maneuver	**Parameter**	**Value**
Plane Change	Burn 1 Duration	50.8745 days = 1.145 km/sec
	Burn 1 Time Offset	-11.5463 days
	Burn 3 Duration	25.4372 days = 0.589 km/sec
Period Change	Burn 2 Duration	13.6736 days = 0.313 km/sec
	Burn 4 Duration	3.6713 days = 0.086 km/sec
Velocity Match	Burn 5 Duration	3.6 hrs = 4 m/sec
	Burn 6 Duration	104.4465 days = 2.518 km/sec
Velocity Match Angles. Angles in heliocentric VNB frame. Azimuth is clockwise from anti velocity vector. Elevation angle is positive in direction of positive Z in GMAT ecliptic coordinates	Azimuth 1/3	28.1673 deg
	Elevation 1/3	0 deg
	Azimuth 2/3	-49.3368 deg
	Elevation 2/3	2.5066 deg
	Azimuth 3/3	-39.2608 deg
	Elevation 3/3	0.1103 deg

system design perspective. Indeed, by assumptions that 100% duty factor is realizable for the full duration of all burns may not be realistic given the necessity of ballistic coast periods for ground tracking purposes. Nevertheless, this trajectory is presented as an existence proof for a solar-electric option to rendezvous with Apophis using a split-plane bi-elliptic trajectory. The margins presented in this document leave ample room for further mission optimization.

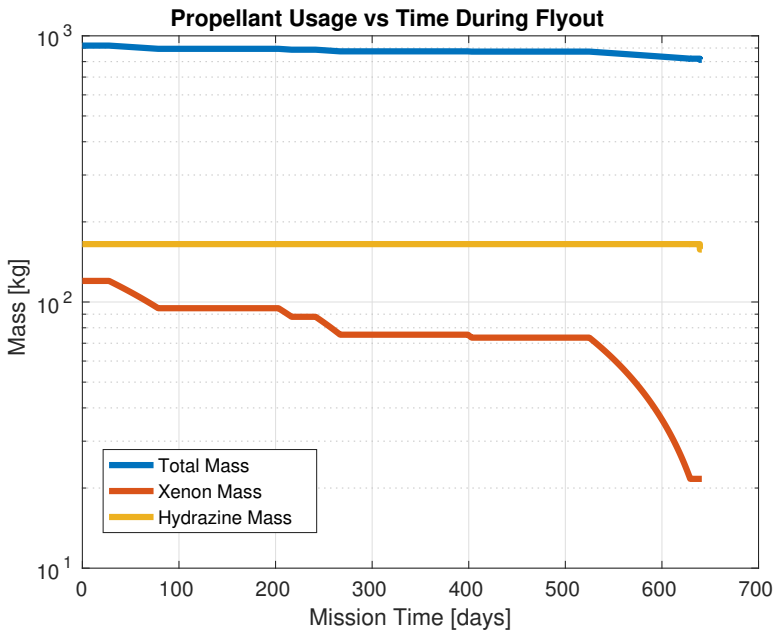

Figure 2.18: Solar-Electric Propellant Usage. Note that use of hydrazine for station-keeping has been ignored and all solar-electric burns are assumed to have 100% duty cycle.

2.4.4 Station-Keeping

Estimates of the asteroid's mass range between 2×10^{10} kg and 8×10^{10}kg [1]. This mass provides sufficient gravitational attraction to allow science operations to take place in an Apophis-centric orbit provided that the stand-off distance is within Apophis's gravitational sphere of influence. The radius of a sphere of influence is given by[9]

$$R_{\text{influence}} = r_{\text{from sun}} \left(\frac{m_{\text{apophis}}}{m_{\text{sun}}} \right)^{2/5} \tag{2.13}$$

Which at a worst-case solar distance of about 0.85 AU and the lower mass estimate works out to 1.2 km on the low end and at 1.05 AU and the higher mass estimate works out to 2.0 km for the upper bound.

In considering station-keeping requirements during science operations, it is necessary to analyze the relative magnitudes of the central gravitational force and the perturbing accelerations. When in orbit of Apophis at a nominal orbital radius on the order of 1km, the gravitational acceleration is on the order of 1 μm/sec^2. Solar radiation pressure acting on the solar panel array is expected to be the dominant perturbation within that sphere of influence. The acceleration due to solar radiation pressure is given by [64]

$$a_{\text{srp}} = \frac{A_{\text{solar panel}}}{m_{\text{satellite}}} \times J_{\text{sun}}/c \tag{2.14}$$

where A is the cross-sectional area of the satellite in square meters, P is the solar insolation in Watts per square meter, and c is the speed of light.

For this analysis, the satellite was assumed to have a nominal solar panel area of about 10m^2 of solar panel and a final dry mass on the order of 500kg. During the initial portion of science operations, Apophis will be at a minimal solar distance of about 0.85 AU at its closest, meaning the power of incidence sunlight will be $1367 \times (1/0.85)^2 = 1900$W/m^2 and the perturbing acceleration will be on the order of 0.12 μm/sec^2, which is a significant fraction of the central gravitational acceleration. This motivates an analysis of the effect of solar radiation pressure on the stability of the science orbit.

Simplified Intuition

An initial analysis was performed with a numerical simulation in two dimensions modeling gravitational acceleration toward the center and a fixed perturbing acceleration in the +x direction. The satellite state was initialized as that of a circular orbit at various altitudes and propagated forward in time. Figure 2.19 shows the result. At higher altitudes, the perturbing acceleration was sufficient to dramatically change the orbit and cause the satellite to crash into the asteroid. This analysis showed the need for continued station-keeping. A more detailed numerical simulation of the control law necessary to maintain the science orbit was performed in GMAT.

Per requirements from the instruments onboard the spacecraft, the radius of the orbit will be between 0.5 and 2 km. The inclination of the orbit, β, will be either 0 degrees or 90 degrees depending on the type of scientific data being collected. Figure 2.20 depicts the two different orbit inclinations, and the points in the orbit at which the station keeping burns will be performed. Stationkeeping will be performed using hydrazine thrusters for actuation, star trackers and science cameras for angle sensing, and the RRT instrument for range to surface. All system requirements for those components are in excess of what is necessary to perform stationkeeping. This section will develop the quantitative requirements for the sensors station-keeping control algorithm.

Detailed Numerical Simulation

The delta-v requirements for both cases as a function of orbital radius are shown in Figures 2.21 and 2.22 below. This analysis showed that to orbit Apophis at $\beta = 0$, on the order of 1 m/sec/year will be required. For $\beta = 90$, between 2-7 m/sec/year will be required.

This analysis was conducted by writing a simulation in General Mission Analysis Tool (GMAT). As shown in Figure 2.20, there are designated locations in the orbit where station-keeping burns will be performed if necessary. At every time step in the simulation, the position and velocity vectors of Apophis and the spacecraft are used to determine whether or not the spacecraft is currently located at one of these points.

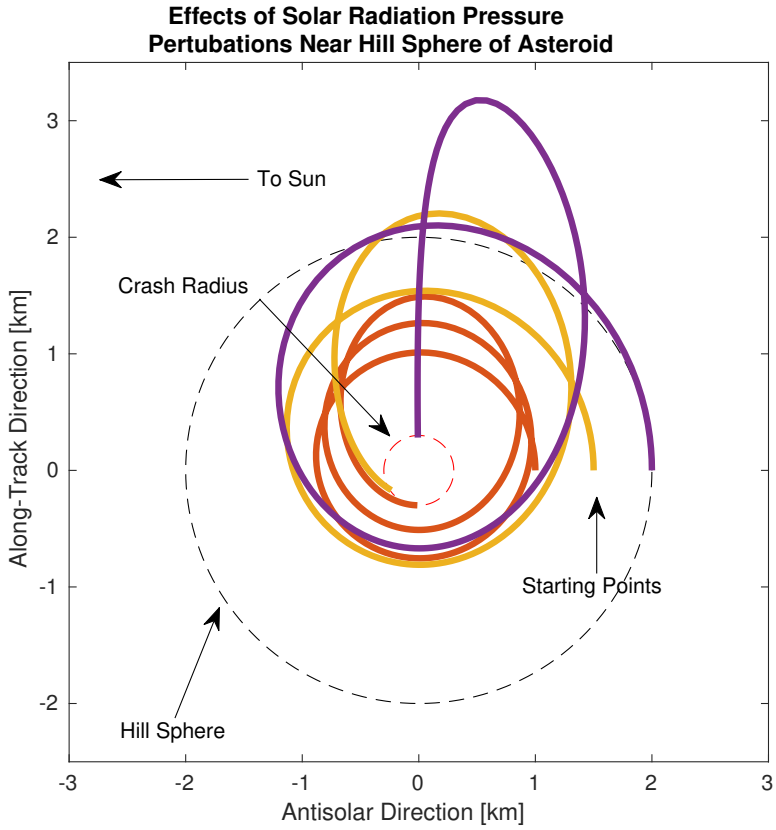

Figure 2.19: Effect of Solar Radiation Pressure on Science Orbits. Simulation of $\beta = 0$ for circular orbits in various starting altitudes inside the Apophis sphere of influence.

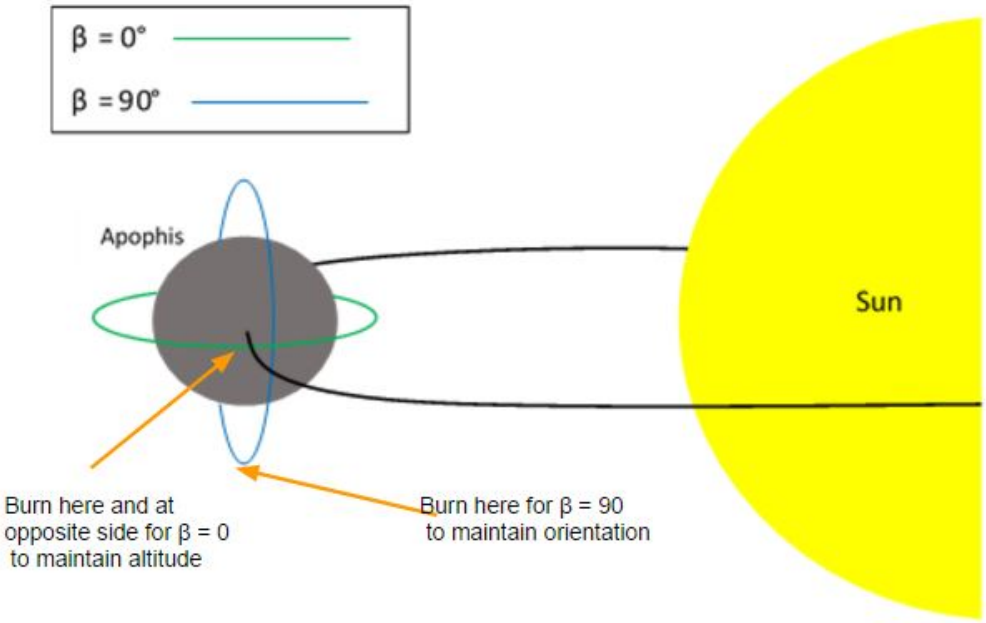

Figure 2.20: Orbital Inclinations and Burn Locations

If so, the magnitude of the burn required to correct the spacecraft's orbit is computed, and the burn is executed. Otherwise, the spacecraft continues in orbit without burning. After each burn, the total amount of delta-v that has been used is updated, and the total delta-v is reported at the end of the simulation.

Altitude Error Tolerance

The magnitude of the burn that is required to keep the spacecraft in orbit is dependent upon the spacecraft's altitude from the center of Apophis. If the sensor reports an incorrect altitude measurement, the burn that is performed could interfere with the spacecraft's ability to stay in orbit. If the burn is too large, the spacecraft could escape Apophis's sphere of influence, and if it is too small, there is a risk of colliding with the surface. This risk is not immediate- the spacecraft will be able to remain its orbit for a minimum of 36 hours without any burns. However, it is necessary to understand how much error in the altitude measurement can be tolerated. This analysis showed that the spacecraft can remain in orbit with up to 10% altitude error.

In order to simulate altitude measurement error, the above-mentioned GMAT simulation was used, and the true altitude of the spacecraft was perturbed by a random number. The simulation was repeated three times, for a random number up to 1%, 5%, and 10% of the spacecraft's true altitude. When the altitude error was increased past 10%, the spacecraft was no longer able to maintain the orbit around Apophis. As expected, the delta-v required to station-keep increased when the error increased since the spacecraft must continually correct for past burns that were not optimal. The delta-v requirements as a function of altitude error are shown in Table 2.9. The key result of this analysis is that up to 10% altitude error in the sensors can be tolerated with respect to station-keeping.

Angles Tolerance

Using the standard star trackers on the bus, we assume we are able to measure absolute angles to the asteroid to an order of several tens of arcseconds. At a circumnavigation rate of about 12 hours in the science orbit, an error of 100 arcsec corresponds to a time error of a few seconds. Our simulation has larger quantization error in the simulation of the science orbit, while remaining in a stable orbit. We therefor conclude that the nominal performance of the star trackers is more than sufficient for stationkeeping.

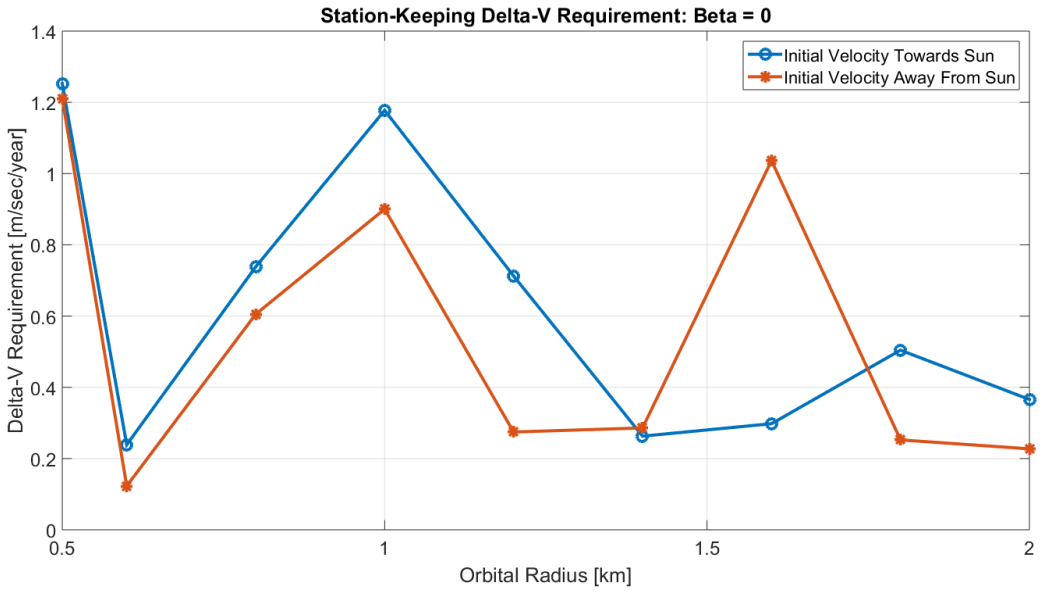

Figure 2.21: Orbital Inclinations and Burn Locations for $\beta = 0$

Altitude Error	0	0-1%	0-5%	0-10%
Delta-V Requirement	1.21	1.28	2.11	3.58

Table 2.9: Delta-V Requirements and Altitude Error

2.5 Rendezvous and Post-encounter Maneuvers

After completing its mission, the SET spacecraft will leave Apophis and enter an elliptic orbit about the sun, as discussed in section 1.1.3. This option was selected to first and foremost mitigate potential planetary protection risks presented by attempting to land the spacecraft on Apophis. However, this risk is extremely small due to the difference in speed of SET and Apophis being on the order of cm/s. Furthermore, there is little more scientific information to be gained from attempting a landing with the onboard instruments. Finally, there may be potential targets in SET's path after leaving Apophis that could be studied with SET's onboard instruments. Such a mission extension would be an added bonus to the scientific data gathered at Apophis.

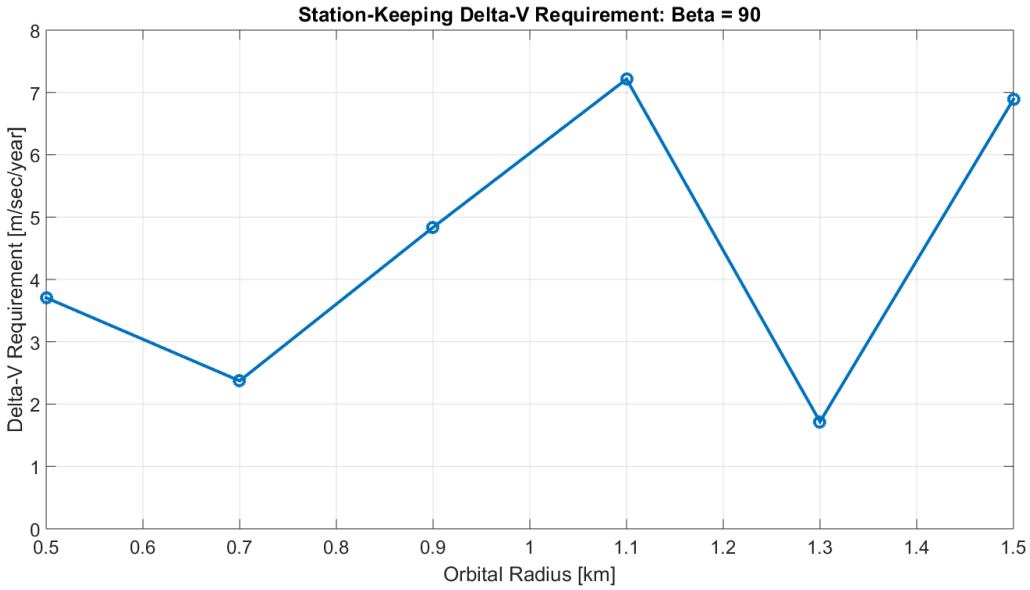

Figure 2.22: Orbital Inclinations and Burn Locations for $\beta = 90$

Chapter 3

Instrumentation

3.1 Overview of Requirements

The payload sub-system requirements have been designed to assure the SET Mission meets its science objectives and takes full advantage of the active "experiment" nature is performing with Apophis. With these requirements instrumentation was selected that not only helps expand knowledge of asteroids through detailed case-study but also allows for observations and measurements of the impact of tidal torques and medium sized (100's of meters in diameter) asteroids. A summary of these requirements can be found in Table 3.1.

PLD.1 aims to collect spatially resolved, spectral measurements of Apophis' surface which will reveal Apophis' surface composition and search for heterogeneities at a scale not detectable from Earth based observations. Most ground based near-IR observations of asteroids range from 0.45 to 2.45μm [19], so SET will cover that range to allow for comparison with ground based observations as well as take advantage of longer wavelengths blocked by the Earth's atmosphere.

Determination of Apophis' rotation rate, spin state, shape, and general surface structure are all accomplished within **PLD.2**. A broad survey of Apophis before and after encounter allows for searches for tidally induced changes to the asteroid's shape, structure, and orbital dynamics.

Before, during, and after the encounter we want to take a more detailed look at Apophis' surface to watch tidal induced surface changes, like the landslides believed to have occurred on Itokawa [63]. **PLD.3** will accomplish this and is based on the gravel size of Itokawa as determined by the Hayabusa mission, with a resolution limit high enough to be able observe surface gravel movement.

PLD.4 uses imaging with multiple filters to bridge the gap between the lower spatial resolution, spectral data and the high spatial resolution data that does not contain spectral information. This will allow for study of possible seismic resurfacing predicted by [69] and [13], as well as provide color imagery of the asteroid.

The purpose of **PLD.5** is to define the depth resolution relevant to characterizing the internal structure of Apophis by using Radio Reflection Tomography. Radio Reflection Tomography (RRT) will be used to produce a map of Apophis's dielectric interfaces [10], which corresponds to the asteroid's interior structure and will ultimately test the hypothesis that Apophis's interior structure is a rubble-pile. Differences before and after the Earth flyby event can confirm this hypothesis. The depth resolution is set to $20m$ because it is the size of the smallest chunk of rock we are interested in determining, which is defined as the size of the body that is responsible for the Chelyabinsk airburst [78].

The next requirement, **PLD.6**, describes the required spacing along the asteroid's surface between RRT samples while in a polar orbit $500m$ from the asteroid's center. This sampling distance along the surface in a polar orbit is necessary for producing a volumetric image of the asteroid's interior [10]. The sampling information comes from the Nyquist condition, which implies that thethe RRT instrument must take samples every $\lambda/2$ meters along the asteroid's surface in order to avoid aliasing. In the case of our RRT instrument, the distance between samples along the surface of Apophis is required to be $10m$, which satisfies the Nyquist condition for an RRT instrument operating at $20MHz$.

The final payload requirement, **PLD.7**, requires measurements of Apophis' thermal properties. Coupled with spin state and rotation rate data, this thermal data will allow for decoding of the coupling between

Table 3.1: Payload Requirements for the SET Mission

ID	Derived Requirements	Parent	Verification
PLD.1	**Composition:** Measure spectra to $20m$ resolution over a wavelength range of 0.45 to $4\mu m$	SYS.6	Testing
PLD.2	**Broad Imaging Survey:** Take observations with at least $1m/pixel$ resolution over at least $540hrs$ (at least 2 rotations) before and after Earth Flyby event	SYS.4, SYS.5	Testing
PLD.3	**High Resolution Imaging:** Image Apophis's surface at $0.01m/pixel$ resolution before, during, and after Earth Flyby event	SYS.6	Testing
PLD.4	**Color Imaging:** Image Apophis's surface at $0.1m/pixel$ resolution in 4 color and NIR filters before and after Earth Flyby event	SYS.6	Testing
PLD.5	**Internal Structure Resolution:** Measure Apophis's internal structure with a depth resolution of $20m$	SYS.7	Testing
PLD.6	**Internal Structure Coverage:** Take observations in PLD.5 with a maximum sampling distance of $10m$ along the asteroid's surface	SYS.7	Testing
PLD.7	**Yarkovsky Drift:** Measure Apophis's spectrum over the $4-50\mu m$ range to characterize mineral composition and thermal emission	SYS.9	Testing

rotation and thermal cycling which results in Yarkovsky drift.

3.2 Instrument Trade Space

The charts shown below are structured in the form of decision matrices showing on the leftmost columns what instruments have been considered, and on other columns some relevant specifications and information that drove our decision making process. Another important feature of these matrices is the color coding which qualitatively indicates how the corresponding value affects our confidence in that instrument's ability to satisfy subsystem requirements. Where green is improves confidence, yellow is slightly weakens confidence, and red is strongly weakens confidence.

Table 3.2 shows the decision matrix for our imaging instruments, where some of the contenders for our missions imaging instrumentation are labeled, including the four instruments we decided on using which are labeled in bold print. The rest of this chart shows important specifications for each instrument such as resolution and spectral range, as well as some information on the heritage of each instrument and the sub-system requirements that they would be able to satisfy.

In order to meet our subsystem requirements PLD. 2 and 3, which deal with imaging the surface of Apophis to specified resolutions and for some specified amount of time, we looked closely at LORRI (Long-Range Reconnaissance Imager) from New Horizons and OSIRIS (Optical, Spectroscopic, and Infrared Remote Imaging System) from Rosetta because they showed the most potential. OSIRIS in particular had the possibility of in addition satisfying PLD.1 because of its spectral imaging capabilities. However, since OSIRIS has at best a resolution of $18.6\mu rad$ [50] with the narrow angle camera (NAC) it would need to be closer than $\sim 538m$ form Apophis' surface in order to satisfy PLD.3, which requires resolution of $0.01m$ per pixel, thereby making it unfeasible since it would be very challenging to get our spacecraft that close.

Table 3.2: Imaging Instrumentation Decision Matrix

Instruments	Heritage	Resolution (microrad)	Spectral Range (microns)	Pixels	Field of View (deg)	Requirement	Ref
LORRI	New Horizons, Lucy	4.95	NA	Black + White	0.2899	PLD.2, 3	1
OSIRIS	Rosetta	18.6 (NAC) 101 (WAC)	NA	Black + White	2.2 x 2.217 (NAC) 11.34 x 12.09 (WAC)	PLD.2	2
LEISA (Ralph)	New Horizons, Lucy	60.83	.45 - 4	Spectral Image	0.8995 x 0.8995 (LEISA)	PLD.1	3 4
VIRS	OSIRIS-REx	~4000	0.4 - 4.3	Spectral Image	0.2292	PLD.1	5 6
MVIC (Ralph)	New Horizons, Lucy	19.77	NA	4 color + NIR	5.701 x 0.03701 (MVIC)	PLD.2, 4	32
TES	OSIRIS-REx , Lucy	~8000	~5 - 50	Spectral Image	.4584	PLD. 8	7
VIRTIS	Rosetta	250	0.2 - 5	Spectral Image	3.667 x 3.667	Partially PLD.8	8 9

LORRI, on the other hand, though it does not have spectral imaging capabilities has a resolution of $4.95\mu rad$ [22], which means that it would only need to get as close as $\sim 2.02km$ in order to image Apophis at $0.01m$ per pixel. Therefore, LORRI was chosen over OSIRIS because it would provide the necessary resolution at a much longer distance.

In addition, LEISA (Linear Etalon Imaging Spectral Array) from New Horizons and VIRS (Visible and Infrared Spectrometer) from OSIRIS-REx were studied because of their potential in acquiring the necessary spectral imaging data needed to satisfy requirement PLD. 1. The VIRS instrument would allow us to meet part of the PLD.1 requirement that demands measurements over the spectral range of 0.45 to $4\mu m$ [83], which is within the instrument's spectral range of 0.4 to $4.3\mu m$. VIRS would also be able to meet the PLD.1 resolution requirement of $20m/pixel$ since it has a resolution of $\sim 4000\mu rad$ [94], which can be met within a distance of $\sim 5km$ from the surface of Apophis. This resolution requirement from PLD.1 can be even more easily met with the LEISA instrument because it has a resolution of $60.83\mu rad$, which gives $20m$ resolution at $328.79km$ from Apophis. Both LEISA and VIRS have the necessary spectral range needed for PLD.1.

One major benefit of using LEISA is that it is coupled with MVIC, which gives us 4 color plus near infrared images, and therefore minimizing the power and weight that would need to be added in order to gain this needed imaging capability. Another advantage that LEISA has over VIRS is that it has a much larger field of view(FOV), where LEISA has a 0.8995° FOV while VIRS has a 0.2293° FOV. This larger FOV would facilitate imaging because LEISA would be able to cover the entirety of the surface with much faster and with less samples.

Table 3.3: Imaging Instrumentation Decision Matrix

Instrument	**Complexity**	**Internal Structure**	**Sensitive to low seismic activity?**	**Satisfies M.O. 2?**
Laser Vibrometer	One spacecraft	Partial	Yes*	Partially
Seismometer	Requires lander	Potentially local	Yes	Yes
High Frequency Camera	One spacecraft	No	No	No
RTT	Two spacecraft	Global	Yes	Yes
RRT	One spacecraft	Global	Yes	Yes

As previously mentioned, MVIC (Multi-spectral Visible Imaging Camera) was included because of the need to capture 4 color plus near infrared images of Apophis in order to satisfy PLD.4. Along with providing colored and near infrared images, MVIC also has a high resolution of $19.77\mu rad$ [83] which would produce $0.1m$ per pixel images within approximately $5km$ from Apophis. Therefore, MVIC was chosen because it has 4 colored plus NIR filters and resolutions that would easily allow for $0.1m/pixel$ thereby fully satisfying the PLD.4 requirement.

TES (Thermal Emission Spectrometer) and VIRTIS (Visible and Infrared Thermal Imaging Spectrometer) were investigated because of the thermal mapping capabilities that are needed for PLD. 7, which is derived from the need to characterize the Yarkovsky effect. The major, decisive difference between the instruments is that TES has a spectral range that is approximately 5 to $50\mu m$[ref], while VIRTIS has a much smaller range from 0.2 to $5\mu m$[ref]. This difference is crucial because the TES range falls close enough to the desire range indicated by PLD.7 of 4 to $50\mu m$ while VIRTIS falls very short of this range. The other important difference between the two instruments is that VIRTIS has a much better resolution of $250\mu rad$[ref] when compared to the the approximately $8000\mu rad$ resolution of TES [ref], however this difference is not as decisive because at $8000\mu rad$ Apophis can be imaged to $20m/pixel$ from a distance within $2.5km$.

In Table 3.3, we can see the instruments we considered for internal structure measurements of Apophis, where RRT is in bold because it is the one we ultimately chose. The first column shows the name of the instruments and the rest show the factors that were important in deciding whether the particular instrument is a better choice than the others. These factors include ability to get a global mapping of internal structure, the complexity attached with the operation of the instrument, and whether or not it is sensitive enough to small internal displacements. The sensitivity requirement is important for measuring changes in internal structure during the near Earth event, which in addition to capturing the internal structure before and after the event would accomplish M.O. 2.

One of the most promising instruments was the laser vibrometer because some sources showed they could be used to measure seismic activity on the surface of Apophis[71], which could give us information about the internal structure. In addition, the high sensitivity of this instrument when coupled with an accelerometer to remove noise added by spacecraft vibrations, would allow it to detect small internal displacements during the near Earth event. However, after further investigation and consultation with a JPL employee (Ryan Park) it became evident that laser vibrometry would not be able map the internal structure of Apophis because the vibrations it would measure would be topical, and so the information on internal structure would be limited in depth giving us only a surface level mapping. This inability to get a global view of internal structure meant that laser vibrometers would only partially satisfy our M.O. 2.

Seismometers were considered because of their ability to accurately and directly measure seismic activity of Apophis. This ability was very important when some of our subsystem requirements included the need to measure seismic activity explicitly, however after further discussion the team redefined its subsystem requirements so that internal structure was emphasized as the primary target and seismic activity became more of a means to that end. The main disadvantage of seismometers is the need to include a lander in our mission architecture, which would increase mission complexity significantly. Furthermore, in order to gather enough information to map out a global internal structure image, several seismometers need to be planted on the surface of Apophis with a wide distribution over the entire surface. This again adds a large amount of complexity to the mission and even if this can be accomplished there is further risk that the seismometers might be located on a rubble pile, in which case the internal structure information it gathers would be limited to to that local rubble pile. The large amount of complexity attached to it and risk that it might not be able to gather enough internal structure information make seismometers an unappealing option.

The high frequency camera was included in our discussions because it had the potential of measuring seismic activity in the near Earth event by observing surface vibrations[111], which would be useful for tracking any changes in the internal structure of Apophis during the event. This instrument was not meant to be used by itself because it can not provide internal structure mapping, instead it was planned to be used with an internal mapping instrument, either RRT or RTT. However, after deeper investigation into the instrument it became apparent that it would not be able to measure the low seismic activity that is expected during the near Earth event.

RTT (Radio Transmission Tomography) and RRT (Radio Reflective Tomography) were the last set of instruments that were investigated. Both these instruments send impulses of radio signals at space bodies in order to collect information about the internal structure of that body. As such both these instruments would be able to gather information about the internal structure of the entire body of Apophis. Furthermore, by increasing the bandwidth frequency of the radio signals, these instruments could be used to detect small internal displacements at the cost of decreasing the penetration depth of the signal. This would allow detection of changes in internal structure during the near Earth event but only in the uppermost layer of Apophis. Despite the limited depth coverage for small internal displacements, both RRT and RTT can meet mission objective two. The main difference between the two instruments is that RTT would require at least two spacecraft in order to function, whereas RRT only needs one spacecraft. This is because RTT operates by sending a signal through the body and out the other side towards a second spacecraft that receives the signal, while RRT operates by transmitting signals through the body and then receiving the reflected signals with the same spacecraft. This gives RRT a great advantage over RTT because a one spacecraft mission has much lower complexity than a two spacecraft mission.

3.3 Final Instrument Choices

Four instruments have been selected to fulfil the payload requirements and scientific objectives of the mission (Figure 3.3). Ralph (subsection 3.3.1)), a panchromatic, color, and spectral imager. LORRI (subsection 3.3.2), a high resolution spectral imager. The RRT instrument (subsection 3.3.3), which will be used for interior structure measurements. And TES (subsection 3.3.4), the thermal instrument used for decoding the Yarkovsky effect.

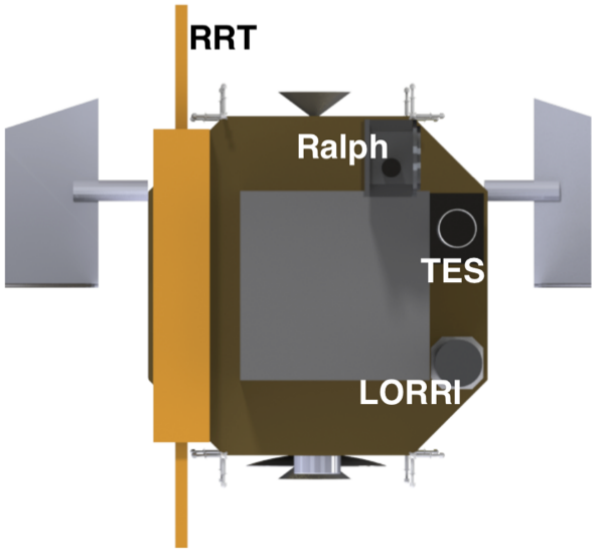

Figure 3.1: CAD Model showing the planned layout for the science instruments on SET (note: the model does not show the full length of the RRT antenna)

3.3.1 Ralph

Ralph is the workhorse of SET's instrument suit. Ralph is based on the Ralph (and L'Ralph) instruments flown on NASA's New Horizons mission and planned for NASA's Lucy mission (a complete, detailed description of New Horizon's Ralph can be found in [83]). Ralph is able to produce panchromatic and color images as well as spatially resolved spectral imaging. It will be used to survey the surface of Apophis to broadly study its shape and surface structure (PLD.3). It will also take imaging used to produce color images as well as broadband absorption maps to monitor Apophis' surface and look for signs of seismic resurfacing (PLD.4). Ralph's spectral capabilities will be used to study Apophis' surface composition (PLD.1). Specifics of imaging capabilities can be found in Table 3.2.

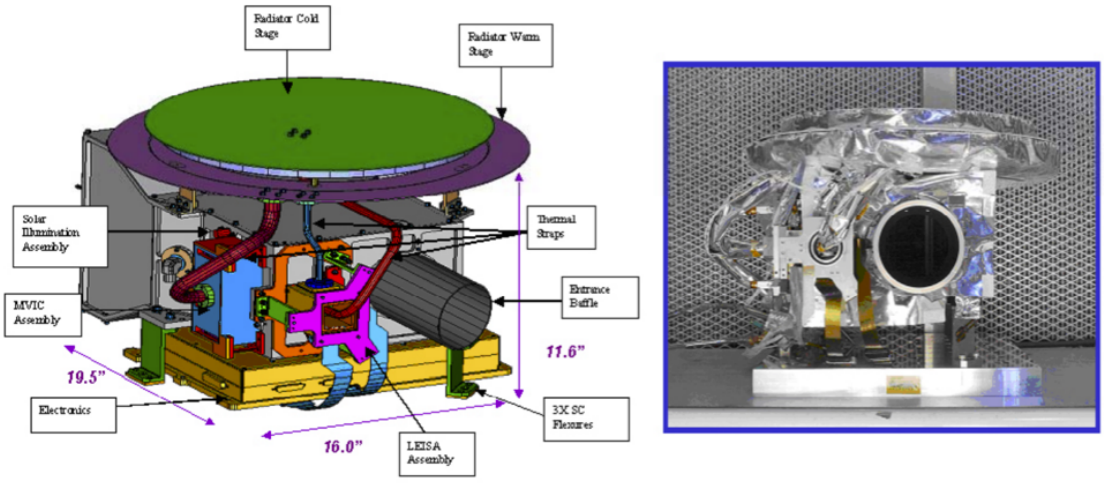

Figure 3.2: (Left) schematic of the Ralph instrument with major structures labeled. (Right) image of the Ralph instrument, looking down the aperture. (credit: Reuter et al. 2008)

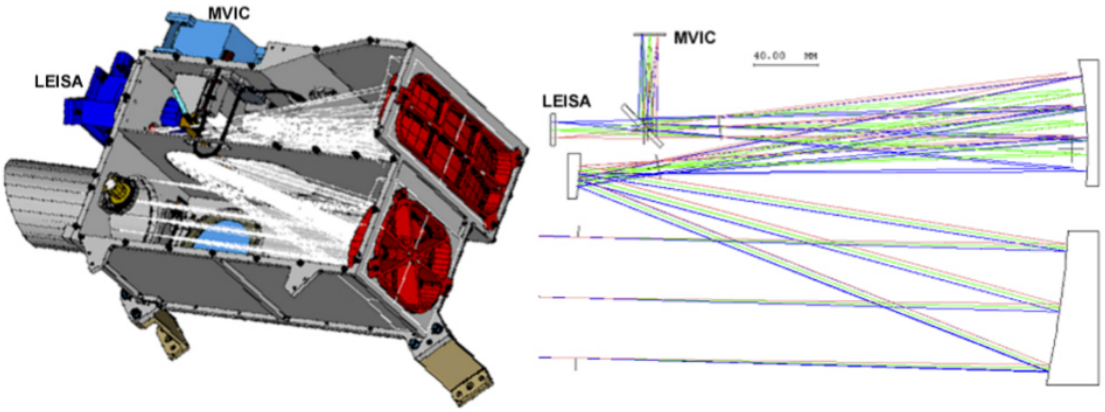

Figure 3.3: (Left) Interior of the Ralph TDA Showing the light path. Note the stainless steel tube loop forming the SIA fiber path. (Right) Raytrace diagram showing the path to the LEISA and MVIC focal planes. (credit: Reuter et al. 2008)

Ralph is comprised of a single telescope with two sets of focal planes. The first is the Multi-spectral Visible Imaging Camera (MVIC), a visible and near-IR imager. The second, Linear Etalon Imaging Spectral Array (LEISA), is a short-wavelength, IR, spectral imager (see Figure 3.2). A diagram of the light patch within the Ralph instrument can be found in Figure 3.3.

MVIC consists of 7 independent CCD arrays on a single substrate that operate in time-delay integration mode (TDI) to produce panchromatic and colored images. Each CCD is 5024×32 pixels (with a field of view of $20 \times 20 \mu rad/pixel$), but by working in TDI mode, the camera is able to produce much broader images than the $32 pixel$ width of the CCDs. For New Horizons' Ralph, 2 CCDs were used for panchromatic imaging, 4 had color filters, and the 7^{th} was a frame transfer CCD. The color filters used were blue ($400 - 550nm$), red ($540 - 700nm$), near IR ($780 - 957nm$), and a narrow band methane filter ($860 - 910nm$) [83]. SET will use different filters better suited for asteroid science, since the data from MVIC will be used to map Apophis' surface in color, distinguish between different possible asteroid classes based on broad band spectroscopy, and we do not expect to see methane (making the $860 - 910nm$ filter not scientifically useful). The exact filter choice is still under consideration.

MVIC is the lead instrument for payload requirements 3 and 4. It will be responsible for broadly surveying Apophis' surface and shape, as well as taking images for color mapping and broadband spectroscopy (Figure 3.4). The data from MVIC will help address questions about Apophis' surface structure and composition, as well as watch for seismic resurfacing or tidal distortion during the close approach to Earth.

LEISA is a wedged filter infra-red spectral imager that creates spatially resolved spectral maps. LEISA is a scanning, imaging instrument, that makes use of a special filter over-which the wavelength varies in one direction. LEISA is scanned across the object in the direction of the filter variation and takes an image at the rate at which the object moves across a single pixel's field of view (Figure 3.5).

For New Horizons, LEISA covered a wavelength range of 1.25 to $2.5 \mu m$ and also included a high-resolution swath from 2.1 to $2.25 \mu m$ [83]. For Lucy, LEISA will not include a high-resolution swath and will cover a broader wavelength range of 1.0 to $3.6 \mu m$ [55]. SET will slightly sacrifice spectral resolution in order to push the wavelength range to 0.45 to $4.0 \mu m$. This wavelength range was selected to provide overlapping coverage with ground-based asteroid spectroscopy (.45 to $2.45 \mu m$) while also taking advantage of the extended wavelength range not available from Earth. This will allow better refinement of Apophis' spectral class as well as search for compositional heterogeneities and any changes in surface composition that may be triggered by Apophis' tidal interaction with the Earth.

Figure 3.4: This map of Pluto was produced by combining images from tree filters and several different observations made by the New Horizons' Ralph/MVIC instrument. Credit: NASA/JHUAPL/SwRI

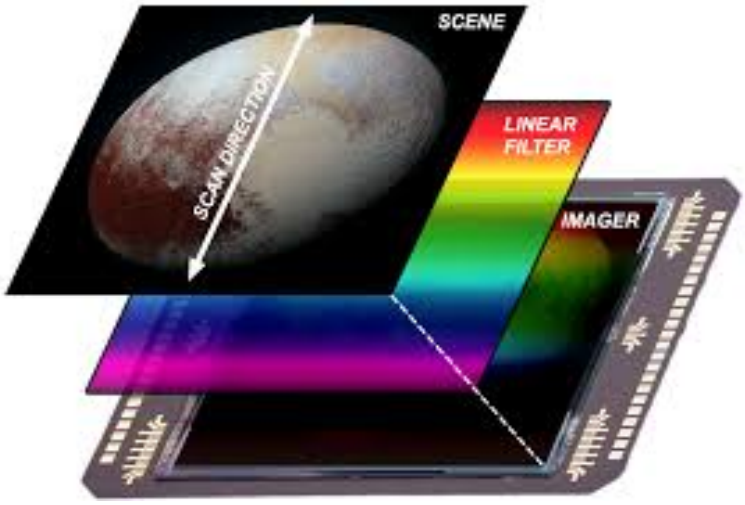

Figure 3.5: Simplified schematic of how the LEISA instrument works. As the scene moves along the scan direction, the imager records a sequence of frames (at the rate the scene moves one pixel width) in order to image each part of the scene through each segment of the linear filter and and build up a spectral map of the entire object. Credit: NASA/JHUAPL/SwRI/Alex Parker

3.3.2 LORRI

The LOng-Range Reconnaissance Imager (LORRI) will be the first instrument to resolve Apophis during the SET's approach to the target and will be responsible for the high-resolution surface imaging of Apophis during the survey phases as well as during Apophis' close approach to the Earth. LORRI is based on the LORRI (and L'LORRI) the high-resolution instruments flown on NASA's New Horizons mission and planned for NASA's Lucy mission (respectively). (A detailed description of the New Horizons' LORRI instrument is provided in [21]).

LORRI is a $20.8cm$ Ritchey-Chrétien telescope with a $1024 \times 1024 pixel$ panchromatic CCD imager (Figure 3.6). Each LORRI pixel has a field of view of $4.95 \mu rad$ (with the instruments' total field of view measuring $0.29° \times 0.29°$). So at as distance of $2km$ from Apophis' surface, it will be able to image Apophis with $0.0099 m/pixel$ resolution.

LORRI is responsible for PLD.3 and will help Ralph/MVIC(pan) with PLD.2 (during the preliminary survey phase). LORRI will survey Apophis' surface at resolution's high enough to detect signs of surface disruption from tidal torques (based on the scale of regolith and suspected landslides observed on the surface a Itokawa [63]. The high resolution imaging provided by LORRI will also be used to better understand Apophis' surface structure which will provide insight into its geologic and dynamic history.

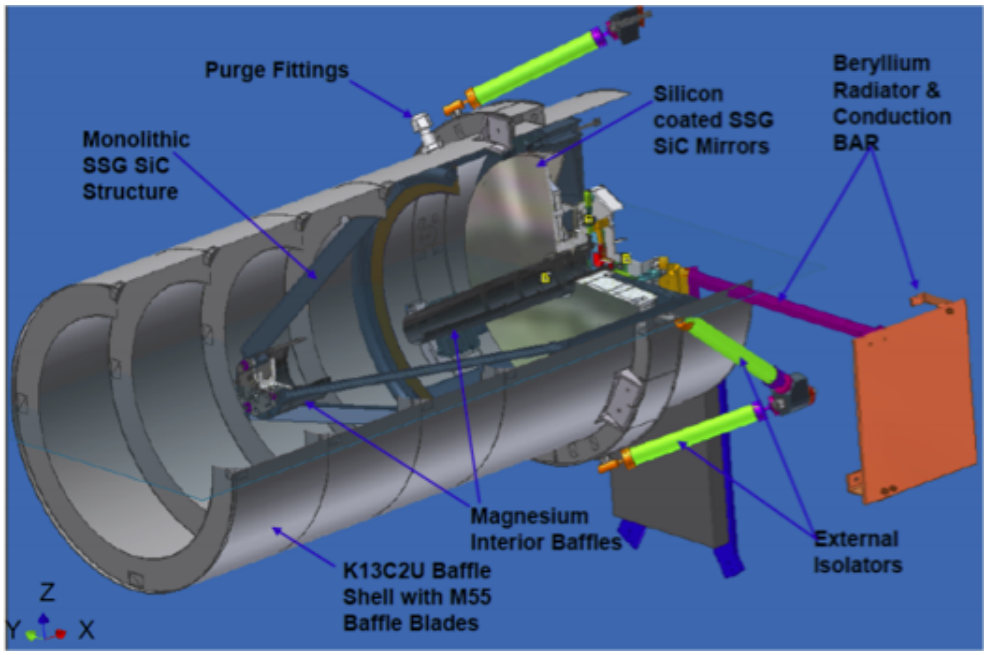

Figure 3.6: Simple schematic of the L'LORRI instrument, with major structures labeled. (Credit: Levison et al. 2016)

In addition to its scientific objectives, LORRI will also play an important role for the protection of the spacecraft. LORRI will be able to resolve Apophis from more than $20,000km$ away, and will be used to observe the asteroid on approach to improve upon ground based measurements of its shape, spin state, and rotation rate, as well as search for any debris or small satellites that could threaten SET.

3.3.3 RRT

The chosen method to satisfy mission requirement SYS.7 and children requirements is Radio Reflection Tomography (RRT). This method measures the differences in dielectric properties of materials in the asteroid by recording the echoes of transmitted low-frequency radio waves, thus providing a way of imaging the internal structure. This method was chosen because unlike seismometry and imaging, it can provide a

reconstruction of the interior based on direct measurements, rather than relying on surface measurements that can be prone to error depending on the cohesion of the asteroid.

The data collected by the RRT instrument are the amplitudes versus time and phases versus time of the radio echoes from the object over the operational bandwidth. This radio echo data are collected in time because our proposed RRT instrument is a pulsed system. The radio echoes are recorded over as many orbits as possible to maximize the number of viewing geometries. Additionally, the radio echoes are not required to be recorded from the same distance for the duration of the recording period. This implies that observations can be made while the spacecraft approaches the target.

The most accurate scheme for inverting the collected data is iterative because the inversion model is non-linear due to the scatterer's (the asteroid's) volumetric properties. Iteration over Apophis's electro-magnetic parameters are done using a gradient search approach driven by minimizing the observed difference between model-predicted radio waves and the actual measured radio data. These iterations yield the dielectric constant distribution inside Apophis, thus revealing the asteroid's internal structure[10].

Similar techniques in space subsurface imaging have been used in the CONSERT instrument on the Rosetta mission as well as the SHARAD instrument on the Mars Reconnaissance Orbiter (MRO) mission. CONSERT used RTT (Radio Transmission Tomography), rather than RRT, in which rather than using one instrument and measuring the echoes, the spacecraft acted as a transmitter and the Philae lander acted as a receiver. Despite the unfavorable landing conditions for the lander, the Rosetta mission successfully characterized the porosity of comet 67P/Churyumov–Gerasimenko, and some conclusions were drawn about the scale of homogeneity of the nucleus as well as the dust to ice ratio[52]. The SHARAD instrument on MRO used a method much more similar to RRT, utilizing a 10 meter dipole antenna transmitting at $20MHz$ with a $10MHz$ bandwidth to image the subsurface structure of the north pole of Mars [82]. The observations provided data of layered deposits up to a few kilometers under the surface. By mapping the time delay and power on the vertical axis, a rough image of the layer interfaces like the one in Figure 3.7 can be constructed. Horizontally, this image spans a distance of a few hundred kilometers, with exaggeration in the vertical axis. This instrument achieved a depth (vertical) resolution between 10 and $15meters$.

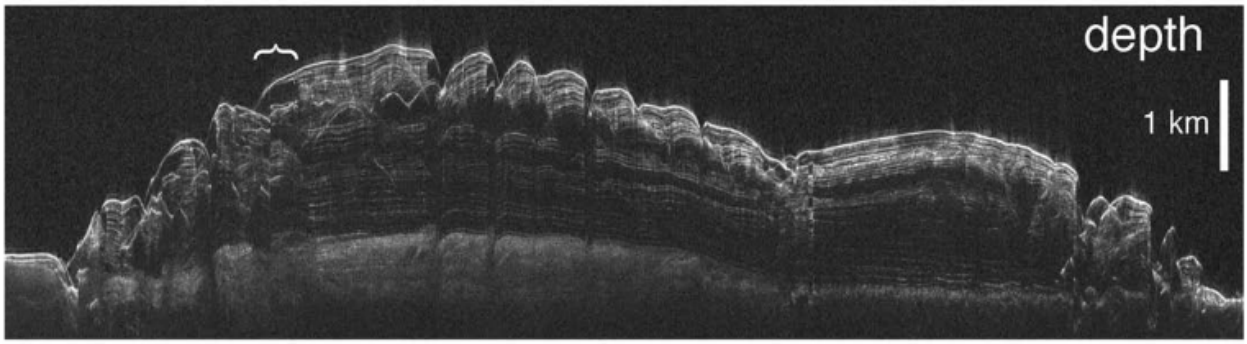

Figure 3.7: SHARAD Sample Layer Interface

Although RRT hasn't specifically been used to image the interior of asteroids, the SHARAD instrument provides promising precedence of how the technique can be used to study subsurface feature. Further, there is literature describing the potential of RRT for imaging asteroids and what the resulting image might look like. In particular, a 2014 paper by Paul Sava et al. provides the results of a simulation of RRT on a model of asteroid 433 Eros[87]. The simulation was carried out with a frequency of $10MHz$, producing the image shown in Figure 3.8 for a slice of the asteroid. (For a better sense of orientation, you can picture the spacecraft orbiting the origin of this image).

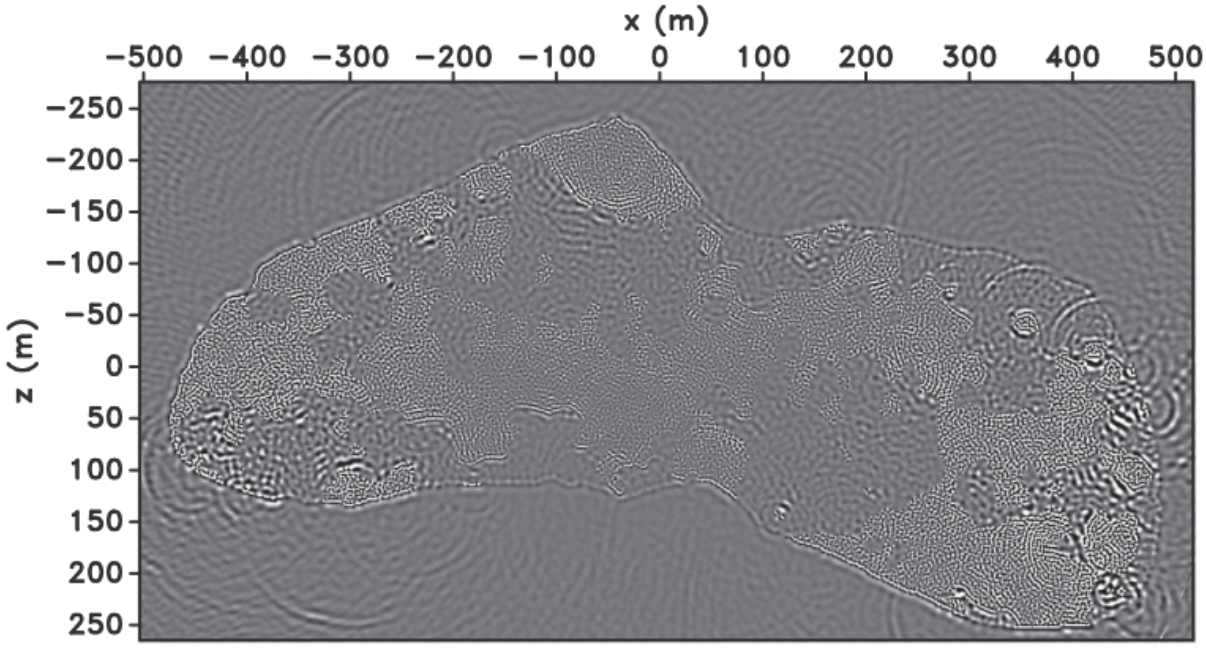

Figure 3.8: RRT Eros Simulation[87]

It is noted in the paper that while this suffers from poor illumination and multi-pathing (propagation of waves through multiple trajectories), it is good enough to give a rough overview of the interior, with room for improvement with more data points. While single-orbiter RRT still produces artifacts in the image, it should provide enough information for the scope of this mission without risking the complexity of multiple orbiters.

Based on the fact that the Eros simulation used a frequency of $10MHz$ to penetrate around 1km of asteroid, as well as the fact that there is heritage instrumentation in SHARAD that used $20MHz$ (meaning a smaller antenna) to penetrate a few kilometers, the proposed transmission frequency for SET's RRT instrument should be around $20MHz$. This sets the resolution perpendicular to transmission (that is, in the "theta" direction about the origin in Figure 3.8) to around $80m$ at an orbital distance of $500m$, which we can make up for with the resolution parallel to transmission (the depth resolution, or the radial direction) given enough samples. The depth resolution depends on the bandwidth based on the formula $r = \frac{c}{2Bn}$, where c is the speed of light, B is the bandwidth, and n is the refractive index[86]. The depth resolution as a function of refractive index is plotted below for a bandwidth of $10MHz$.

Assuming a refractive index similar to Itokawa[45], the resolution comes out to around $8.5m$, and is still under $20m$ in the worst case scenario (a vacuum). This meets PLD. 5 with room for margin, and is smaller than the size of the Chelyabinsk asteroid, which makes it significant from a planetary protection perspective.

PLD. 6 states that the internal structure should be sampled with a spatial resolution of $10m$ along the surface. Since we're concerned with imaging sizes in the $20m$ range for planetary protection purposes, this is in accordance with the Nyquist Theorem in the spatial domain, which states that a sampling distance half the size of the largest item to be resolved is required for accurate imaging. A terminator orbit can ensure full coverage of the surface at this resolution, given that the maximum distance between any two sampled points along the surface is less than or equal to $10m$. 70 orbits at $500m$ from the surface ensures an average separation of around $8m$ on the surface, and the spacecraft can be pointed away in areas of dense coverage to compensate for areas of low coverage. This orbit would take 30 days and the total number of samples is around 50,400, or a sample every 120 seconds. This orbit effectively rotates the equivalent of the slice in Figure 3.8 around the volume of the asteroid, by taking advantage of the asteroid's rotation.

The hardware to be used for RRT is the same instrument used for SHARAD[30], since it was designed to transmit $20MHz$ and is space tested. It consists of a $10m$ dipole antenna that can be folded for launch, and deployed solely with the elastic properties of the encasing tube, as well as an electronics box for signal

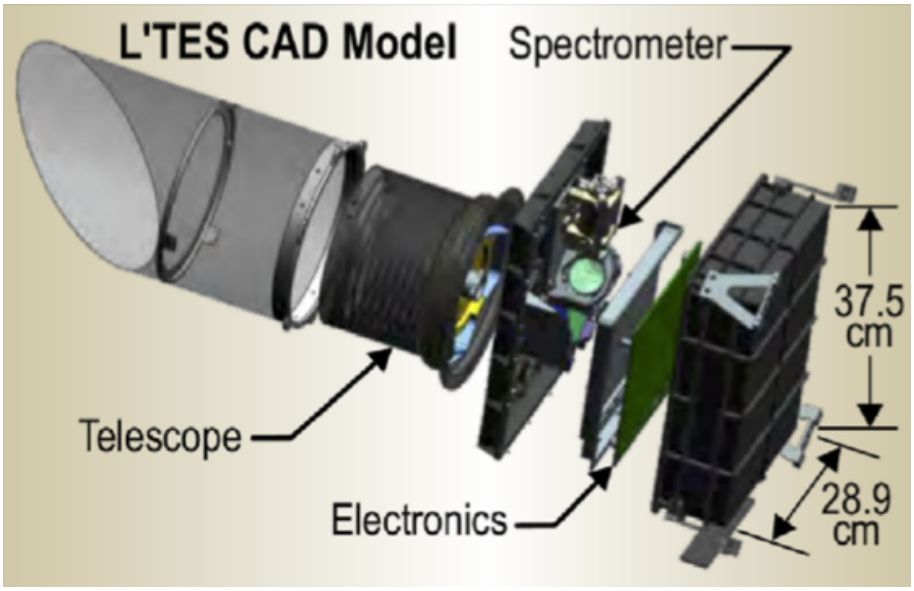

Figure 3.9: Simple L'TES CAD model with major structures labeled (credit: Levison et al. 2016)

generation and power amplification.

3.3.4 TES

The Thermal Emission Spectrometer (TES) will be based on the OTES instrument flying on NASA's OSIRIS-REx mission [26] and the L'TES instrument planned for NASA's Lucy mission [55]. These instruments were developed from the TES instruments on Mars Observer and Mars Global Surveyor [28, 24] the two Mars Exploration Rover Miniature TES instruments [25] and the Mars Odyssey Thermal Emission Imaging System (THEMIS) instrument [27]. TES will consist of a telescope, interferometer assembly, electronics, and support structure (Figure 3.9). TES achieves its spectral range by implementing an interferometer, beam splitter, and moving mirror assembly which can be adjusted to sample different wavelengths along the desired spectral resolution by changing the interference pattern created when the light reflected of the fixed and moving mirror recombine (Figure 3.10).

TES will map mineralogical and thermophysical properties of Apophis with a spectral range of 6 to $100\mu m$. TES uses a single detector with a field of view of $8mrad$, so at a distance of $2km$ it will have a field of view on Apophis' surface of roughly $16 \times 16m$. The data from TES will serve a number of purposes. TES can provide insight into Apophis' mineralogy, globally map the material distribution, and determine regolit physical properties (e.g. grain size and subsurface structure) based on diurnal temperature measurements [26]. Most importantly, the thermal measurements from TES (which satisfy PLD.7), combined with imaging and ground-based radar tracking, will help decode the coupling of thermal cycling and rotation which results in Yarkovsky drift. Improving understanding of Yarkovsky will aid in not only refining future predictions of Apophis' orbit, but also the orbits of other potentially hazardous asteroids.

3.4 Instrumentation Subsystem Risks

The instruments we chose for the mission are low risk because they all record data at a distance, and each of the instruments already has space heritage. Though the instruments are low risk, there still exist risks specific to the instrumentation subsystem. The table on the right identifies and describes the various risks and presents the current mitigation strategy. Figure 3.11 shown below is the risk matrix describing the risk of the identified subsystem risks. The instrumentation subsystem specifics risks are:

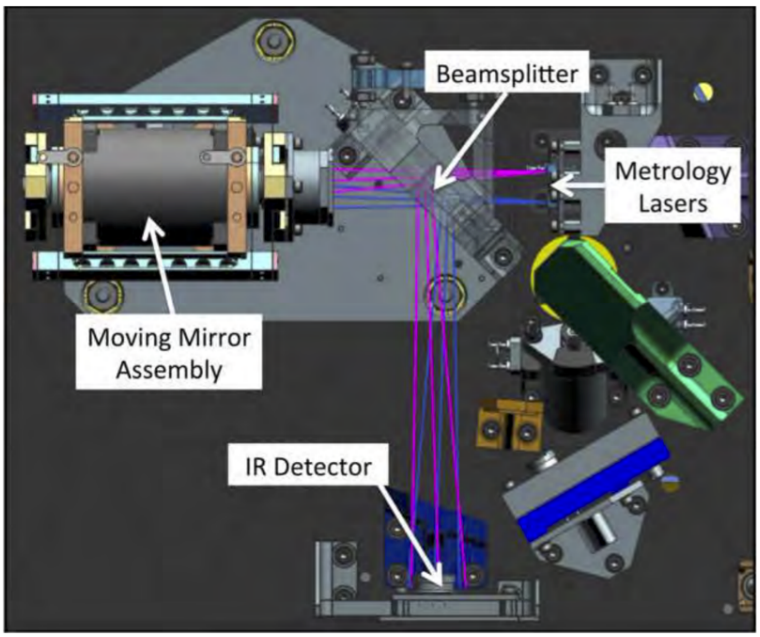

Figure 3.10: The OTES CAD model showing the interferometer layout on the optics plate (credit: Christensen et al. 2017)

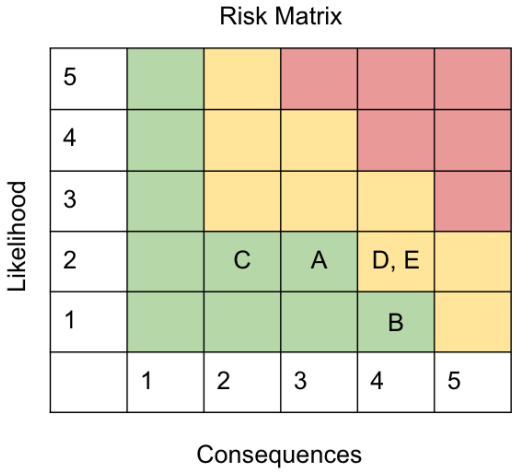

Figure 3.11: Risk Matrix for the Instrumentation Subsystem

- **A:** Debris dislodged from Apophis's surface during the near Earth flyby event poses a risk to the instrumentation subsystem as a whole. For example, material dislodged from the asteroid during the flyby could prevent the spacecraft from conducting its RRT sampling orbit, thus failing to satisfy SYS.7. This debris could also prevent the cameras on the spacecraft from collecting data at the meter/pixel quality outlined by the instrumentation subsystem requirements.

  To mitigate this risk, it is recommended a numerical study of Apophis be conducted where it is assumed that the asteroid has a rubble-pile type interior with the intent of evaluating the legitimacy of the presented risk. If the models show that debris can be dislodged from Apophis's surface during the flyby, then the instrumentation team will consider whether/how the system requirements can be met given this obstacle.

- **B:** Solar interference is a risk for RALPH, LORRI, and TES because it would prevent the instruments from collecting valid data. Instead of recording data relevant to Apophis, the instruments would be collecting data relevant only to the sun.

  This risk is mitigated by coordinating with the LNAC and Bus subsystems to assure that the instruments are consistently pointed in the correct direction. As it currently is, the risk is minor and does not need further consideration.

- **C:** The RRT instrument's antenna unfolding can impart a moment onto the spacecraft. Depending on the magnitude of the moment, the spacecraft's trajectory and/or orbit can be perturbed. This moment could cause the spacecraft to tumble and cause further problems for the other instruments in terms of affecting the instruments' proper orientation for data collection.

  To mitigate this risk, it is recommended that the magnitude of the moment imparted on the spacecraft due to the antenna's unfolding be determined for the SHARAD instrument. If the magnitude of the moment is significant (which would be determined by LNAC), then the concept of minimizing this moment should be one of the major goals of the detailed design of the RRT antenna.

- **D:** The RRT antenna failing to unfold correctly poses a risk to characterizing the interior of Apophis. This would prevent the transmission and receiving of the signals required for conducting tomography.

  This risk can be mitigated by studying how the heritage SHARAD instrument managed to successfully deploy its antenna. Additionally, testing of the antenna's unfolding mechanism will aid in mitigating this risk.

- **E:** The RRT components could burnout at some point during the mission because it is essentially a high power radar. This would prevent the spacecraft from collecting the data relevant to tomography.

  To mitigate this, we have identified an instrument that has already been proven to work in space. Further testing of the instruments would fully mitigate this risk.

3.5 Derived Requirements

Table 3.4 below summarizes the derived requirements relevant to the Communications and Data, and Spacecraft Bus subteams:

Table 3.4: Derived instrumentation requirements for other subsystems. ∗Cost using a data rate of 1160 kbps (based on 100Gb total data with 86400s observing time) with technology readiness level of 7

Instrument	Heritage	Dimensions [cm]	Power Input [W]	Mass [kg]	Data Output [Mbps]	Cost Estimate (thousands of USD)	Thermal Requirement Survival (Deg C)	Thermal Requirement Operational (Deg C)
LORRI	New Horizons	27.7 x 27.7 x 61.5	15	9.8	12	$14,900	-	Electronics: 0 to 40 CCD: -125 to 40 (ideal <70)
Ralph	New Horizons	49.5 x 40.6 x 29.5	8	11	13.2	$12,000	-	Electronics: 0 to 40 Leisa CCD: ideal -140 MVIC CCD: Ideal -98
TES	OSIRIS-Rex	37.5 × 28.9 × 52.2	10.8	6.27	0.0576	$10,100	-25 to 55	w/in spec: 10 to 40 out of spec: -15 to 45
RRT	Mars Reconna-issance Orbiter	Launch: 152.4 x 24.1 x 19 Deployed: 10m Dipole Antenna Electronics 45 x 37 x 19	41	17.1	0.0917	$22,600*	-120 to 120	-100 -100

Chapter 4

Communications and Data

4.1 Overview of Sub-System Requirements

The communications requirements define the required properties of the subsystem necessary to support the communication and data handling functions of the mission. These functions include storage of collected data, downlink of science data, uplink and downlink of telemetry and command-and-control data, and long-term tracking of the spacecraft. All of the communications requirements derive from SYS.3, which requires the spacecraft to communicate with Earth, except for the long-term tracking requirement, which derives from SYS.8. The subsystem requirements are shown in Table 4.1. Additionally, a description and rationale for each requirement is included below.

CD.1 defines a requirement that the downlink of the Post-Flyby Survey data be completed within a certain time frame. Six months was chosen as a reasonable time frame to perform the Post-Flyby Survey and complete downlinking the data. Because the distance between Earth and the spacecraft is rapidly increasing, the maximum data varies over time, so a specific science downlink data rate requirement was deemed inappropriate. This requirement additionally allows trading of downlink time against data rate, and provides flexibility in the design.

CD.2 defines the minimum data rate requirements for the spacecraft throughout the trajectory. This imposes a minimum data rate requirement for transmitting spacecraft telemetry and command-and-control data during normal operations at maximum range. 10 kbps was selected as the minimum data rate for normal operations based on the data rates given in SMAD, Chapter 21.[18]

CD.3 requires the spacecraft to maintain communication with Earth throughout the Earth Flyby. This is necessary to monitor the spacecraft status as Apophis undergoes its disturbances, and allows preliminary science data in real time, as well as return preliminary science data during the Earth Flyby.

CD.4 defines a requirement that the system be capable of transmitting at a minimum data rate even when the spacecraft is unable to fine-point an antenna. The need to transmit without fine pointing control would arise in the case of a reaction wheel failure or the spacecraft being safe-moded. 50 bits/s was selected as the required data rate based on the example safe mode data rates given in SMAD, Chapter 21.[18]

CD.5 defines the required quantity of data storage. The 3 Tbit value for required data storage was produced by calculating the expected quantity of science data collected during the Pre-Flyby Survey, Earth Flyby, and Post-Flyby Survey and adding a margin of over 1 Tbit for engineering and miscellaneous data.

CD.6 requires the communication system to track the spacecraft's position, in support of the long-term tracking mission objective. Spacecraft tracking is performed using the communication system, and to satisfy the mission objectives our system must be trackable Post-Flyby. The Yarkovsky effect is expected to accumulate to about 400 m/year, so the requirement is set to an accuracy of 50 m to allow for 10 significant samples per year.

Table 4.1: Communication and Data Subsystem Requirements

ID	Statement	Parent	Verification
CD.1	Subsystem shall transmit all science data collected during Post-Flyby Survey within 6 months from Earth Flyby.	SYS.3	Analysis: link budget and downlink scheduling
CD.2	Subsystem shall be capable of communicating data between the ground and spacecraft, uplink and downlink, at no less than 10 kbps at any point on trajectory.	SYS.3	Analysis: link budget
CD.3	Subsystem shall be capable of communicating at a rate of at least 50 kbps uplink and downlink throughout the Earth Flyby.	SYS.3	Analysis: link budget
CD.4	Subsystem shall be capable of communicating at a rate of at least 50 bps when in safe mode or if pointing control is lost at any point on the trajectory	SYS.3	Analysis: link budget
CD.5	Subsystem shall be capable of storing up to 3 Tbits of data.	SYS.3	Inspection: data recorder specifications
CD.6	Subsystem shall track spacecraft position to an accuracy of at least 50 m.	SYS.8	Analysis: tracking capability and estimation

4.2 Summary of Subsystem

The communications and data subsystem is responsible for storing and communicating all science and command-and-control data on the spacecraft. This section of the design document includes a data budget, communication system design, link budgets, and data downlink schedule. The data budget details the data volumes produced by each instrument and the command-and-control data being handled. Based on these data volumes, a communication system is presented that is capable of meeting the subsystem requirements with that quantity of data. The communication system design includes spacecraft hardware, ground station selection, and coding scheme. Using the parameters of this communication system, requirements CD.2-CD.4 are validated by performing a link analysis. An analysis of science data downlink is performed to validate CD.6, and a data storage and downlink schedule is presented that validates CD.1 and CD.5. The use of the communication system to track the spacecraft is presented. Finally, an analysis of risks to the communication system is presented.

4.3 Data Budget

The total amount of science data, including packaging, is expected to be about 1725 Gbits total for the Pre-Flyby Survey, Earth Flyby, and Post-Flyby Survey. A month of engineering data, at 20 Gbits/day, brings the total to 2325 Gbits of storage, which validates CD.5 because it is less than the 3 Tbits of storage provided on the spacecraft bus. This was a preliminary worst-case analysis, however the plan is for the spacecraft to downlink the data from each Survey before the following survey begins.

Table 4.2 shows the expected volume of data received from the spacecraft's instrument payload for the Pre-Flyby Survey, Earth Flyby, and Post-Flyby Survey. When available, specifications from heritage instruments were used to quantify the data volumes. Images are taken at a rate of 1 per minute, which yields unique

images. This figure is based on the orbital period of the spacecraft around Apophis and Apophis's rotation rate. A study conducted by CNES, the French Space Agency, estimates that a full RRT characterization of Apophis can be done with 100 Gbits.[8] Table 4.2 shows 200 Gbits for the RRT instrument because Apophis will be fully characterized during the Pre- and Post-Flyby Surveys. A factor of 2 was applied to the raw science data for packaging information, including timestamps, pixel information, orientation information, etc.

In addition to science data, the spacecraft will be collecting and transmitting engineering data, also known as housekeeping data. The worst case storage requirement was estimated to be 20 Gbits/day, based on a 15 Gbits/day example from SMAD involving the Lunar Reconnaissance Orbiter.[36] Section 4.9.2 discusses how much engineering data is transmitted to Earth.

Table 4.2: Data Budget

LORRI	**Pre-Encounter**	**Encounter**	**Post-Encounter**	**TOTAL**
Resolution (pixels)		1052672		
Sensitivity (bits/pixel)		8		
Number of Images	16200	1800	16200	34200
Data Generated (Gbits)	**136**	**15**	**136**	**288**
Ralph LEISA				
Resolution (pixels)		643072		
Sensitivity (bits/pixel)		8		
Number of Images	16200	0	16200	32400
Data Generated (Gbits)	**83**	**0**	**83**	**167**
Ralph MVIC				
Resolution (pixels)		65536		
Sensitivity (bits/pixel)		40		
Number of Images	16200	0	16200	32400
Data Generated (Gbits)	**42**	**0**	**42**	**85**
TES				
Sample Rate (Hz)		100		
Sensitivity (bits/sample)		600		
Number of Images	16200	1800	16200	34200
Data Generated (Gbits)	**58**	**6**	**58**	**123**
RRT Instrument				
Data Generated (Gbits)	**100**	**0**	**100**	**200**
Instrumentation Subtotal with Packaging				
Data Generated (Gbits)	**841**	**43**	**841**	**1725**
Engineering Data				
Data Generated (Gbits/month)	**600**	**600**	**600**	**600**
TOTAL (Gbits)				**2325**
PROVIDED STORAGE (Gbits)				**3000**

4.4 Trades, Downselect, and Rationale

4.4.1 Frequency band Trade

X-band and Ka-band were chosen as the two communication bands for the SET mission. The options considered include S-band, X-band, and Ka-band, three radio bands commonly used for deep space commu-

nication systems. Additionally, laser communication (lasercom) was considered as it is a rapidly developing technology that will have deep space heritage in 2026.

The frequency options were compared based on data rate at 0.15 AU, whether they satisfy requirement CD.1, heritage and ground station availability. An order of magnitude data rate for each radio band at 0.15 AU from Earth was calculated. The Deep Space Optical Communication payload under development at NASA JPL was used as the reference for laser communication.[101] 0.15 AU corresponds to 54 days after Earth Flyby, and was selected as a representative distance for data downlink. Whether or not the data rate for each option satisfies requirement CD.1 was also evaluated. Finally, heritage and ground station availability for each architecture were documented. All three radio bands have extensive heritage and numerous ground stations, while lasercom has no current deep-space heritage and limited current ground station options. An overview of the criteria used in this trade is given in Table 4.3.

Table 4.3: Frequency band Decision Matrix

Decision Matrix	Data Rate at 0.15 AU (mbps)	Comm Time to return 3 Tb (h)	Satisfies CD.1?	Heritage	Groundstation
Lasercom	~300	~3	Yes	None for deep space	JPL OCTL
Ka-Band	~6	~138	Yes	MRO, JWST Iridium, etc.	DSN, Near Earth Network
X-Band	~2	~416	Yes	Hayabusa, MRO, etc.	DSN, Near Earth Network
S-Band	0.8	1041.6	No	Numerous	DSN, Near Earth Network

Laser communication was not selected because radio is sufficient to satisfy the mission requirements and lasercom little heritage compared to radio frequency. Additionally, there are few existing ground stations for lasercom, as compared to the numerous ground station options for the other options. S-band was eliminated because it does not produce sufficient data rates at deep-space distances.

An X-band communication system alone is sufficient to meet CD.1. However, the communication system requires redundancy which can be achieved with a dual X-band and Ka-band system. As detailed in Section 4.5, transponders exist that transmit in both Ka- and X-band, and the only additional hardware required for Ka-band communication are another traveling wave tube amplifier and more switches for the RF network. The additional hardware adds only 4 kg to the system, and is not more expensive. The pointing requirement of Ka-band is less than that of the instruments, so a Ka-band system imposes no additional pointing requirement. Additionally, the higher data rate of Ka-band allows the mission to use a smaller high gain antenna and less DSN time, negating some of the mass penalty of the additional amplifier and increasing downlink schedule flexibility.

4.4.2 Selected Bands and Frequencies

The gain on the DSN 34 m antennas for X-band and Ka-band are based on reference frequencies from the DSN Link Design Handbook, shown in Table 4.4.[96] These are not the frequencies that the final mission will use because exact frequencies are selected closer to the launch date. X-band and Ka-band are defined frequency bands that are partially reserved for deep space communication, but the specific frequencies used by SET will depend on spectrum availability at the time of launch. However, the impact of the difference between the final frequency and the reference frequencies on the design and analysis of the subsystem is negligible.

Table 4.4: Communication and Data Subsystem Requirements

Band, Application	Frequency
X-band Uplink	7.145 GHz
X-band Downlink	8.42 GHz
Ka-band Downlink	32 GHz

4.4.3 Pre-Processing Discussion

The team chose not to pre-process data in the interest of preserving scientific value, particularly because it is unclear what changes will occur during the Earth Flyby. Because most the data will be collected very close to Earth, it is not difficult to transmit all the raw data back to Earth.

4.5 Spacecraft Hardware Design

4.5.1 Spacecraft Hardware Overview

Figure 4.1 shows the high level block diagram for the communication subsystem. The subsystem was designed based on the Mars Reconnaissance Orbiter and Juno missions, both of which used X-band and Ka-band.[65, 108] The 3D blocks indicate redundancy. A combined X- and Ka-band transponder will encode information received from the spacecraft bus and will send the signal to the traveling wave tube amplifier (TWTA) for the appropriate band. From there, the signal will go through a switching network to the appropriate antenna. Ka-band is for transmission only, so no diplexer is required to separate transmitted and received signals. Only one low gain antenna will be used at a time, but collectively the beam pattern of the three cover most of the space around the spacecraft, as shown in Figure 4.2. The Communication Subsystem Master Equipment List (MEL) is shown in Table 4.5, and includes mass and power budgets.

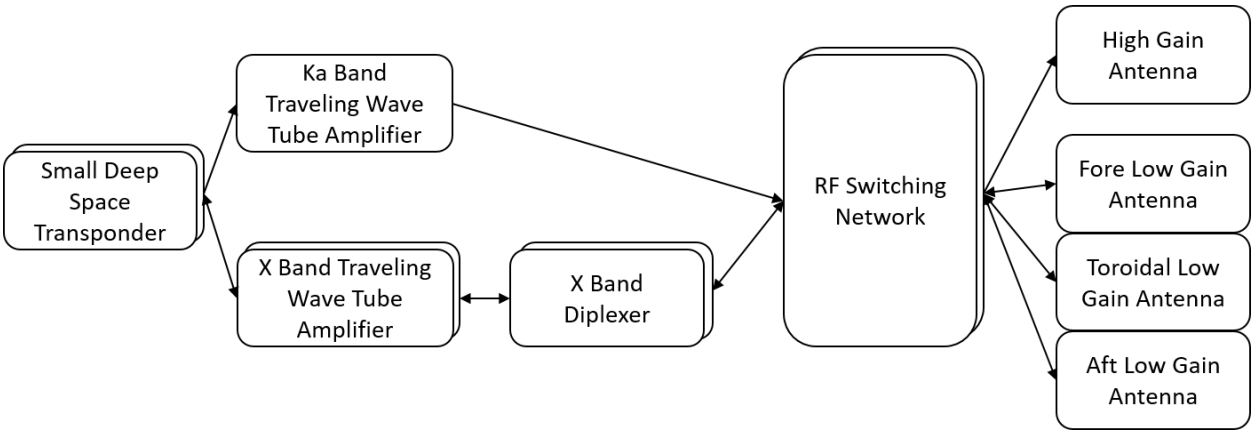

Figure 4.1: High level communication subsystem block diagram.

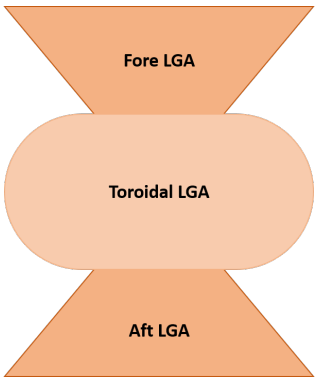

Figure 4.2: The beam pattern of the low gain antenna subsystem.

Table 4.5: Communication Subsystem Master Equipment List.

Part	Description	Power (W)	Qty	Unit Mass (kg)	Total Mass (kg)
SDST	Transponder, Ka and X	19.5	2	3.2	6.4
Ultrastable Oscillator	Spacecraft Clock	5	2	1.75	3.5
Diplexer	Splits transmitted and received X-Band signals	0	2	0.4	0.8
X TWTA	100 w X Band Power Amplifier	172	2	0.85	1.7
KA TWTA	34 w Ka Band Power Amplifier	81	1	0.8	0.8
X Power Converter		0	2	1.5	3
Ka Power Converter		0	1	1.5	1.5
Misc Microwave		0	1	1	1
Waveguides and Coax		0	1	8.3	8.3
Switches		0	5	0.44	2.2
TLGA	Toroidal Low Gain Antenna	0	1	1.9	1.9
LGA	Horn Low Gain Antenna	0	2	0.5	1
HGA	0.75 m Parabolic Dish	0	1	4	4
	Total: X-Band	196.5		Total	36.1
	Total: Ka-Band	105.5			

4.5.2 Data Storage

The LeoStar-3 bus can be equipped with 3 Tbits of storage, which will accommodate the science data, engineering data, and margin in case of missed downlinks.[74] Section 4.9 discusses the data volume expected over the course of the mission.

4.5.3 Redundancy

Full redundancy in the transmission and receiving system is ensured by having two available bands. The X-band system is fully redundant on its own, however the Ka-band system is not. The X-band system will be used for the long-term tracking of the spacecraft, so is required to survive for the entirety of the mission. The Ka-band system is used to return science data from the Pre-Flyby Survey, Earth Flyby, and Post-Flyby Survey, but is not required to survive as long as the X-band system. In addition, the X-band system can meet the mission requirements alone, while the Ka-band system cannot because it is only a transmitter, not a receiver.

The data storage system is not redundant, but includes margin. This is discussed in more depth in Section 4.9.

4.6 Ground Stations

As a part of the communication system design, ground stations for the spacecraft were selected. The NASA Deep Space Network (DSN) 34 m antennas were selected for use while the spacecraft is in deep space. A combination of the NASA Near Earth Network (NEN) and the ESA ESTrack network was selected for communication during the Earth Flyby,

Ground stations for use during the Earth Flyby were considered separately from the ground station used during the deep-space section of the mission. The distance between Earth and the spacecraft varies by orders of magnitude between those two mission phases. Additionally, during the Earth Flyby SET will be taking observations and will be unable to point its high gain antenna. As a result, it will be necessary to use different ground stations during these two mission phases.

Key performance metrics of ground stations include the gain of the antenna, geographic distribution of the stations, and whether the station is capable of transmitting and receiving in the communication bands that the spacecraft is using. Ground stations were selected that were capable of supporting communication with the spacecraft at the data rates and times dictated by the subsystem requirements.

4.6.1 Deep Space

The DSN 34 m dishes will be used to communicate with SET while the spacecraft is in deep space. Before and after the Earth Flyby the distance between the spacecraft and Earth will vary from 0 AU to 2.32 AU. To sustain a reasonable data rate at these distances, an antenna with tens of dB gain and millidegree pointing control is necessary. The DSN is used to support all NASA deep space spacecraft and is a natural choice to support this need.

The DSN is capable of supporting both uplink and downlink in X-band, and downlink in Ka-band.[96] It will be used for two way X-band communication during cruise and normal operations, and science data downlink with Ka-band after surveys of the asteroid.

Each DSN station is has several 34 m and one 72 m dish.[96] For SET, the 34 m Beam Waveguide dishes were selected. The 72 m dish is not necessary to close the link, and is more expensive. There are two types of 34 m dishes: Beam Waveguide dishes, and High Efficiency dishes. The BWG are more modern and there are at least two at each location, while there is only one HEF dish at each ground station location. Consequently, the 34 m BWG dish was selected as the deep space communication ground station. An image of a 34 m dish is shown in figure 4.3.[105]

There are three DSN locations: Goldstone, California; Madrid, Spain; and Melbourne, Australia. Combined, these stations provide global coverage and the ability to communicate with the spacecraft regardless of its direction from Earth.

Table 4.6 lists the relevant specifications of the DSN 34 m dish. These parameters will be used in the link analysis to validate the subsystem requirements.[96]

Figure 4.3: Image of 34 Meter DSN dish in Goldstone, CA.

Table 4.6: DSN 34 Meter BWG Antenna Parameters

Parameter	**Value**
X-Band Receive Frequency	8.20-8.60 GHz
Ka-Band Receive Frequency	31.80–32.30 GHz
X-Band Transmit Frequency	7.145-7.235 GHz
Dish Diameter	34 m
Transmit Power	17.4 kW
X-Band Receive Gain	68.30 dBi at 8.42 GHz
Ka-Band Receive Gain	79.18 dBi at 32 GHz
X-Band Transmit Gain	67.09 dBi at 7.145 GHz
X-Band System Noise Temperature	25 K
Ka-Band System Noise Temperature	36
Locations	Goldstone, California; Madrid, Spain; Canberra, Australia

DSN Cost Calculation

A significant consideration for ground station is the cost of using the ground station. For our mission, the DSN 34 m dish will cost approximately $1691.2. This estimate is based on the DSN costing in 2015, and will change by the time that SET launches.

The DSN fee/hour is calculated as:

$$Fee/Hour = \$1057 \cdot A_w \cdot (0.9 + 0.1 \cdot \frac{\#Passes}{Week}) \tag{4.1}$$

where A_w is a weighting for the aperture being used.

A_w equals 1 for the 34 m BWG array. Currently, the spacecraft is planned to use 1 pass per day for a rate of 7 passes/week. With these parameters, the hourly fee for the DSN is calculated as $1691.2.

4.6.2 Near Earth

A combination of the NASA Near Earth Network (NEN) and the ESA ESTRACK network will be used for two-way communication with SET through the Earth Flyby. These two networks include 4 antennas capable of both transmitting and receiving X-band, and ten additional antennas capable of receiving X-band. The networks include ground stations owned by NASA, ESA, and private industry.[33, 68]

These two networks will be used during the Earth Flyby because they provide global coverage of X-band ground stations capable of supporting near Earth missions. The dishes vary in size, but all are smaller than the DSN and consequently have lower gain. However, the gain of these dishes is still sufficient to achieve the data rates required by CD.3 for during the Earth flyby. A map showing the X-band capable ground stations for both the NEN and ESTRACK is included in Figure 4.4.

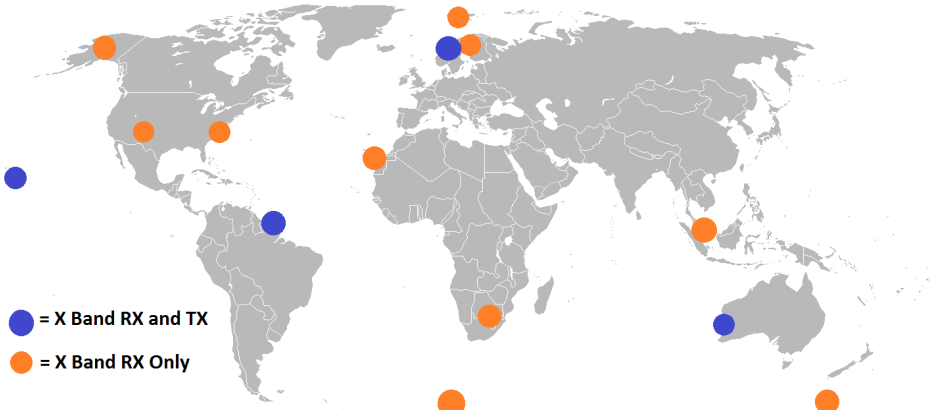

Figure 4.4: Map of NEN and ESTrack X-band Ground Stations

Because the two networks consist of a range of different ground stations, the properties of the antennas vary between sites. The 11 m dish at the Wallops Island station of the NEN was used as a reference ground station for this study. Table 4.7 lists the relevant specifications of the Wallops Island 11 m dish, which is representative of the X-band antennas at the various locations.

Table 4.7: Wallops Island 11 Meter Dish Specifications

Parameter	**Value**
X-Band Receive Frequency	8.00-8.50 GHz
Dish Diameter	11 meters
Gain	56.8 dBi

4.7 Coding

The information transmitted on a radio wave can be encoded with different coding schemes that have different properties. SET will use rate 1/2 convolutional coding when within 0.3 AU of Earth, and will use turbo coding when farther than 0.3 AU. The DSN has different maximum decoding data rates for the two codes, and the two codes have different required bit energy to noise ratios. As a result, a higher data rate

is achievable with turbo coding while in deep space, and a higher data rate is possible with convolutional coding when near Earth.

Turbo coding is a scheme commonly used for deep space missions. It has low spectral efficiency compared to other options, but requires a lower bit error to noise ratio. As a result, it works well for deep space missions that have large path losses.[95] Convolutional has better spectral efficiency than turbo coding, but requires a higher bit energy to noise ratio. As a result, convolutional coding is commonly used for communication satellites and Earth orbiting missions which have more competition for spectrum but lower path losses.[95] The maximum data DSN decoding rate for turbo coding is 1.6 Mbps, and the maximum DSN decoding rate for convolutional coding is 6.6 Mbps.[96] The parameters of the two coding schemes are summarized in Table 4.8.

Table 4.8: Coding Scheme Specifications

Parameter	**Value, Turbo Coding**	**Value, Convolutional Coding**
Required Bit Energy/Noise	1 dB	5.5 dB
DSN Maximum Decoding Rate	1.6 Mbps	0.6 Mbps

4.8 Link Budgets

The sections of this chapter so far have described the expected data produced by the mission and the design of the communication system. Using the parameters of the communication system, required data rates, and operational scenarios, link budgets were produced validate subsystem requirements CD.2, CD.3, and CD.4. The link budgets show that the communication system designed is capable of closing the link at the required data rates in the operational scenarios of these three requirements.

These link budgets do not describe science data downlink or requirement CD.1. Science data downlink is instead covered in Section 4.9.

4.8.1 Link Budget Methodology

A link budget is a set of calculations that characterizes a radio link between a transmitter and receiver. The budget uses the data rate and the parameters of the transmitter, receiver, and free space channel to calculate a link margin. The link margin is a single number that describes the strength of the link: if the link margin is positive, the link between the transmitter and receiver is said to close and the inputted data rate can be sustained. Standard practice is to keep at least 3 dB of link margin.[18, 95]

The link budget is comprised of several steps that model the signal as it moves from the transmitter through free space channel to the receiver, and calculates the power received. From the power received, the link margin is calculated using the data rate and system noise, and the required bit energy to noise ratio of the coding scheme being used. The values involved span orders of magnitude, so standard practice is to use all values in decibels to enable easy manipulation. Equations for each of these steps are given below.

The strength of the transmitted signal is described by the equivalent isotropic radiated power, or EIRP, which is the power that the transmitter would emit if it radiated evenly in all directions, rather than a narrow beam. The EIRP is calculated as

$$EIRP = P_{TX} + G_{TX} - L_{TX} \tag{4.2}$$

where P_{TX} is the power of the transmitter in dBm, G_{TX} is the gain of the transmit antenna in dB, and L_{TX} is the line loss and other losses in dB of the transmitter.

The transmitted signal loses strength as it propagates from the receiver to the transmitter. The losses of the free space channel can be calculated as

$$L_{FS} = L_{path} - L_{atm} - L_{pointing} \tag{4.3}$$

where L_{path} is the path loss caused by the signal spreading as it propagates, L_{atm} is the loss caused by atmospheric interference, and $L_{pointing}$ is the loss caused by pointing errors in the transmitter or receiver.

The power collected by the receiver is calculated as

$$P_{RX} = EIRP - L_{propagation} + G_{RX} - L_{RX} \tag{4.4}$$

where G_{RX} is the gain of the receiving antenna in dBi, L_{RX} are losses in the receiving electronics in dB. From the received power, the link margin can be calculated as

$$LinkMargin = P_{RX} - T - R_b - (E_b/N_0)_{required} \tag{4.5}$$

where T is the receiver system noise temperature in dBK, R_b is the data rate of the transmission in dBbps, and $(E_b/N_0)_{required}$ is the required bit energy to noise ratio in dB, which is determined by the coding scheme being used.

The following budgets use the methodology described here, combined with the system parameters detailed in earlier sections and relevant details of the operational scenario. In each budget the link margin is shown to be positive, validating the relevant requirement.

4.8.2 X-band High Gain Downlink, Maximum Distance

This budget shows that the link closes at 10 kbps at maximum Earth-SET distance when transmitting with X-band and the high gain antenna (HGA). The link margin is substantially higher when transmitting on Ka-band. For smaller Earth-SET distances path loss is lower, so the link margin will be greater than or equal to 10.26 dB for the entire mission duration. Therefore, this link budgets shows that the spacecraft will be able to sustain the data rate necessary for normal operations for every point on the trajectory.

Table 4.9: Link Budget, Deep Space X-band HGA Downlink

Parameter	Units	Value	Notes
Downlink Frequency	GHz	8.42	X-Band Reference Frequency
Data Rate	kbps	10	Requirement CD.2
Satellite Antenna Gain	dBi	34.20	0.75 m parabolic antenna
Tx Power	W	100	100 Watt TWTA
EIRP	dBm	82.20	Sum of Tx Power, Antenna Gain, Line Loss
Path Length	AU	2.32	Maximum Earth-SET Distance
Net Propagation Loss	dB	-282.86	Propagation loss, 3 dB pointing loss, 1 dB atmospheric loss
Ground Station Antenna Gain	dBi	68.30	DSN 34 meter dish
Received Carrier Power	dBm	-133.36	Sum of gains and losses
Link Margin	dB	**10.26**	Turbo Coding, system noise density of -184.62 dBm/hz

4.8.3 X-band High Gain Uplink, Maximum Distance

This budget shows that the link closes at maximum Earth-SET distance when uplinking at 10 kpbs with the DSN 34 m dish and receiving with the HGA on the spacecraft. As for the previous link budget, the link margin will be equal to or greater than 30.66 dB throughout the trajectory, so this link budget validates the uplink portion of requirement CD.2.

Table 4.10: Link Budget, Deep Space X-band HGA Uplink

Parameter	Units	Value	Source
Uplink Frequency	GHz	7.145	Reference X-Band Uplink frequency
Data Rate	kbps	10	Requirement CD.2
Ground Station Antenna Gain	dBi	67.09	DSN 34 m Tx gain
Tx Power	kW	17.4	DSN 34 m max Tx power
EIRP	dBm	138.50	Sum of Tx Power, Antenna Gain, Line Loss
Path Length	AU	2.32	Maximum Earth-SET Distance
Net Propagation Loss	dB	-281.43	Propagation loss, 3 dB pointing loss, 1 dB atmospheric loss
Satellite Antenna Gain	dBi	32.77	0.75 m parabolic antenna
Received Carrier Power	dBm	-112.17	Sum of gains and losses
Link Margin	dB	**30.66**	Turbo Coding, system noise density of -183.81 dBm/hz

4.8.4 X-band Low Gain Downlink, During Earth Flyby

This budget is for the spacecraft-Earth link during the Earth Flyby, when the spacecraft will be observing the asteroid and will be unable to point the HGA. The budget shows that the link closes at lunar distance when transmitting at 10 kbps with coding with the toroidal low gain antenna (TLGA), and receiving with the Wallops Island 11 m dish. Additionally, 3dB of pointing loss is included, corresponding to a 10 degree off-point. During the Earth Flyby we will be at or within lunar distance, so the link margin will be greater than or equal to 10.77 dB. This budget shows that the subsystem will be capable of closing the link at greater than 50 kbps through the Earth Flyby, verifying requirement CD.3.

Table 4.11: Link Budget, During Earth Flyby X-band TLGA Downlink

Parameter	Units	Value	Notes
Downlink Frequency	GHz	8.42	X-Band Reference Frequency
Data Rate	kbps	50	Requirement CD.2
Satellite Antenna Gain	dBi	.6.5	Juno Heritage Toroidal Low Gain Antenna
Tx Power	W	100	100 Watt TWTA
EIRP	dBm	54.50	Sum of Tx Power, Antenna Gain, Line Loss
Path Length	km	406700	Lunar Distance
Net Propagation Loss	dB	-227.13	Propagation loss, 3 dB pointing loss, 1 dB atmospheric loss
Ground Station Antenna Gain	dBi	56.80	Wallops 13m, NEN representative
Received Carrier Power	dBm	-116.83	Sum of gains and losses
Link Margin	dB	**10.77**	Convolutional Coding, system noise density of -175.59 dBm/hz

4.8.5 X-band Low Gain Downlink, Maximum Distance

The budget is for communication with the spacecraft at maximum distance using the low gain antenna (LGA). The budget shows that the link closes when transmitting with the TLGA, with 10 degrees of pointing error, at the most distant point on the trajectory and receiving with the DSN 34 m dish. This scenario would arise if the spacecraft is safe-moded, or if a reaction wheel fails and pointing control is lost, and is unable to point the HGA. This budget validates requirement CD.4 and shows that communication with the spacecraft is possible even when pointing control is lost, at any point in the mission.

Table 4.12: Link Budget, Maximum Distance X-band TLGA Downlink

Parameter	Units	Value	Source
Downlink Frequency	GHz	8.42	X-Band Reference Frequency
Data Rate	bps	50	Requirement CD.4
Satellite Antenna Gain	dBi	6.50	Juno heritage toroidal low gain antenna
Tx Power	W	100	100 Watt TWTA
EIRP	dBm	54.50	Sum of Tx Power, Antenna Gain, Line Loss
Path Length	AU	2.32	Maximum Earth-SET Distance
Net Propagation Loss	dB	-285.76	Propagation loss, 3 dB pointing loss, 1 dB atmospheric loss
Ground Station Antenna Gain	dBi	68.30	DSN 34 meter dish
Received Carrier Power	dBm	-163.96	Sum of gains and losses
Link Margin	dB	**2.67**	Turbo Coding, system noise density of -184.6 dBm/hz

4.9 Downlink Planning

4.9.1 Downlink Data Rate

Because the distance between SET and Apophis varies between 0 AU and 2.3 AU over the course of the mission, a traditional link budget was deemed as insufficient to analyze the science data downlink. Instead, the high gain data rates for X- and Ka-band with 3 dB of link margin were calculated for every day through the course of the mission.

The data rate with 3 dB of link margin throughout the course of the mission is shown in Figure 4.5. The maximum data rate is limited by the DSN's capability to decode the received signal. As described in Section 4.7, the maximum data rate is 1.6 Mbps for turbocoding and 6.6 Mbps for convolutional coding. SET switches between the two when it is close to Earth. This property of the communication system accounts for the flat portions and kinks present in the data rate plot.

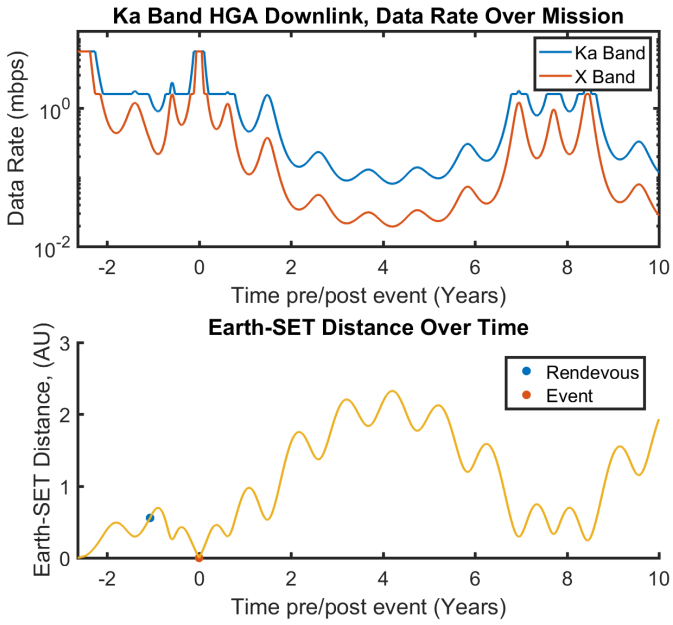

Figure 4.5: The high gain downlink rate throughout the mission, for X- and Ka-Band

This data rate was used in combination with the rates of data collection and downlink scheduling to show that the spacecraft can downlink all science data collected in a reasonable time. This analysis is presented in the following sections.

4.9.2 Downlink Schedule

Measurements from the Coarse Survey of Apophis will be transmitted back to Earth as soon as available. This will allow the team to more accurately predict what events are expected to take place during the Earth Flyby, and adjust the data acquisition strategy as necessary. The Pre-Flyby Survey data will also be transmitted back to Earth as soon as it is complete. Between the Pre-Flyby Survey and the Earth Flyby, the spacecraft will make monthly downlinks with any additional science data collected. The team will be able to communicate with the spacecraft during Earth Flyby using the LGAs, but the science mission dominates the spacecraft pointing and prevents using the HGA. The data from the Earth Flyby will be transmitted back immediately for publicity. The spacecraft's proximity to Earth allows this to be completed in a matter of days, after which the Post-Flyby Survey can begin.

A worst-case data volume simulation shows that CD.1 can be met using Ka-band if the spacecraft collects no more than 13 Gbits/day of engineering data for transmission back to Earth. The peak volume of data

for transmission to Earth is 2 Tbits, leaving a 1 Tbit margin for engineering data being temporarily stored but not transmitted, missed downlinks, and other unexpected data. The same analysis for X-band yeilds a maximum of 1.5 Gbits/day of engineering data for transmission, and a margin of 2 Tbits.

The simulation assumed the spacecraft would collect 1 Gbit/day of miscellaneous data starting a month after the Pre-Flyby Survey until 2 days before the Earth Flyby, and again starting a month after the Post-Flyby Survey. The schedule is based on monthly downlinks for 6 hours a day, for as many days as is necessary to downlink all stored data. The simulation is worst-case because it assumes that there are no downlinks during any of the Surveys. Only the time from the start of the Pre-Flyby Survey through a year after the Earth Flyby were simulated because this is the most data-intensive portion of the mission. The results of the simulation are displayed graphically in Figure 4.6, plotted below a graph of the spacecraft's distance from Earth. The red lines indicate the 3 Tbit storage limit.

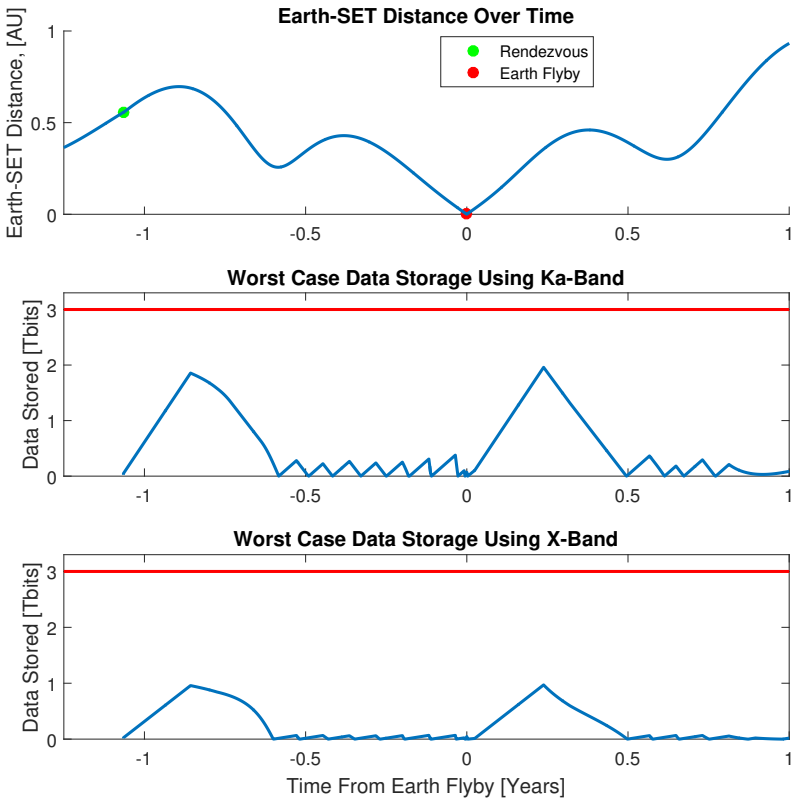

Figure 4.6: The amount of data stored on the spacecraft for worst case Ka- and X-band scenarios.

4.10 Tracking

The spacecraft will use the instrument payload and optical navigation techniques to determine the relative position of Apophis. The spacecraft's position will be determined using Delta Differential One-way Ranging (ΔDOR) for angular position, Sequential Ranging for line-of-sight range, and Doppler ranging for line-of-sight velocity. All these techniques will use the spacecraft's X-band communication system. These techniques, when combined with multiple observations and an orbit-estimation algorithm, will satisfy CD.6.

ΔDOR is a technique that uses two ground stations and a reference source with a well-known position (usually a quasar) to determine a spacecraft's angle from Earth. A nominal system using ΔDOR has a root-sum-square random error of less than 2.25 nrad, which corresponds to a maximum cross-position error

of 707 m at 2.1 AU. For trajectory estimation purposes, systematic errors can be eliminated by the model. The DSN Telecommunications Link Design Handbook, Module 210, discusses ΔDOR in depth.

Sequential ranging is a technique that uses period signals and Doppler shift to determine a spacecraft's line-of-sight range. The range error is on the order of 10 m and depends on the specifications of the clock on the spacecraft. The DSN Telecommunications Link Design Handbook, Module 203, discusses Sequential ranging in depth.

Doppler shift for determining line-of-sight velocity is simply a measurement of the Doppler phase shift of signals sent from the spacecraft, and has a 1-sigma accuracy of 0.05 mm/s over a 60 s integration time. The DSN Services Catalog discusses Doppler ranging briefly in section 3.3.1.3.

4.11 Subsystem Risks

The communication and data system designed for SET is comparable to previous deep space missions, and as a result there are no risks unique to the mission. Several risks that the communication system faces are presented below. Tables 4.11 and 4.13 show these risks on a standard heat-map.

1. **Missed downlink windows -** Lack of DSN availability, weather attenuation on Ka-band, or other factors could cause SET to miss science downlink windows. This would lead to additional data stored on the spacecraft. This risk is mitigated by having enough data storage margin to accommodate a delay in downlinking data, and by having the flexibility to downlink at any point on the mission trajectory

2. **More data collected than planned -** Changes to the observation plan could result in additional measurements and the collection of more data than expected. To mitigate this risk data storage margin is included so that no additional data will be lost.

3. **Communication hardware failure -** The failure of a transponder, traveling wave tube amplifier, or switch could affect the operation of the communication system. This is mitigated by full redundancy in X-band communication hardware, and the ability to satisfy the subsystem requirements if the Ka-band system fails.

4. **Loss of ability to point HGA -** Safe-moding of the spacecraft or failure of a reaction wheel could prevent the spacecraft from pointing its high gain antenna to communicate. This risk is mitigated by the ability to communicate using the low gain antennas so that communication with the spacecraft can be maintained even if pointing control is lost.

Table 4.13: Communication and Data Risk Chart Descriptions

ID	**Description**	**Mitigation**
A	Missed downlink windows	Data storage margin, downlink scheduling flexibility
B	More data collected than planned	Data storage margin
C	Communication system hardware failure	Fully redundant hardware
D	Loss of ability to point high gain antenna	Low gain antennas X-band antennas as backup

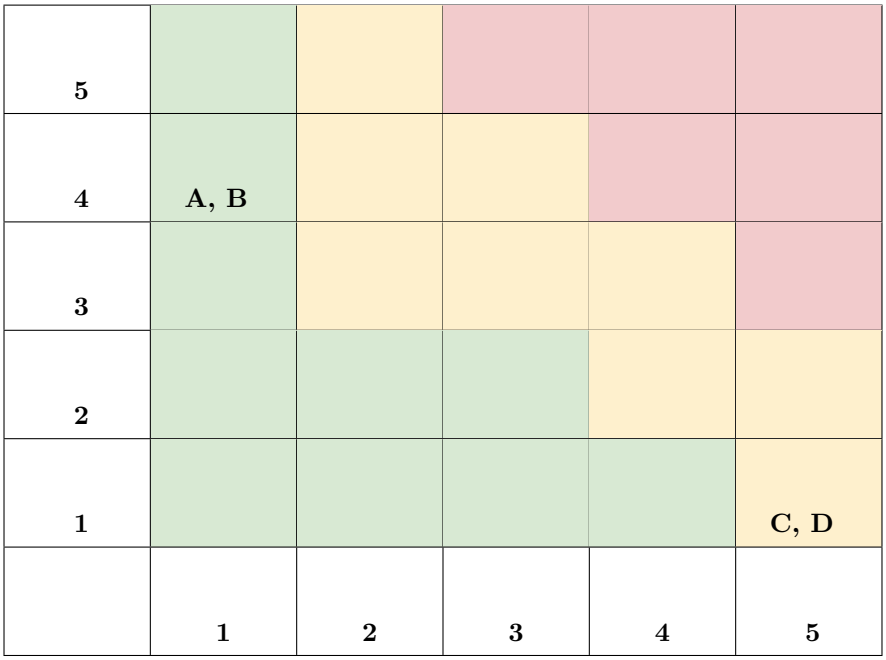

Figure 4.7: Communication and Data Risk Chart

Chapter 5

Spacecraft Bus

5.1 Overview of Requirements

To develop the requirements, the bus team determined the structural, thermal, power, and volume needs of the instruments the bus would support as well as the bus's required propulsive and control capabilities. These requirements can be found in Table 5.1.

The spacecraft bus must first survive launch to fulfil mission requirements. SB.1 was developed to comply with the launch company's structural requirements, which will ensure that the bus can bear launch loads.

The bus needs to bring the payload to Apophis and maintain the appropriate orbit to collect measurements. To fulfill these system requirements, the bus will need a propulsion system that can support all maneuvers as stated in SB.2.

System requirements 2 and 3, the requirements on taking measurements and transmitting data, necessitate a pointing system. SB.3 states that the bus must meet LNAC's pointing requirements.

The bus needs to withstand the environment in deep space to continue taking measurements. The bus team developed SB.4 based on the worst-case scenario of inert black body in Earth's shadow, to ensure the bus will weather the environment.

Not only must the bus resist external temperature fluctuations, it also must maintain a suitable internal temperature for the instruments to function properly. This bus requirement meets the system requirement that the spacecraft shall maintain appropriate conditions to take data, and is reflected in SB.5.

To support the instruments, the bus must provide sufficient power and space for the instruments. These requirements are reflected in SB.6 and SB.7 respectively.

5.2 Spacecraft Bus Trade Space

5.2.1 Commercial-off-the-shelf (COTS) vs. Custom bus

The first high level decision that the spacecraft bus team made was whether to use a commercial bus or to design a new bus specific to this mission. The decision was made early on to use a commercial option. The rationales below were the primary drivers of this decision.

1. **Time and personnel constraints**: The spacecraft bus team was initially composed of four members, none of which has had extensive experience designing large spacecraft bus systems. Additionally, the class and consequently the project had a duration of roughly three and a half months, from the beginning of February to mid-May. It was deemed that the team had neither time nor resources to design a custom spacecraft bus that would be suitable for the mission profile.

2. **Availability of commercial options**: Spacecraft of all sizes and mission types have used commercial busses for decades. There are a wide variety of commercial spacecraft busses readily available in the market from a number of well known and reliable manufacturers. The team anticipated that it could both save money and not sacrifice capabilities by choosing the commercial bus option. Companies

Table 5.1: Spacecraft bus requirements

ID	Statement	Parent	Verification
SB.1	Bus structure and internal instruments shall withstand 10g axial and 8g lateral launch loads, as well as acoustic loads and vibrations due to launch[75]	SYS.1	Vibration, stress testing
SB.2	Bus shall support spacecraft maneuvers from launch vehicle separation until end of mission.	SYS.1, SYS.2	Analysis
SB.3	Bus shall satisfy Instrumentation and LNAC pointing requirements.	SYS.2, SYS.3	Analysis
SB.4	Bus shall withstand external temperature in ranges -95 to 35 C.	SYS.2	Thermal vacuum testing
SB.5	Bus shall regulate the internal temperature to support all onboard sensors and equipment in ranges 0-40 degrees Celsius. Instruments with more stringent requirements shall be supported individually[49].	SYS.2	Thermal vacuum testing
SB.6	Bus power system shall provide sufficient and reliable power to all subsystems in ranges 11.5 kW.	SYS.2	Analysis, day in the life testing
SB.7	Bus layout shall sufficiently support all onboard sensors and equipment	SYS.2	Analysis

including Boeing, Lockheed Martin, Northrop Grumman, Orbital ATK, and Airbus are the largest manufacturers that we initially surveyed.

3. **Heritage in space**: An advantage commercial busses had that we considered was the heritage and proven reliability of many spacecraft busses. There is a large amount of inherent risk in flying new designs that we could avoid by using a commercial bus. Furthermore, we knew our mission would share many features with other previous deep space missions, and more specifically with asteroid and comet probes such as NASA's Dawn or JAXA's Hayabusa. A commercial bus with proven deep space heritage would be significantly lower cost and less risky than a new design.

5.2.2 Choice of Bus

The team chose the LEOStar-3 spacecraft bus from Orbital ATK. To determine the optimal bus, the team researched many commercial bus options from suppliers including Lockheed Martin, Northrop Grumman, Orbital ATK, and Airbus. Tables 5.2 - 5.4 compare data about the leading busses produced by each supplier and denote how well each bus fit the requirements. Green boxes denote that the bus meets requirements, yellow boxes denote that the bus can meet requirements with some modification, and red boxes denote that the bus cannot meet requirements.

Some of the bus data was not available to the team. Since all the candidate busses are currently in use, the bus team assumed that all busses could meet requirements SB.1, and SB.4: launch loads and external temperature resistance, respectively. The team assumed that SB.5, internal temperature regulation, could be easily met with a standard radiator.

Although there are no requirements on maximum mass, cost, or heritage, the bus team collected data on these areas in order to inform their decision. The team chose busses that have heritage with deep space

Table 5.2: Performance of bus candidates with regards to requirements SB.1 - SB.3

Bus Name	**Manufacturer**	**SB.1: Launch Loads**	**SB.2: Delta-V**	**SB.3: Pointing**
LEOStar-3	Orbital ATK	Yes	170 m/s with monopropellant[74]	Knowledge: 10/15 arcsec standard, sub-arcsec knowledge achievable w/ upgraded sensors. Stability < 1 arcsec/sec[74].
6U CubeSat	Various, including MIT's SSL, STAR Lab, and SPL	Yes	Impulse: 300 (monopropellant), 43000+ N-s (ion)[2]	Knowledge: 1.3 arcmin[15], pointing accuracy: 3 degrees[47]
Custom Eurostar-3000EOR/ Eurostar-NEO	Airbus	Yes	Customizable for mission; specific data not available	Customizable for mission; specific data not available
OSIRIS-REx Bus	Lockheed Martin	Yes	Delta-V: 1400 m/s; impulse: 230s[12], Chemical monopropellant[32]	Uses star trackers, reaction wheels, sun sensors and IMUs; specific data not available[32]
Boeing 702	Boeing	Yes	Data not available	Data not available
Eagle-3 GEO	Northrop Grumman	Yes	Delta-V: 2100 m/s+, monoprop[72]	Knowledge: 10 arcsec Control: 9 arcsec[72]

missions and busses that typically carry payloads similar to or larger than the SET payload to ensure that the busses would be able to meet the requirements.

The team narrowed down the options to the LEOStar-3 and the custom Eurostar-3000 EOR primarily because neither bus failed any requirements. In addition, both companies provide many customization options and both have experience designing busses for science missions. Since the team found more data supporting Orbital ATK's ability to produce a spacecraft to the specifications, the team chose Orbital ATK's LEOStar-3 bus for this mission.

5.3 Technical Characteristics

5.3.1 Bus Characteristics

The LEOStar-3 has the capabilities listed below prior to customization. More details can be found in the LEOStar-3 Fact Sheet.[74]

The pointing system will fulfill all pointing requirements imposed by instrumentation and communications, thus no customization is necessary. The LEOStar-3 has the following pointing capabilities:

- 10 arcsec pointing knowledge, but sub arcsec knowledge is achievable with enhanced star trackers
- 15 arcsec pointing accuracy
- 3-axis Zero Momentum Bias, with pitch momentum bias and spin stabilized configurations also available

Table 5.3: Performance of bus candidates with regards to requirements SB.4 - SB.7.

Bus Name	SB.4: Temperature Range	SB.5: Internal Temperature Regulation	SB.6: Power	SB.7: Volume
LEOStar-3	Yes	Yes	150 - 800 W for payload[74]	1.8m x 1.8m x 2m bus volume; 1.8m x 1.8m x 1.4m payload bay, but can be customized[74]
6U CubeSat	Yes	Yes	45 W[109]	10 cm x 10 cm x 20 or 30 cm[109]
Custom Eurostar-3000EOR/ Eurostar-NEO	Yes	Yes	7 - 25 kW[4]	From spacecraft images, standard is 3 - 4.5m tall and about 2m in diameter, but it is customizable
OSIRIS-REx Bus	Yes	Yes	1 - 3 kW[56]	2.43m x 2.43m x 3.15m[56]
Boeing 702	Yes	Yes	3 kW - 12+ kW[17]	Data not available
Eagle-3 GEO	Yes	Yes	5.5+ kW[72]	Data not available

Table 5.4: Performance of seven bus candidates in categories of typical payload mass, typical dry mass, design lifetime, cost, and mission heritage.

Bus Name	Payload Mass	Total Dry Mass	SYS.8: Lifetime	Cost	Heritage
LEOStar-3	150 kg - 3000 kg[74]	300 - 4000 kg[74]	1-10 years[74]	$130 M[42]	Yes[74]
6U CubeSat	3-5 kg[66]	12 kg[109]	1-2 years	$30K	Used for science missions on a smaller scale
Custom Eurostar-3000EOR/ Eurostar-NEO	1200 kg[106]	5800 kg - 6400 kg[35]	15 yrs[106]	Data not available	Yes, in future missions[34]
OSIRIS-REx Bus	Data not available	880 kg[56]	Data not available	Data not available	Yes[56]
Boeing 702	200 - 2000 kg[17]	Data not available	15 years[92]	$274M[92]	No[17]
Eagle-3 GEO	1100 kg[72]	Data not available	15 years[72]	Data not available	Yes[67]

- Sub arcsec/sec pointing stability

The LEOStar-3 has a blowdown monopropellant hydrazine[74] fuel system. Based on recommendations from the Launch, Navigation, and Attitude Control team, the Bus team chose to add a solar electric propulsion (SEP) system. The hydrazine fuel system has the following characteristics:

- 170 m/sec delta-V for 4300 kg satellite with 350 kg propellant
- Propellant and delta-V are adjustable

The spacecraft bus will provide the necessary data and communications to meet the Communication team's requirements. The bus's communications capabilities are included below:

- Data Storage: up to 3 Tbit
- Data Downlink: 2-4 Mbps S-Band, 740 Mbps X-Band, or 622 Mbps Ka-band
- Command Uplink: 2-1042 Kbps S-Band

The bus will also provide sufficient volume and Orbital ATK has launched spacecraft similar or higher masses. The bus typically uses less power than the SET mission requires, but Orbital ATK specifies that the power system is customizable.

- Size: 1.8m x 1.8m x 2m bus volume; 1.8m x 1.8m x 1.4m payload bay, but can be customized.
- Total Mass: 300 to over 4,000 kg, including payload
- Payload Mass: 150 kg - over 3,000 kg
- Payload Orbit Average Power: 150 - 800 W, but higher power payloads can be accommodated

Other points of interest on the LEOStar-3 include its lifetime, sufficient for our mission, unique mission services provided by Orbital ATK, and the bus's heritage for science missions. Details are included below.

- Lifetime: 1 - 10 years
- Delivery Time: 30 - 36 months
- Launch Vehicle Compatibility: Pegasus, Minotaur, Antares, Delta, Atlas, and Falcon 9
- Mission Services: can include just LEOStar-3 bus up to mission design, payload integration, test, launch services, and mission operations
- Science Mission Heritage: Fermi, Swift, Coriolis, RHESSI, Mighty Sat II.I, Deep Space I

After reviewing these capabilities and others included on the fact sheet, the bus team determined that the propulsion, thermal, and pointing systems will require increased capabilities to meet the mission requirements. This analysis is included in the following sections.

5.3.2 Fuel System Changes

As determined by the requirements set forth from Launch, Navigation, and Attitude Control, the SET spacecraft will be performing navigation burns as well as attitude control burns. The navigation burns will be performed with NASA's NEXT solar electric thruster, and the attitude control burns will be performed with the LEOStar-3's onboard monopropellant thrusters. The addition of the NEXT thrusters will require that the onboard fuel system be adapted to carry xenon, the propellant utilized by NEXT, as well as hydrazine for the monopropellant thrusters.

To perform the mission, the SET spacecraft will require customized fuel tanks. This arises due to the fact that the LEOStar-3 is not commercially advertised as providing xenon propellant. Furthermore, the SET spacecraft requires a non-standard load of hydrazine fuel for the onboard monopropellant thrusters.

For the propulsive maneuvers set forth by LNAC, the SET spacecraft must be capable of providing 5.02 km/s of delta-v for navigation burns, as outlined previously in the LNAC requirements. At full power, the NEXT thrusters provide 4190 seconds of specific impulse [44]. Thus, knowing that the dry mass of the spacecraft is 633.7 kg, application of the Tsiolkovsky rocket equation states that the NEXT thrusters will require 103.8 kg of xenon fuel to complete the mission.

The monopropellant thrusters feature a maximum thrust of 1 N, making them nearly four times more powerful than the NEXT-C thrusters[74]. Consequently, the monopropellant thrusters will be used for attitude control and also will be used to provide any additional thrust required by the mission. For these purposes, LNAC has budgeted 0.5 km/s of required delta-v. Knowing that these thrusters feature 200 seconds of specific impulse, from another application of the Tsiolkovsky equation, the SET spacecraft will require 165.3kg of hydrazine.

These propellants can be then sized volumetrically with knowledge of the densities of hydrazine and xenon. The hydrazine is stored as a liquid with a known density of 1.02 g/cm$\hat{3}$. Storage density for the xenon propellant will be done utilizing heritage reasoning. In the Dawn mission, this propellant was pressurized to a density of 1.50 g/cm$\hat{3}$ [53]. As the mission was successful, the SET spacecraft will also store its xenon propellant at this density. Consequently, the spacecraft requires 0.162 m$\hat{3}$ of hydrazine and 0.069 m$\hat{3}$ of xenon.

To ensure that these tanks fit within the spacecraft, the tanks were designed to be "pill shaped," essentially cylinders with hemispheres at each end. The hydrazine tank is currently sized with a diameter of 0.5m and a length of 1.0m. The xenon tank is currently sized with a diameter of 0.4m, and a length of 0.68m.

5.3.3 Pointing System

The pointing subsystem of the bus is most important with respect to the LNAC team and to the Instrumentation team. From an attitude control perspective, the pointing subsystem must be able to accommodate any attitude control maneuvers required by the LNAC team. Furthermore, from an instrumentation perspective, the bus demonstrates stability in pointing to a degree that is smaller than the angular resolution provided by the instrument, thus ensuring that any measurements taken by the instrument are accurate, and that any pictures would not be blurred.

In order to satisfy all requirements, the bus will be improved via the inclusion of higher performance star trackers, as advertised by Orbital ATK. The addition of these star trackers lowers the pointing knowledge of the bus to a sub-arcsecond level. This improved pointing knowledge, along with the arcsecond level pointing stability advertised by the bus, is necessary to fully meet the requirements of LNAC and Instrumentation.

To satisfy the LNAC requirements, the bus must provide a maximum slew rate larger than the expected maximum slewing rate the spacecraft will encounter during the mission. This occurs during orbits about Apophis. The minimum period the SET spacecraft will encounter during an orbit of Apophis is estimated to be about six hours, which thus constitutes a slew rate of 0.017 degrees per second. The LEOStar-3 bus provides a maximum slew rate of 3 degrees per second, easily satisfying the LNAC requirement[74].

The angular resolution specifications for the onboard instruments is provided in Table 5.5. The pointing control provided by the LEOStar-3 bus is lower than all field of view measurements, and consequently the onboard pointing system is sufficient for all pointing requirements.

As the bus provides 4.85 μrad/sec of pointing stability, and the minimum angular resolution is 4.95 μrad, the bus thus nominally satisfies the pointing requirements of all instrumentation. However, this metric passes by a thin margin (2.02% of the nominal requirement), and so the quality of image resolution is still

Table 5.5: Instrumentation fields of view

Instrument	**Angular Resolution (arc-sec)**	**Angular Resolution (μrad)**
Ralph (MVIC)[83]	4.08	19.77
Ralph (LEISA)[83]	12.5	60.83
LORRI[21]	1.02	4.95
TES[40]	1650	8000
RRT[59]	1440	6981

in question. However, the instrument in question, LORRI, was successfully operated on the New Horizons mission, which boasted a pointing stability of 25 μrad/sec by utilizing quick measurement periods, in the range of 50 to 200 milliseconds, constraining the spacecraft jitter to a maximum of 7 μrad during the measurement period[21]. As the SET spacecraft operates with increased pointing stability, the spacecraft is expected to produce a quality of measurement at least as good as that provided from New Horizons.

5.3.4 Thermal Control System

Requirements

The thermal control systems were tailored to ensure that the onboard instrumentation, communications systems, and solar panels were kept within acceptable temperature ranges. Table 5.6 provides the temperature limits of components that have been accounted for thermally.

Table 5.6: Required Temperature Limits

Component	**Temperature Limits [K]**
TES[40]	283-313
LORRI[21]	273-313
Ralph[83]	273-313
RRT[59]	173-373
Communications Antennae/TWTA[112]	173-373
Solar Panels[112]	173-373

Assumptions

In performing thermal analyses for each component, it was assumed that the spacecraft components would be experiencing a worst-case scenario with regard to the heat fluxes seen by the spacecraft. Thus, for the radiators, it was assumed any projected heat flux areas were equal to the area of the radiator, physically indicating direct incidence of any heat fluxes. Furthermore, any heat transfers were evaluated with view factors equivalent to unity, again physically indicating direct incidence between components. This will not be the case during the entirety of the mission, and can be mitigated by splitting radiator areas about multiple faces of the spacecraft to ensure direct incidence across the entirety of the radiator area never occurs, but

using these assumptions is a method of ensuring that the thermal control systems can fully protect the components.

When applying the conservation of energy to perform power balances among components, the steady state assumption was employed. This assumption thus fails to capture any transients present during the mission, particularly during eclipse while in Low Earth Orbit, but otherwise is not a bad assumption.

For internal spacecraft components, the only method of heat transfer was assumed to be conductive. Therefore, internal components cannot radiate heat to each other. As the internal environment is to be kept within "room temperature" limits, the steady state temperatures of all internal components are relatively close to each other, and thus there is minimal radiative heat transfer, and this transfer is negligible compared to heat transfer via conduction.

Analyzed Scenarios

Thermal control analyses were performed at mission perihelion, mission aphelion, and during Low Earth Orbit, ignoring eclipse. Eclipse was ignored as overheating is considered more dangerous and more difficult to protect against. Even during eclipse, the spacecraft is inherently protected against cool temperatures due to internal components dissipating heat from their power inputs. The expected solar flux the spacecraft would encounter during each scenario is presented in Table 5.7.

Table 5.7: Expected Solar Flux for Analyzed Scenarios

Scenario	**Distance to Sun [AU]**	**Solar Flux** $[W/m^2]$
Low Earth Orbit	1	1366
Mission Perihelion	0.74	2495
Mission Aphelion	1.31	796

Aside from the included solar flux present during Low Earth Orbit, an analysis of this scenario includes albedo from Earth as well as the infrared radiation present from Earth. These values have been determined to be $410W/m^2$ (30% albedo from Earth) and $239W/m^2$, respectively[51]. Therefore, the entire heat flux absorbed by the spacecraft is determined to be $2015W/m^2$.

External Components

The external components consist of the RRT instrument, the communications antennae, and the solar panels. In performing a thermal analysis for these instruments, the heat flux entering the instruments was assumed to be the total heat flux present in the analyzed scenario, as well as the power input to the instrument. A figure accurately describing the heat flow present throughout these antennas are presented in Figure 5.1:

The antennas were then assumed to have white paint coatings, which is typical of spacecraft antennae, as described by Martinez. The properties of these coatings as well as the thermo-optical properties of the solar panels are presented in Table 5.8.

The direct mathematical approach utilizing the assumptions valid for external components as outlined in the previous section is outlined via the following analysis:

$$Q_{FLUX} + Q_{ANT} = Q_{EMIT} \tag{5.1}$$

$$Q_{FLUX} + Q_{ANT} = \sigma\varepsilon({T_{ANT}}^4 - {T_{SPC}}^4) \tag{5.2}$$

$$(\frac{Q_{ANT} + Q_{FLUX}}{\sigma\varepsilon} + {T_{SPC}}^4)^{\frac{1}{4}} = T_{ANT} \tag{5.3}$$

Here, Q_{ANT} and Q_{ANT} denote the power input of the antenna and the flux seen in each thermal scenario, respectively. To fully define the value of Q_{FLUX}, the input flux in each scenario must be multiplied by the absorptivity of the external component being considered, as outlined previously in Table 33. T_{ANT} is the

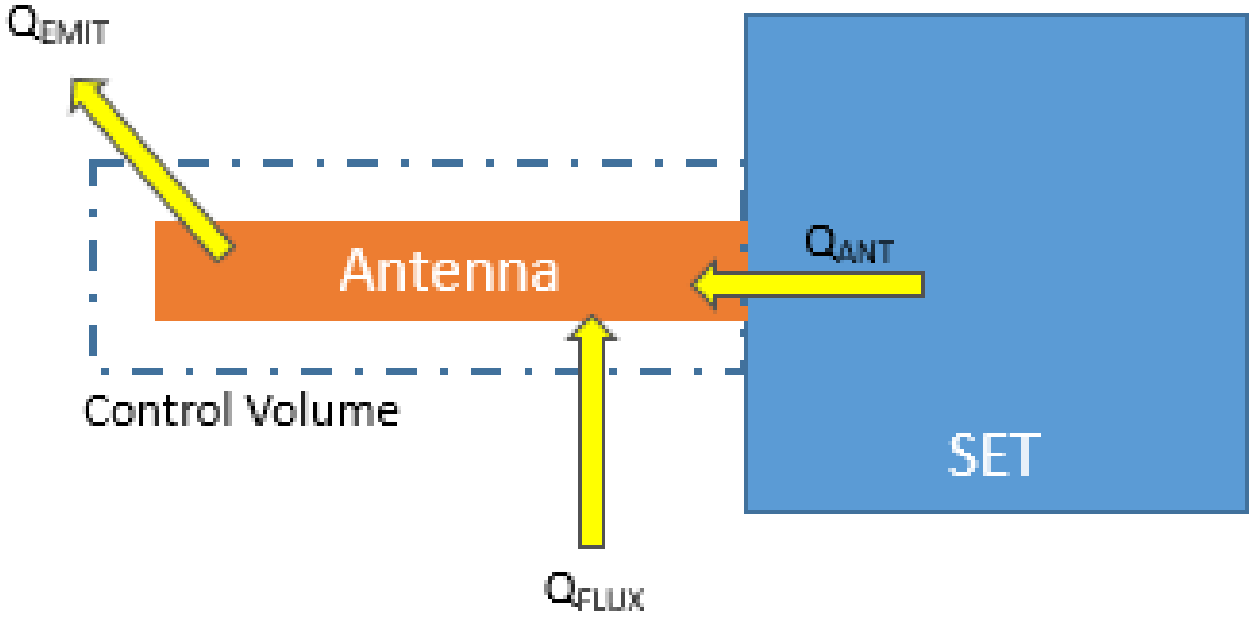

Figure 5.1: Model of External Component Heat Fluxes

Table 5.8: Thermo-optical Properties of External Components[60]

Component	**Coating**	**Absorptance**	**Emissivity**
Communications Antennas/TWTA	White Paint	0.20	0.85
RRT	White Paint	0.20	0.85
Solar Panels	-	0.75	0.75

steady-state temperature of the external component, and T_{SPC} is the temperature of deep space, taken to be 2.7 K in this analysis. The value of epsilon denotes the emissivity of the external component, again as denoted in Table 33. Finally, sigma is the Stefan-Boltzmann constant, empirically known to be $5.67\times10^{-8}Wm^{-1}K^{-4}$.

With these coatings, the external antennae do well in all thermal scenarios, and are able to stay within their specified temperature ranges without any active thermal control. The solar panels, however, have a tendency to slightly overheat during mission perihelion. However, this analysis assumed a worst-case scenario of direct incidence to the sun during mission perihelion. In reality, as the solar flux is much larger during perihelion, the solar arrays will need be tilted with respect to the sun in order to lower the incoming power, as the power provided from direct incidence to the sun during perihelion will be significantly higher than the peak power required at any point during the mission. Thus, this action provides an implicit mitigation strategy which will ensure that the solar arrays never have a steady state temperature outside of the specified limit.

The steady-state temperatures for each scenario are presented in Table 5.9 and are shaded green (indicating within specified temperature ranges), yellow (indicating marginally outside of temperature ranges), or red (indicating significantly outside of specified temperature ranges).

Table 5.9: External Component Steady-State Temperatures

Component	**LEO Temp. [K]**	**Perihelion Temp. [K]**	**Aphelion Temp. [K]**
Comms. Antennas/TWTA	348.36	331.21	265.70
RRT	345.75	328.17	259.69
Solar Panels	359.25	375.95	310.82

Internal Components

The internal components consist of Ralph, TES, LORRI, and NEXT. To control the temperature of Ralph, TES, and LORRI, all three of these instruments are connected to a common radiator which is exposed to the cold space environment. This radiator keeps the instruments within the specified temperature ranges for mission perihelion. NEXT is modeled separately from these instruments due to the fact that the thruster is physically separated from the instrument deck on the SET spacecraft. A full model of the heat fluxes present within the SET spacecraft is presented below in 5.2:

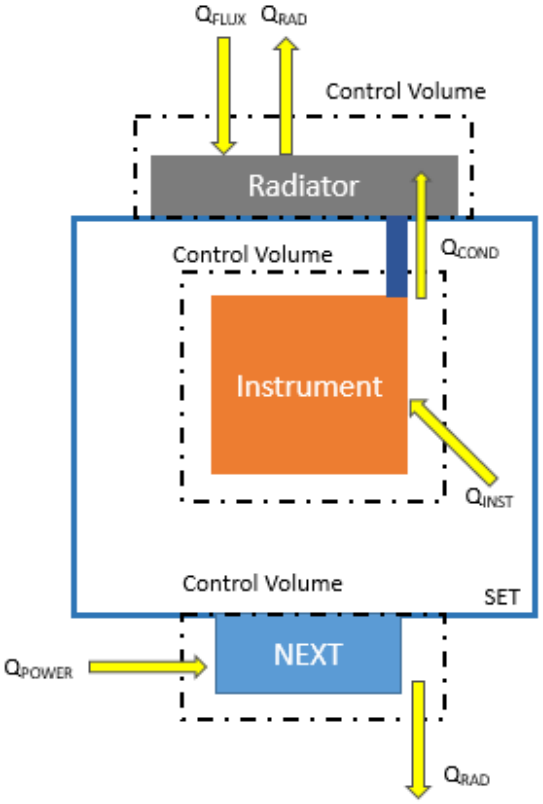

Figure 5.2: Model of Internal Component Heat Fluxes

At aphelion and during LEO, these instruments are below their specified temperature ranges. One method of ensuring that the instruments will not become too cold is to keep louvers on the radiator, which essentially act as "valves" for the radiator which can be opened and closed as necessary to expose a variable area of the radiator to the cold space environment[49].

Important to note is how heat transfer occurs within this model. As the name implies, the radiator uses radiation as the sole method to transfer heat between itself and the cold space environment. The

instruments transfer heat to the radiator via conduction. For the instruments, this conduction is assumed to occur through ten steel bolts. This is a generally accepted method of heat transfer between onboard components and radiators, though in a higher-fidelity model of thermal control, in which there will likely be multiple radiators such that the view factors and project areas can be manipulated to facilitate thermal control as necessary, this conduction will likely occur through heat pipes and thermal straps through which the heat transfer is controlled.

In determining the steady state temperature of Ralph, TES, and LORRI, a two step analysis had to be performed. First, radiator temperature is determined as follows.

$$Q_{COND} + Q_{FLUX} = Q_{RAD} \tag{5.4}$$

$$Q_{COND} + Q_{FLUX} = \sigma\varepsilon({T_{RAD}}^4 - {T_{SPC}}^4) \tag{5.5}$$

$$(\frac{Q_{COND} + Q_{FLUX}}{\sigma\varepsilon} + {T_{SPC}}^4)^{\frac{1}{4}} = T_{INST} \tag{5.6}$$

For this analysis, Q_{COND} is taken as the sum of the power inputs of Ralph, TES, and LORRI. This physically implies that the entirety of the instrumentation power input is dissipated as heat energy which is then absorbed by the radiator. Furthermore, Q_{FLUX} is the external heat flux seen by the radiator in each thermal scenario, and is determined by taking the external heat flux explicitly present in each scenario and multiplying it by the radiator absorptivity, taken to be 0.08, as determined from a reference source[60]. Finally, the deep space temperature is taken to be 2.7 K.

With the steady-state radiator temperatures now known from the above analysis, the individual temperatures of each instrument can be calculated via the following analysis.

$$Q_{INST} = Q_{COND} \tag{5.7}$$

$$Q_{INST}\, n_{bolt}\, k_{bolt}\, A_{bolt}\, (T_{INST} - T_{RAD}) \tag{5.8}$$

$$\frac{Q_{INST}}{n_{bolt}\, k_{bolt}\, A_{bolt}} + T_{RAD} = T_{INST} \tag{5.9}$$

Here, Q_{INST} denotes the individual power input to each instrument. Conduction was assumed to occur through ten steel bolts, as mentioned within the assumption subsection. Consequently, n_{bolt} is taken to be equal to 10, and for space-grade steel bolts, the value of k_{bolt} is taken as 52 $Wm^{-1}K^{-1}$. Furthermore, the area of the steel bolt exposed to the instrument was estimated as being 6 cm^2.

Although there are no instances of louvers failing during a mission[79], an analysis was implemented to see how much heat would need to be provided to the instruments during each scenario should the louver fail to close and the radiator was constantly exposed to the space environment. This analysis is tabulated in Table 35 and finds that a maximum of 55 W needs to be made available to the instruments via heat pipes. As the thermal subsystem is budgeted roughly 320 W, this heating is viable even for low-efficiency heat pipes.

To determine the steady-state temperatures of the Ralph, TES, and LORRI, the following mathematical analysis was performed:

Table 5.10: Internal Component Steady-State Temperatures

Component	**LEO Temp. [K]**	**Heat Addition [W]**	**Perihelion Temp. [K]**	**Heat Addition [W]**	**Aphelion Temp. [K]**	**Heat Addition [W]**
Ralph	284.22	5	281.16	0	285.56	20
LORRI	295.52	0	306.48	0	294.86	15
TES	296.08	5	293.02	0	297.42	20

NEXT was disincluded from a full analysis within the three thermal scenarios, as NEXT will be isolated from the external fluxes seen by the spacecraft. Thus, the analysis to determine the steady-state temperature of the NEXT thrusters can be denoted as follows:

$$Q_{POWER} = Q_{RAD} \tag{5.10}$$

$$Q_{POWER} = \sigma\varepsilon({T_{NEXT}}^4 - {T_{SPC}}^4) \tag{5.11}$$

$$(\frac{Q_{POWER}}{\sigma\varepsilon} + {T_{SPC}}^4)^{\frac{1}{4}} = T_{NEXT} \tag{5.12}$$

Here, it is important to note that Q_{POWER} is physically the waste heat produced by the NEXT thruster. Knowing that the overall efficiency of NEXT is 0.67[70], and that the input power to NEXT is 7 kW, Q_{POWER} is then equivalent to 2.31 kW. The analysis is then rounded out by utilizing an emissivity of unity (thus stating that the NEXT thruster is modeled as a blackbody) and by once again utilizing a deep space temperature value of 2.7 K. With these inputs, the steady state temperature of NEXT is 453 K.

As stated by Van Noord, the most heat sensitive component on the NEXT thruster is an exit wire harness, which is only rated to a maximum temperature of 423 K[110]. The thermal control of NEXT is a current research area internally at NASA, with Benson, Riehl, and Oleson citing the use of external radiators and heat pipes to keep the NEXT thruster cool[11]. The SET spacecraft will aim to utilize the thermal control methods established in this report.

Furthermore, an important aspect of Ralph and LORRI is that these instruments contain CCDs which must be kept cool during operation. The Ralph instrument was designed to have internal thermal control systems which keep the CCD within its specified temperature range[83]. Thus, this thermal analysis is not explicitly performed, as the CCD is being actively cooled by the instrument itself. The LORRI instrument is designed such that the cryogenic components of the instrument are kept within a chamber which can be opened to the cold space environment. This strategy has worked in the prior implementation of the LORRI instrument, and so this analysis is also not explicitly performed, but the strategy will be implemented onboard the spacecraft bus[21].

Temperature Sensing

As mentioned previously, the thermal control systems include several active components to ensure that all components are kept within their temperature limits. These active components include heat pipes or heaters to keep the internal instrumentation safe in the case that the spacecraft falls below specified temperature ranges, as well as changing the heat flux through the radiators through the use of louvers. To ensure that these components are mitigating the required heat fluxes, the thermal control system needs to monitor the current temperature of the internal and external components. This monitoring will be done via an array of temperature sensors, placed around each component being thermally controlled. A previous MIT SSL based report utilized 50 sensors to thermally monitor the temperatures of four onboard instruments, as well as 75 sensors to thermally monitor additional spacecraft bus based components, along with an additional 150 sensors to monitor optics based components[61]. As the SET spacecraft contains many of the same components, noting that much of the instrumentation is optics based and contains components which require low temperatures, the SET spacecraft will utilize the same number of sensors, distributed in a similar manner.

5.3.5 Power System

The spacecraft will use solar arrays and batteries to provide electrical power throughout the mission in order to support all propulsion requirements, spacecraft operations and control, and science operations. These solar arrays are designed to meet the identified power requirement of the spacecraft during its peak power usage. Peak power usage is detailed in Table 5.11. The period at which spacecraft power usage is maximal has been identified to be during the cruise phase of the mission from Earth to Apophis. During this time, the solar electric propulsion (SEP), communications system, and all spacecraft support systems will be operating. The SEP is by far the system that draws the most power on the spacecraft.

In order to determine the final power requirement for the spacecraft, appropriate margins were added onto the nominal requirement at peak usage. A 10% mission margin was added as a standard safety margin

Table 5.11: Peak Power Consumption Budget

Item (Mission Phase 2: Cruise to Apophis)	**Power Usage (W)**
Solar Electric Propulsion	6900.0
Communications	330.0
Power Management/Distribution, Command & Data Handling	181.21
Attitude Control System	217.45
Thermal Control	328.16
Other	18.12
Total Power Requirement at Peak Usage	**7,974.9**

for spacecraft solar arrays that have heritage in space. An additional 20% manufacturing margin was added to account for potential changes in the spacecraft design or instrument power requirements that may occur in redesign or fabrication. These margins were. Further justification for these margins is found in De Luca's paper detailing architectural design criteria for spacecraft solar arrays[57]. These margins are detailed in Table /reftab:PowerMargins.

Table 5.12: Power Margins

Expected Peak Power Consumption	7,974.9
10% Mission Margin	797.5 W
20% Additional Manufacturing Margin	1754.5 W
Total Design Power Requirement	**10526.9 W**

The bus team has chosen the Orbital ATK UltraFlex solar arrays in order to provide power to the spacecraft. These solar arrays are volume, mass, and cost efficient, well tested in various space environments, and compatible with the chosen Orbital ATK LEOStar-3 spacecraft bus. The UltraFlex arrays are stowed during launch and deploy as two identical decagonal arrays on either side of the spacecraft. More information about these solar arrays can be found in a publicly available fact sheet[76].

Peak power consumption for the spacecraft will occur during the beginning of the mission at distances of roughly 1.0 to 1.1 AU from Earth. To meet the design power requirement of 10,526.9 W, the UltraFlex solar arrays need to provide this power at 1.1AU at the beginning of life (BOL) of the solar panels.

The UltraFlex solar array can produce approximately 237.5 W/m^2 at 1 AU at BOL according to the available data. Given an estimated solar irradiance of 1,361 W/m^2 at 1 AU,[29] these panels have an efficiency of 17.45%. In order to meet the power requirement of 10,526.9 W at 1.1 AU, each solar array will need an area of 26.817 m^2, for a total area of 53.633 m^2. Each decagonal panel will be 6.041 m across.

The solar arrays will degrade over time due to interactions with energetic particles and micrometeoroid impacts[58]. The expected rate of decay of power provided by the solar panels is -2.741% per year. This was based on models developed for a similar system design study conducted by NASA engineers in 2011[97]. Figure 5.3 illustrates the expected rate of decline in provided solar power over a period of 15 years.

Solar array efficiency over 10 years is expected to decline to 13.2%, providing 179.9 W at 1.0 AU. It is additionally important to note that neither the orbit of Apophis nor the spacecraft is circular, so panel power will fluctuate according to the spacecraft's position in its orbit. This is illustrated in Figure 5.4 (5).

Solar power performance will degrade throughout the mission and vary according to the spacecraft's

Table 5.13: UltraFlex Solar Array Specifications

Efficiency	17.45%
Number of Individual Panels	2
Total Area	53.633 m^2
Individual Panel Area	26.817 m^2
Panel Cross Length	6.041 m

distance from the Sun. However, the solar panels have been designed to support the peak power usage during the cruise to Apophis, which is known to be at around 1.1 AU and BOL. Current models show that with the included margins, the spacecraft can sustain its peak power requirement of 7.9 kW after 10 years in flight at 1.1 AU.

It is useful to note that the SEP system is throttleable and if the solar panels can not meet the 6.9 kW required to power the SEP at 100% during some point in the mission, it can be throttled down as necessary in order to provide power to both propulsion and other necessary spacecraft subsystems.

It is beyond the scope of this design study to specify all spacecraft power conversion mechanisms, although preliminary analysis based on the analogous Dawn mission suggests a solar array voltage in the range of 85 V to 140 V and a down-converted unregulated bus voltage for subsystem and instrument usage of 22 V to 35 V, with 28 V being the industry standard[107].

Additionally, the spacecraft is not expected to be in eclipse or shadow for any significant period of time. Therefore it is expected that the standard battery provided by Orbital ATK on the LEOStar-3 will be sufficient for this mission. Further analysis based on data that is not publicly available is necessary to justify this assumption.

5.3.6 CAD Model

To ensure that the bus would meet requirement SB.7, components of the spacecraft bus were modeled in Computer Aided Design (CAD) software. Many of the components included with the bus, such as the reaction wheels and communication and data handling system, were not modeled. Orbital ATK ensures that these components fit inside the spacecraft bus during design of specific missions, and little relevant data on these systems were available to the team to do the analysis themselves. Additional features, such as payload instruments, communications antennas, and the solar electric propulsion tank were included in the CAD model.

All the components were placed to ensure that each subsystem's requirements were met. The two decagonal solar panels were placed opposite each other on the spacecraft bus to maximize solar energy absorbed[76]. The solar panels are gimballed and the spacecraft will be oriented such that the panels face the sun as often as possible.

The high gain dish was placed on one of the remaining bus faces such that it faces Earth prior to Apophis flyby. For the same reason, one of the low gain antennas is on the same face but below as the high gain antenna. The low gain antennas perform best when placed 180 degrees apart, so the second low gain antenna is on the opposite face. The toroidal antenna is placed near the payload bay on this face to provide coverage to the areas that the high and low gain antennas cannot reach, since the toroidal antenna transmits radially and the high and low gain antennas transmit perpendicular to the spacecraft bus face.

Figure 5.5 shows the full render of the spacecraft bus, specifically the communications equipment and solar panels.

All the instruments were placed in the payload bay with their sensors pointing up. This face of the bus will always be facing Apophis so the payload sensors will be able to take data. Ralph was placed outside the spacecraft for its New Horizons mission, so it will be mounted on exterior of the payload bay covering[83]. LORRI, also used on New Horizons, was placed on the interior of the spacecraft, and thus was placed inside

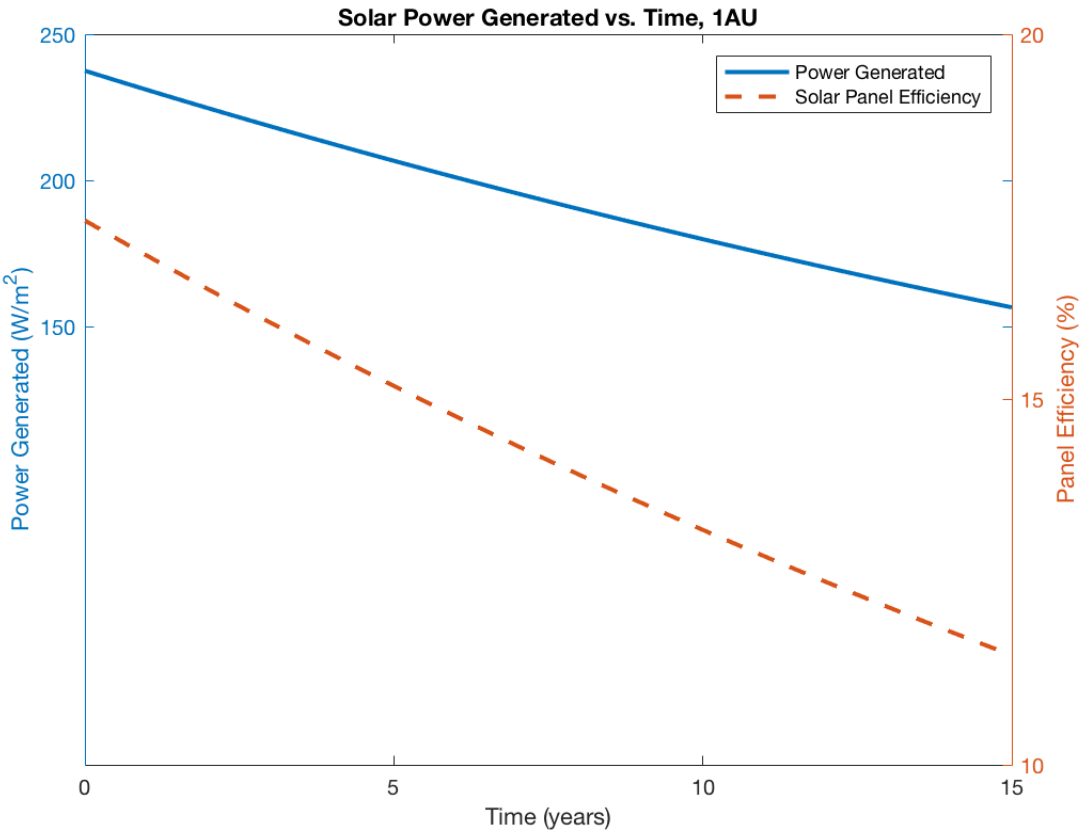

Figure 5.3: Modeled degredation of solar panels at 1 AU

the spacecraft bus[21]. The payload bay will open such that the sensors on LORRI will be unobscured. These sensors need to be kept at low temperatures, so exposing them to the exterior of the bus will satisfy the thermal requirements. TES, the remaining payload instrument, will be placed inside the payload bay. TES's sun shade, however, will be exposed to the exterior as it was in OSIRIS-REx[26]. In the middle of the payload bay is a radiator to keep the instruments at the appropriate temperature.

The RRT antenna, in gold, was placed on the same face as the solar panels so that it could not expand into one of the solar panels during deployment[59]. For the RRT antenna to take data, it must not have an antenna facing directly toward Apophis, so it was placed horizontally on the side of the bus. The team found no indication that the RRT nor any other instrumentation will interfere with the communications, so this is not a concern.

Figure 5.6 shows the layout of the payload bay.

The hydrazine thrusters are placed on each bus corner, with one thruster facing along each axis, in order to provide adequate control[73]. The solar electric propulsion (SEP) thruster is placed at the base of the spacecraft to be aligned with the spacecraft's center of mass[90]. The hydrazine and xenon tanks are placed in the center of the spacecraft bus, with the xenon tank on top of the hydrazine.

Figure 5.7 highlights the propulsion system.

5.4 Testing Requirements

Prior to flight, the spacecraft must be tested to ensure it is capable of satisfying all mission requirements. These tests involve testing to ensure the spacecraft can safely carry the maximum expected loading during launch and during the mission, testing to ensure the thermal control systems work as expected, and testing

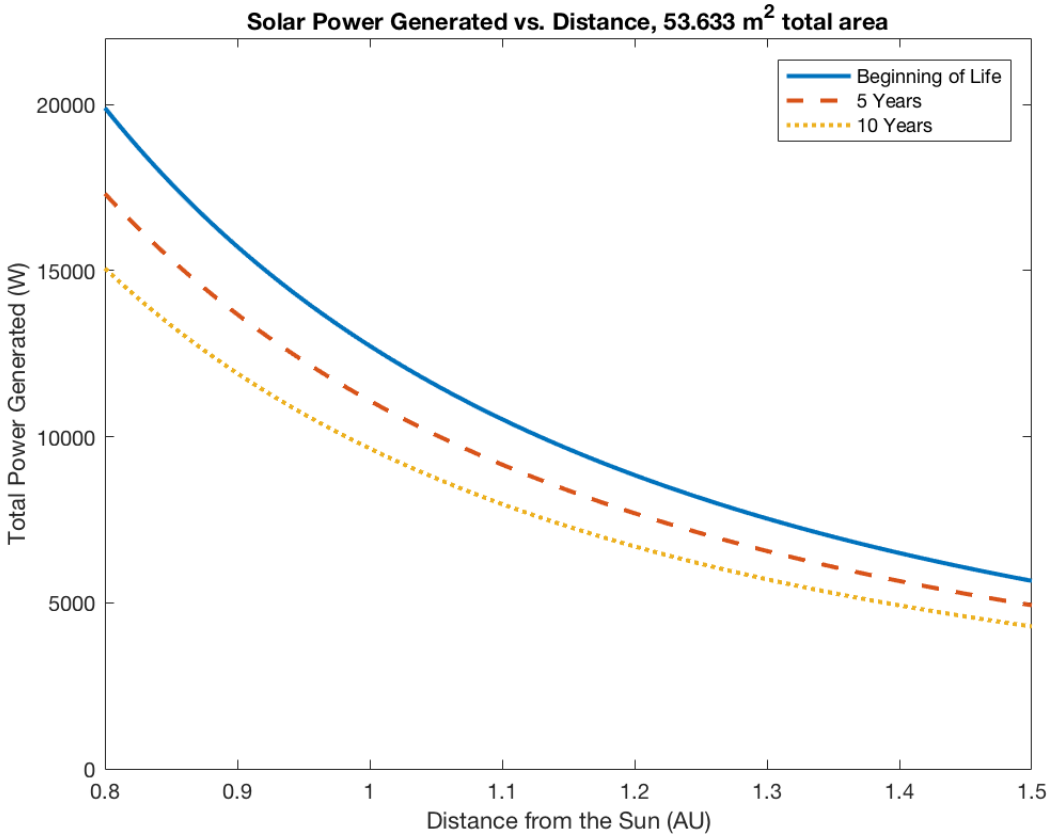

Figure 5.4: Modeled solar panel power generation at various orbital positions

to ensure the bus is capable of powering all components as needed.

5.4.1 Maximum Load

Vibration testing is utilized to ensure that the spacecraft can survive the high levels of vibration present during launch. General vibration testing involves bolting the spacecraft to a shaker stand, which is capable of shaking the spacecraft in all three directions. The spacecraft will be tested in a frequency range from 5 – 2000 Hz to ensure that the bus and the internal components are capable of surviving launch[93]. As Orbital ATK possesses the necessary facilities to carry out this testing, they will perform these tests[74].

Further vibration testing will be performed via vibroacoustic testing, in which the spacecraft is placed in a chamber and exposed to external acoustic pressures induced via large speakers. This testing method allows for "sine sweeps" in which the acoustic frequencies are slowly modified, allowing for the discovery of resonant frequencies within the bus[93].

5.4.2 Thermal Control

To ensure that the thermal control systems onboard the bus are working as required, thermal vacuum testing will be utilized. In this method of testing, the spacecraft is placed within a vacuum chamber and exposed to the expected thermal radiation levels that are expected to be encountered during the mission. The spacecraft is then monitored to ensure that the thermal control systems work as expected, allowing the internals components to stay within their specified temperature ranges.

In producing the thermal environment the spacecraft is expected to see during Low Earth Orbit, the bus will further be exposed to thermal cycling, in which the thermal control systems are tested to see how

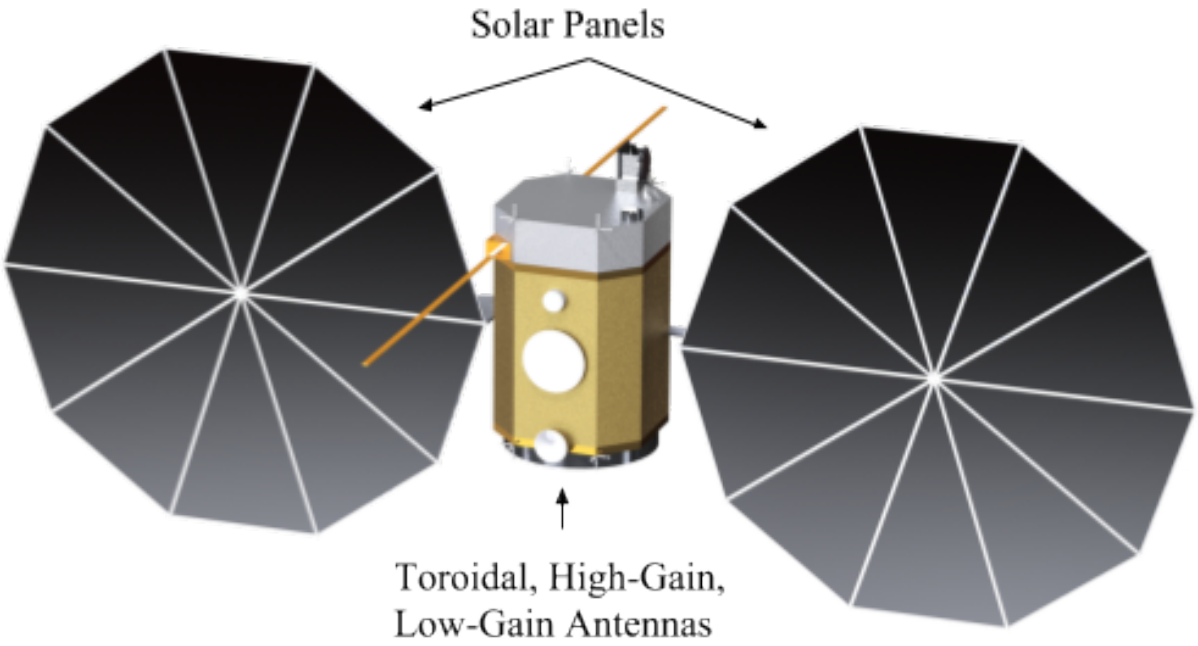

Figure 5.5: Render of spacecraft bus

they would respond as the spacecraft moves into and out of Earth's shadow during eclipse. These cycles are often performed at more stressing temperatures than expected during operation to ensure the systems are robust[100].

5.4.3 Powering Components

In this testing phase, the spacecraft will be powered on and operated in various configurations to ensure that the bus is capable of powering all internal components and instrumentation. Not all components will be powered by the bus for the entirety of the mission, so testing these various configurations is important to ensure that no failures occur during the mission. Furthermore, the power system will be cycled to ensure that the spacecraft is capable of power cycling during the mission if necessary.

5.5 SWaP Budget

The bus was approximated as a 1.8m cube with a 1.8m x 1.8m x 1.4m payload bay. The bus team expects the bus to have a dry mass of 554.9 kg and require 8058 watts to run the bus and SEP system.

Unfortunately, size, weight, and power data for specific bus components was not readily available. Orbital ATK specified the payload bay dimensions, 1.8m x 1.8m x 1.4m, so the bus team used this information to determine the size limitations on the components in the payload bay[74]. Since no other size data was available, the bus team assumed that the bus structure would be sufficient to house all the internal components that would be purchased commercially with the bus.

No data on the weight of the LEOStar-3 was available. To estimate the masses of bus components, the team made the assumption that the bus mass would scale with payload and communications masses. Thus, to estimate the spacecraft bus mass, the bus team first determined the expected dry mass from the initial communications and instrumentation masses. Then, the team used the historical percentages to estimate the masses of bus subsystems. The communications and instrumentation masses have decreased slightly since these initial estimates, but the team chose to keep the larger bus masses as an extra margin.

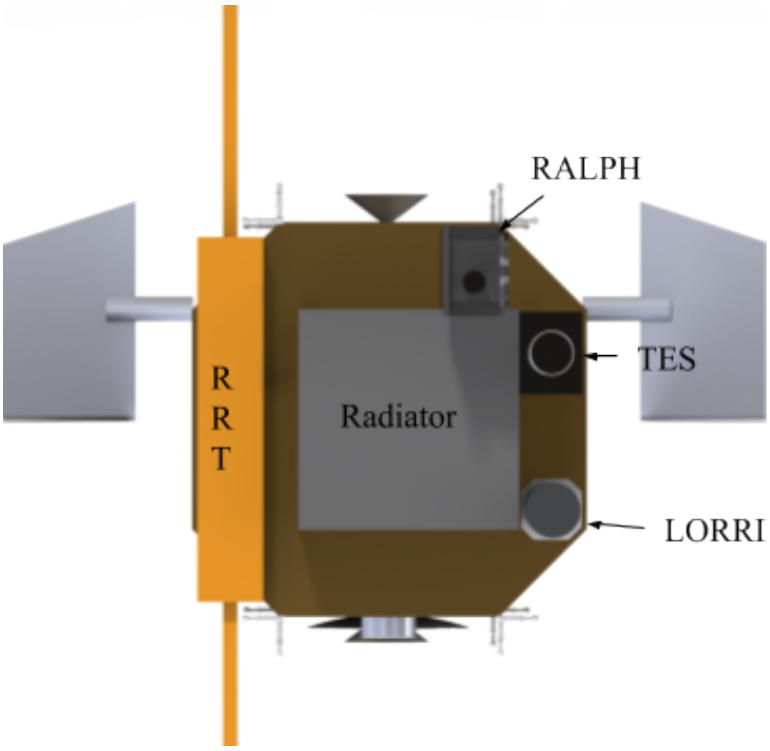

Figure 5.6: Render of payload bay

The same procedure was used to estimate the power requirements of bus components. The power requirements of instrumentation and communications decreased since the initial estimates, but the bus team chose to keep the bus estimates as an extra margin. Since SEP is not included in the historical mass budgets, the bus team did not scale other bus power components with the SEP system but instead added the power after estimating the other components. Since SEP falls into the category of power required to operate the bus's propulsion system, the SEP power requirement of 6900 W was included with bus components. Table 39 summarizes the current mass and power estimates.

5.6 Subsystem Risks

The spacecraft was designed with the goal of using high heritage and low risk systems in order to ensure the reliability of the spacecraft. The most significant risks that the team has identified are described below.

1. Solar electric propulsion systems are relatively new technology and subject to non-negligible failure rates. Failure of the spacecraft's SEP system could render the leave the spacecraft in an incorrect orbit, leaving it unable to complete the mission. This risk is mitigated by redundancy through the inclusion of two SEP thrusters.

2. Chemical propulsion systems are complex and have non-negligible failure rates. The failure of the spacecraft's chemical propulsion system could lead to mission failure if it is unable to complete attitude adjustments and station keeping necessary for mission success.

3. Mechanical risks include the failure of mechanical systems on the spacecraft to operate properly, some of which are mission critical. Critical identified mechanical system risks are the failure of the solar array deployment mechanisms and reaction wheels. Mitigation is provided by redundancy in solar arrays and attitude control systems.

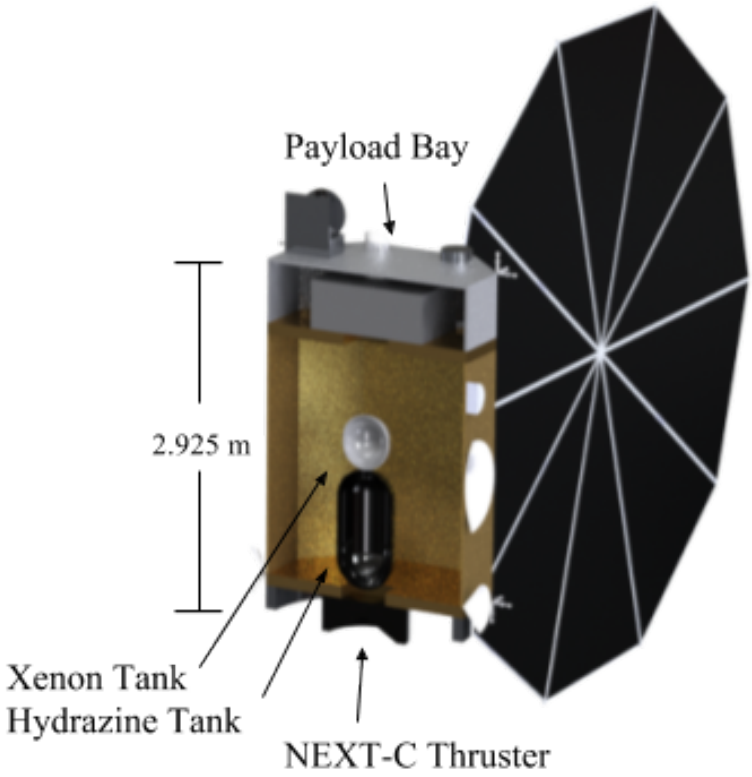

Figure 5.7: Cross-sectional view of spacecraft bus

4. Thermal control systems need to operate properly in order for the various onboard equipment to function properly.

5. Power systems need to operate properly to keep all onboard equipment functioning properly.

6. Modifications to the commercial LEOStar-3 bus introduce potential risk. One of the primary reasons for choosing the LEOStar-3 bus was its heritage in space and demonstrated reliability. However, every LEOStar-3 bus is different as Orbital ATK manufactures to customer specifications. The addition of new components introduces risk in that new designs that have never flown are inherently risky due to design oversights or manufacturing issues. This can be mitigated through robust testing and analysis prior to flight.

Table 5.14: Estimated bus component masses and power requirements

	Current Best Estimate (kg)	**Current Power (W)**
Bus- Structure	168.0	18.0
Bus- Thermal	32.0	326.0
Bus- Power	142.0	181.0
Bus- Attitude Determination	38.0	217.0
Bus- Propulsion	155.9	7117.0
Bus- Processing	19.0	199.0
Allocated Margin	0.0	0.0
Total	554.9	8058.0

Table 5.15: Bus Risk Chart Descriptions

ID	**Description**	**Mitigation**
A	Propulsion system failure	Redundancy, heritage
B	Mechanical systems (ie solar array deployment, reaction wheels) fail	Testing, limited redundancy, heritage
C	Thermal control, power systems fail	Testing, heritage
D	Modifications to LEOStar-3 cause bus system to fail	Testing, heritage

5					
4					
3					
2					
1				**B**	**A,C,D**
	1	**2**	**3**	**4**	**5**

Figure 5.8: Bus Risk Chart

Chapter 6

System-Level Summary

6.1 Consolidated SWaP Budget

The bus team developed the system-level size, weight, and power (SWaP) budget based on historical mission data and standard margins.

To develop size constraints, the bus team first made the assumption that the components included with the bus would fit inside the main bus compartment. Any additional payload instruments would need to fit in the $1.8m \times 1.8m \times 1.4m$ payload bay, so the bus team allotted this space to instrumentation, and size constraints were primarily tracked in the Computer Aided Design (CAD) model.

Table 6.1: Average mass allotments for historic missions

Averages	**Total Mass**	**Wet Mass**	**Dry Total Mass**	**Payload Mass**	**Payload %**
Small spacecraft (total wet mass <1000 kg)	599.5	599.5	389.75	50.5	14%
Medium spacecraft (1000 <wet mass <2500)	1718.6	1487.6	904	163.6	13%
Large spacecraft (total wet mass >5000 kg)	4510	3412.5	1842.5	409	20%
Small payload(<60 kg)	952.2	721.1	405.4	38.4	9%
Medium payload (60 <payload <200 kg)	1690.5	1141.75	715.25	96.75	16%
Large payload (>200 kg)	3690.5	3690.5	2170	609.5	29%

The weight and power budgets required a two step process. The team first reviewed the average allotment across subsystems for historical deep space missions. A spreadsheet of mass and power budgets for the 11 planetary spacecraft in Space Mission Engineering: The New SMAD was created. To ensure that the averages were appropriate for a mission of this size, the team decided to split the data based on mission and payload size and average the allotments in these subgroups. The allotments can be seen in Tables 6.1 through 6.4. The green rows highlight the allotments for the appropriate spacecraft and payload size.

The bus team allotted percentages of total mass and power based on an average of the highlighted data above. Using the estimated mass and power requirements from each team, the basic mass budget for the spacecraft was developed.

Table 6.2: Average mass allotments for historic missions

AVERAGES	Structure and Mech Mass %	Thermal Mass %	Power Mass %	TTC Mass %	Processing Mass %	ACDS Mass %	Prop Mass %
Small spacecraft (total wet mass <1000 kg)	25%	5%	27%	7%	5%	5%	13%
Medium spacecraft (1000 <wet mass <2500)	26%	7%	20%	6%	3%	7%	14%
Large spacecraft (total wet mass >5000 kg)	21%	4%	16%	8%	5%	7%	13%
Small payload(<60 kg)	26%	7%	22%	6%	4%	6%	13%
Medium payload (60 <payload <200 kg)	25%	4%	25%	7%	4%	6%	12%
Large payload (>200 kg)	16%	4%	14%	5%	4%	7%	15%

Table 6.3: Average Power Allotments for Historic Missions

Averages	Payload Power [W]	Payload %	Structure and Mech Power %	Thermal Power %
Small spacecraft (total wet mass <1000 kg)	61	12%	0%	17%
Medium spacecraft (1000 <wet mass <2500)	120.67	17%	2%	17%
Large spacecraft (total wet mass >5000 kg)	745	28%	0%	11%
Small payload(<60 kg)	94.5	13%	0%	12%
Medium payload (60 <payload <200 kg)	92.33	14%	2%	19%
Large payload (>200 kg)	745	56%	0%	11%

Reserves were added to the mass and power budgets as the second step in their development. Since component masses increase between the Critical Design Review (CDR) and project completion, a mass growth allowance (MGA) was added to the components, per AIAA standard[3]. Since the payload and instrumentation masses are based on components in production, a 3% MGA was added. The bus masses, however, are based on historical data, so a 7% MGA was added. A 2% mass margin was added to the predicted mass to allow buffer between the predicted and maximum allowable mass[3]. A 10% management

reserve was added to the maximum allowable mass[14].

A similar process of buffers was applied to the power budget. A 10% management reserve was added to the basic power requirement[14], then another 20% margin in the event that manufacturers cannot meet their power specifications[31].

Tables 6.5 and 6.6 summarize the mass and power budgets.

Table 6.4: Average Power Allotments for Historic Missions, cont.

Averages	**PMAD Power %**	**TTC Power %**	**Processing Power %**	**ACDS Power %**	**Prop Power %**
Small spacecraft (total wet mass <1000 kg)	11%	15%	13%	9%	25%
Medium spacecraft (1000 <wet mass <2500)	11%	21%	9%	15%	7%
Large spacecraft (total wet mass >5000 kg)	4%	No data	11%	11%	7%
Small payload(<60 kg)	9%	14%	6%	13%	33%
Medium payload (60 <payload <200 kg)	9%	18%	12%	9%	17%
Large payload (>200 kg)	4%	0%	11%	11%	7%

Table 6.5: Mass Budget for Spacecraft Including Margins

	Dry Mass % Allowed (SMAD)	**Dry Mass % Allowed (SEP)**	**Basic Mass [kg]**	**Predicted Mass [kg]**	**Allowable Mass [kg]**	**Mass Limit [kg]**	**Wet Mass % Predicted**	**Wet Mass Predicted [kg]**	**Current Best Estimate [kg]**	**% Allotted Mass Used**
Fuel - Hydrazine	N/A	N/A	N/A	N/A	N/A	N/A	28.68%	350	350	100.00%
Fuel - Xenon	N/A	N/A	N/A	N/A	N/A	N/A	4.65%	56.7	41	72.31%
Comms	6.00%	5.36%	41.51	42.76	43.61	48	3.75%	43.61	36.1	72.25%
Bus - Structure	26.00%	23.24%	168.30	180.08	189.09	208	15.49%	189.09	168	80.77%
Bus - Thermal	5.00%	4.47%	32.37	34.64	36.37	40	2.98%	36.37	32	79.99%
Bus - Power	22.00%	19.67%	142.45	152.42	160.04	176	13.11%	160.04	142	80.66%
Bus - Attitude Determination	6.00%	5.36%	38.82	41.53	43.61	48	3.57%	43.61	38	79.21%
Bus - Propulsion	12.00%	21.34%	154.54	165.36	173.63	191	14.23%	173.63	155.90	81.63%
Inst. - Payload	14.00%	12.52%	96.96	99.87	101.87	112	8.35%	101.87	42.47	37.90%
Bus - Processing	3.00%	2.68%	19.41	20.77	21.81	24	1.79%	21.81	19.00	79.21%
Allocated Margin	6.00%	5.36%	38.82	41.53	43.61	48	3.57%	43.61	0	0.00%
Total	**100.00%**	**100.00%**	**733.18**	**698**	**814**	**895**	**100%**	**1220.34**	**1024.47**	**83.95%**

Table 6.6: Power Budget for Spacecraft Including Margins, cont.

	Power % Allowed (SMAD)	Power % Allowed (adjusted for SEP)	Basic Power [W]	Design Power Limit [W]	Manufacturing Power Limit [W]	Current Power [W]	% Allotted Power Used
Fuel - Hydrazine	N/A	N/A	N/A	N/A	N/A	N/A	N/A
Fuel - Xenon	N/A	N/A	N/A	N/A	N/A	N/A	N/A
Comms	20.00%	4.16%	362.42	398.67	478.40	277.50	69.61%
Bus - Structure	1.00%	0.21%	18.12	19.93	23.92	18.00	90.30%
Bus - Thermal	18.00%	3.74%	326.18	358.80	430.56	326.00	90.86%
Bus - Power	10.00%	2.08%	181.21	199.33	239.2	181.00	90.80%
Bus - Attitude Determination	12.00%	2.50%	217.45	239.20	287.04	217.00	90.72%
Bus - Propulsion	12.00%	81.70%	7117.45	7829.20	9395.04	7117.00	90.90%
Inst. - Payload	16.00%	3.33%	289.94	318.93	382.72	74.80	23.45%
Bus - Processing	11.00%	2.29%	199.33	219.27	263.12	199.00	90.76%
Allocated Margin	0.00%	0.00%	0.00	0.00	0.00	0.00	0.00%
Total	100.00%	100.00%	8712.12	9583.33	11500	8410.30	87.76%

6.2 Master Equipment List

The Master Equipment List (MEL) contains information on each individual component of the spacecraft. For ease of inclusion it has been split into two broad categories: a qualitative section which lists the function, requirement satisfied, and heritage of the equipment; and a quantitative section which lists the dimensions, power, mass, data budget, cost estimate, and thermal requirements.

Table 6.7: Qualitative Master Equipment List

	Functionality	Requirement(s) Satisfied	Heritage
Instrumentation			
LORRI	Panchromatic imaging	PLD.2; PLD.3	New Horizons, Lucy
Ralph	Color and spectral imaging	PLD.1; PLD.4	New Horizons, Lucy
TES	Thermal Imaging	PLD.8	OSIRIS-REx, Lucy
RRT	Internal structure mapping	PLD.5 - PLD.7	None
LNAC			
Solar Electric Propulsion System (thruster + tank)	Delta V for orbital plane change, phasing burn, station keeping	LNAC.1; LNAC.4	Dawn
Xenon Propellant	SEP Propellant	LNAC.1; LNAC.4	Dawn
Hydrazine Propellant	Chemical propulsion for final velocity match maneuver	LNAC.1	Standard LEOStar-3 feature
Falcon 9	Launch Vehicle	LNAC.3	Extensive
Bus			
LEOStar-3 Bus	Provides structure	SB.1 - SB.7	Dawn, Deep Space 1
Solar Panels (x2)	Provides power	SB.6	Extensive
Comm			
Ultrastable oscillator (x2)	Part of RF system	CD.1	Extensive
K_a Band High Gain Antenna	Primary comms	CD.1	Kepler, others
K_a Band Waveguide	Guides waves	CD.1	Kepler, others
K_a Band TWTA (x2)	K_a band amplifier	CD.1	Kepler, others
K_aBand Exciter (x2)	K_a band modulation	CD.1	Kepler, others
X Band Low Gain Antenna(x2)	Redundant comms	CD.1 - CD.3	Extensive
X Band Cables	Part of RF System	CD.1 - CD.3	Extensive
x Band Switching Network (x2)	Controls comms mode	CD.1 - CD.3	Extensive

X Band Diplexer (x2)	Part of RF system	CD.1 - CD.3	Extensive
X Band TWTA (x2)	X Band amplifier	CD.1 - CD.3	Extensive
X Band Transponder (x2)	Modulation and demodulation	CD.1 - CD.3	Extensive

Table 6.8: Quantitative Master Equipment List

	Dimensions [cm]	Power Input[W]	Mass [kg]	Data Output [Mbps]	Cost Estimate [thousands of $]	Thermal Requirement Survival (Deg C)	Thermal Requirement Operational (Deg C)
Instrumentation							
LORRI	27.7x 27.7x 61.5	15	8.6	1.575 (Total:18.1 Gb)	14,900		Electronics: 0 to 40 CCD: -125 to 40 (ideal <70)
Ralph	49.5x 40.6x 29.5	8	10.5	1.65 (Total: 1.8Gb)	12,000		Electronics: 0 to 40 Leisa CCD: ideal -140 MVIC CCD: Ideal -98
TES	37.5x 28.9x 52.2	10.8	6.27	.0072 (Total: 5.28Gb)	10,100	-25 to 55	w/in spec: 10 to 40 out of spec: -15 to 45
RRT	166x 30	41	5.5	1.16	25,000	-120 - 120	-100 - 100
RRT Electronics Box	45x 37x 19	Included in RRT	11.6				
LNAC							
Solar Electric Propulsion System (thruster + tank)	30x 30x 60	6900 (included in Bus)	95.9 (included in Bus)		1,000		
Xenon Propellant	30x 30x 60x	0	120		160		

Hydrazine Tanks	71x 71x 71	217 (included in Bus)	60 (included in Bus)				
Hydrazine Propellant	71x 71x 71	0	165.3		11.7		
Falcon 9	N/A	N/A	N/A	N/A	60,000		
Bus							
LEOStar-3 Bus	360x 180	8058	554.9	0	130,000		
Solar Panels (x2)	216x 216x 2	- 10525.9	included in Bus	0	included in Bus		
Comm							
SDST (x2)	18.1x 16.6x 11.4	19.5	6.4	0	3,955.2	-120 - 120	-40 - 60
Ultrastable Oscillator (x2)	7.62x 7.62 x 16.7	5	3.5	0	2,163	-28 - 90	0 - 55
Diplexer (x2)		0	.8	0	494.4	-120 - 120	-100 - 100
X TWTA		172	1.7	0	1,050.6	-120 - 120	-100 - 100
K_a TWTA		81	.8	0	494.4	-120 - 120	-100 - 100
X Power Converter (x2)		0	3	0	1,854	-120 - 120	-100 - 100
K_a Power Converter		0	1.5	0	927	-120 - 120	-100 - 100
Misc. Microwave		0	1	0	618	-120 - 120	-100 - 100
Waveguides and Coax		0	8.3	0	5,129.4	-120 - 120	-100 - 100
Switches (x5)		0	2.2	0	1,359.6	-120 - 120	-100 - 100
Toroidal Low Gain Antenna		0	1.9	0	1,174.2	-120 - 120	-100 - 100
Low Gain Antenna (x2)		0	1	0	618	-120 - 120	-100 - 100

High Gain Antenna		0	4	0	2,472	-120 - 120	-100 - 100
Totals		-2116.6	918.77		275,469.8		
Including Management Reserve 15%		-1799.1	1056.6				

6.3 Programmatic Risk

Of the previously defined subsystems risks, a few elements have both a unique risk to our mission and risk level significant to the systems level. These risks are graphed in the Figure below and described more fully in the two following sections: Functional and Political.

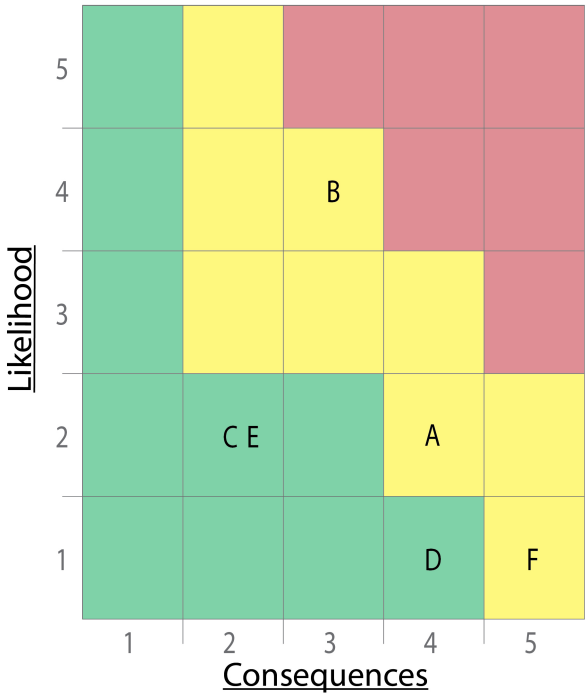

Figure 6.1: A - RRT Instrumentation Failure, B - Time Sensitivity for Launch, C - Science Product Risk, D - Asteroid Breaks Apart During Event, E - Post-Event Orbital Characteristic, F - Collision with Asteroid During Operations. The red regions indicate implement new process or change system, yellow regions indicate aggressively manage or consider change, and the green indicates ongoing monitoring

6.3.1 Functional

A - RRT Instrumentation Failure

This risk encapsulates those described in the Instrumentation sections including RRT antenna deployment failure, component burnout, and moment imparted to craft during deployment. This risk is highlighted at

a system level due to the low heritage of the instrument, and the history of deployment on highly tested instruments failing.

Mitigation Strategy: Design and on the ground testing are the primary methods of mitigation that should be pursued for this risk.

B - Time Sensitivity for Launch

The launch window to arrive at Apophis a year before the event is sizable, but if this window were to be missed, the Mission Objectives would be severely compromised. The following launch window would allow only a month of characterization time before the event which would most notably reduce our opportunity to accomplish M.O.2. We would still be able to accomplish the two other Mission Objectives.

Mitigation Strategy: This risk will be aggressively managed in the development schedule to work out any delays from fabrication and design. The launch will then be affected primarily by the weather and launch vehicle funding which are outside of the scope of this study.

C - Science Product Risk

There are many questions currently about what will actually take place during the flyby event from a scientific standpoint. This risk comes from the possibility that the asteroid does nothing or the effects are finer than our system requirements demand we achieve as it passes by. While this still would provide a wealth of new knowledge on asteroids and the Yarkovsky effect, the effects of tidal forces, one of the primary reasons this mission and why this event are so unique, would not gain as much new knowledge.

Mitigation Strategy: This risk cannot be solved on the ground short of researching the level of detail at which we must measure in order to see all the effects of the event.

D - Asteroid Breaks Apart During Event

There is a small risk that the asteroid breaks apart during the event as was seen with Shoemaker-Levy 9 on Jupiter. While this is highly improbable, the result could cause damage to the spacecraft, loss of mission objectives, or a rapid re-evaluation of the operations as we would have to modify orbit to follow a single piece. The loss of mission objectives would be slightly acceptable due to byproducts of breaking apart such as the high resolution imaging occurring of an extremely rare event such as this and the interior structure would be exposed and separate providing more in-depth fracture information than our RRT experiments.

Mitigation Strategy: This risk is mitigated by operational adaptation once the initial characterization and assessment has occurred. The spacecraft will need to be a safe distance away during the event.

E - Post-Event Orbital Characteristic

This risk is the most likely to occur of all previously mentioned. Following the Earth flyby event the orbital characteristics of the asteroid are unknown. If the obliquity is near 90 degrees, pointing toward the sun, the stationkeeping will require more fuel and the risk of drifting to collision will increase during the RRT characterization period.

Mitigation Strategy: This risk will be primarily dealt with through margin. The time margin following the event is sizable, up to three years, meaning a more distant orbit could be used, reducing the proximity and increasing the orbital period.

6.3.2 Political

F - Collision with Asteroid During Operations

Throughout the entire mission development to this point, the political risk of affecting the orbit of a Potentially Hazardous Asteroid has been highlighted. Worst-case analysis has allowed us to rule out trajectory options that can have large effects on the orbit of the asteroid leading up to the 2029 Earth flyby and

subsequent close approaches.
Mitigation Strategy: The mission will be using a fail-miss approach with low closing velocities and maintaining a low escape velocity when in close orbit with the asteroid to allow easy bail-out to an escape orbit.

6.4 Projected Development Schedule and Cost

Throughout the design of the SET mission, heritage was used to buy down the risk associated with a new spacecraft mission. As a result, the spacecraft has a robust instrument suite in terms of cost and risk. A first-order analysis on the potential schedule and budget was performed.

The major subsystems selected were contracted by the following companies for their respective missions:

Table 6.9: Contractors for Previous Missions

Subsystem	**Contractor**
RRT Instrument	Northrop Grumman/Astro Aerospace
TES	Moog, NASA Goddard, Arizona State
LORRI	Johns Hopkins University Applied Physics Laboratory
Ralph	Ball Aerospace
NEXT-C	Aerojet Rocketdyne
LEOStar-3	Orbital ATK
Hydrazine Thrusters	Airbus Space & Defense
Antennas	General Dynamics & Orbital ATK

Based on these, we can baseline our spacecraft cost estimates, and the option of a competitive contract for an instrument may also reduce the cost.

Based on the NASA project management handbook and the OSIRIS-REx mission timeline [16], the following projected life cycle was developed:

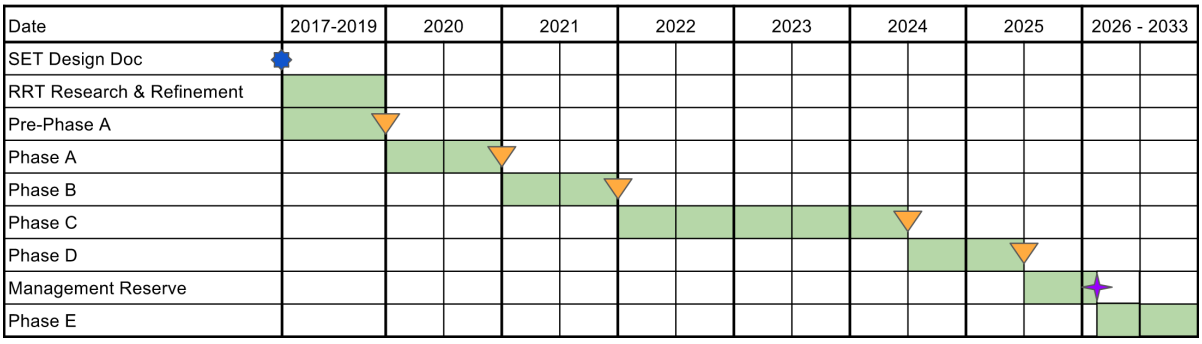

Figure 6.2: Projected Life Cycle, by NASA Mission Phase

The proposed timeline is 68 months, and 12 months of management reserve are available if the project begins in January 2020. These dates take into account the maximum build time from Orbital ATK for the LEOStar-3 bus[74], and allows time to develop and improve the instruments as necessary to fulfill mission requirements.

Based on the Master Equipment List (Figure 6.8), we project the cost of the spacecraft to be $320 million. Based on the USCM8 Cost Estimation Relationships, and a 15% management reserve to account for the

current TRL of the instruments**??**, this results in a program cost of $800 million. The projected breakdown of cost by phase is below. Some underlying assumptions that were made included applying program cost and overhead cost evenly by year. This will result in a skewed cost rollup towards phases A and B, because the overhead will reasonably increase during phase C due to the need for additional facilities for flight hardware.

Table 6.10: Estimated Total Cost

Item	Description	Cost (2016 $K)	Est. Error	Source
SET Spacecraft	Estimated cost of the spacecraft	275,469.8	10%	MEL
I&T	Integration and Testing Cost	41,790.4	37%	[36]
Program Cost	Estimated Program Cost	106,505.7	40%	[36]
Aerospace Ground Equipment	Estimated Ground Equipment cost	216,098.4	37%	[36]
Overhead	50% Overhead rate	222,687.9	50%	
15% Management Reserve	Based on TRL's of Instruments	100,209.6	N/A	[62]
Total		768,273	23.36%	

The SET mission projects a similar cost to that of OSIRIS-REx[56], and has a flexible schedule in Phase C pending more information about the build time of the various subsystems from their respective vendors. The similarity to OSIRIS-REx provides some confidence in our cost model.

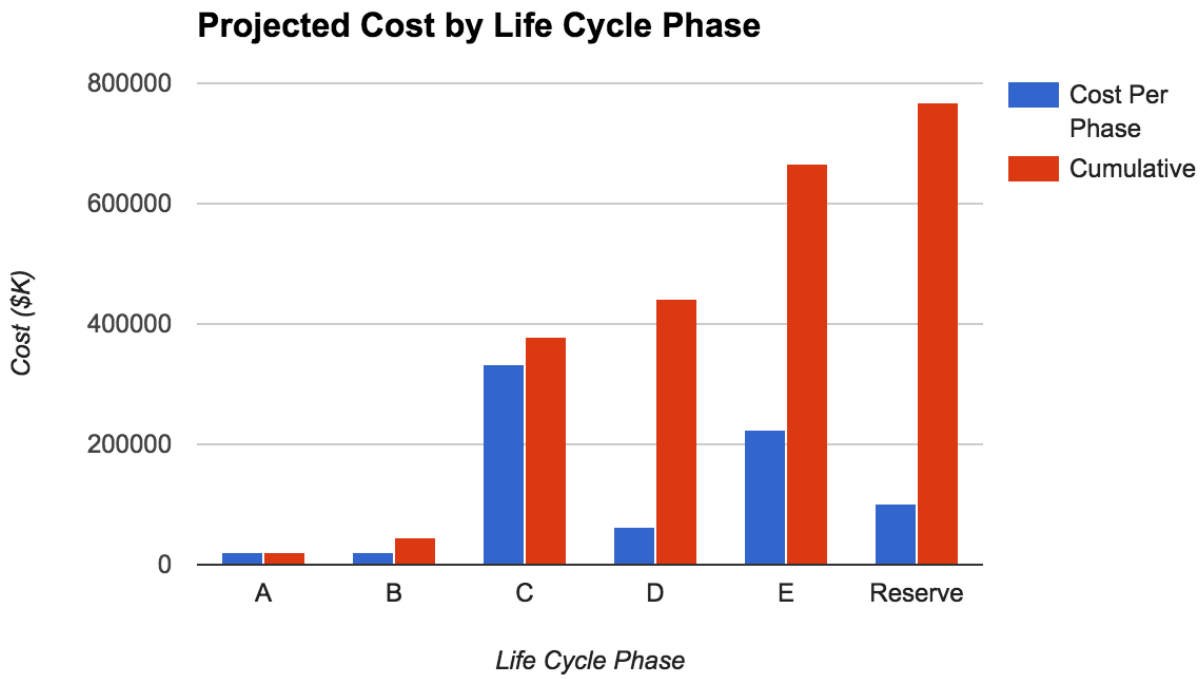

Figure 6.3: Life Cycle Cost breakdown, assuming even distribution of overhead and program cost.

Chapter 7

Conclusion

Project SET will accomplish our mission objectives for the Apophis opportunity by observing Apophis before, during, and after an encounter with Earth on April 13, 2029. By leveraging commercial options and flight-proven instruments, we propose a single-satellite instrument suite contracted by Orbital ATK and launched by in August 2026 to inform our knowledge of the structure and composition of NEOs while decoding the Yarkovsky effect. Based on our analysis, we have a projected cost of $275 million dollars for the spacecraft, and $768 million dollars accounting for overhead and operational costs.

Bibliography

[1] *99942 Apophis (2004 MN4)*. URL: https://ssd.jpl.nasa.gov/sbdb.cgi?sstr=99942;cad=1.

[2] Accion Systems. *Tile*. URL: http://www.accion-systems.com/tile/.

[3] AIAA and The International Society of Allied Weight Engineers. *American National Standard Mass Properties Control for Space Systems*. electronic. 2015.

[4] Airbus Defense and Space. *Eurostar Series*. 2015. URL: https://airbusdefenceandspace.com/our-portfolio/space-systems/telecommunications-satellites/eurostar-series/.

[5] United Launch Alliance. *Atlas V Launch Services User's Guide*. 2010.

[6] United Launch Alliance. *Delta IV Launch Services User's Guide*. 2013.

[7] Arianespace. *Ariane 5 User's Manual*. 2016.

[8] M Antonietta Barucci et al. "The flybys of asteroids (2867) Šteins,(21) Lutetia, and (4179) Toutatis". In: *et al., Asteroids IV, Univ. of Arizona, Tucson* (2015), pp. 433–450.

[9] Richard H Battin. *An introduction to the mathematics and methods of astrodynamics*. Aiaa, 1999.

[10] M. J. S. Belton. *Mitigation of hazardous comets and asteroids.* Cambridge ; New York : Cambridge University Press, 2004., 2004. ISBN: 0521827647. URL: https://search.ebscohost.com/login.aspx?direct=true&db=cat00916a&AN=mit.001339107&site=eds-live&scope=site.

[11] Scott W Benson, John P Riehl, and Steven R Oleson. "NEXT Ion Propulsion System Configurations and Performance for Saturn System Exploration". In: *The 43rd AIAA/ASME/SAE/ASEE Joint Propulsion Conference and Exhibit* (2007), pp. 1–15. URL: https://ntrs.nasa.gov/archive/nasa/casi.ntrs.nasa.gov/20080006604.pdf.

[12] Edward Beshore et al. "The OSIRIS-REx asteroid sample return mission". In: *IEEE Aerospace Conference Proceedings* 2015-June.520 (2015). ISSN: 1095323X. DOI: 10.1109/AERO.2015.7118989.

[13] R. P. Binzel et al. "Earth encounters as the origin of fresh surfaces on near-Earth asteroids". In: *Nature* 463 (Jan. 2010), pp. 331–334. DOI: 10.1038/nature08709.

[14] R. Bitten and S. A. Shinn. *Historical Mass, Power, Schedule, and Cost Growth for NASA Science Instruments*. Tech. rep. Big Sky, MT: IEEE Aerospace Conference, 2014.

[15] Blue Canyon Technologies. *XACT*. URL: http://bluecanyontech.com/xact/.

[16] Michael P Blythe et al. "NASA Space Flight Program and Project Management Handbook". In: (2014).

[17] Boeing. *Boeing Satellite Family*. 2017. URL: http://www.boeing.com/space/boeing-satellite-family/.

[18] Robert S. Bokulic and Christopher C. DeBoy. "Space Mission Engineering: The New SMAD". In: Hawthorne, CA: Microcosm Press, 2015. Chap. Communications Payloads.

[19] S. J. Bus et al. "Bus-DeMeo Taxonomy: Extending Asteroid Taxonomy Into The Near-infrared". In: *AAS/Division for Planetary Sciences Meeting Abstracts #40*. Vol. 40. Bulletin of the American Astronomical Society. Sept. 2008, p. 440.

[20] *Celestrak Software*. URL: https://celestrak.com/software/vallado-sw.asp.

[21] A. F. Cheng et al. “Long-Range Reconnaissance Imager on New Horizons”. In: *Space Science Reviews* 140 (Oct. 2008), pp. 189–215. DOI: 10.1007/s11214-007-9271-6. arXiv: 0709.4278.

[22] AF Cheng et al. “Long-range reconnaissance imager on New Horizons”. In: *Space Science Reviews* 140.1-4 (2008), pp. 189–215.

[23] S. R. Chesley et al. “Direct Detection of the Yarkovsky Effect by Radar Ranging to Asteroid 6489 Golevka”. In: *Science* 302 (Dec. 2003), pp. 1739–1742. DOI: 10.1126/science.1091452.

[24] P. R. Christensen et al. “Mars Global Surveyor Thermal Emission Spectrometer experiment: Investigation description and surface science results”. In: *Journal of Geophysical Research* 106 (Oct. 2001), pp. 23823–23872. DOI: 10.1029/2000JE001370.

[25] P. R. Christensen et al. “Morphology and Composition of the Surface of Mars: Mars Odyssey THEMIS Results”. In: *Science* 300 (June 2003), pp. 2056–2061. DOI: 10.1126/science.1080885.

[26] P. R. Christensen et al. “The OSIRIS-REx Thermal Emission Spectrometer (OTES) Instrument”. In: *ArXiv e-prints* (Apr. 2017). arXiv: 1704.02390 [astro-ph.IM].

[27] P. R. Christensen et al. “The Thermal Emission Imaging System (THEMIS) for the Mars 2001 Odyssey Mission”. In: *Space Science Review* 110 (Jan. 2004), pp. 85–130. DOI: 10.1023/B:SPAC.0000021008.16305.94.

[28] P. R. Christensen et al. “Thermal emission spectrometer experiment - Mars Observer mission”. In: *Journal of Geophysical Research* 97 (May 1992), pp. 7719–7734. DOI: 10.1029/92JE00453.

[29] O Coddington et al. “A Solar Irradiance Climate Data Record”. In: *Bulletin of the American Meteorological Society* 97.7 (Dec. 2015), pp. 1265–1282. ISSN: 0003-0007. DOI: 10.1175/BAMS-D-14-00265.1. URL: http://dx.doi.org/10.1175/BAMS-D-14-00265.1.

[30] Renato Croci et al. “SHARAD design and operation”. In: *Geoscience and Remote Sensing Symposium, 2007. IGARSS 2007. IEEE International*. IEEE. 2007, pp. 1611–1615.

[31] Antonio De Luca. *Architectural Design Criteria for Spacecraft Solar Arrays*. Tech. rep. Germany: VEGA Space GmbH.

[32] Earth Observation Portal. *OSIRIS-REx*. 2017. URL: https://directory.eoportal.org/web/eoportal/satellite-missions/o/osiris-rex.

[33] *ESTRACK: ESA’ S Deep Space Tracking Network*. Tech. rep. European Space Agency, 2015. URL: http://www.esa.int/Our%7B%5C_%7DActivities/Operations/Estrack.

[34] European Space Agency. *ESA Science and Technology: Jupiter Mission Contract Ceremony*. Dec. 2015. URL: http://sci.esa.int/juice/57014-jupiter-mission-contract-ceremony/.

[35] European Space Agency. *Eurostar E3000 Large Mechanical Platform Development*. Feb. 2014. URL: https://artes.esa.int/projects/eurostar-e3000-large-mechanical-platform-development.

[36] David F. Everett. “Space Mission Engineering: The New SMAD”. In: Hawthorne, CA: Microcosm Press, 2015. Chap. Overview of Spacecraft Design.

[37] D. Farnocchia et al. “Orbits, Long-Term Predictions, Impact Monitoring”. In: *Asteroids IV*. Ed. by P. Michel, F. E. DeMeo, and W. F. Bottke. 2015, pp. 815–834. DOI: 10.2458/azu_uapress_9780816532131-ch041.

[38] William M Folkner et al. “The planetary and lunar ephemerides DE430 and DE431”. In: *Interplanet. Netw. Prog. Rep* 196 (2014), p. C1.

[39] Chris Gebhardt. *U.S. debates Atlas V RD-180 engine ban, ULA’s non-bid for military launch*. Jan. 2016. URL: https://www.nasaspaceflight.com/2016/01/u-s-debates-atlas-v-rd-180-ban-ulas-non-bid-military/.

[40] Victoria Hamilton and Philip Christensen. “The OSIRIS-REx thermal emission spectrometer (OTES)”. In: *EGU General Assembly Conference Abstracts*. Vol. 16. 2014, p. 4687.

[41] A. W. Harris and G. D’Abramo. “The population of near-Earth asteroids”. In: *Icarus* 257 (Sept. 2015), pp. 302–312. DOI: 10.1016/j.icarus.2015.05.004.

[42] Caleb Henry. *NASA Awards $130 Million Landsat 9 Contract to Orbital ATK*. Oct. 2016.

[43] Daniel A. Herman. *NASA's Evolutionary Xenon Thruster (NEXT) Project Qualification Propellant Throughput Milestone: Performance, Erosion, and Thruster Service Life Prediction After 450 kg*. Nov. 2010. URL: https://ntrs.nasa.gov/archive/nasa/casi.ntrs.nasa.gov/20110000521.pdf.

[44] Daniel A. Herman. "NASA's Evolutionary Xenon Thruster (NEXT) Project Qualification Propellant Throughput Milestone: Performance, Erosion, and Thruster Service Life Prediction After 450 kg". In: November (2010), NASA/TM–2010–216816.

[45] Takahiro Hiroi et al. "Developing space weathering on the asteroid 25143 Itokawa". In: *Nature* 443.7107 (2006), pp. 56–58.

[46] Richard. Hofer and et al. *Development Approach and Status of the 12.5 kW HERMeS Hall Thruster for the Solar Electric Propulsion Technology Demonstration Mission*. July 2015. URL: erps.spacegrant.org/uploads/images/2015Presentations/IEPC-2015-186_ISTS-2015-b-186.pdf.

[47] Siegfried W Janson and Richard P Welle. "The NASA Optical Communication and Sensor Demonstration Program". In: *27th Annual AIAA/USU Conference on Small Satellites* (2013), pp. 1–10.

[48] *JPL HORIZONS Database*. URL: https://ssd.jpl.nasa.gov/horizons.cgi.

[49] John E Keesee. *Spacecraft Thermal Control Systems*.

[50] Horst Uwe Keller et al. "OSIRIS–The scientific camera system onboard Rosetta". In: *Space Science Reviews* 128.1 (2007), pp. 433–506.

[51] KK Associates. *Earth's Thermal Environment*. URL: http://www.tak2000.com/data/planets/earth.htm.

[52] Wlodek W Kofman et al. "Cosmochemical implications of CONSERT permittivity characterization of 67P/CG". In: *AGU fall Meeting 2016*. 2016, P43A–2084.

[53] Jet Propulsion Laboratory. *Technology ¿ Ion Propulsion — Dawn Mission*. URL: https://dawn.jpl.nasa.gov/technology/ion_prop.asp.

[54] D. Lauretta. "The Physical, Geological, and Dynamical Nature of Asteroid (101955) Bennu - Target of OSIRIS-REx". In: *AAS/Division for Planetary Sciences Meeting Abstracts*. Vol. 46. AAS/Division for Planetary Sciences Meeting Abstracts. Nov. 2014, p. 503.01.

[55] H. F. Levison and Lucy Science Team. "Lucy: Surveying the Diversity of the Trojan Asteroids, the Fossils of Planet Formation". In: *Lunar and Planetary Science Conference*. Vol. 47. Lunar and Planetary Science Conference. Mar. 2016, p. 2061.

[56] Lockheed Martin. *OSIRIS-REx*. 2017. URL: http://lockheedmartin.com/us/products/osirisrex.html.

[57] Antonio De Luca. "Architectural Design Criteria for Spacecraft Solar Arrays". In: (2011). URL: http://cdn.intechopen.com/pdfs/22805.pdf.

[58] S. Makham, G. C. Sun, and J. C. Bourgoin. "Modelling of solar cell degradation in space". In: *Solar Energy Materials and Solar Cells* 94.6 (2010), pp. 971–978. ISSN: 09270248. DOI: 10.1016/j.solmat.2010.01.026. URL: http://dx.doi.org/10.1016/j.solmat.2010.01.026.

[59] G. W. Marks, M. T. Reilly, and R. L. Huff. *The Lightweight Deployable Antenna for the MARSIS Experiment on the Mars Express Spacecraft*.

[60] Isodoro Martinez. "Thermo-Optical Properties". In: (), pp. 1–2.

[61] David W Miller. *Tradespace Investigation of a Telescope Architecture for Next-generation Space Astronomy and Exploration*. May 2014.

[62] David W Miller, Col John Keesee, and Mr Cyrus Jilla. *Space systems cost modeling*. 2003.

[63] H. Miyamoto et al. "Regolith Migration and Sorting on Asteroid Itokawa". In: *Science* 316 (May 2007), p. 1011. DOI: 10.1126/science.1134390.

[64] Oliver Montenbruck and Eberhard Gill. *Satellite Orbits: Models, Methods and Applications*. Springer, 2000.

[65] R Mukai et al. "Juno Telecommunications". In: *NASA DESCANSO Design and Performance Summary Series* (2012).

[66] NASA. *NASA Awards Contract for Series of CubeSat Technology Missions*. Jan. 2017. URL: https://www.nasa.gov/directorates/spacetech/small_spacecraft/feature/CubeSat_Technology_Missions.

[67] NASA Rapid Spacecraft Development Office. *Eagle Spacecraft*. URL: https://rsdo.gsfc.nasa.gov/images/catalog/Eagle.pdf.

[68] *Near Earth Network (NEN) Users' Guide*. Tech. rep. Greenbelt, MD: NASA Goddard Space Flight Center, 2016. URL: sbir.gsfc.nasa.gov/sites/default/files/453-NENUG%20R2.pdf.

[69] D. Nesvorný et al. "Evidence for asteroid space weathering from the Sloan Digital Sky Survey". In: *Icarus* 173 (Jan. 2005), pp. 132–152. DOI: 10.1016/j.icarus.2004.07.026.

[70] "NEXT Ion Propulsion System Development Status and Performance". In: July (2007), pp. 1–17. ISSN: 2007-5199. DOI: 10.2514/6.2007-5199.

[71] Osamu Nishizawa et al. "Laboratory studies of seismic wave propagation in inhomogeneous media using a laser Doppler vibrometer". In: *Bulletin of the Seismological Society of America* 87.4 (1997), pp. 809–823.

[72] Northrop Grumman. *Eagle-3*. 2013.

[73] Orbital ATK. *High Performance Green Propulsion (HGPG)*. 2015.

[74] Orbital ATK. *LEOStar-3 Bus*. 2017.

[75] Orbital ATK. "Pegasus User's Guide". In: October (2015). DOI: 10.1007/SpringerReference_27988.

[76] Orbital ATK. "UltraFlex Solar Array Systems". In: (2011). URL: https://www.orbitalatk.com/space-systems/space-components/solar-arrays/docs/FS007%7B%5C_%7D15%7B%5C_%7D0A%7B%5C_%7D3862%20UltraFlex.pdf.

[77] Peter. Peterson and et al. *NASA HERMeS Hall Thruster Electrical Configuration Characterization*. 2016. URL: https://ntrs.nasa.gov/archive/nasa/casi.ntrs.nasa.gov/20170000958.pdf.

[78] O. P. Popova et al. "Chelyabinsk Airburst, Damage Assessment, Meteorite Recovery, and Characterization". In: *Science* 342 (Nov. 2013), pp. 1069–1073. DOI: 10.1126/science.1242642.

[79] Ed Powers. *Spacecraft Thermal Design Overview*. Oct. 2015.

[80] P. Pravec et al. "The tumbling spin state of (99942) Apophis". In: *Icarus* 233 (May 2014), pp. 48–60. DOI: 10.1016/j.icarus.2014.01.026.

[81] N. E. Putzig et al. "Subsurface structure of Planum Boreum from Mars Reconnaissance Orbiter Shallow Radar soundings". In: *Icarus* 204 (Dec. 2009), pp. 443–457. DOI: 10.1016/j.icarus.2009.07.034.

[82] Nathaniel E Putzig et al. "Subsurface structure of Planum Boreum from Mars Reconnaissance Orbiter shallow radar soundings". In: *Icarus* 204.2 (2009), pp. 443–457.

[83] D. C. Reuter et al. "Ralph: A Visible/Infrared Imager for the New Horizons Pluto/Kuiper Belt Mission". In: *Space Science Reviews* 140 (Oct. 2008), pp. 129–154. DOI: 10.1007/s11214-008-9375-7. arXiv: 0709.4281.

[84] D. C. Richardson, W. F. Bottke, and S. G. Love. "Tidal Distortion and Disruption of Earth-Crossing Asteroids". In: *Icarus* 134 (July 1998), pp. 47–76. DOI: 10.1006/icar.1998.5954.

[85] Christopher T. Rusell. *Dawn*. URL: https://nssdc.gsfc.nasa.gov/nmc/spacecraftDisplay.do?id=2007-043A.

[86] A Safaeinili et al. "Probing the interior of asteroids and comets using radio reflection tomography". In: *Meteoritics & Planetary Science* 37.12 (2002), pp. 1953–1963.

[87] Paul Sava et al. "Radio reflection imaging of asteroid and comet interiors I: Acquisition and imaging theory". In: *Advances in Space Research* 55.9 (2015), pp. 2149–2165.

[88] D. J. Scheeres et al. "Abrupt alteration of Asteroid 2004 MN4's spin state during its 2029 Earth flyby". In: *Icarus* 178 (Nov. 2005), pp. 281–283. DOI: 10.1016/j.icarus.2005.06.002.

[89] D. J. Scheeres et al. "Effects of Gravitational Interactions on Asteroid Spin States". In: *Icarus* 147 (Sept. 2000), pp. 106–118. DOI: 10.1006/icar.2000.6443.

[90] Schmidt et al. *The NASA Evolutionary Xenon Thruster (NEXT): The Next Step for U.S. Deep Space Propulsion*. 2008.

[91] George R. Schmidt, Michael J. Patterson, and Scott W. Benson. *The NASA Evolutionary Xenon Thruster (NEXT): The Next Step for U.S. Deep Space Propulsion*. 2008. URL: https://ntrs.nasa.gov/archive/nasa/casi.ntrs.nasa.gov/20080047732.pdf.

[92] Peter B Selding. *Astrium Picked To Build DirecTV 15 Telecom Satellite*. 2011. URL: http://spacenews.com/astrium-picked-build-directv-15-telecom-sate.

[93] Carl Shenk. *Vibration Testing*. DOI: 10.1016/0301-679X(78)90120-2.

[94] Amy Simon. *THE OSIRIS-REX VISIBLE AND NEAR-IR SPECTROMETER (OVIRS) – MEASURING THE CHEMISTRY AND REFLECTANCE OF BENNU*. May 2014. URL: https://dslauretta.com/2014/05/28/the-osiris-rex-visible-and-near-ir-spectrometer-ovirs-measuring-the-chemistry-and-reflectance-of-bennu/.

[95] Rabindra Singh, Ed Pentaleri, and Kent M. Price. "Space Mission Engineering: The New SMAD". In: Hawthorne, CA: Microcosm Press, 2015. Chap. Communications Payloads.

[96] Stephen D. Slobin. *DSN Telecommunications Link Design Handbook; 34-m BWG Stations Telecommunications Interfaces*. Tech. rep. Pasadena, CA: NASA Jet Propulsion Laboratory, 2015. URL: https://evt.grc.nasa.gov/rfp-industry-briefing-2016/wp-content/blogs.dir/52/files/sites/10/Deep-Space-Network-Telecommunications-Link-Design-Handbook-810-005.pdf.

[97] John Steven Snyder, Thomas M Randolph, and Damon F Landau. "Power and Propulsion System Design for Near-Earth Object Robotic Exploration". In: August (2011), pp. 1–16.

[98] J. Souchay et al. "Rotational changes of the asteroid 99942 Apophis during the 2029 close encounter with Earth". In: *Astronomy and Astrophysics* 563, A24 (Mar. 2014), A24. DOI: 10.1051/0004-6361/201322364.

[99] J. S. Sovey, V. K. Rawlin, and M. J. Patterson. *NASA Solar Electric Propulsion Technology Application Readiness (NSTAR)*. Apr. 2009. URL: https://www.grc.nasa.gov/WWW/ion/past/90s/nstar.htm.

[100] "Space Based Infrared System Geosynchronous (GEO-1) Thermal Vacuum Testing". In: ().

[101] *Space Technology Game Changing Development: Deep Space Optical Communications (DSOC)*. Tech. rep. NASA, 2015. URL: https://www.nasa.gov/sites/default/files/atoms/files/fs%7B%5C_%7Ddsoc%7B%5C_%7Dfactsheet%7B%5C_%7D150910.pdf.

[102] SpaceX. *Falcon 9 Launch Vehicle Payload User's Guide*. 2013.

[103] SpaceX. *Launch Manifest*. 2017. URL: www.spacex.com/missions.

[104] SpaceX. *SES-10 Launch - world's first reflight of an orbital class rocket*. Mar. 2017. URL: https://www.flickr.com/photos/spacex/33616913981/.

[105] *Speaking in Phases*. 2001. URL: https://www.jpl.nasa.gov/edu/teach/activity/speaking-in-phases/.

[106] Marc-Jean Stephan. "Electric Propulsion Activities for Eurostar 3000". In: *Spacecraft Propulsion, Third International Conference* (Dec. 2000). URL: http://adsabs.harvard.edu/full/2000ESASP.465...81S.

[107] Jim Taylor. "Dawn Telecommunications". In: *NASA DESCANSO Design and Performance Summary Series* 13 (2009).

[108] Jim Taylor, Dennis K Lee, and Shervin Shambayati. "Mars Reconnaissance Orbiter Telecommunications". In: *NASA DESCANSO Design and Performance Summary Series* (2006).

[109] California Polytechnic State University. "6U CubeSat Design Specification Rev . PROVISIONAL". In: Rev. Provisional (2016). URL: http://static1.squarespace.com/static/5418c831e4b0fa4ecac1bacd/t/573fa2fee321400346075f01/1463788288448/6U%7B%5C_%7DCDS%7B%5C_%7D2016-05-19%7B%5C_%7DProvisional.pdf.

[110] JL Van Noord. "NEXT Ion Thruster Thermal Model". In: July (2010), pp. 1–21. ISSN: 2007-5218. URL: http://arc.aiaa.org/doi/pdf/10.2514/6.2007-5218.

[111] James D Walker et al. "Scale size effect in momentum enhancement". In: *Procedia Engineering* 58 (2013), pp. 240–250.

[112] James R. Wertz, David F. Everett, and Jeffery J. Puschell. "Space Mission Engineering: The New SMAD". In: Hawthorne, CA: Microcosm Press, 2015. Chap. Mass and Power Distribution for Spacecraft.

[113] Y. Yu et al. "Numerical predictions of surface effects during the 2029 close approach of Asteroid 99942 Apophis". In: *Icarus* 242 (Nov. 2014), pp. 82–96. DOI: 10.1016/j.icarus.2014.07.027. arXiv: 1408.0168 [astro-ph.EP].

Appendix A

Model-Based Systems Engineering Approach

A.1 MBSE Approach and Product

The SET project implemented a digital system model as part of a movement towards a Model-Based Systems Engineering (MBSE) approach in the MIT Space Systems Engineering course. Generally, the goal of an MBSE model is to represent the system, its requirements, and their satisfaction in a consolidated format. The fidelity of a system model may vary, depending on the scope and goals of the modelling effort. Ultimately, model creation benefits the project through centralized information, consistent organization, and the opportunity to automate.

The SET MBSE model was created in Cameo Systems Modeler, software built on the industry-standard Systems Modelling Language (SysML). Users create and interact with the model through a primarily-graphical interface which depicts objects and connections. "Blocks" are the fundamental unit of the model which can be assigned to nearly any level or type of component. Values or parts can be assigned to blocks and values can also be assigned to parts where appropriate. Connections of various types are formed between blocks, values, or parts. Requirements are a separate section of the model and have their own specific building block called, appropriately, requirements. Special types of relations can be formed between requirements and the rest of the model to denote requirement satisfaction by model components. Additional component types may be integrated such as activities which are discussed in the section on future applications. Nonetheless, the model and its outputs are built largely from humble components.

The project's duration determined the level of fidelity achieved by the MBSE model. From the discussed components of the model – blocks, values, parts, requirements, and connectors – the MBSE model includes:

- Requirements and requirement derivation/satisfaction relationships
- Structural diagrams including system components and interfaces
- Component properties and parametric roll-ups of system values in various states
- And a representation of the mission's CONOPS with component associations

In addition to housing the elements and relations which define the model, Cameo Systems Modeler generated summary diagrams and tables, which aid in representing and evaluating the system as a whole.

A.1.1 Applications

This section will take the previous section's discussion of the components of the model and use that to outline what can and has been done with the model in its current form. It will walk through the model's contributions to the requirements, the structural and functional diagrams, the CONOPS, and the master equipment list. In each case a brief discussion of how the model differs from traditional systems engineering

will be included, as well as notable pros and cons. The section concludes with a list of the tables and diagrams created by the model.

Requirements

The model was first applied to the organization of requirements. As the project progressed, the requirements underwent several iterations that, in turn, affected the flow down from system requirements to subsystem requirements to equipment. At each turn, the updated requirements and their derivation relationships were incorporated into the model. The exercise of explicitly stating the requirement derivation relationships was useful in documenting the information, as well as presenting it in a holistic context for evaluation. For example, this revision utility led to the rephrasing of M.O. 2 from seismologically-inclined language to the current wording, which widened the design space for internal structure determination methods.

A SysML "derive requirements matrix" was implemented in the model to create and update the connections between system and subsystem requirements. This tool allowed for the viewing and editing of all connections between the two requirements levels at once and facilitated derivation verification –that is, ensuring that all subsystem requirements are derived from system-level requirements, and that there were no system requirements without derived subsystem requirements.

A related "satisfy requirements matrix" was used to perform a similar task with respect to requirements and equipment. This analysis verified that all requirements were satisfied by at least one piece of equipment and that no equipment was included that did not satisfy any requirements. For instance, the analysis proved useful in identifying a system requirement that specified a need for automation on the part of spacecraft. The matrices indicated that the automation requirement did not link to any subsystem requirements or equipment. This prompted a reevaluation of the need for that system level requirement and eventually led to its removal. A similar assessment resulted in the incorporation of a thermal imaging requirement (now SYS.9) since the TES instrument did not link directly to any requirements.

Structural and Functional Diagrams

The system's structural and functional diagrams are main staples of the MBSE model. Both diagrams represent components of the system and the physical links between them. The distinction lies in emphasis: a structural diagram emphasizes a specificity hierarchy while a functional diagram makes explicit the connections between the components.

One of the key benefits of model based systems engineering via SysML is its graphical interface, meaning that much of the work required to create structural and functional diagrams is completed in the process of constructing the model itself (i.e. the components and connections). In this area, the model offers the advantage that if a part needs to be replaced that action can be performed directly in the diagram and will be reflected everywhere that part is referenced. A difficulty of the model that became apparent here was the challenge of dealing with different levels of abstraction. That is, it is organizationally useful to have a block named "Payload" which links all the instruments on the spacecraft to the bus. However, that instrumentation block would be logically placed between the spacecraft bus and each instrument, meaning that the instruments are not directly linked to the bus in the model. The only way discovered to include both sets of information would be duplicate structural diagrams, one which contains multiple levels of abstraction and one which does not, which might lead to its own set of problems. Fortunately, duplicate structural diagrams were not required in this case, but if the project were to move forward it may be beneficial to include both.

Using the components created for the structural diagram, it is possible to create the functional diagrams for power consumption and data flow across different parts of the spacecraft. Each component has its own value properties for parameters such as power consumption and data usage, if applicable. The functional diagram contains connections between values of the same type that are present in different components. For instance, the instrumentation receives power from the power management and handling component so there would be a link between the two. By displaying all the connections of a given type it is possible to visualize the entire power or data system in a single image. The image can then be used to quickly verify that all components that require power are connected to the power system. The benefit of the model in this case is that it would allow for the specification of the connection type down to the precise wires and ports required, if that information exists. Additionally, as with structural diagrams, a change in one of the components will

automatically be reflected in the diagram. One of the downsides of the model in this case is that initial form of the functional diagram is not easily readable or presentable. For this reason, earlier iterations of the functional diagram were given to another member of the team for data visualization improvements. The latest version of the functional diagram demonstrates that with significant effort it can be made readable, but that it will generally not be presented in the optimal form for successful information transfer.

Instances and Parametrics

A useful area of the model, and one which especially stands out compared to traditional systems engineering, is the way in which it deals with the parameter values of the equipment through a tool called an instance. Similar to traditional systems the model includes values for the power, mass, data, and price of spacecraft components. However, instances also allow for two key uses of the parameter values of equipment.

To begin, an instance is the model's representation of a particular state or mode of the system. Part of the value of the model lies in the creation of an instance for each phase of the mission. Some examples of instances are science and safe modes. The instances of these time period will reflect which equipment is required – scientific instruments, communication systems etc. – and which is not required. By having an instance for each phase of the mission, it becomes possible to track exactly equipment usage across the entire mission. Since these instances use the underlying structure of the model, a change to a piece of equipment will be reflected in each instance in the model. If, for instance, the mission switched from K_a-band to X-band as the primary communication system, that change could be made at the level of the structural diagram and, if done properly, would automatically propagate through all instances.

Instances also enable the use of parametric diagrams, which allow the specification of calculations from value properties within the model. Thus, system values can be computed by expressing equations in "constraint" blocks and solving them using Paramagic, a plug-in for Cameo Systems Modeler. Though parametric possibilities abound, mass and power "roll-ups" (i.e. sums) appear to be the most useful and simple, and thus were implemented in the model for any given mode. Though components' property values (such as power consumption) are set to their maximum value by default, an instance overrides the default value to represent the relevant mode.

To make clear how the model operates in this context, it is useful to step through an example. Consider a post-arrival, pre-event, science imaging mode instance. Though several systems are active at that time, the solar electric propulsion system and the RALPH instrument illustrate the point. In that instance, the solar electric propulsion power consumption is set to zero because it is not in use. This does not change the default power consumption of the solar electric propulsion and it allows for a summation of power consumption that does not go over-budget by including equipment that is not in use. Now consider the use of RALPH in that instance. Without further specification, the default consumption value is assumed. If that default value is changed, the power consumption of RALPH in the instance will automatically change. However, in a hypothetical scenario where the maximum power consumption of RALPH remained constant but the amount of power it consumed in this particular instance changed, then it would be necessary to change that manually in the instance. The value of RALPH's power consumption in the instance would then be a separate value from RALPH's default power consumption and would have to be updated independently. From this example, it is clear that the model in its current form is most useful when equipment is either running at maximum or off, but that it is less useful with gradations. Despite this limitation, the capacity to track parameters through different mission phases is a very useful one and one of the significant contributions of model-based systems engineering.

CONOPS

The model also contributed to the creation of the CONOPS. As with a traditional CONOPS it details the stages of the mission and what operations will be conducted during those stages. The traditional CONOPS provide an excellent overview of the mission as a whole, however, the model offers a significant improvement in linking the operations in the CONOPS with the equipment that will complete that operation. As an example, consider the "cruise" stage of the mission, in which the spacecraft will travel to Apophis. In the model, this stage is represented by a package titled "Cruise" containing the stage's components, such as the plane and period changes necessary to travel to Apophis. Each component is then linked to a piece of equipment. For example, plane changes are linked to the solar electric propulsion system. This helps ground

the CONOPS in the physical mission equipment and helps guarantee that spacecraft has the necessary equipment to complete each phase of the mission.

Master Equipment List

The relationship between the master equipment list and the model is an interesting one. Naturally, all the information in the master equipment list should be present in the model so it should be a trivial task to produce the master equipment list from the model. However, prior to inputting the equipment information into the model it was necessary to compile the information in a single spreadsheet to make entry easier. That document simply became the master equipment list. Moving forward the model is certainly capable of producing a master equipment list but, as of yet, it has not been called upon to do so. A related reason for this is that the model requires special software to open and change while a simple cloud-shared spreadsheet can be viewed and edited by the entire team and was therefore more appropriate.

List of Diagrams and Tables related to MBSE

1. Requirements list, maps, and matrices
2. Structural, functional block diagrams
3. Structural satisfaction matrices
4. CONOPS and structural association matrices
5. Parametric instances and diagrams
6. Master Equipment List
7. Modes/Functionality Table

A.2 Potential Applications

There are two broad categories into which potential future uses of a SysML model fall: expansions of current applications and entirely novel components or applications. Both are worth discussing, though naturally expansions can be discussed in greater detail.

A.2.1 Expansions

One key area for expansion of the model's capabilities lies within Cameo Systems Modeler's powerful plugins. Currently, the model utilizes only one plugin, ParaMagic, which performed the parametric calculations discussed in the previous section. This plugin could also be used to perform calculations on other useful parameters such as thermal state or data usage. These calculations were not included in the current iteration due to their relative complexity, i.e. both would require calculations beyond simple addition, but are within the capabilities of the ParaMagic plugin.

More broadly, Cameo Systems Modeler allows for the use of a wide variety of plugins to increase the utility of the model. One group of plugins that appear especially promising for communication purposes enable Cameo to interact with Microsoft Excel. The CSV import plugin would add in creating the model while the Excel Import Plugin, despite its name, enables the export of model components to Excel. If both plugins could be made operational it would greatly speed the creation of the project and similarly aid in communicating outputs of the model in a ubiquitous format.

Beyond plugins, there are expansions to the model itself that would be useful if the project were to continue. One of the strengths of Cameo is its capacity to organize systems down to the smallest component. This level of detail was not required in this project due both to its short time frame and to the level fact that this information often was not available. However, future editions of the model would likely contain the precise equipment in each component. This would include, for example, both the structural nuts and bolts that make up the physical construction and the wires and ports of the power system.

A.2.2 Novel Applications and Components

There are a number of diagram types that the model is capable of creating that were not used in this case, partially because it was beyond the scope of this project to apply all of them. However, one that stood out as especially potentially useful was an Activity Diagram. An Activity Diagram is meant to represent the completion of internally generated actions. It would likely be beneficial to create an activity diagram for each of the positional blocks present in the CONOPS. So, for instance, station keeping would have its own activity diagram that details the firing of the propulsion, the communication with ground systems, and all the other steps that would be necessary for the spacecraft to complete a station keeping operation. This diagram would then be linked to the appropriate CONOPS block so that a user could view the CONOPS and immediately navigate to the activities involved in a given step.

Moving from novel components in the model to novel applications for its use, one area demands greater development: communication of the contents of the model. While creating the model for this project the MBSE team repeated ran into difficulties in communicating relevant parts of the model. Direct outputs of the modeling software do not lend themselves to presentation and accessing the model directly generally requires specialized and licensed software. Workarounds, such as carefully curated image and videos, were developed, but if the project were to move forward more focus would need to be placed on strategies for the communication of the model.

Two known tools could be beneficial for this effort. The more complicated of the two is a collaboration server offered by the company behind Cameo Systems Modeler. It allows multiple people to work on the model at once by "checking out" the part they are working on, leaving it in a read-only state for everyone else. If this was set up and every team had one person responsible for updating their part of the model then the model could serve as a real time representation of the state of the system. The downside is that this would require additional people install and learn to use Cameo Systems Modeler, which can be an onerous task. The simpler tool is open source software that allows for the viewing of Cameo files. Assuming the team responsible for the model can maintain an updated version on the cloud, this software would allow all members of the project to access the model. This could provide the benefits of having a centralized source for information on a project without the downside of requiring every member to learn and use the complicated systems modelling software. It also would prevent version control issues since only the people on the modelling team would be able to edit the model. The application of either of these tools would help in realizing and communicating the tangible benefits that model-based systems engineering has to offer.

A.3 Mode Functionality Table

The modes functionality table springs partially from the MBSE construction of instances. It includes the power and the data usage of the spacecraft in eight different phases of the mission: safe mode, instrumentation test, cruise, imaging, internal measurements, Earth flyby event, long term tracking, and disposal. Also included are roll-ups of the power and data usage for each mode. The units of power are in watts consumed so a negative value indicates that there are that number of watts available above and beyond what is being used. Data is a more complicated case. The output of the communication equipment is not always greater than the rate of data coming in from the instrumentation. However, there is three terabytes of on board data storage to cover for this mismatch when it occurs. Taking this into account, there are sufficient data handling capabilities to ensure that no data is lost.

Table A.1: Mode/Functionality Table 1

	Mode							
	Safe		Test		Cruise		Imaging(M.O.1)	
	Power Consumed (W)	Data Produced (Mbps)	Power Consumed (W)	Data Produced (Mbps)	Power Consumed (W)	Data Produced (Mbps)	Power Consumed (W)	Data Produced (Mbps)
Instrumentation								
LORRI	0	0	15	1.575	0	0	15	1.575
Ralph	0	0	8	1.65	0	0	8	1.65
TES	0	0	10.8	.0072	0	0	10.8	.0072
RRT	0	0	41	1.16	0	0	0	0
LNAC								
Solar Electric Propulsion	0	0	0	0	6900	0	0	0
Chemical Propulsion	0	0	0	0	0	0	217	0
Bus								
Power(harnesses)	181	0	181	0	181	0	181	0
Thermal	326	0	326	0	326	0	326	
Attitude Determination	217	0	217	0	217	0	217	0
Processing	199	0	199	0	199	0	199	0
Structure	18	0	18	0	18	0	18	0
Solar Panels	-10526.9	0	-10526.9	0	-10526.9	0	-10526.9	0
Comm								
X/K_a SDST	19.5	-.00005	19.5	-1	19.5	-.01	19.5	-1
X-band TWTA	172	0	0	0	172	0	0	0
K_a-band TWTA	0	0	81	0	0	0	81	0
Ultra Stable Oscillator	5	0	5	0	5	0	5	0
Totals	-9389.4	-.00005	-9405.6	3.3922	-2489.4	-.01	-9229.6	2.2322

Table A.2: Mode/Functionality Table 2

	Mode							
	Internal (M.O.2)		Event		Tracking (M.O.3)		Disposal	
	Power Consumed (W)	Data Produced (Mbps)	Power Consumed (W)	Data Produced (Mbps)	Power Consumed (W)	Data Produced (Mbps)	Power Consumed (W)	Data Produced (Mbps)
Instrumentation								
LORRI	0	0	15	1.575	0	0	0	0
Ralph	0	0	8	1.65	0	0	0	0
TES	0	0	10.8	.0072	10.8	.0072	0	0
RRT	0	0	0	0	0	0	0	0
LNAC								
Solar Electric Propulsion	0	0	0	0	0	0	0	0
Chemical Propulsion	217	0	217	0	217	0	217	0
Bus								
Power(harnesses)	181	0	181	0	181	0	181	0
Thermal	326	0	326	0	326	0	326	
Attitude Determination	217	0	217	0	217	0	217	0
Processing	199	0	199	0	199	0	199	0
Structure	18	0	18	0	18	0	18	0
Solar Panels	-10526.9	0	-10526.9	0	-10526.9	0	-10526.9	0
Comm								
X/K_a SDST	19.5	-1	19.5	-.05	19.5	-.05	0	0
X-band TWTA	0	0	172	0	172	0	0	0
K_a-band TWTA	81	0	0	0	0	0	0	0
Ultra Stable Oscillator	5	0	5	0	5	0	5	0
Totals	-9222.4	.16	-9138.6	3.1822	-9166.6.4	-.0428	-9368.9	0

Appendix B

Compiled Requirements

This Appendix combines all the requirements referenced earlier in the document in a concise location.

Table B.1: Mission Objectives

ID	Title	Requirement	Rationale
M.O.1	Bulk Physical Properties	Characterize Apophis's shape, size, density, surface topography and composition, rotation rate, and spin state	To inform planetary defense initiatives and the scientific community
M.O.2	Internal Structure	Characterize internal structure of Apophis before and after Earth Flyby event	To improve knowledge of tidal stresses on asteroids' internal structure
M.O.3	Orbit Characterization	Characterize Apophis's orbit, accounting for the influencing factors of the Yarkovsky Effect	To improve knowledge of Apophis's orbit, the Yarkovsky Effect, and NEO orbital dynamics

Table B.2: LNAC Subsystem Requirements

ID	Derived Requirements	Parent	Verification
LNAC.1	**Trajectories.** LNAC shall compute launch windows and trajectories to intercept and rendezvous with Apophis before 2029 Earth flyby event. Trajectory options will quantify trades between launch opportunity, flight duration, and payload mass delivered.	SYS.2	Analysis
LNAC.2	**Rendezvous & Divert Hazard.** Intercept trajectories shall be quantified in terms of closing velocity and worst-case effect on long-term orbit of Apophis. Worst-case impact shall not perturb Apophis at 2029 near-Earth event by more than Yarkovsky drift effect.	SYS.1-2	Analysis
LNAC.3	**Launch Vehicle/Propulsion.** Launch vehicle shall be capable of meeting criteria developed in LNAC.1 within mission budget; propulsion shall execute all trajectory correction maneuvers with 50% margin.	SYS.1	Analysis
LNAC.4	**Science Operations.** System shall circumnavigate Apophis at an altitude of no higher than 2 km and no lower than 0.5 km in multiple planes; attitude control systems and propulsion hardware shall provide attitude control to 1 arcsec and 5 arcsec/sec during science observations.	SYS.1-2 PLD.2-4,6	Analysis
LNAC.5	**End of Mission Orbit.** System shall depart Apophis at the conclusion of science operations into an orbit that will not encounter Apophis or Earth, or contaminate other bodies.	SYS.8	Analysis

Table B.3: Payload

ID	Derived Requirements	Parent	Verification
PLD.1	**Composition:** Measure spectra to 20 meter resolution over a wavelength range of 0.45 to 4 micrometers	SYS.6	Testing
PLD.2	**Broad Imaging Survey:** Take observations with at least 1 meter/pixel resolution over at least 540 hrs (at least 2 rotations) before and after Earth Flyby event	SYS.4, SYS.5	Testing
PLD.3	**High Resolution Imaging:** Image Apophis's surface at 0.01 meter/pixel resolution before, during, and after Earth Flyby event	SYS.6	Testing
PLD.4	**Color Imaging:** Image Apophis's surface at 0.1 meter/pixel resolution in 4 color and NIR filters before and after Earth Flyby event	SYS.6	Testing
PLD.5	**Internal Structure Resolution:** Measure Apophis's internal structure with a depth resolution of 20 meters	SYS.7	Testing
PLD.6	**Internal Structure Coverage:** Take observations in PLD.5 with a maximum sampling distance of 10 m along the asteroid's surface	SYS.7	Testing
PLD.7	**Yarkovsky Drift:** Measure Apophis's spectrum over the 4-50 micron range to characterize mineral composition and thermal emission	SYS.9	Testing

Table B.4: Communications and Data

ID	**Statement**	**Parent**	**Verification**
CD.1	Subsystem shall transmit all science data collected during near-Earth event within 6 months from event.	SYS.3	Analysis: link budget and downlink scheduling
CD.2	Subsystem shall be capable of communicating data between the ground and spacecraft, uplink and downlink, at no less than 10 kbps at any point on trajectory.	SYS.3	Analysis: link budget
CD.3	Subsystem shall be capable of communicating at a rate of at least 50 kbps uplink and downlink throughout near-Earth event.	SYS.3	Analysis: link budget
CD.4	Subsystem shall be capable of communicating at a rate of at least 50 bps when in safe mode or if pointing control is lost at any point on the trajectory	SYS.3	Analysis: link budget
CD.5	Subsystem shall be capable of storing up to 3 terabits of data.	SYS.3	Inspection: data recorder specifications
CD.6	Subsystem shall track spacecraft position to a precision of at least 50 radially m and 20 millidegrees angularly	SYS.8	Inspection: ground station tracking capability

Table B.5: Spacecraft Bus

ID	Statement	Parent	Verification
SB.1	Bus structure and internal instruments shall withstand 10g axial and 8g lateral launch loads, as well as acoustic loads and vibrations due to launch	SYS.1	Vibration, stress testing
SB.2	Bus shall support spacecraft maneuvers from launch vehicle separation until end of mission.	SYS.1, SYS.2	Analysis
SB.3	Bus shall satisfy Instrumentation and LNAC pointing requirements.	SYS.2, SYS.3	Analysis
SB.4	Bus shall withstand external temperature in ranges -95 to 35 C.	SYS.2	Thermal vacuum testing
SB.5	Bus shall regulate the internal temperature to support all onboard sensors and equipment in ranges 0-40 degrees Celsius. Instruments with more stringent requirements shall be supported individually.	SYS.2	Thermal vacuum testing
SB.6	Bus power system shall provide sufficient and reliable power to all subsystems in ranges 11.5 kW.	SYS.2	Analysis, day in the life testing
SB.7	Bus layout shall sufficiently support all onboard sensors and equipment	SYS.2	Analysis

Appendix C

Team Organization

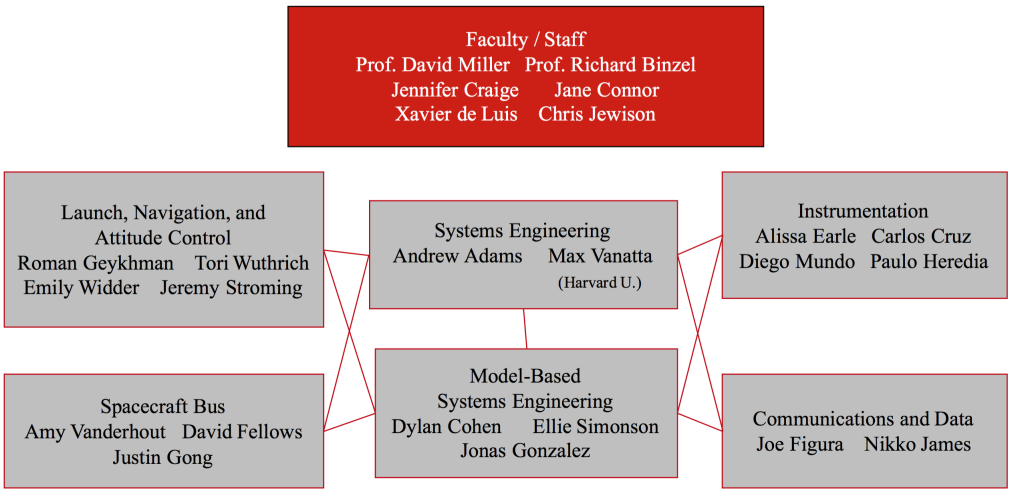

Figure C.1: Team Organization Chart

Appendix D

Launch Window

D.1 Launch Windows

The following table lists nominal launch windows using simplified impulsive calculations for all possible launch dates and rendezvous dates for the bi-elliptic trajectory. A single plane change burn is executed on the first nodal crossing, a single period change at first aphelion, and a final velocity match to rendezvous at a subsequent Apophis/spacecraft aphelion point.

Launch Date	Vinf	PlnCh	Total	PdChange	Vmatch	Arrival Date
	km/s	km/s	km/s	km/s	km/s	
2017-Aug-24	0.781	1.649	2.263	-0.536	-1.726	2020-Mar-31
2017-Aug-24	0.781	1.649	2.263	-1.053	-1.210	2021-Feb-17
2017-Aug-24	0.781	1.649	2.263	-0.499	-1.751	2026-Jun-13
2017-Aug-24	0.781	1.649	2.263	-1.332	-0.929	2022-Jan-07
2017-Aug-24	0.781	1.649	2.263	-1.506	-0.757	2022-Nov-27
2018-Aug-24	0.778	1.650	2.265	-1.158	-1.109	2021-Feb-17
2018-Aug-24	0.778	1.650	2.265	-0.452	-1.801	2026-Jun-13
2018-Aug-24	0.778	1.650	2.265	-1.503	-0.761	2022-Jan-07
2018-Aug-24	0.778	1.650	2.265	-0.648	-1.605	2027-May-03
2018-Aug-24	0.778	1.650	2.265	-1.684	-0.582	2022-Nov-27
2018-Aug-24	0.778	1.650	2.265	-1.796	-0.470	2023-Oct-16
2019-Aug-24	0.780	1.650	2.265	-1.478	-0.790	2021-Feb-17
2019-Aug-24	0.780	1.650	2.265	-0.387	-1.867	2026-Jun-13
2019-Aug-24	0.780	1.650	2.265	-1.857	-0.408	2022-Jan-07
2019-Aug-24	0.780	1.650	2.265	-0.618	-1.636	2027-May-03
2019-Aug-24	0.780	1.650	2.265	-1.990	-0.277	2022-Nov-27
2019-Aug-24	0.780	1.650	2.265	-0.799	-1.456	2028-Mar-22
2019-Aug-24	0.780	1.650	2.265	-2.057	-0.210	2023-Oct-16
2020-Aug-24	0.779	1.649	2.263	-0.587	-1.664	2027-May-02
2020-Aug-24	0.779	1.649	2.263	-0.797	-1.455	2028-Mar-21
2020-Aug-24	0.779	1.649	2.263	-0.961	-1.292	2029-Feb-08
2021-Aug-24	0.781	1.650	2.263	-0.531	-1.720	2027-May-03
2021-Aug-24	0.781	1.650	2.263	-0.784	-1.467	2028-Mar-22
2021-Aug-24	0.781	1.650	2.263	-0.972	-1.279	2029-Feb-09
2022-Aug-24	0.779	1.651	2.263	-0.455	-1.796	2027-May-03
2022-Aug-24	0.779	1.651	2.263	-0.771	-1.480	2028-Mar-22
2022-Aug-24	0.779	1.651	2.263	-0.993	-1.258	2029-Feb-09
2023-Aug-24	0.781	1.651	2.263	-0.752	-1.499	2028-Mar-22
2023-Aug-24	0.781	1.651	2.263	-1.023	-1.228	2029-Feb-09
2024-Aug-24	0.778	1.651	2.262	-0.728	-1.531	2028-Mar-21
2024-Aug-24	0.778	1.651	2.262	-1.074	-1.185	2029-Feb-08
2025-Aug-24	0.777	1.652	2.262	-0.667	-1.596	2028-Mar-21
2025-Aug-24	0.777	1.652	2.262	-1.149	-1.114	2029-Feb-08
2026-Aug-24	0.773	1.652	2.264	-0.494	-1.771	2028-Mar-21
2026-Aug-24	0.773	1.652	2.264	-1.308	-0.957	2029-Feb-08
2027-Aug-25	0.774	1.651	2.263	-1.838	-0.425	2029-Feb-08

D.2 Launch Day Margin

The following table lists the ΔV penalty for launching earlier or later than the launch window in six selected years. Penalty is expressed in terms of additional required V_∞ ("Launch") or additional required velocity at the first period change burn ("Period") under the constraint that the early or late launch joins the nominal trajectory after completing the period change burn.

Launch	Delay	Penalty [km/s]	
	days	Launch	Period
2022-Jul-25	-30	-0.138	+0.068
2022-Aug-04	-20	-0.100	+0.036
2022-Aug-14	-10	-0.056	+0.035
2022-Aug-24	0	-0.000	+0.000
2022-Sep-03	10	+0.038	+0.010
2022-Sep-13	20	+0.080	+0.040

Launch	Delay	Penalty [km/s]	
	days	Launch	Period
2023-Jul-25	-30	-0.135	+0.095
2023-Aug-04	-20	-0.098	+0.057
2023-Aug-14	-10	-0.056	+0.040
2023-Aug-24	0	-0.000	-0.000
2023-Sep-03	10	+0.035	+0.032
2023-Sep-13	20	+0.075	+0.079

Launch	Delay	Penalty [km/s]	
	days	Launch	Period
2024-Jul-25	-30	-0.134	+0.132
2024-Aug-04	-20	-0.098	+0.097
2024-Aug-14	-10	-0.056	+0.079
2024-Aug-24	0	-0.000	+0.000
2024-Sep-03	10	+0.031	+0.092
2024-Sep-13	20	+0.068	+0.143

Launch	Delay	Penalty [km/s]	
	days	Launch	Period
2025-Jul-25	-30	-0.139	+0.082
2025-Aug-04	-20	-0.101	+0.047
2025-Aug-14	-10	-0.058	+0.034
2025-Aug-24	0	-0.000	+0.000
2025-Sep-03	10	+0.035	+0.014
2025-Sep-13	20	+0.076	+0.061

Launch	Delay	Penalty [km/s]	
	days	Launch	Period
2026-Jul-25	-30	-0.132	+0.099
2026-Aug-04	-20	-0.096	+0.062
2026-Aug-14	-10	-0.000	+0.000
2026-Aug-24	0	-0.008	+0.033
2026-Sep-03	10	+0.037	+0.041
2026-Sep-13	20	+0.076	+0.088

Launch	Delay	Penalty [km/s]	
	days	Launch	Period
2027-Jul-26	-30	-0.132	+0.126
2027-Aug-05	-20	-0.096	+0.091
2027-Aug-15	-10	-0.000	+0.000
2027-Aug-25	0	-0.010	+0.068
2027-Sep-04	10	+0.034	+0.086
2027-Sep-14	20	+0.071	+0.138

D.3 Station-Keeping Simulation GMAT Files

D.3.1 $\beta = 0$ Case

```
% Tori Wuthrich
% Email: toriw@mit.edu
% Beta = 0 Station-Keeping Analysis


%----------------------------------------
%---------- User-Defined Celestial Bodies
%----------------------------------------

Create Asteroid Apophis;
GMAT Apophis.NAIFId = 2099942;
% To re-run, change this line
GMAT Apophis.OrbitSpiceKernelName = {'C:\Users\toriw\Downloads\wld27924.15'};
GMAT Apophis.OrbitColor = Salmon;
GMAT Apophis.TargetColor = DarkGray;
GMAT Apophis.EquatorialRadius = 0.15;
GMAT Apophis.Flattening = 0.0033527;
GMAT Apophis.Mu = 2.6680e-9;
GMAT Apophis.PosVelSource = 'SPICE';
GMAT Apophis.CentralBody = 'Sun';
GMAT Apophis.RotationDataSource = 'IAUSimplified';
GMAT Apophis.OrientationEpoch = 21545;
GMAT Apophis.SpinAxisRAConstant = 0;
GMAT Apophis.SpinAxisRARate = -0.641;
GMAT Apophis.SpinAxisDECConstant = 90;
GMAT Apophis.SpinAxisDECRate = -0.5570000000000001;
GMAT Apophis.RotationConstant = 190.147;
GMAT Apophis.RotationRate = 360.9856235;
GMAT Apophis.TextureMapFileName = 'GenericCelestialBody.jpg';
GMAT Apophis.3DModelFile = '';
GMAT Apophis.3DModelOffsetX = 0;
GMAT Apophis.3DModelOffsetY = 0;
GMAT Apophis.3DModelOffsetZ = 0;
GMAT Apophis.3DModelRotationX = 0;
GMAT Apophis.3DModelRotationY = 0;
GMAT Apophis.3DModelRotationZ = 0;
GMAT Apophis.3DModelScale = 10;

%----------------------------------------
%---------- Spacecraft
%----------------------------------------

Create Spacecraft sc;
GMAT sc.DateFormat = UTCModJulian;
GMAT sc.Epoch = '28849';
GMAT sc.CoordinateSystem = ApophisCentric;
GMAT sc.DisplayStateType = Cartesian;
GMAT sc.X = -65544127.48899682;
GMAT sc.Y = 13557950.20462532;
GMAT sc.Z = 6006559.022108644;
GMAT sc.VX = -2.757395192237148;
GMAT sc.VY = -12.56753145908596;
GMAT sc.VZ = -0.5721100087969084;
GMAT sc.DryMass = 1000;
GMAT sc.Cd = 2.2;
GMAT sc.Cr = 1;
GMAT sc.DragArea = 15;
GMAT sc.SRPArea = 10;
GMAT sc.NAIFId = -10003001;
GMAT sc.NAIFIdReferenceFrame = -9003001;
GMAT sc.OrbitColor = Red;
GMAT sc.TargetColor = Teal;
GMAT sc.EstimationStateType = 'Cartesian';
```

```
GMAT sc.OrbitErrorCovariance = [ 1e+070 0 0 0 0 0 ; 0 1e+070 0 0 0 0 ; 0 0 1e+070 0 0 0 ; 0
    0 0 1e+070 0 0 ; 0 0 0 0 0 1e+070 0 ; 0 0 0 0 0 0 1e+070 ];
GMAT sc.CdSigma = 1e+070;
GMAT sc.CrSigma = 1e+070;
GMAT sc.Id = 'SatId';
GMAT sc.Attitude = CoordinateSystemFixed;
GMAT sc.SPADSRPScaleFactor = 1;
GMAT sc.ModelFile = 'aura.3ds';
GMAT sc.ModelOffsetX = 0;
GMAT sc.ModelOffsetY = 0;
GMAT sc.ModelOffsetZ = 0;
GMAT sc.ModelRotationX = 0;
GMAT sc.ModelRotationY = 0;
GMAT sc.ModelRotationZ = 0;
GMAT sc.ModelScale = 1;
GMAT sc.AttitudeDisplayStateType = 'Quaternion';
GMAT sc.AttitudeRateDisplayStateType = 'AngularVelocity';
GMAT sc.AttitudeCoordinateSystem = EarthMJ2000Eq;
GMAT sc.EulerAngleSequence = '321';

%----------------------------------------
%---------- ForceModels
%----------------------------------------

Create ForceModel ACFM;
GMAT ACFM.CentralBody = Apophis;
% add more planets here
GMAT ACFM.PointMasses = {Sun, Earth, Apophis};
GMAT ACFM.Drag = None;
GMAT ACFM.SRP = On;
GMAT ACFM.RelativisticCorrection = On;
GMAT ACFM.ErrorControl = RSSStep;
GMAT ACFM.SRP.Flux = 1367;
GMAT ACFM.SRP.SRPModel = Spherical;
GMAT ACFM.SRP.Nominal_Sun = 149597870.691;

%----------------------------------------
%---------- Propagators
%----------------------------------------

Create Propagator ACP;
GMAT ACP.FM = ACFM;
GMAT ACP.Type = RungeKutta89;
GMAT ACP.InitialStepSize = 60;
GMAT ACP.Accuracy = 1e-08;
GMAT ACP.MinStep = 10;
GMAT ACP.MaxStep = 2700;
GMAT ACP.MaxStepAttempts = 50;
GMAT ACP.StopIfAccuracyIsViolated = false;

%----------------------------------------
%---------- Burns
%----------------------------------------

Create ImpulsiveBurn burn;
GMAT burn.CoordinateSystem = Local;
GMAT burn.Origin = Apophis;
GMAT burn.Axes = VNB;
GMAT burn.Element1 = 1e-008;
GMAT burn.Element2 = 0;
GMAT burn.Element3 = 0;
GMAT burn.DecrementMass = false;
GMAT burn.Isp = 300;
GMAT burn.GravitationalAccel = 9.810000000000001;

%----------------------------------------
%---------- Coordinate Systems
%----------------------------------------
```

```
131
132 Create CoordinateSystem ApophisCentric;
133 GMAT ApophisCentric.Origin = Apophis;
134 GMAT ApophisCentric.Axes = MJ2000Ec;
135
136 Create CoordinateSystem HelioCentric;
137 GMAT HelioCentric.Origin = Sun;
138 GMAT HelioCentric.Axes = MJ2000Ec;
139
140 %----------------------------------------
141 %---------- Subscribers
142 %----------------------------------------
143
144 Create ReportFile Rreport;
145 GMAT Rreport.SolverIterations = Current;
146 GMAT Rreport.UpperLeft = [ 0 0 ];
147 GMAT Rreport.Size = [ 0 0 ];
148 GMAT Rreport.RelativeZOrder = 0;
149 GMAT Rreport.Maximized = false;
150 GMAT Rreport.Filename = 'C:\Users\toriw\Documents\apophis_report_r.txt';
151 GMAT Rreport.Precision = 16;
152 GMAT Rreport.WriteHeaders = true;
153 GMAT Rreport.LeftJustify = On;
154 GMAT Rreport.ZeroFill = Off;
155 GMAT Rreport.FixedWidth = true;
156 GMAT Rreport.Delimiter = ' ';
157 GMAT Rreport.ColumnWidth = 23;
158 GMAT Rreport.WriteReport = true;
159
160 Create ReportFile DVreport;
161 GMAT DVreport.SolverIterations = Current;
162 GMAT DVreport.UpperLeft = [ 0 0 ];
163 GMAT DVreport.Size = [ 0 0 ];
164 GMAT DVreport.RelativeZOrder = 0;
165 GMAT DVreport.Maximized = false;
166 GMAT DVreport.Filename = 'C:\Users\toriw\Documents\apophis_report_dv.txt';
167 GMAT DVreport.Precision = 16;
168 GMAT DVreport.WriteHeaders = true;
169 GMAT DVreport.LeftJustify = On;
170 GMAT DVreport.ZeroFill = Off;
171 GMAT DVreport.FixedWidth = true;
172 GMAT DVreport.Delimiter = ' ';
173 GMAT DVreport.ColumnWidth = 23;
174 GMAT DVreport.WriteReport = true;
175
176 Create ReportFile POSreport;
177 GMAT POSreport.SolverIterations = Current;
178 GMAT POSreport.UpperLeft = [ 0 0 ];
179 GMAT POSreport.Size = [ 0 0 ];
180 GMAT POSreport.RelativeZOrder = 0;
181 GMAT POSreport.Maximized = false;
182 GMAT POSreport.Filename = 'C:\Users\toriw\Documents\apophis_report_pos.txt';
183 GMAT POSreport.Precision = 16;
184 GMAT POSreport.WriteHeaders = true;
185 GMAT POSreport.LeftJustify = On;
186 GMAT POSreport.ZeroFill = Off;
187 GMAT POSreport.FixedWidth = true;
188 GMAT POSreport.Delimiter = ' ';
189 GMAT POSreport.ColumnWidth = 23;
190 GMAT POSreport.WriteReport = true;
191
192 %----------------------------------------
193 %---------- Arrays, Variables, Strings
194 %----------------------------------------
195
196 % Define Variables
197
198 Create Array X[1,3] V[1,3] N[1,3] T[1,3] Va[1,3] vcrosst[1,3] radii[1,9] dv_values[1,9];
```

```
199 Create Variable startingMJD currentMJD theta vdottTol dv mu r1 r2 dvTot vdott;
200 Create Variable absvdott xdott vFinal e r_alpha absXdott idx b time_increment
        delay_burn_flag vmag dt_burn;
201
202
203
204 %----------------------------------------
205 %---------- Mission Sequence
206 %----------------------------------------
207
208
209 BeginMissionSequence;
210
211 GMAT mu = 2.6680e-9;
212 GMAT vdottTol = 1 - 1e-2;
213
214 GMAT radii(1) = 0.5;
215 GMAT radii(2) = 0.6;
216 GMAT radii(3) = 0.8;
217 GMAT radii(4) = 1.0;
218 GMAT radii(5) = 1.2;
219 GMAT radii(6) = 1.4;
220 GMAT radii(7) = 1.6;
221 GMAT radii(8) = 1.8;
222 GMAT radii(9) = 2.0;
223
224
225 GMAT startingMJD = 28849;
226
227 % For each starting radius
228 For idx = 1:1:1;
229
230    GMAT currentMJD = startingMJD;
231    Write currentMJD { Style = Concise, LogFile = false, MessageWindow = true }
232
233    % IC for in-plane case (vary the orbital radius)
234    GMAT sc.ApophisCentric.X = radii(idx);
235    GMAT sc.ApophisCentric.Y = 0;
236    GMAT sc.ApophisCentric.Z = 0;
237    GMAT sc.ApophisCentric.VX = 0;
238    GMAT sc.ApophisCentric.VY = sqrt(6.67e-11*4e10*1e-9/radii(idx));
239    GMAT sc.ApophisCentric.VZ = 0;
240
241    GMAT r_alpha = radii(idx);
242
243    GMAT currentMJD = 0;
244    GMAT dvTot = 0;
245
246          time_increment = 0.025;
247
248          delay_burn_flag = 0;
249
250          While currentMJD < 20
251
252
253       %  Report report sc.UTCGregorian sc.ApophisCentric.X sc.ApophisCentric.Y sc.
              ApophisCentric.Z sc.ApophisCentric.VX sc.ApophisCentric.VY sc.ApophisCentric.VZ sc
              .SMA sc.ECC Apophis.X;
254       Propagate ACP(sc) {sc.ElapsedDays = time_increment};
255                 Apophis.UTCModJulian = sc.UTCModJulian;
256       GMAT currentMJD = currentMJD + time_increment;
257
258                 % EarthMJ2000Ec
259
260       % Get vector from Sun to Apophis (normalized)
261       GMAT X(1,1) = Apophis.HelioCentric.X/sqrt(Apophis.HelioCentric.X^2 + Apophis.
              HelioCentric.Y^2 + Apophis.HelioCentric.Z^2);
```

```
262         GMAT X(1,2) = Apophis.HelioCentric.Y/sqrt(Apophis.HelioCentric.X^2 + Apophis.
                HelioCentric.Y^2 + Apophis.HelioCentric.Z^2);
263         GMAT X(1,3) = Apophis.HelioCentric.Z/sqrt(Apophis.HelioCentric.X^2 + Apophis.
                HelioCentric.Y^2 + Apophis.HelioCentric.Z^2);
264
265         % Get velocity vector of Apophis (normalized)
266         GMAT V(1,1) = Apophis.HelioCentric.VX/sqrt(Apophis.HelioCentric.VX^2 + Apophis.
                HelioCentric.VY^2 + Apophis.HelioCentric.VZ^2);
267         GMAT V(1,2) = Apophis.HelioCentric.VY/sqrt(Apophis.HelioCentric.VX^2 + Apophis.
                HelioCentric.VY^2 + Apophis.HelioCentric.VZ^2);
268         GMAT V(1,3) = Apophis.HelioCentric.VZ/sqrt(Apophis.HelioCentric.VX^2 + Apophis.
                HelioCentric.VY^2 + Apophis.HelioCentric.VZ^2);
269
270         GMAT N = cross(X,V);
271
272         GMAT V(1,1) = sc.ApophisCentric.VX/sqrt(sc.ApophisCentric.VX^2 + sc.ApophisCentric.VY
                ^2 + sc.ApophisCentric.VZ^2);
273         GMAT V(1,2) = sc.ApophisCentric.VY/sqrt(sc.ApophisCentric.VX^2 + sc.ApophisCentric.VY
                ^2 + sc.ApophisCentric.VZ^2);
274         GMAT V(1,3) = sc.ApophisCentric.VZ/sqrt(sc.ApophisCentric.VX^2 + sc.ApophisCentric.VY
                ^2 + sc.ApophisCentric.VZ^2);
275
276         % Calculate N and T
277         GMAT T = cross(N,X);
278
279         % Calculate dot product of T and V to check if they are perpendicular
280         GMAT vdott = T(1,1)*V(1,1) + T(1,2)*V(1,2) + T(1,3)*V(1,3);
281         GMAT absvdott = abs(vdott);
282
283         GMAT dv = 0;
284
285         GMAT xdott = abs(sc.ApophisCentric.X*T(1,1) + sc.ApophisCentric.Y*T(1,2) + sc.
                ApophisCentric.Z*T(1,3))/(sqrt(sc.ApophisCentric.X^2 + sc.ApophisCentric.Y^2 + sc.
                ApophisCentric.Z^2)*sqrt(T(1)^2 + T(2)^2 + T(3)^2));
286
287         GMAT absXdott = abs(xdott);
288
289         % If v and T are perpendicular (within vdottTol), then execute a burn (x dot t)
290         % Check dot product to make sure that it is 1 where it shoudl be
291         If absXdott > 0.98
292
293            % Calculate starting radius, end radius is known. Add a random number to the radius
294 %                        GMAT r1 = sqrt(sc.ApophisCentric.X^2 + sc.ApophisCentric.Y^2 + sc.
    ApophisCentric.Z^2) + 0.01*rand()*sqrt(sc.ApophisCentric.X^2 + sc.ApophisCentric.Y^2 +
    sc.ApophisCentric.Z^2);
295            GMAT r1 = sqrt(sc.ApophisCentric.X^2 + sc.ApophisCentric.Y^2 + sc.ApophisCentric.Z
                   ^2);
296
297            GMAT r2 = r_alpha;
298
299
300            GMAT vFinal = sqrt(mu*((2.0/r1) - (1.0/(0.5*(r1 + r2)))));
301
302            GMAT dv = vFinal - sqrt(sc.ApophisCentric.VX^2 + sc.ApophisCentric.VY^2 + sc.
                   ApophisCentric.VZ^2);
303
304                           % Propogate the sc forward by a small time increment to simulate
                                  angle error
305                           vmag = (sc.ApophisCentric.VX^2 + sc.ApophisCentric.VY^2 + sc.
                                  ApophisCentric.VZ^2)^0.5
306                           time_increment = (3.5e-4*r1/vmag)/86400.0;
307
308                           Propagate ACP(sc) {sc.ElapsedDays = time_increment};
309                           GMAT currentMJD = currentMJD + time_increment;
310
311            GMAT burn.Element1 = dv;
312            Maneuver burn(sc);
313            GMAT dvTot = dvTot + abs(dv);
```

```
314
315                             % sc.Apophis.MM: rad/sec
316                             % for 0.5 km: use 0.025
317                             dt_burn = 0.15/sc.Apophis.MM;
318                             Propagate ACP(sc) {sc.ElapsedSecs = dt_burn};
319                             Apophis.UTCModJulian = sc.UTCModJulian;
320                             GMAT currentMJD = currentMJD + dt_burn/86400.0;
321
322                     Else
323                             dv = 0;
324
325         EndIf;
326
327         Report POSreport sc.UTCGregorian sc.UTCModJulian sc.ApophisCentric.X sc.ApophisCentric
                .Y sc.ApophisCentric.Z sc.ApophisCentric.VX sc.ApophisCentric.VY sc.ApophisCentric
                .VZ Apophis.HelioCentric.X Apophis.HelioCentric.Y Apophis.HelioCentric.Z T(1) T(2)
                T(3) N(1) N(2) N(3) xdott vdott absXdott vFinal dv;
328
329     EndWhile;
330
331     GMAT dv_values(idx) = dvTot;
332     Write dvTot { Style = Concise, LogFile = false, MessageWindow = true }
333
334 EndFor;
335
336 Report DVreport dv_values;
337 Report Rreport radii;
338 Write dv_values
```

D.3.2 $\beta = 90°$ Case

```
1  % Tori Wuthrich
2  % Email: toriw@mit.edu
3  % Station-keeping analysis script for beta = 90
4
5  %---------------------------------------
6  %---------- User-Defined Celestial Bodies
7  %---------------------------------------
8
9  Create Asteroid Apophis;
10 GMAT Apophis.NAIFId = 2099942;
11 % To rerun, change this
12 GMAT Apophis.OrbitSpiceKernelName = {'C:\Users\toriw\Downloads\wld27924.15'};
13 GMAT Apophis.OrbitColor = Salmon;
14 GMAT Apophis.TargetColor = DarkGray;
15 GMAT Apophis.EquatorialRadius = 0.15;
16 GMAT Apophis.Flattening = 0.0033527;
17 GMAT Apophis.Mu = 2.6e-009;
18 GMAT Apophis.PosVelSource = 'SPICE';
19 GMAT Apophis.CentralBody = 'Sun';
20 GMAT Apophis.RotationDataSource = 'IAUSimplified';
21 GMAT Apophis.OrientationEpoch = 21545;
22 GMAT Apophis.SpinAxisRAConstant = 0;
23 GMAT Apophis.SpinAxisRARate = -0.641;
24 GMAT Apophis.SpinAxisDECConstant = 90;
25 GMAT Apophis.SpinAxisDECRate = -0.5570000000000001;
26 GMAT Apophis.RotationConstant = 190.147;
27 GMAT Apophis.RotationRate = 360.9856235;
28 GMAT Apophis.TextureMapFileName = 'GenericCelestialBody.jpg';
29 GMAT Apophis.3DModelFile = '';
30 GMAT Apophis.3DModelOffsetX = 0;
31 GMAT Apophis.3DModelOffsetY = 0;
32 GMAT Apophis.3DModelOffsetZ = 0;
33 GMAT Apophis.3DModelRotationX = 0;
34 GMAT Apophis.3DModelRotationY = 0;
35 GMAT Apophis.3DModelRotationZ = 0;
36 GMAT Apophis.3DModelScale = 10;
37
```

```
%----------------------------------------
%---------- Spacecraft
%----------------------------------------

Create Spacecraft sc;
GMAT sc.DateFormat = UTCModJulian;
GMAT sc.Epoch = '28849';
GMAT sc.CoordinateSystem = ApophisCentric;
GMAT sc.DisplayStateType = Cartesian;
GMAT sc.X = -65544127.48899682;
GMAT sc.Y = 13557950.20462532;
GMAT sc.Z = 6006559.022108644;
GMAT sc.VX = -2.757395192237148;
GMAT sc.VY = -12.56753145908596;
GMAT sc.VZ = -0.5721100087969084;
GMAT sc.DryMass = 1000;
GMAT sc.Cd = 2.2;
GMAT sc.Cr = 1;
GMAT sc.DragArea = 15;
GMAT sc.SRPArea = 10;
GMAT sc.NAIFId = -10003001;
GMAT sc.NAIFIdReferenceFrame = -9003001;
GMAT sc.OrbitColor = Red;
GMAT sc.TargetColor = Teal;
GMAT sc.EstimationStateType = 'Cartesian';
GMAT sc.OrbitErrorCovariance = [ 1e+070 0 0 0 0 0 ; 0 1e+070 0 0 0 0 ; 0 0 1e+070 0 0 0 ; 0
    0 0 1e+070 0 0 ; 0 0 0 0 1e+070 0 ; 0 0 0 0 0 1e+070 ];
GMAT sc.CdSigma = 1e+070;
GMAT sc.CrSigma = 1e+070;
GMAT sc.Id = 'SatId';
GMAT sc.Attitude = CoordinateSystemFixed;
GMAT sc.SPADSRPScaleFactor = 1;
GMAT sc.ModelFile = 'aura.3ds';
GMAT sc.ModelOffsetX = 0;
GMAT sc.ModelOffsetY = 0;
GMAT sc.ModelOffsetZ = 0;
GMAT sc.ModelRotationX = 0;
GMAT sc.ModelRotationY = 0;
GMAT sc.ModelRotationZ = 0;
GMAT sc.ModelScale = 1;
GMAT sc.AttitudeDisplayStateType = 'Quaternion';
GMAT sc.AttitudeRateDisplayStateType = 'AngularVelocity';
GMAT sc.AttitudeCoordinateSystem = EarthMJ2000Eq;
GMAT sc.EulerAngleSequence = '321';

%----------------------------------------
%---------- ForceModels
%----------------------------------------

Create ForceModel ACFM;
GMAT ACFM.CentralBody = Apophis;
% add more planets here
GMAT ACFM.PointMasses = {Sun, Earth, Apophis};
GMAT ACFM.Drag = None;
GMAT ACFM.SRP = On;
GMAT ACFM.RelativisticCorrection = On;
GMAT ACFM.ErrorControl = RSSStep;
GMAT ACFM.SRP.Flux = 1367;
GMAT ACFM.SRP.SRPModel = Spherical;
GMAT ACFM.SRP.Nominal_Sun = 149597870.691;

%----------------------------------------
%---------- Propagators
%----------------------------------------

Create Propagator ACP;
GMAT ACP.FM = ACFM;
GMAT ACP.Type = RungeKutta89;
```

```
GMAT ACP.InitialStepSize = 60;
GMAT ACP.Accuracy = 1e-08;
GMAT ACP.MinStep = 10;
GMAT ACP.MaxStep = 2700;
GMAT ACP.MaxStepAttempts = 50;
GMAT ACP.StopIfAccuracyIsViolated = false;

%----------------------------------------
%---------- Burns
%----------------------------------------

Create ImpulsiveBurn burn;
GMAT burn.CoordinateSystem = Local;
GMAT burn.Origin = Apophis;
GMAT burn.Axes = VNB;
GMAT burn.Element1 = 1e-008;
GMAT burn.Element2 = 0;
GMAT burn.Element3 = 0;
GMAT burn.DecrementMass = false;
GMAT burn.Isp = 300;
GMAT burn.GravitationalAccel = 9.810000000000001;

%----------------------------------------
%---------- Coordinate Systems
%----------------------------------------

Create CoordinateSystem ApophisCentric;
GMAT ApophisCentric.Origin = Apophis;
GMAT ApophisCentric.Axes = MJ2000Ec;

Create CoordinateSystem HelioCentric;
GMAT HelioCentric.Origin = Sun;
GMAT HelioCentric.Axes = MJ2000Ec;

%----------------------------------------
%---------- Subscribers
%----------------------------------------

Create ReportFile Rreport;
GMAT Rreport.SolverIterations = Current;
GMAT Rreport.UpperLeft = [ 0 0 ];
GMAT Rreport.Size = [ 0 0 ];
GMAT Rreport.RelativeZOrder = 0;
GMAT Rreport.Maximized = false;
GMAT Rreport.Filename = 'C:\Users\toriw\Documents\apophis_report_r_b90.txt';
GMAT Rreport.Precision = 16;
GMAT Rreport.WriteHeaders = true;
GMAT Rreport.LeftJustify = On;
GMAT Rreport.ZeroFill = Off;
GMAT Rreport.FixedWidth = true;
GMAT Rreport.Delimiter = ' ';
GMAT Rreport.ColumnWidth = 23;
GMAT Rreport.WriteReport = true;

Create ReportFile DVreport;
GMAT DVreport.SolverIterations = Current;
GMAT DVreport.UpperLeft = [ 0 0 ];
GMAT DVreport.Size = [ 0 0 ];
GMAT DVreport.RelativeZOrder = 0;
GMAT DVreport.Maximized = false;
GMAT DVreport.Filename = 'C:\Users\toriw\Documents\apophis_report_dv_b90.txt';
GMAT DVreport.Precision = 16;
GMAT DVreport.WriteHeaders = true;
GMAT DVreport.LeftJustify = On;
GMAT DVreport.ZeroFill = Off;
GMAT DVreport.FixedWidth = true;
GMAT DVreport.Delimiter = ' ';
GMAT DVreport.ColumnWidth = 23;
```

```
GMAT DVreport.WriteReport = true;

Create ReportFile POSreport;
GMAT POSreport.SolverIterations = Current;
GMAT POSreport.UpperLeft = [ 0 0 ];
GMAT POSreport.Size = [ 0 0 ];
GMAT POSreport.RelativeZOrder = 0;
GMAT POSreport.Maximized = false;
GMAT POSreport.Filename = 'C:\Users\toriw\Documents\apophis_report_pos_b90.txt';
GMAT POSreport.Precision = 16;
GMAT POSreport.WriteHeaders = true;
GMAT POSreport.LeftJustify = On;
GMAT POSreport.ZeroFill = Off;
GMAT POSreport.FixedWidth = true;
GMAT POSreport.Delimiter = ' ';
GMAT POSreport.ColumnWidth = 23;
GMAT POSreport.WriteReport = true;

%----------------------------------------
%---------- Arrays, Variables, Strings
%----------------------------------------

% Define Variables

Create Array X[1,3] V[1,3] N[1,3] T[1,3] Va[1,3] vcrosst[1,3] radii[1,6] dv_values[1,6];
Create Variable startingMJD currentMJD theta vdottTol dv mu r1 r2 dvTot;
Create Variable absvdott xdott vFinal e r_alpha absXdott idx b xdottTol thetaVT vdotx vdott
    abstheta;



%----------------------------------------
%---------- Mission Sequence
%----------------------------------------


BeginMissionSequence;

GMAT mu = 2.6e-9;
GMAT vdottTol = 1 - 1e-2;
GMAT xdottTol = 0.01;

GMAT radii(1) = 0.5;
GMAT radii(2) = 0.7;
GMAT radii(3) = 0.9;
GMAT radii(4) = 1.1;
GMAT radii(5) = 1.3;
GMAT radii(6) = 1.5;




GMAT startingMJD = 28849;

% For each starting radius
For idx = 1:1:6;

   GMAT currentMJD = startingMJD;
   Write currentMJD { Style = Concise, LogFile = false, MessageWindow = true }

   % IC for in-plane case (vary the orbital radius)
   GMAT sc.ApophisCentric.X = 0;
   GMAT sc.ApophisCentric.Y = 0;
   GMAT sc.ApophisCentric.Z = radii(idx)
   GMAT sc.ApophisCentric.VX = sqrt(6.67e-11*4e10*1e-9/radii(idx));
   GMAT sc.ApophisCentric.VY = 0;
   GMAT sc.ApophisCentric.VZ = 0;

```

```
240     GMAT r_alpha = radii(idx);
241
242     GMAT currentMJD = 0;
243     GMAT dvTot = 0;
244
245     While currentMJD < 10
246
247        %  Report report sc.UTCGregorian sc.ApophisCentric.X sc.ApophisCentric.Y sc.
               ApophisCentric.Z sc.ApophisCentric.VX sc.ApophisCentric.VY sc.ApophisCentric.VZ sc
               .SMA sc.ECC Apophis.X;
248        Propagate ACP(sc) {sc.ElapsedDays = 0.025};
249        GMAT currentMJD = currentMJD + 0.025;
250
251        % Get vector from Sun to Apophis (normalized)
252        GMAT X(1,1) = Apophis.HelioCentric.X/sqrt(Apophis.HelioCentric.X^2 + Apophis.
               HelioCentric.Y^2 + Apophis.HelioCentric.Z^2);
253        GMAT X(1,2) = Apophis.HelioCentric.Y/sqrt(Apophis.HelioCentric.X^2 + Apophis.
               HelioCentric.Y^2 + Apophis.HelioCentric.Z^2);
254        GMAT X(1,3) = Apophis.HelioCentric.Z/sqrt(Apophis.HelioCentric.X^2 + Apophis.
               HelioCentric.Y^2 + Apophis.HelioCentric.Z^2);
255
256        % Get velocity vector of Apophis (normalized)
257        GMAT V(1,1) = Apophis.HelioCentric.VX/sqrt(Apophis.HelioCentric.VX^2 + Apophis.
               HelioCentric.VY^2 + Apophis.HelioCentric.VZ^2);
258        GMAT V(1,2) = Apophis.HelioCentric.VY/sqrt(Apophis.HelioCentric.VX^2 + Apophis.
               HelioCentric.VY^2 + Apophis.HelioCentric.VZ^2);
259        GMAT V(1,3) = Apophis.HelioCentric.VZ/sqrt(Apophis.HelioCentric.VX^2 + Apophis.
               HelioCentric.VY^2 + Apophis.HelioCentric.VZ^2);
260
261        GMAT N = cross(X,V);
262
263        GMAT V(1,1) = sc.ApophisCentric.VX/sqrt(sc.ApophisCentric.VX^2 + sc.ApophisCentric.VY
               ^2 + sc.ApophisCentric.VZ^2);
264        GMAT V(1,2) = sc.ApophisCentric.VY/sqrt(sc.ApophisCentric.VX^2 + sc.ApophisCentric.VY
               ^2 + sc.ApophisCentric.VZ^2);
265        GMAT V(1,3) = sc.ApophisCentric.VZ/sqrt(sc.ApophisCentric.VX^2 + sc.ApophisCentric.VY
               ^2 + sc.ApophisCentric.VZ^2);
266
267        % Calculate N and T
268        GMAT T = cross(N,X);
269
270        GMAT xdott = abs(sc.ApophisCentric.X*T(1,1) + sc.ApophisCentric.Y*T(1,2) + sc.
               ApophisCentric.Z*T(1,3))/(sqrt(sc.ApophisCentric.X^2 + sc.ApophisCentric.Y^2 + sc.
               ApophisCentric.Z^2)*sqrt(T(1)^2 + T(2)^2 + T(3)^2));
271
272        GMAT absXdott = abs(xdott);
273
274        % Check the alignment of X with T- if they are perpendicular, may need to burn
275        If absXdott < 0.02
276
277                           vdotx = V(1)*X(1) + V(2)*X(2) + V(3)*X(3);
278                           vdott = V(1)*T(1) + V(2)*T(2) + V(3)*T(3);
279
280                           theta = atan2(vdotx, vdott);
281
282                          % If V and T are approximately aligned, don't need to burn.
                                   Otherwise, need to burn.
283                           abstheta = abs(theta);
284
285                           If abstheta > 0.01745
286
287                                   % Calculate Required magnitude of dv (dv = v*tan(theta/2))
288                                   dv = sqrt(sc.ApophisCentric.VX^2 + sc.ApophisCentric.VY^2 +
                                           sc.ApophisCentric.VZ^2)*sin(abstheta);
289
290                                   burn.Element1 = -dv*sin(theta)
291                                   burn.Element2 = dv*cos(theta)
292
```

```
293                                     % Perform Manuever and increment dv usage
294                                     Maneuver burn(sc)
295                                     dvTot = dvTot + abs(dv);
296                                     Propagate ACP(sc) {sc.ElapsedDays = 0.025};
297                                     GMAT currentMJD = currentMJD + 0.025;
298
299                             Else
300
301                                     dv = 0;
302
303                             EndIf;
304
305                     Else
306
307                             dv = 0;
308
309                     EndIf
310
311                     Report POSreport sc.UTCGregorian sc.UTCModJulian sc.ApophisCentric.X sc.
                            ApophisCentric.Y sc.ApophisCentric.Z sc.ApophisCentric.VX sc.
                            ApophisCentric.VY sc.ApophisCentric.VZ Apophis.EarthMJ2000Ec.X Apophis.
                            EarthMJ2000Ec.Y Apophis.EarthMJ2000Ec.Z Apophis.EarthMJ2000Ec.VX Apophis
                            .EarthMJ2000Ec.VY Apophis.EarthMJ2000Ec.VZ T(1) T(2) T(3) xdott thetaVT
                            dv;
312
313     EndWhile;
314
315     GMAT dv_values(idx) = dvTot;
316     Write dvTot { Style = Concise, LogFile = false, MessageWindow = true }
317
318  EndFor;
319
320  Report DVreport dv_values;
321  Report Rreport radii;
322  Write dvTot
```

D.4 Impulsive Trajectory File

```
1  % 2017/05/09 MIT 16.83 Apophis Mission CDR
2  % High fidelity GMAT simulation of launch on 26 Aug 2026 and
3  % Rendezvous with Apophis in May 2028.
4  %
5  % All SPICE kernels obtained from JPL Horizons Telnet Interface
6  % Values for Big-16 asteroid masses from Farnocchia et al in Asteroids IV
7  % Runs with GMAT 2016a using DE-424(?) planetary ephemerides
8  %
9  %
10 % Simulates solar-electric trajectory with a single NEXT-C thruster at 236 mN and 100% duty
       factor running at 7kW
11 % To run,
12 %
13 % Obtain SPICE kernels for Apophis and the Big 16 asteroids out of the HORIZONS system and
       change fully qualified paths below
14 %
15 % Contact:
16 % Roman Geykhman
17 % geykhman@mit.edu
18 %----------------------------------------
19 %---------- User-Defined Celestial Bodies
20 %----------------------------------------
21
22 Create Asteroid Apophis;
23 GMAT Apophis.NAIFId = 2099942;
24 GMAT Apophis.OrbitSpiceKernelName = {'apophis.bsp'};
25 GMAT Apophis.Mu = 1e-09;
26 GMAT Apophis.PosVelSource = 'SPICE';
27 GMAT Apophis.CentralBody = 'Sun';
```

```
28
29 %% The 16 largest main belt asteroids and their masses from Farnochia et al in Asteroids IV,
       Table 2:
30
31 Create Asteroid Ceres;
32 GMAT Ceres.NAIFId = 2000001;
33 GMAT Ceres.OrbitSpiceKernelName = {'ceres.bsp'};
34 GMAT Ceres.Mu = 63.13
35 GMAT Ceres.PosVelSource = 'SPICE';
36 GMAT Ceres.CentralBody = 'Sun';
37 GMAT Ceres.EquatorialRadius = 0.5;
38
39 Create Asteroid Pallas;
40 GMAT Pallas.NAIFId = 2000002;
41 GMAT Pallas.OrbitSpiceKernelName = {'pallas.bsp'};
42 GMAT Pallas.Mu = 13.73;
43 GMAT Pallas.PosVelSource = 'SPICE';
44 GMAT Pallas.CentralBody = 'Sun';
45 GMAT Pallas.EquatorialRadius = 0.5;
46
47 Create Asteroid Juno;
48 GMAT Juno.NAIFId = 2000003;
49 GMAT Juno.OrbitSpiceKernelName = {'juno.bsp'};
50 GMAT Juno.Mu = 1.82;
51 GMAT Juno.PosVelSource = 'SPICE';
52 GMAT Juno.CentralBody = 'Sun';
53 GMAT Juno.EquatorialRadius = 0.5;
54
55 Create Asteroid Vesta;
56 GMAT Vesta.NAIFId = 2000004;
57 GMAT Vesta.OrbitSpiceKernelName = {'vesta.bsp'};
58 GMAT Vesta.Mu = 17.2903;
59 GMAT Vesta.PosVelSource = 'SPICE';
60 GMAT Vesta.CentralBody = 'Sun';
61 GMAT Vesta.EquatorialRadius = 0.5;
62
63 Create Asteroid Hebe;
64 GMAT Hebe.NAIFId = 2000006;
65 GMAT Hebe.OrbitSpiceKernelName = {'hebe.bsp'};
66 GMAT Hebe.Mu = 0.93;
67 GMAT Hebe.PosVelSource = 'SPICE';
68 GMAT Hebe.CentralBody = 'Sun';
69 GMAT Hebe.EquatorialRadius = 0.5;
70
71 Create Asteroid Iris;
72 GMAT Iris.NAIFId = 2000007;
73 GMAT Iris.OrbitSpiceKernelName = {'iris.bsp'};
74 GMAT Iris.Mu = 0.86;
75 GMAT Iris.PosVelSource = 'SPICE';
76 GMAT Iris.CentralBody = 'Sun';
77 GMAT Iris.EquatorialRadius = 0.5;
78
79 Create Asteroid Hygiea;
80 GMAT Hygiea.NAIFId = 2000010;
81 GMAT Hygiea.OrbitSpiceKernelName = {'hygiea.bsp'};
82 GMAT Hygiea.Mu = 5.78;
83 GMAT Hygiea.PosVelSource = 'SPICE';
84 GMAT Hygiea.CentralBody = 'Sun';
85 GMAT Hygiea.EquatorialRadius = 0.5;
86
87 Create Asteroid Eunomia;
88 GMAT Eunomia.NAIFId = 2000015;
89 GMAT Eunomia.OrbitSpiceKernelName = {'eunomia.bsp'};
90 GMAT Eunomia.Mu = 2.10;
91 GMAT Eunomia.PosVelSource = 'SPICE';
92 GMAT Eunomia.CentralBody = 'Sun';
93 GMAT Eunomia.EquatorialRadius = 0.5;
94
```

```
Create Asteroid Psyche;
GMAT Psyche.NAIFId = 2000016;
GMAT Psyche.OrbitSpiceKernelName = {'psyche.bsp'};
GMAT Psyche.Mu = 1.81;
GMAT Psyche.PosVelSource = 'SPICE';
GMAT Psyche.CentralBody = 'Sun';
GMAT Psyche.EquatorialRadius = 0.5;

Create Asteroid Amphitrite;
GMAT Amphitrite.NAIFId = 2000029;
GMAT Amphitrite.OrbitSpiceKernelName = {'amphitrite.bsp'};
GMAT Amphitrite.Mu = 0.86;
GMAT Amphitrite.PosVelSource = 'SPICE';
GMAT Amphitrite.CentralBody = 'Sun';
GMAT Amphitrite.EquatorialRadius = 0.5;

Create Asteroid Europa;
GMAT Europa.NAIFId = 2000052;
GMAT Europa.OrbitSpiceKernelName = {'europa.bsp'};
GMAT Europa.Mu = 1.59;
GMAT Europa.PosVelSource = 'SPICE';
GMAT Europa.CentralBody = 'Sun';
GMAT Europa.EquatorialRadius = 0.5;

Create Asteroid Cybele;
GMAT Cybele.NAIFId = 2000065;
GMAT Cybele.OrbitSpiceKernelName = {'cybele.bsp'};
GMAT Cybele.Mu = 0.91;
GMAT Cybele.PosVelSource = 'SPICE';
GMAT Cybele.CentralBody = 'Sun';
GMAT Cybele.EquatorialRadius = 0.5;

Create Asteroid Sylvia;
GMAT Sylvia.NAIFId = 2000087;
GMAT Sylvia.OrbitSpiceKernelName = {'sylvia.bsp'};
GMAT Sylvia.Mu = 0.99;
GMAT Sylvia.PosVelSource = 'SPICE';
GMAT Sylvia.CentralBody = 'Sun';
GMAT Sylvia.EquatorialRadius = 0.5;

Create Asteroid Thisbe;
GMAT Thisbe.NAIFId = 2000088;
GMAT Thisbe.OrbitSpiceKernelName = {'thisbe.bsp'};
GMAT Thisbe.Mu = 1.02;
GMAT Thisbe.PosVelSource = 'SPICE';
GMAT Thisbe.CentralBody = 'Sun';
GMAT Thisbe.EquatorialRadius = 0.5;

Create Asteroid Davida;
GMAT Davida.NAIFId = 2000511;
GMAT Davida.OrbitSpiceKernelName = {'davida.bsp'};
GMAT Davida.Mu = 2.26;
GMAT Davida.PosVelSource = 'SPICE';
GMAT Davida.CentralBody = 'Sun';
GMAT Davida.EquatorialRadius = 0.5;

Create Asteroid Interamnia;
GMAT Interamnia.NAIFId = 2000704;
GMAT Interamnia.OrbitSpiceKernelName = {'interamnia.bsp'};
GMAT Interamnia.Mu = 2.19;
GMAT Interamnia.PosVelSource = 'SPICE';
GMAT Interamnia.CentralBody = 'Sun';
GMAT Interamnia.EquatorialRadius = 0.5;

%----------------------------------------
%---------- Coordinate Systems
%----------------------------------------

```

```
Create CoordinateSystem SunEcliptic;
GMAT SunEcliptic.Origin = Sun;
GMAT SunEcliptic.Axes = MJ2000Ec;

Create CoordinateSystem EarthEcliptic;
GMAT EarthEcliptic.Origin = Earth;
GMAT EarthEcliptic.Axes = MJ2000Ec;

Create CoordinateSystem ApophisEcliptic;
GMAT ApophisEcliptic.Origin = Apophis;
GMAT ApophisEcliptic.Axes = MJ2000Ec;

%----------------------------------------
%---------- Spacecraft
%----------------------------------------

%hydrazine
Create ChemicalTank hydrazineTank
hydrazineTank.AllowNegativeFuelMass = false
hydrazineTank.FuelMass = 300
hydrazineTank.Pressure = 1500
hydrazineTank.Temperature = 20
hydrazineTank.RefTemperature = 20
hydrazineTank.Volume = 0.75
hydrazineTank.FuelDensity = 1260
hydrazineTank.PressureModel = PressureRegulated

Create ElectricTank xenonTank;
xenonTank.FuelMass = 180;
xenonTank.AllowNegativeFuelMass = true;

% Electric power system and Solar-Electric thruster:
Create SolarPowerSystem powerSystem;
powerSystem.InitialMaxPower = 7; %kw

Create ElectricThruster nextThruster;
nextThruster.Axes = VNB;
nextThruster.CoordinateSystem = Local;
nextThruster.DecrementMass = true;
nextThruster.Origin = Sun;
nextThruster.Tank = xenonTank;
nextThruster.ThrustModel = ConstantThrustAndIsp;
nextThruster.ConstantThrust = 0.236;
nextThruster.Isp = 4190;

%don't create a ChemicalThruster object; low fidelity modeling of hydrazine thruster through
     impulsive burn objects

%% Force Models and Propagator objects

%----------------------------------------
%---------- ForceModels
%----------------------------------------

Create ForceModel HelioProp_ForceModel;
GMAT HelioProp_ForceModel.CentralBody = Sun;
GMAT HelioProp_ForceModel.PointMasses = {Sun, Mercury, Venus, Earth, Luna, Mars, Jupiter,
     Saturn, Uranus, Neptune, Pluto, Ceres, Pallas, Juno, Vesta, Hebe, Iris, Hygiea, Eunomia,
      Psyche, Amphitrite, Europa, Cybele, Sylvia, Thisbe, Davida, Interamnia, Apophis};
GMAT HelioProp_ForceModel.Drag = None;
GMAT HelioProp_ForceModel.SRP = On;
GMAT HelioProp_ForceModel.RelativisticCorrection = On;
GMAT HelioProp_ForceModel.ErrorControl = RSSStep;


%----------------------------------------
%---------- Propagators
%----------------------------------------
```

```
228
229 Create Propagator HelioProp;
230 GMAT HelioProp.FM = HelioProp_ForceModel;
231 GMAT HelioProp.Type = RungeKutta89;
232 GMAT HelioProp.InitialStepSize = 86400;
233 GMAT HelioProp.Accuracy = 1e-8;
234 GMAT HelioProp.MinStep = 1000;
235 GMAT HelioProp.MaxStep = 86400;
236 GMAT HelioProp.MaxStepAttempts = 50;
237 GMAT HelioProp.StopIfAccuracyIsViolated = false;
238
239 Create Propagator GeoProp;
240 GMAT GeoProp.FM = HelioProp_ForceModel;
241 GMAT GeoProp.Type = RungeKutta89;
242 GMAT GeoProp.InitialStepSize = 40;
243 GMAT GeoProp.Accuracy = 1e-8;
244 GMAT GeoProp.MinStep = 10;
245 GMAT GeoProp.MaxStep = 400;
246 GMAT GeoProp.MaxStepAttempts = 50;
247 GMAT GeoProp.StopIfAccuracyIsViolated = false;
248
249
250 Create Propagator NearApophis;
251 GMAT NearApophis.FM = HelioProp_ForceModel;
252 GMAT NearApophis.Type = RungeKutta89;
253 GMAT NearApophis.InitialStepSize = 60;
254 GMAT NearApophis.Accuracy = 1e-8;
255 GMAT NearApophis.MinStep = 1;
256 GMAT NearApophis.MaxStep = 8640;
257 GMAT NearApophis.MaxStepAttempts = 50;
258 GMAT NearApophis.StopIfAccuracyIsViolated = false;
259
260 %% Spacecraft objects. Create several objects for aids to calculation as well as main
      mission sequence
261
262 Create Spacecraft sc0;
263 GMAT sc0.DateFormat = UTCModJulian;
264 GMAT sc0.Epoch = '31276'; %august 2026 launch
265 GMAT sc0.CoordinateSystem = SunEcliptic;
266 GMAT sc0.DisplayStateType = Cartesian;
267 GMAT sc0.DryMass = 500;
268 GMAT sc0.Cd = 2.2;
269 GMAT sc0.Cr = 1;
270 GMAT sc0.DragArea = 15;
271 GMAT sc0.SRPArea = 15;
272 GMAT sc0.Tanks = {hydrazineTank, xenonTank};
273 GMAT sc0.PowerSystem = powerSystem;
274 GMAT sc0.Thrusters = nextThruster;
275
276 Create Spacecraft sc1;
277 sc1 = sc0;
278
279 % Data subscribers
280 Create ReportFile trajreport;
281 GMAT trajreport.SolverIterations = Current;
282 GMAT trajreport.UpperLeft = [ 0 0 ];
283 GMAT trajreport.Size = [ 0 0 ];
284 GMAT trajreport.RelativeZOrder = 0;
285 GMAT trajreport.Maximized = false;
286 GMAT trajreport.Filename = 'output_solar_system_ecliptic.txt';
287 GMAT trajreport.Precision = 16;
288 GMAT trajreport.WriteHeaders = true;
289 GMAT trajreport.LeftJustify = On;
290 GMAT trajreport.ZeroFill = Off;
291 GMAT trajreport.FixedWidth = true;
292 GMAT trajreport.Delimiter = ' ';
293 GMAT trajreport.ColumnWidth = 23;
294 GMAT trajreport.WriteReport = true;
```

```
GMAT trajreport.Add = {sc0.UTCGregorian sc0.UTCModJulian  sc0.SunEcliptic.X sc0.SunEcliptic.Y sc0.SunEcliptic.Z  sc0.SunEcliptic.VX sc0.SunEcliptic.VY sc0.SunEcliptic.VZ sc0.TotalMass sc0.xenonTank.FuelMass sc0.hydrazineTank.FuelMass  };

Create ReportFile trajreport_apophis;
GMAT trajreport_apophis.SolverIterations = Current;
GMAT trajreport_apophis.UpperLeft = [ 0 0 ];
GMAT trajreport_apophis.Size = [ 0 0 ];
GMAT trajreport_apophis.RelativeZOrder = 0;
GMAT trajreport_apophis.Maximized = false;
GMAT trajreport_apophis.Filename = 'output_apophis_system_ecliptic.txt';
GMAT trajreport_apophis.Precision = 16;
GMAT trajreport_apophis.WriteHeaders = true;
GMAT trajreport_apophis.LeftJustify = On;
GMAT trajreport_apophis.ZeroFill = Off;
GMAT trajreport_apophis.FixedWidth = true;
GMAT trajreport_apophis.Delimiter = ' ';
GMAT trajreport_apophis.ColumnWidth = 23;
GMAT trajreport_apophis.WriteReport = true;
GMAT trajreport_apophis.Add = {sc0.UTCGregorian sc0.UTCModJulian  sc0.ApophisEcliptic.X sc0.ApophisEcliptic.Y sc0.ApophisEcliptic.Z  sc0.ApophisEcliptic.VX sc0.ApophisEcliptic.VY sc0.ApophisEcliptic.VZ };

Create ReportFile trajreport_earth;
GMAT trajreport_earth.SolverIterations = Current;
GMAT trajreport_earth.UpperLeft = [ 0 0 ];
GMAT trajreport_earth.Size = [ 0 0 ];
GMAT trajreport_earth.RelativeZOrder = 0;
GMAT trajreport_earth.Maximized = false;
GMAT trajreport_earth.Filename = 'output_earth_system_ecliptic.txt';
GMAT trajreport_earth.Precision = 16;
GMAT trajreport_earth.WriteHeaders = true;
GMAT trajreport_earth.LeftJustify = On;
GMAT trajreport_earth.ZeroFill = Off;
GMAT trajreport_earth.FixedWidth = true;
GMAT trajreport_earth.Delimiter = ' ';
GMAT trajreport_earth.ColumnWidth = 23;
GMAT trajreport_earth.WriteReport = true;
GMAT trajreport_earth.Add = {sc0.UTCGregorian sc0.UTCModJulian  sc0.EarthEcliptic.X sc0.EarthEcliptic.Y sc0.EarthEcliptic.Z  sc0.EarthEcliptic.VX sc0.EarthEcliptic.VY sc0.EarthEcliptic.VZ };



%burns and trajectory correction maneuvers
Create ImpulsiveBurn EscapeBurn;
GMAT EscapeBurn.CoordinateSystem = Local;
GMAT EscapeBurn.Origin = Earth;
GMAT EscapeBurn.Axes = VNB;
GMAT EscapeBurn.Element1 = 4.000;
GMAT EscapeBurn.Element2 = 0;
GMAT EscapeBurn.Element3 = 0;
GMAT EscapeBurn.DecrementMass = false;
GMAT EscapeBurn.Isp = 300;
GMAT EscapeBurn.GravitationalAccel = 9.81;


Create ImpulsiveBurn TCM_Launch;
TCM_Launch.CoordinateSystem = Local;
TCM_Launch.Origin = Sun;
TCM_Launch.Axes = VNB;
TCM_Launch.Element1 = 0;
TCM_Launch.Element2 = 0;
TCM_Launch.Element3 = 0;
TCM_Launch.DecrementMass = false;
TCM_Launch.Isp = 220;
TCM_Launch.GravitationalAccel = 9.81;
TCM_Launch.Tank = hydrazineTank;
```

```
357
358 Create ImpulsiveBurn TCM_Launch_SEP;
359 TCM_Launch_SEP.CoordinateSystem = Local;
360 TCM_Launch_SEP.Origin = Sun;
361 TCM_Launch_SEP.Axes = VNB;
362 TCM_Launch_SEP.Element1 = 0;
363 TCM_Launch_SEP.Element2 = 0;
364 TCM_Launch_SEP.Element3 = 0;
365 TCM_Launch_SEP.DecrementMass = false;
366 TCM_Launch_SEP.Isp = 220;
367 TCM_Launch_SEP.GravitationalAccel = 9.81;
368 TCM_Launch_SEP.Tank = hydrazineTank;
369
370
371 Create ImpulsiveBurn TCM_PlaneChange;
372 TCM_PlaneChange.CoordinateSystem = Local;
373 TCM_PlaneChange.Origin = Sun;
374 TCM_PlaneChange.Axes = VNB;
375 TCM_PlaneChange.Element1 = 0;
376 TCM_PlaneChange.Element2 = -1.7;
377 TCM_PlaneChange.Element3 = 0;
378 TCM_PlaneChange.DecrementMass = false;
379 TCM_PlaneChange.Isp = 220;
380 TCM_PlaneChange.GravitationalAccel = 9.81;
381 TCM_PlaneChange.Tank = hydrazineTank;
382
383 Create ImpulsiveBurn TCM_PeriodChange;
384 TCM_PeriodChange.CoordinateSystem = Local;
385 TCM_PeriodChange.Origin = Sun;
386 TCM_PeriodChange.Axes = VNB;
387 TCM_PeriodChange.Element1 = -0.5;
388 TCM_PeriodChange.Element2 = 0;
389 TCM_PeriodChange.Element3 = 0;
390 TCM_PeriodChange.DecrementMass = false;
391 TCM_PeriodChange.Isp = 220;
392 TCM_PeriodChange.GravitationalAccel = 9.81;
393 TCM_PeriodChange.Tank = hydrazineTank;
394
395 Create ImpulsiveBurn TCM_VelocityMatch;
396 TCM_VelocityMatch.CoordinateSystem = SunEcliptic;
397 TCM_VelocityMatch.Origin = Sun;
398 TCM_VelocityMatch.Axes = MJ2000Eq;
399 TCM_VelocityMatch.Element1 = -0.5;
400 TCM_VelocityMatch.Element2 = 0;
401 TCM_VelocityMatch.Element3 = 0;
402 TCM_VelocityMatch.DecrementMass = false;
403 TCM_VelocityMatch.Isp = 220;
404 TCM_VelocityMatch.GravitationalAccel = 9.81;
405 TCM_VelocityMatch.Tank = hydrazineTank;
406
407 Create ImpulsiveBurn TCM_R1;
408 TCM_R1.CoordinateSystem = Local;
409 TCM_R1.Origin = Sun;
410 TCM_R1.Axes = VNB;
411 TCM_R1.Element1 = 0;
412 TCM_R1.Element2 = 0;
413 TCM_R1.Element3 = 0;
414 TCM_R1.DecrementMass = false;
415 TCM_R1.Isp = 220;
416 TCM_R1.GravitationalAccel = 9.81;
417 TCM_R1.Tank = hydrazineTank;
418
419 Create ImpulsiveBurn TCM_R2;
420 TCM_R2.CoordinateSystem = Local;
421 TCM_R2.Origin = Apophis;
422 TCM_R2.Axes = LVLH;
423 TCM_R2.Element1 = 0;
424 TCM_R2.Element2 = 0;
```

```
425 TCM_R2.Element3 = 0;
426 TCM_R2.DecrementMass = false;
427 TCM_R2.Isp = 220;
428 TCM_R2.GravitationalAccel = 9.81;
429 TCM_R2.Tank = hydrazineTank;
430
431 Create ImpulsiveBurn TCM_R3;
432 TCM_R3.CoordinateSystem = Local;
433 TCM_R3.Origin = Sun;
434 TCM_R3.Axes = VNB;
435 TCM_R3.Element1 = 0;
436 TCM_R3.Element2 = 0;
437 TCM_R3.Element3 = 0;
438 TCM_R3.DecrementMass = false;
439 TCM_R3.Isp = 220;
440 TCM_R3.GravitationalAccel = 9.81;
441 TCM_R3.Tank = hydrazineTank;
442
443 Create ImpulsiveBurn TCM_R4;
444 TCM_R4.CoordinateSystem = Local;
445 TCM_R4.Origin = Apophis;
446 TCM_R4.Axes = VNB;
447 TCM_R4.Element1 = 0;
448 TCM_R4.Element2 = 0;
449 TCM_R4.Element3 = 0;
450 TCM_R4.DecrementMass = false;
451 TCM_R4.Isp = 220;
452 TCM_R4.GravitationalAccel = 9.81;
453 TCM_R4.Tank = hydrazineTank;
454
455 Create FiniteBurn sepBurn;
456 sepBurn.Thrusters = nextThruster;
457
458 %Create calculation variables and differential corrector objects
459
460 Create Variable pi, negpi, twopi, ThetaOut, EscapeTime, PlaneChangeDT ZDotDesired;
461 Create Variable phiNow, phiPln, nuBurn, eaBurn, maBurn, dtBurn, dtApo, dtApo2, dtApToNode;
462
463 Create Variable ATheta, MTheta, DTheta, DR, DZ, DRdot DV;
464
465
466
467 Create Variable T_vmm T_rendezvous0;
468
469 Create DifferentialCorrector DC;
470 DC.DerivativeMethod = CentralDifference;
471
472 %Impulsive end-to-end
473 BeginMissionSequence;
474
475 pi = 3.14159265358979323846264338327950;
476 negpi = -1*pi;
477 twopi = 2*pi;
478
479
480 %start in 2026 August around the Earth in a circular parking orbit
481 sc0.Epoch = 31279;
482 sc0.CoordinateSystem = EarthEcliptic;
483 sc0.EarthEcliptic.X =  6371 + 185;
484 sc0.EarthEcliptic.Y = 0;
485 sc0.EarthEcliptic.Z = 0;
486 sc0.EarthEcliptic.VX = 0;
487 sc0.EarthEcliptic.VY = sqrt(398600.4415/ ( 6371 + 185) ) + 0.01;
488 sc0.EarthEcliptic.VZ = 0;
489
490
491 %Target an escape burn to achieve an asymptote direction in the plane of the ecliptic going
        out
```

```
%with aphelion selected by setting the outgoing C3 to 0.78 (km/sec)^2

ThetaOut = atan2( Earth.SunEcliptic.VY, Earth.SunEcliptic.VX )*180/pi;

Target DC

   Vary DC ( EscapeBurn.Element1 = 3.23, {Lower = 3.0, Upper = 5.0} );
   Vary DC ( EscapeTime = 8957.0, {Lower = 2700, Upper = 11000, Perturbation = 60} );

   Propagate GeoProp(sc0) {sc0.ElapsedSecs = EscapeTime};

   DV = sqrt( sc0.EarthEcliptic.VX^2 + sc0.EarthEcliptic.VY^2 + sc0.EarthEcliptic.VZ^2);
   DR = sqrt( sc0.EarthEcliptic.X^2 + sc0.EarthEcliptic.Y^2 + sc0.EarthEcliptic.Z^2);



   Maneuver EscapeBurn(sc0);

   DV = sqrt( sc0.EarthEcliptic.VX^2 + sc0.EarthEcliptic.VY^2 + sc0.EarthEcliptic.VZ^2);
   DR = sc0.Earth.Altitude;
   DZ = sc0.Earth.SMA



   Propagate GeoProp(sc0) {sc0.ElapsedDays = 1.5}; %get some altitude before computing C3

   Achieve DC( sc0.Earth.OutgoingC3Energy = 0.600, {Tolerance = 1e-6} );
   Achieve DC( sc0.EarthEcliptic.OutgoingRHA = ThetaOut, {Tolerance = 1e-4} );

EndTarget;

sc1 = sc0;

%now execute the trajectory correction manuever post-launch, plane change, period change,
    and velocity match maneuver within a single optimization

%approximate time of rendezvous after the final vmm
nuBurn = (204.457189)*pi/180;
eaBurn = atan2( sin(nuBurn)/sqrt(1 - sc0.Sun.ECC^2 ), sc0.Sun.ECC + cos( nuBurn ) );
maBurn = eaBurn - sc0.Sun.ECC * sin(eaBurn);

dtApToNode = (maBurn - pi);

If dtApToNode < 0
  dtApToNode = dtApToNode + 2*pi;
EndIf;
dtApToNode = dtApToNode / (sc0.Sun.MM * 86400);

Target DC

   Vary DC(TCM_Launch.Element1 = -0.056, {Lower = -0.25, Upper = 0.25, MaxStep = 0.01});
   Vary DC(TCM_PlaneChange.Element2 = -1.709, {Lower = -2.5, Upper = 2.4, Perturbation =
       0.05, MaxStep = 0.05});
   Vary DC(TCM_PeriodChange.Element1 = -0.33, {Lower = -.7, Upper = 0.7, Perturbation =
       0.01, MaxStep = 0.05});
   Vary DC(PlaneChangeDT             = 0, {Lower = -20, Upper = 20, Perturbation = 0.1,
       MaxStep = 1});


   Maneuver TCM_Launch(sc0);

   %Apophis RAAN is 204.457189 degrees, so we need to figure out how long it takes to get
       there
   %
   % we will do this by computing nu at the present time, and MA at the present time
   % these two will come from the spacecraft state
   %
   % we then compute the nu corresponding to 204 degrees and the MA corresponding to that
```

```
      time
% and then compute the time to propagate via dt = MA / n
%

phiNow = atan2( sc0.SunEcliptic.Y, sc0.SunEcliptic.X)*180/pi;
phiPln = 204.457189 - 180.0;

nuBurn = (phiPln - phiNow + sc0.Sun.TA)*pi/180;

If nuBurn < 0
   nuBurn = nuBurn + 2*pi;
EndIf;

eaBurn = atan2( sin(nuBurn)/sqrt(1 - sc0.Sun.ECC^2 ), sc0.Sun.ECC + cos( nuBurn ) );
maBurn = eaBurn - sc0.Sun.ECC * sin(eaBurn);

dtBurn = (maBurn - sc0.Sun.MA*pi/180);

If dtBurn < 0
    dtBurn = dtBurn + 2*pi;
EndIf;

dtBurn = dtBurn / (sc0.Sun.MM * 86400) + PlaneChangeDT;

dtApo  = (pi - maBurn) / (sc0.Sun.MM * 86400) - dtBurn - PlaneChangeDT;

Propagate HelioProp(sc0) {sc0.ElapsedDays = dtBurn};

Maneuver  TCM_PlaneChange(sc0);

Propagate HelioProp(sc0) {sc0.ElapsedDays = dtApo};

Maneuver  TCM_PeriodChange(sc0);

Propagate HelioProp(sc0) {sc0.ElapsedDays = 30};

dtApo2 = (pi - sc0.Sun.MA*pi/180);

If dtApo2 < 0
    dtApo2 = dtApo2 + 2*pi;
EndIf;

dtApo2  = dtApo2 / (sc0.Sun.MM * 86400);

Propagate HelioProp(sc0) {sc0.ElapsedDays = dtApo2};

Apophis.UTCModJulian = sc0.UTCModJulian;

ATheta = atan2( Apophis.SunEcliptic.Y, Apophis.SunEcliptic.X);
MTheta = atan2( sc0.SunEcliptic.Y, sc0.SunEcliptic.X);

DTheta = ATheta - MTheta;

If DTheta > pi
  DTheta = DTheta - 2*pi;
EndIf;

If DTheta <= negpi
   DTheta = DTheta + 2*pi;
EndIf;


DZ =  Apophis.SunEcliptic.Z - sc0.SunEcliptic.Z;

DR =  sqrt(Apophis.SunEcliptic.X^2 + Apophis.SunEcliptic.Y^2) - sqrt( sc0.SunEcliptic.X^2
     + sc0.SunEcliptic.Y^2);

ZDotDesired = -200/(86400*dtApToNode);
```

```
621
622     Achieve DC( DTheta = 0, {Tolerance = 1e-10});
623     Achieve DC( DZ = 200, {Tolerance = 10}); %miss by 40 km intentionally
624     Achieve DC( DR =  0, {Tolerance = 10});
625     Achieve DC( sc0.ApophisEcliptic.VZ =  ZDotDesired , {Tolerance = 1e-3});
626
627
628 EndTarget; %period change
629
630 TCM_VelocityMatch.Element1 = Apophis.SunEcliptic.VX - sc0.SunEcliptic.VX;
631 TCM_VelocityMatch.Element2 = Apophis.SunEcliptic.VY - sc0.SunEcliptic.VY;
632 TCM_VelocityMatch.Element3 = 0;
633
634 T_vmm                      = sc0.UTCModJulian;
635
636
637
638 Maneuver TCM_VelocityMatch(sc0);
639
640
641 phiNow = atan2( sc0.SunEcliptic.Y, sc0.SunEcliptic.X)*180/pi;
642 phiPln = 204.457189;
643
644 nuBurn = (phiPln - phiNow + sc0.Sun.TA)*pi/180;
645 eaBurn = atan2( sin(nuBurn)/sqrt(1 - sc0.Sun.ECC^2 ), sc0.Sun.ECC + cos( nuBurn ) );
646 maBurn = eaBurn - sc0.Sun.ECC * sin(eaBurn);
647
648 dtBurn = (maBurn - sc0.Sun.MA*pi/180);
649
650 If dtBurn < 0
651    dtBurn = dtBurn + 2*pi;
652 EndIf;
653
654 dtBurn = dtBurn / (sc0.Sun.MM * 86400);
655
656 T_rendezvous0 = dtBurn + sc0.UTCModJulian;
657
658 Write EscapeBurn TCM_Launch TCM_PlaneChange TCM_PeriodChange T_vmm TCM_VelocityMatch
       T_rendezvous0
659
660 Target DC
661
662     Vary DC(TCM_R1.Element1 = 0, {Lower = -0.25, Upper = 0.25, Perturbation=0.001, MaxStep =
          0.005});
663     Vary DC(TCM_R1.Element2 = 0, {Lower = -0.25, Upper = 0.25, Perturbation=0.001, MaxStep =
          0.005});
664     Vary DC(TCM_R1.Element3 = 0, {Lower = -0.25, Upper = 0.25, Perturbation=0.001, MaxStep =
          0.005});
665
666     Maneuver TCM_R1(sc0);
667
668
669     Propagate HelioProp(sc0){ sc0.ElapsedDays = dtBurn};
670
671     Apophis.UTCModJulian = sc0.UTCModJulian;
672
673     ATheta = atan2( Apophis.SunEcliptic.Y, Apophis.SunEcliptic.X);
674     MTheta = atan2( sc0.SunEcliptic.Y, sc0.SunEcliptic.X);
675
676     DTheta = ATheta - MTheta;
677
678     If DTheta > pi
679       DTheta = DTheta - 2*pi;
680     EndIf;
681
682     If DTheta <= negpi
683        DTheta = DTheta + 2*pi;
684     EndIf;
```

```
685
686
687     DZ =  Apophis.SunEcliptic.Z - sc0.SunEcliptic.Z;
688
689     DR =  sqrt(Apophis.SunEcliptic.X^2 + Apophis.SunEcliptic.Y^2) - sqrt( sc0.SunEcliptic.X^2
            + sc0.SunEcliptic.Y^2);
690
691     Achieve DC( DTheta = 0, {Tolerance = 1e-10});
692     Achieve DC( DZ = 10, {Tolerance = 0.1});
693     Achieve DC( DR =  0, {Tolerance = 0.01});
694
695 EndTarget
696
697 %now can do b-plane targetting and enter orbit. but first we need to make a small impulse
        toward the asteroid
698
699 TCM_R2.Element1 = -0.01;
700 Maneuver TCM_R2(sc0);
701
702
703 Target DC
704
705     Vary DC(TCM_R3.Element1 = 0, {Lower = -0.05, Upper = 0.05, Perturbation=0.001, MaxStep =
            0.005});
706     Vary DC(TCM_R3.Element2 = 0, {Lower = -0.05, Upper = 0.05, Perturbation=0.001, MaxStep =
            0.005});
707     Vary DC(TCM_R3.Element3 = 0, {Lower = -0.05, Upper = 0.05, Perturbation=0.001, MaxStep =
            0.005});
708
709     Maneuver TCM_R3(sc0);
710
711     Achieve DC( sc0.ApophisEcliptic.BdotT = 0, {Tolerance = .01});
712     Achieve DC( sc0.Apophis.IncomingRadPer = 1.2, {Tolerance = .01});
713 EndTarget
714
715 dtBurn = -sc0.Apophis.MA * pi / (180*sc0.Apophis.MM);
716
717 Propagate NearApophis(sc0){ sc0.ElapsedSecs = dtBurn};
718
719 TCM_R4.Element1 = sqrt( 1e-09 / sc0.Apophis.RMAG ) - sc0.ApophisEcliptic.VMAG;
720 TCM_R4.Element2 = 0;
721 TCM_R4.Element3 = 0;
722
723 Maneuver TCM_R4(sc0);
724 Write dtBurn TCM_R4
725 Propagate NearApophis(sc0) {sc0.ElapsedDays = 2};
```

D.5 Solar-Electric Trajectory File

```
1  % 2017/05/09 MIT 16.83 Apophis Mission CDR
2  % High fidelity GMAT simulation of launch on 26 Aug 2026 and
3  % Rendezvous with Apophis in May 2028.
4  %
5  % All SPICE kernels obtained from JPL Horizons Telnet Interface
6  % Values for Big-16 asteroid masses from Farnocchia et al in Asteroids IV
7  % Runs with GMAT 2016a using DE-424(?) planetary ephemerides
8  %
9  %
10 % Simulates solar-electric trajectory with a single NEXT-C thruster at 236 mN and 100% duty
       factor running at 7kW
11 % To run,
12 %
13 % Obtain SPICE kernels for Apophis and the Big 16 asteroids out of the HORIZONS system and
       change fully qualified paths below
14 %
15 % Contact:
16 % Roman Geykhman
```

```
17 % geykhman@mit.edu
18
19 %----------------------------------------
20 %---------- User-Defined Celestial Bodies
21 %----------------------------------------
22
23 %Need to edit and recompile source code for DE430 to work, otherwise default is DE421
24 %SolarSystem.EphemerisSource = 'DE430';
25 %SolarSystem.DEFilename = 'de430.dat';
26
27 Create Asteroid Apophis;
28 GMAT Apophis.NAIFId = 2099942;
29 GMAT Apophis.OrbitSpiceKernelName = {'apophis.bsp'};
30 GMAT Apophis.Mu = 1e-09;
31 GMAT Apophis.PosVelSource = 'SPICE';
32 GMAT Apophis.CentralBody = 'Sun';
33
34 %% The 16 largest main belt asteroids and their masses from Farnochia et al in Asteroids IV,
       Table 2:
35
36 Create Asteroid Ceres;
37 GMAT Ceres.NAIFId = 2000001;
38 GMAT Ceres.OrbitSpiceKernelName = {'ceres.bsp'};
39 GMAT Ceres.Mu = 63.13
40 GMAT Ceres.PosVelSource = 'SPICE';
41 GMAT Ceres.CentralBody = 'Sun';
42 GMAT Ceres.EquatorialRadius = 0.5;
43
44 Create Asteroid Pallas;
45 GMAT Pallas.NAIFId = 2000002;
46 GMAT Pallas.OrbitSpiceKernelName = {'pallas.bsp'};
47 GMAT Pallas.Mu = 13.73;
48 GMAT Pallas.PosVelSource = 'SPICE';
49 GMAT Pallas.CentralBody = 'Sun';
50 GMAT Pallas.EquatorialRadius = 0.5;
51
52 Create Asteroid Juno;
53 GMAT Juno.NAIFId = 2000003;
54 GMAT Juno.OrbitSpiceKernelName = {'juno.bsp'};
55 GMAT Juno.Mu = 1.82;
56 GMAT Juno.PosVelSource = 'SPICE';
57 GMAT Juno.CentralBody = 'Sun';
58 GMAT Juno.EquatorialRadius = 0.5;
59
60 Create Asteroid Vesta;
61 GMAT Vesta.NAIFId = 2000004;
62 GMAT Vesta.OrbitSpiceKernelName = {'vesta.bsp'};
63 GMAT Vesta.Mu = 17.2903;
64 GMAT Vesta.PosVelSource = 'SPICE';
65 GMAT Vesta.CentralBody = 'Sun';
66 GMAT Vesta.EquatorialRadius = 0.5;
67
68 Create Asteroid Hebe;
69 GMAT Hebe.NAIFId = 2000006;
70 GMAT Hebe.OrbitSpiceKernelName = {'hebe.bsp'};
71 GMAT Hebe.Mu = 0.93;
72 GMAT Hebe.PosVelSource = 'SPICE';
73 GMAT Hebe.CentralBody = 'Sun';
74 GMAT Hebe.EquatorialRadius = 0.5;
75
76 Create Asteroid Iris;
77 GMAT Iris.NAIFId = 2000007;
78 GMAT Iris.OrbitSpiceKernelName = {'iris.bsp'};
79 GMAT Iris.Mu = 0.86;
80 GMAT Iris.PosVelSource = 'SPICE';
81 GMAT Iris.CentralBody = 'Sun';
82 GMAT Iris.EquatorialRadius = 0.5;
83
```

```
84  Create Asteroid Hygiea;
85  GMAT Hygiea.NAIFId = 2000010;
86  GMAT Hygiea.OrbitSpiceKernelName = {'hygiea.bsp'};
87  GMAT Hygiea.Mu = 5.78;
88  GMAT Hygiea.PosVelSource = 'SPICE';
89  GMAT Hygiea.CentralBody = 'Sun';
90  GMAT Hygiea.EquatorialRadius = 0.5;
91
92  Create Asteroid Eunomia;
93  GMAT Eunomia.NAIFId = 2000015;
94  GMAT Eunomia.OrbitSpiceKernelName = {'eunomia.bsp'};
95  GMAT Eunomia.Mu = 2.10;
96  GMAT Eunomia.PosVelSource = 'SPICE';
97  GMAT Eunomia.CentralBody = 'Sun';
98  GMAT Eunomia.EquatorialRadius = 0.5;
99
100 Create Asteroid Psyche;
101 GMAT Psyche.NAIFId = 2000016;
102 GMAT Psyche.OrbitSpiceKernelName = {'psyche.bsp'};
103 GMAT Psyche.Mu = 1.81;
104 GMAT Psyche.PosVelSource = 'SPICE';
105 GMAT Psyche.CentralBody = 'Sun';
106 GMAT Psyche.EquatorialRadius = 0.5;
107
108 Create Asteroid Amphitrite;
109 GMAT Amphitrite.NAIFId = 2000029;
110 GMAT Amphitrite.OrbitSpiceKernelName = {'amphitrite.bsp'};
111 GMAT Amphitrite.Mu = 0.86;
112 GMAT Amphitrite.PosVelSource = 'SPICE';
113 GMAT Amphitrite.CentralBody = 'Sun';
114 GMAT Amphitrite.EquatorialRadius = 0.5;
115
116 Create Asteroid Europa;
117 GMAT Europa.NAIFId = 2000052;
118 GMAT Europa.OrbitSpiceKernelName = {'europa.bsp'};
119 GMAT Europa.Mu = 1.59;
120 GMAT Europa.PosVelSource = 'SPICE';
121 GMAT Europa.CentralBody = 'Sun';
122 GMAT Europa.EquatorialRadius = 0.5;
123
124 Create Asteroid Cybele;
125 GMAT Cybele.NAIFId = 2000065;
126 GMAT Cybele.OrbitSpiceKernelName = {'cybele.bsp'};
127 GMAT Cybele.Mu = 0.91;
128 GMAT Cybele.PosVelSource = 'SPICE';
129 GMAT Cybele.CentralBody = 'Sun';
130 GMAT Cybele.EquatorialRadius = 0.5;
131
132 Create Asteroid Sylvia;
133 GMAT Sylvia.NAIFId = 2000087;
134 GMAT Sylvia.OrbitSpiceKernelName = {'sylvia.bsp'};
135 GMAT Sylvia.Mu = 0.99;
136 GMAT Sylvia.PosVelSource = 'SPICE';
137 GMAT Sylvia.CentralBody = 'Sun';
138 GMAT Sylvia.EquatorialRadius = 0.5;
139
140 Create Asteroid Thisbe;
141 GMAT Thisbe.NAIFId = 2000088;
142 GMAT Thisbe.OrbitSpiceKernelName = {'thisbe.bsp'};
143 GMAT Thisbe.Mu = 1.02;
144 GMAT Thisbe.PosVelSource = 'SPICE';
145 GMAT Thisbe.CentralBody = 'Sun';
146 GMAT Thisbe.EquatorialRadius = 0.5;
147
148 Create Asteroid Davida;
149 GMAT Davida.NAIFId = 2000511;
150 GMAT Davida.OrbitSpiceKernelName = {'davida.bsp'};
151 GMAT Davida.Mu = 2.26;
```

```
GMAT Davida.PosVelSource = 'SPICE';
GMAT Davida.CentralBody = 'Sun';
GMAT Davida.EquatorialRadius = 0.5;

Create Asteroid Interamnia;
GMAT Interamnia.NAIFId = 2000704;
GMAT Interamnia.OrbitSpiceKernelName = {'interamnia.bsp'};
GMAT Interamnia.Mu = 2.19;
GMAT Interamnia.PosVelSource = 'SPICE';
GMAT Interamnia.CentralBody = 'Sun';
GMAT Interamnia.EquatorialRadius = 0.5;

%----------------------------------------
%---------- Coordinate Systems
%----------------------------------------

Create CoordinateSystem SunEcliptic;
GMAT SunEcliptic.Origin = Sun;
GMAT SunEcliptic.Axes = MJ2000Ec;

Create CoordinateSystem EarthEcliptic;
GMAT EarthEcliptic.Origin = Earth;
GMAT EarthEcliptic.Axes = MJ2000Ec;

Create CoordinateSystem ApophisEcliptic;
GMAT ApophisEcliptic.Origin = Apophis;
GMAT ApophisEcliptic.Axes = MJ2000Ec;

%----------------------------------------
%---------- Spacecraft
%----------------------------------------

%hydrazine
Create ChemicalTank hydrazineTank
hydrazineTank.AllowNegativeFuelMass = false
hydrazineTank.FuelMass = 300
hydrazineTank.Pressure = 1500
hydrazineTank.Temperature = 20
hydrazineTank.RefTemperature = 20
hydrazineTank.Volume = 0.75
hydrazineTank.FuelDensity = 1260
hydrazineTank.PressureModel = PressureRegulated

Create ElectricTank xenonTank;
xenonTank.FuelMass = 180;
xenonTank.AllowNegativeFuelMass = false;

% Electric power system and Solar-Electric thruster:
Create SolarPowerSystem powerSystem;
powerSystem.InitialMaxPower = 7; %kw

Create ElectricThruster nextThruster;
nextThruster.Axes = VNB;
nextThruster.CoordinateSystem = Local;
nextThruster.DecrementMass = true;
nextThruster.Origin = Sun;
nextThruster.Tank = xenonTank;
nextThruster.ThrustModel = ConstantThrustAndIsp;
nextThruster.ConstantThrust = 0.236;
nextThruster.Isp = 4190;

%don't create a ChemicalThruster object; low fidelity modeling of hydrazine thruster through
     impulsive burn objects

%% Force Models and Propagator objects

%----------------------------------------
%---------- ForceModels
```

```
%----------------------------------------

Create ForceModel HelioProp_ForceModel;
GMAT HelioProp_ForceModel.CentralBody = Sun;
GMAT HelioProp_ForceModel.PointMasses = {Sun, Mercury, Venus, Earth, Luna, Mars, Jupiter,
     Saturn, Uranus, Neptune, Pluto, Ceres, Pallas, Juno, Vesta, Hebe, Iris, Hygiea, Eunomia,
      Psyche, Amphitrite, Europa, Cybele, Sylvia, Thisbe, Davida, Interamnia, Apophis};
GMAT HelioProp_ForceModel.Drag = None;
GMAT HelioProp_ForceModel.SRP = On;
GMAT HelioProp_ForceModel.RelativisticCorrection = On;
GMAT HelioProp_ForceModel.ErrorControl = RSSStep;


%----------------------------------------
%---------- Propagators
%----------------------------------------

Create Propagator HelioProp;
GMAT HelioProp.FM = HelioProp_ForceModel;
GMAT HelioProp.Type = RungeKutta89;
GMAT HelioProp.InitialStepSize = 86400;
GMAT HelioProp.Accuracy = 1e-8;
GMAT HelioProp.MinStep = 1000;
GMAT HelioProp.MaxStep = 86400;
GMAT HelioProp.MaxStepAttempts = 50;
GMAT HelioProp.StopIfAccuracyIsViolated = false;

Create Propagator GeoProp;
GMAT GeoProp.FM = HelioProp_ForceModel;
GMAT GeoProp.Type = RungeKutta89;
GMAT GeoProp.InitialStepSize = 40;
GMAT GeoProp.Accuracy = 1e-8;
GMAT GeoProp.MinStep = 10;
GMAT GeoProp.MaxStep = 400;
GMAT GeoProp.MaxStepAttempts = 50;
GMAT GeoProp.StopIfAccuracyIsViolated = false;


Create Propagator NearApophis;
GMAT NearApophis.FM = HelioProp_ForceModel;
GMAT NearApophis.Type = RungeKutta89;
GMAT NearApophis.InitialStepSize = 60;
GMAT NearApophis.Accuracy = 1e-8;
GMAT NearApophis.MinStep = 1;
GMAT NearApophis.MaxStep = 8640;
GMAT NearApophis.MaxStepAttempts = 50;
GMAT NearApophis.StopIfAccuracyIsViolated = false;

%% Spacecraft objects. Create several objects for aids to calculation as well as main
     mission sequence

Create Spacecraft sc0;
GMAT sc0.DateFormat = UTCModJulian;
GMAT sc0.Epoch = '31276'; %august 2026 launch
GMAT sc0.CoordinateSystem = SunEcliptic;
GMAT sc0.DisplayStateType = Cartesian;
GMAT sc0.DryMass = 500;
GMAT sc0.Cd = 2.2;
GMAT sc0.Cr = 1;
GMAT sc0.DragArea = 15;
GMAT sc0.SRPArea = 15;
GMAT sc0.Tanks = {hydrazineTank, xenonTank};
GMAT sc0.PowerSystem = powerSystem;
GMAT sc0.Thrusters = nextThruster;

Create Spacecraft sc1;
sc1 = sc0;

```

```
284
285 Create Spacecraft sc4;
286 sc4 = sc0;
287
288 Create Spacecraft scFinal;
289 scFinal = sc0;
290
291 % Data subscribers
292
293 Create ReportFile trajreport_Final;
294 GMAT trajreport_Final.SolverIterations = Current;
295 GMAT trajreport_Final.UpperLeft = [ 0 0 ];
296 GMAT trajreport_Final.Size = [ 0 0 ];
297 GMAT trajreport_Final.RelativeZOrder = 0;
298 GMAT trajreport_Final.Maximized = false;
299 GMAT trajreport_Final.Filename = 'Solar_Electric_Trajectory.txt';
300 GMAT trajreport_Final.Precision = 16;
301 GMAT trajreport_Final.WriteHeaders = true;
302 GMAT trajreport_Final.LeftJustify = On;
303 GMAT trajreport_Final.ZeroFill = Off;
304 GMAT trajreport_Final.FixedWidth = true;
305 GMAT trajreport_Final.Delimiter = ' ';
306 GMAT trajreport_Final.ColumnWidth = 23;
307 GMAT trajreport_Final.WriteReport = true;
308 GMAT trajreport_Final.Add = {scFinal.UTCGregorian scFinal.UTCModJulian  scFinal.SunEcliptic.
    X scFinal.SunEcliptic.Y scFinal.SunEcliptic.Z  scFinal.SunEcliptic.VX scFinal.
    SunEcliptic.VY scFinal.SunEcliptic.VZ scFinal.TotalMass scFinal.xenonTank.FuelMass
    scFinal.hydrazineTank.FuelMass scFinal.ApophisEcliptic.X scFinal.ApophisEcliptic.Y
    scFinal.ApophisEcliptic.Z  scFinal.ApophisEcliptic.VX scFinal.ApophisEcliptic.VY scFinal
    .ApophisEcliptic.VZ };
309
310
311 %burns and trajectory correction maneuvers
312 Create ImpulsiveBurn EscapeBurn;
313 GMAT EscapeBurn.CoordinateSystem = Local;
314 GMAT EscapeBurn.Origin = Earth;
315 GMAT EscapeBurn.Axes = VNB;
316 GMAT EscapeBurn.Element1 = 4.000;
317 GMAT EscapeBurn.Element2 = 0;
318 GMAT EscapeBurn.Element3 = 0;
319 GMAT EscapeBurn.DecrementMass = false;
320 GMAT EscapeBurn.Isp = 300;
321 GMAT EscapeBurn.GravitationalAccel = 9.81;
322
323
324 Create ImpulsiveBurn TCM_Launch;
325 TCM_Launch.CoordinateSystem = Local;
326 TCM_Launch.Origin = Sun;
327 TCM_Launch.Axes = VNB;
328 TCM_Launch.Element1 = 0;
329 TCM_Launch.Element2 = 0;
330 TCM_Launch.Element3 = 0;
331 TCM_Launch.DecrementMass = false;
332 TCM_Launch.Isp = 220;
333 TCM_Launch.GravitationalAccel = 9.81;
334 TCM_Launch.Tank = hydrazineTank;
335
336
337 Create ImpulsiveBurn TCM_R1;
338 TCM_R1.CoordinateSystem = Local;
339 TCM_R1.Origin = Sun;
340 TCM_R1.Axes = VNB;
341 TCM_R1.Element1 = 0;
342 TCM_R1.Element2 = 0;
343 TCM_R1.Element3 = 0;
344 TCM_R1.DecrementMass = true;
345 TCM_R1.Isp = 220;
346 TCM_R1.GravitationalAccel = 9.81;
```

```
347 TCM_R1.Tank = hydrazineTank;
348
349 Create ImpulsiveBurn TCM_R2;
350 TCM_R2.CoordinateSystem = Local;
351 TCM_R2.Origin = Apophis;
352 TCM_R2.Axes = LVLH;
353 TCM_R2.Element1 = 0;
354 TCM_R2.Element2 = 0;
355 TCM_R2.Element3 = 0;
356 TCM_R2.DecrementMass = true;
357 TCM_R2.Isp = 220;
358 TCM_R2.GravitationalAccel = 9.81;
359 TCM_R2.Tank = hydrazineTank;
360
361 Create ImpulsiveBurn TCM_R3;
362 TCM_R3.CoordinateSystem = Local;
363 TCM_R3.Origin = Sun;
364 TCM_R3.Axes = VNB;
365 TCM_R3.Element1 = 0;
366 TCM_R3.Element2 = 0;
367 TCM_R3.Element3 = 0;
368 TCM_R3.DecrementMass = true;
369 TCM_R3.Isp = 220;
370 TCM_R3.GravitationalAccel = 9.81;
371 TCM_R3.Tank = hydrazineTank;
372
373 Create ImpulsiveBurn TCM_R4;
374 TCM_R4.CoordinateSystem = Local;
375 TCM_R4.Origin = Apophis;
376 TCM_R4.Axes = VNB;
377 TCM_R4.Element1 = 0;
378 TCM_R4.Element2 = 0;
379 TCM_R4.Element3 = 0;
380 TCM_R4.DecrementMass = true;
381 TCM_R4.Isp = 220;
382 TCM_R4.GravitationalAccel = 9.81;
383 TCM_R4.Tank = hydrazineTank;
384
385 Create FiniteBurn sepBurn;
386 sepBurn.Thrusters = nextThruster;
387
388 %Create calculation variables and differential corrector objects
389
390 Create Variable pi, negpi, twopi, ThetaOut, EscapeTime, PlaneChangeDT ZDotDesired;
391 Create Variable phiNow, phiPln, nuBurn, eaBurn, maBurn, dtBurn, dtApo, dtApo2, dtApToNode;
392
393 Create Variable ATheta, MTheta, DTheta, DR, DZ, DRdot, DV;
394
395 %variables for SEP trajectory optimization
396 Create Variable PlaneChange_Time_SEP PlaneChange_Time_SEP_0;
397 Create Variable PlaneChangeDT_SEP PlaneChangeDT_SEP_0;
398 Create Variable PeriodChange_Time_SEP PeriodChange_Time_SEP_0;
399 Create Variable PeriodChange_TimePer_SEP PeriodChange_TimePer_SEP_0;
400
401 Create Variable VelocityMatchTime_SEP VelocityMatchTime_SEP_0;
402 Create Variable VelocityMatchTimePer_SEP VelocityMatchTimePer_SEP_0;
403
404 Create Array    VelocityMatchAngle_SEP[3,2] VelocityMatchAngle_SEP_0[3,2];
405 Create Variable iSepAngle BoostPer
406 Create Variable VelocityMatchAnglePer_SEP VelocityMatchAnglePer_SEP_0;
407
408 Create Variable SepTcm_Az SepTcm_El SepTcm_Time;
409 Create Variable SepTcm_Az0 SepTcm_El0 SepTcm_Time0;
410
411 Create Variable T_vmm T_rendezvous0 TmpValue;
412
413 Create DifferentialCorrector DC;
414 DC.DerivativeMethod = CentralDifference;
```

```
415
416 Create DifferentialCorrector DC2;
417 DC2.DerivativeMethod = CentralDifference;
418 DC2.MaximumIterations = 100;
419
420 %
421
422
423 %values of all the impulsive maneuvers as computed by the _impulsive script:
424
425 EscapeTime = 9011.07023136;
426
427 EscapeBurn.CoordinateSystem = 'Local';
428 EscapeBurn.Origin = 'Earth';
429 EscapeBurn.Axes = 'VNB';
430 EscapeBurn.Element1 = 3.25515;
431 EscapeBurn.Element2 = 0;
432 EscapeBurn.Element3 = 0;
433 EscapeBurn.DecrementMass = false;
434 EscapeBurn.Isp = 300;
435 EscapeBurn.GravitationalAccel = 9.81;
436
437 TCM_Launch.CoordinateSystem = 'Local';
438 TCM_Launch.Origin = 'Sun';
439 TCM_Launch.Axes = 'VNB';
440 TCM_Launch.Element1 = -0.05965;
441 TCM_Launch.Element2 = 0;
442 TCM_Launch.Element3 = 0;
443 TCM_Launch.DecrementMass = false;
444 TCM_Launch.Tank = {'hydrazineTank'};
445 TCM_Launch.Isp = 220;
446 TCM_Launch.GravitationalAccel = 9.81;
447
448 PlaneChangeDT = 1.45826535069;
449
450
451
452 T_vmm = 31856.48787856432;
453
454 %Impulsive end-to-end
455 BeginMissionSequence;
456
457 pi = 3.14159265358979323846264338327950;
458 negpi = -1*pi;
459 twopi = 2*pi;
460
461
462 %start in 2026 August around the Earth in a circular parking orbit
463 scFinal.Epoch = 31279;
464 scFinal.CoordinateSystem = EarthEcliptic;
465 scFinal.EarthEcliptic.X =  6371 + 185;
466 scFinal.EarthEcliptic.Y = 0;
467 scFinal.EarthEcliptic.Z = 0;
468 scFinal.EarthEcliptic.VX = 0;
469 scFinal.EarthEcliptic.VY = sqrt(398600.4415/ ( 6371 + 185) ) + 0.01;
470 scFinal.EarthEcliptic.VZ = 0;
471
472 scFinal.DryMass = 634; %2017/05/07 value
473 scFinal.hydrazineTank.FuelMass = 165;
474 scFinal.xenonTank.FuelMass = 120;
475
476
477 %now execute the trajectory correction manuever post-launch, plane change, period change,
        and velocity match maneuver within a single optimization
478
479 Propagate GeoProp(scFinal) {scFinal.ElapsedSecs = EscapeTime};
480
481 Maneuver EscapeBurn(scFinal);
```

```
482
483 Propagate GeoProp(scFinal) {scFinal.ElapsedDays = 0.5}; %get some altitude before computing
    C3
484
485 %End-to-End with real tanks
486
487 PlaneChange_Time_SEP_0 = 50.8736477336
488 PeriodChange_Time_SEP_0 = 10.0022504659
489 PeriodChange_TimePer_SEP_0 = 3.67136510001
490 PlaneChangeDT_SEP_0 = -11.544474133
491
492 T_vmm = 31856.48787856432;
493 T_rendezvous0 = 31918.26991319591;
494
495 Target DC2
496
497    Vary DC2(PlaneChange_Time_SEP          = PlaneChange_Time_SEP_0, {Lower = 2, Upper = 120,
       Perturbation = 1, MaxStep = 5});
498    Vary DC2(PeriodChange_Time_SEP         = PeriodChange_Time_SEP_0, {Lower = 1, Upper = 40,
       Perturbation = 1, MaxStep = 5})
499    Vary DC2(PeriodChange_TimePer_SEP      = PeriodChange_TimePer_SEP_0, {Lower = 0.1, Upper =
        5.0, Perturbation = 0.1, MaxStep = 0.2});
500    Vary DC2(PlaneChangeDT_SEP             = PlaneChangeDT_SEP_0, {Lower = -20, Upper = 20,
       Perturbation = 0.5, MaxStep = 1.0});
501
502
503    Maneuver TCM_Launch(scFinal);
504
505    phiNow = atan2( scFinal.SunEcliptic.Y, scFinal.SunEcliptic.X)*180/pi;
506    phiPln = 204.457189 - 180.0;
507
508    nuBurn = (phiPln - phiNow + scFinal.Sun.TA)*pi/180;
509    eaBurn = atan2( sin(nuBurn)/sqrt(1 - scFinal.Sun.ECC^2 ), scFinal.Sun.ECC + cos( nuBurn )
       );
510    maBurn = eaBurn - scFinal.Sun.ECC * sin(eaBurn);
511
512    dtBurn = (maBurn - scFinal.Sun.MA*pi/180);
513
514    If dtBurn < 0
515       dtBurn = dtBurn + 2*pi;
516    EndIf;
517
518    dtBurn = dtBurn / (scFinal.Sun.MM * 86400) + PlaneChangeDT_SEP - 0.25*
       PlaneChange_Time_SEP;
519
520
521
522    Propagate HelioProp(scFinal) { scFinal.ElapsedDays = dtBurn};
523
524    %set up for a plane change
525    scFinal.nextThruster.ThrustDirection1 = 0;
526    scFinal.nextThruster.ThrustDirection2 = -1;
527    scFinal.nextThruster.ThrustDirection3 = 0;
528
529    BeginFiniteBurn sepBurn(scFinal);
530
531    Propagate HelioProp(scFinal) { scFinal.ElapsedDays = PlaneChange_Time_SEP};
532
533    EndFiniteBurn sepBurn(scFinal);
534
535
536    %set up for the period change burn
537    dtBurn = (pi - scFinal.Sun.MA*pi/180);
538
539    If dtBurn < 0
540       dtBurn = dtBurn + 2*pi;
541    EndIf;
542
```

```
543     dtBurn = dtBurn / (scFinal.Sun.MM * 86400) - 0.5*( PeriodChange_Time_SEP +
            PeriodChange_TimePer_SEP);
544
545
546
547     Propagate HelioProp(scFinal) { scFinal.ElapsedDays = dtBurn};
548
549     %set up for a period change
550     scFinal.nextThruster.ThrustDirection1 = -1;
551     scFinal.nextThruster.ThrustDirection2 = 0;
552     scFinal.nextThruster.ThrustDirection3 = 0;
553
554     BeginFiniteBurn sepBurn(scFinal);
555     dtBurn =  PeriodChange_Time_SEP + PeriodChange_TimePer_SEP;
556     Propagate HelioProp(scFinal) { scFinal.ElapsedDays = dtBurn};
557     EndFiniteBurn sepBurn(scFinal);
558
559     %second half of plane change
560     %execute the other half of the plane change
561     phiNow = atan2( scFinal.SunEcliptic.Y, scFinal.SunEcliptic.X)*180/pi;
562     phiPln = 204.457189;
563
564     nuBurn = (phiPln - phiNow + scFinal.Sun.TA)*pi/180;
565
566
567     eaBurn = atan2( sin(nuBurn)/sqrt(1 - scFinal.Sun.ECC^2 ), scFinal.Sun.ECC + cos( nuBurn )
            );
568     maBurn = eaBurn - scFinal.Sun.ECC * sin(eaBurn);
569
570     dtBurn = (maBurn - scFinal.Sun.MA*pi/180);
571
572     If dtBurn < 0
573         dtBurn = dtBurn + 2*pi;
574     EndIf;
575     If dtBurn > twopi
576         dtBurn = dtBurn - 2*pi;
577     EndIf;
578
579     dtBurn = dtBurn / (scFinal.Sun.MM * 86400);
580     dtBurn = dtBurn  - 0.25*PlaneChange_Time_SEP;
581
582     Propagate HelioProp(scFinal) { scFinal.ElapsedDays = dtBurn};
583
584     %set up for a plane change in the opposite direction
585     scFinal.nextThruster.ThrustDirection1 = 0;
586     scFinal.nextThruster.ThrustDirection2 = 1;
587     scFinal.nextThruster.ThrustDirection3 = 0;
588
589     BeginFiniteBurn sepBurn(scFinal);
590     dtBurn = PlaneChange_Time_SEP / 2.0;
591     Propagate HelioProp(scFinal) { scFinal.ElapsedDays = dtBurn};
592     EndFiniteBurn sepBurn(scFinal);
593
594
595
596
597     dtBurn = (0 - scFinal.Sun.MA*pi/180);
598
599     If dtBurn < 0
600         dtBurn = dtBurn + 2*pi;
601     EndIf;
602
603     dtBurn = dtBurn / (scFinal.Sun.MM * 86400) - 0.5*( PeriodChange_TimePer_SEP);
604
605
606     Propagate HelioProp(scFinal) { scFinal.ElapsedDays = dtBurn};
607
608     %set up for a profelactic aphelion raise
```

```
609     scFinal.nextThruster.ThrustDirection1 = 1;
610     scFinal.nextThruster.ThrustDirection2 = 0;
611     scFinal.nextThruster.ThrustDirection3 = 0;
612
613
614     BeginFiniteBurn sepBurn(scFinal);
615     dtBurn =  PeriodChange_TimePer_SEP;
616     Propagate HelioProp(scFinal) { scFinal.ElapsedDays = dtBurn};
617     EndFiniteBurn sepBurn(scFinal);
618
619
620     dtBurn = T_vmm - scFinal.UTCModJulian;
621
622     sc4 = scFinal;
623     Propagate HelioProp(sc4) { sc4.ElapsedDays = dtBurn};
624
625     Apophis.UTCModJulian = sc4.UTCModJulian;
626
627     ATheta = atan2( Apophis.SunEcliptic.Y, Apophis.SunEcliptic.X);
628     MTheta = atan2( sc4.SunEcliptic.Y, sc4.SunEcliptic.X);
629
630     DTheta = ATheta - MTheta;
631
632     If DTheta > pi
633       DTheta = DTheta - 2*pi;
634     EndIf;
635
636     If DTheta <= negpi
637        DTheta = DTheta + 2*pi;
638     EndIf;
639
640
641     DZ =  Apophis.SunEcliptic.Z - sc4.SunEcliptic.Z;
642
643     DR    =  sqrt(Apophis.SunEcliptic.X^2 + Apophis.SunEcliptic.Y^2) - sqrt( sc4.SunEcliptic.
          X^2 + sc4.SunEcliptic.Y^2);
644
645     Achieve DC2( DTheta = 0, {Tolerance = 1e-10});
646     Achieve DC2( DZ = 200, {Tolerance = 10}); %miss by 40 km intentionally
647     Achieve DC2( DR =  0, {Tolerance = 10});
648     Achieve DC2( sc4.ApophisEcliptic.VZ =  ZDotDesired , {Tolerance = 1e-4});
649
650 EndTarget;
651
652 VelocityMatchAngle_SEP_0(1,1) = 28.1620990235
653 VelocityMatchAngle_SEP_0(2,1) = -49.3306717497
654 VelocityMatchAngle_SEP_0(3,1) = -39.2586311381
655
656 VelocityMatchAngle_SEP_0(1,2) = 0;
657 VelocityMatchAngle_SEP_0(2,2) = 2.5510313936
658 VelocityMatchAngle_SEP_0(3,2) = 0;
659
660 VelocityMatchTime_SEP_0 = 104.444828578
661
662
663 Target DC2;
664    Vary DC2(VelocityMatchAngle_SEP(1,1)    = VelocityMatchAngle_SEP_0(1,1), {Lower = -190,
          Upper = 190.0, Perturbation = .2, MaxStep = 10});
665    Vary DC2(VelocityMatchAngle_SEP(2,1)    = VelocityMatchAngle_SEP_0(2,1), {Lower = -190,
          Upper = 190.0, Perturbation = .2, MaxStep = 10});
666    Vary DC2(VelocityMatchAngle_SEP(3,1)    = VelocityMatchAngle_SEP_0(3,1), {Lower = -190,
          Upper = 190.0, Perturbation = .2, MaxStep = 10});
667
668    Vary DC2(VelocityMatchAngle_SEP(2,2)    = VelocityMatchAngle_SEP_0(2,2), {Lower = -190,
          Upper = 190.0, Perturbation = .2, MaxStep = 10});
669    Vary DC2(VelocityMatchAngle_SEP(3,2)    = VelocityMatchAngle_SEP_0(3,2), {Lower = -190,
          Upper = 190.0, Perturbation = .2, MaxStep = 10});
670
```

```
671     Vary DC2(VelocityMatchTime_SEP         = VelocityMatchTime_SEP_0, {Lower = 10.0, Upper =
            160.0, Perturbation = .2, MaxStep = 10});
672
673      scFinal.nextThruster.ThrustDirection1 = 1;
674      scFinal.nextThruster.ThrustDirection2 = 0;
675      scFinal.nextThruster.ThrustDirection3 = 0;
676      BoostPer = .15
677      BeginFiniteBurn sepBurn(scFinal);
678      Propagate HelioProp(scFinal) { scFinal.ElapsedDays = BoostPer};
679      EndFiniteBurn sepBurn(scFinal);
680
681
682     dtBurn = T_rendezvous0 - scFinal.UTCModJulian - VelocityMatchTime_SEP - 10;
683
684
685     Propagate HelioProp(scFinal) { scFinal.ElapsedDays = dtBurn};
686
687
688      For iSepAngle = 1:3
689
690          scFinal.nextThruster.ThrustDirection1 = -cos( VelocityMatchAngle_SEP(iSepAngle,1)*pi
                /180)*cos(VelocityMatchAngle_SEP(iSepAngle,2)*pi/180);
691          scFinal.nextThruster.ThrustDirection2 = sin(VelocityMatchAngle_SEP(iSepAngle,2)*pi
                /180)
692          scFinal.nextThruster.ThrustDirection3 = sin( VelocityMatchAngle_SEP(iSepAngle,1)*pi
                /180)*cos(VelocityMatchAngle_SEP(iSepAngle,2)*pi/180)
693
694
695          BeginFiniteBurn sepBurn(scFinal);
696          dtBurn =  VelocityMatchTime_SEP/3;
697          If iSepAngle==3
698                  Propagate NearApophis(scFinal) { scFinal.ElapsedDays = dtBurn};
699          Else
700                  Propagate HelioProp(scFinal) { scFinal.ElapsedDays = dtBurn};
701          EndIf;
702          EndFiniteBurn sepBurn(scFinal);
703      EndFor;
704
705
706
707
708
709     Apophis.UTCModJulian = scFinal.UTCModJulian;
710
711     ATheta = atan2( Apophis.SunEcliptic.Y, Apophis.SunEcliptic.X);
712     MTheta = atan2( scFinal.SunEcliptic.Y, scFinal.SunEcliptic.X);
713
714     DTheta = ATheta - MTheta;
715
716     If DTheta > pi
717       DTheta = DTheta - 2*pi;
718     EndIf;
719
720     If DTheta <= negpi
721        DTheta = DTheta + 2*pi;
722     EndIf;
723
724
725     DZ =  Apophis.SunEcliptic.Z - scFinal.SunEcliptic.Z;
726
727     DR    =  sqrt(Apophis.SunEcliptic.X^2 + Apophis.SunEcliptic.Y^2) - sqrt( scFinal.
            SunEcliptic.X^2 + scFinal.SunEcliptic.Y^2);
728
729     DV    =  sqrt(2.0/scFinal.Sun.RMAG - 1.0/scFinal.Sun.SMA);
730     DV    =  DV - sqrt(2.0/sqrt(Apophis.SunEcliptic.X^2+Apophis.SunEcliptic.Y^2+Apophis.
            SunEcliptic.Z^2) -  1.0/(1.379933884271476e+08));
731     DV = DV *sqrt(1.3271244001e11);
732
```

```
733     Achieve DC2( DTheta =  0, {Tolerance = 1e-9})
734     Achieve DC2( DR =  0, {Tolerance = 10});
735
736     Achieve DC2( scFinal.ApophisEcliptic.VY =0, {Tolerance = 0.1});
737     Achieve DC2( scFinal.ApophisEcliptic.VX =0, {Tolerance = 0.1});
738
739     Achieve DC2( DZ = 50, {Tolerance = 5});
740     Achieve DC2( scFinal.ApophisEcliptic.VZ =  0 , {Tolerance = 1e-3});
741
742  EndTarget;
743
744  %rendezvous burn immediately
745
746  Target DC
747
748     Vary DC(TCM_R1.Element1 = 0, {Lower = -0.25, Upper = 0.25, Perturbation=0.01, MaxStep =
          0.05});
749     Vary DC(TCM_R1.Element2 = 0, {Lower = -0.25, Upper = 0.25, Perturbation=0.01, MaxStep =
          0.05});
750     Vary DC(TCM_R1.Element3 = 0, {Lower = -0.55, Upper = 0.55, Perturbation=0.01, MaxStep =
          0.05});
751
752     Maneuver TCM_R1(scFinal);
753
754     dtBurn = T_rendezvous0 - scFinal.UTCModJulian;
755     Propagate NearApophis(scFinal){ scFinal.ElapsedDays = dtBurn};
756
757     Apophis.UTCModJulian = scFinal.UTCModJulian;
758
759     ATheta = atan2( Apophis.SunEcliptic.Y, Apophis.SunEcliptic.X);
760     MTheta = atan2( scFinal.SunEcliptic.Y, scFinal.SunEcliptic.X);
761
762     DTheta = ATheta - MTheta;
763
764     If DTheta > pi
765       DTheta = DTheta - 2*pi;
766     EndIf;
767
768     If DTheta <= negpi
769        DTheta = DTheta + 2*pi;
770     EndIf;
771
772
773     DZ =  Apophis.SunEcliptic.Z - scFinal.SunEcliptic.Z;
774
775     DR =  sqrt(Apophis.SunEcliptic.X^2 + Apophis.SunEcliptic.Y^2) - sqrt( scFinal.SunEcliptic
          .X^2 + scFinal.SunEcliptic.Y^2);
776
777     Achieve DC( DTheta = 0, {Tolerance = 1e-10});
778     Achieve DC( DZ = 10, {Tolerance = 0.1});
779     Achieve DC( DR =  0, {Tolerance = 0.01});
780
781  EndTarget
782
783  %%and the final rendezvous
784
785  %now can do b-plane targetting and enter orbit. but first we need to make a small impulse
       toward the asteroid
786
787  TCM_R2.Element1 = -0.004;
788  TCM_R2.Element2 = 0;
789  TCM_R2.Element3 = 0;
790
791  Maneuver TCM_R2(scFinal);
792
793  Propagate HelioProp(scFinal) {scFinal.ElapsedSecs = 100}
794
795
```

```
796 Target DC
797
798    Vary DC(TCM_R3.Element1 = 0, {Lower = -0.09, Upper = 0.09, Perturbation=0.001, MaxStep =
           0.005});
799    Vary DC(TCM_R3.Element2 = 0, {Lower = -0.09, Upper = 0.09, Perturbation=0.001, MaxStep =
           0.005});
800    Vary DC(TCM_R3.Element3 = 0, {Lower = -0.09, Upper = 0.09, Perturbation=0.001, MaxStep =
           0.005});
801
802    Maneuver TCM_R3(scFinal);
803
804    Achieve DC( scFinal.ApophisEcliptic.BdotT = 0, {Tolerance = .01});
805    Achieve DC( scFinal.Apophis.IncomingRadPer = 1.2, {Tolerance = .01});
806 EndTarget
807
808 dtBurn = -scFinal.Apophis.MA * pi / (180*scFinal.Apophis.MM);
809
810 Propagate NearApophis(scFinal){ scFinal.ElapsedSecs = dtBurn};
811
812 TCM_R4.Element1 = sqrt( 1e-09 / scFinal.Apophis.RMAG ) - scFinal.ApophisEcliptic.VMAG;
813 TCM_R4.Element2 = 0;
814 TCM_R4.Element3 = 0;
815
816 Maneuver TCM_R4(scFinal);
817
818 Propagate NearApophis(scFinal) {scFinal.ElapsedDays = 2};
819
820 Write TCM_R1 TCM_R2 TCM_R3 TCM_R4
```

Appendix E

Science Orbits

This section briefly shows the body-fixed frame orbits for the Terminator I and Terminator II science orbits. The orbital characteristics of the asteroid rotation, obliquity, and precession are taken from Pravec et al.[80] and are as follows-

Rotation: 263 Hours
Obliquity: 165 Degrees
Precession: 27.38 Hours

E.1 $2km$ Terminator I Orbit

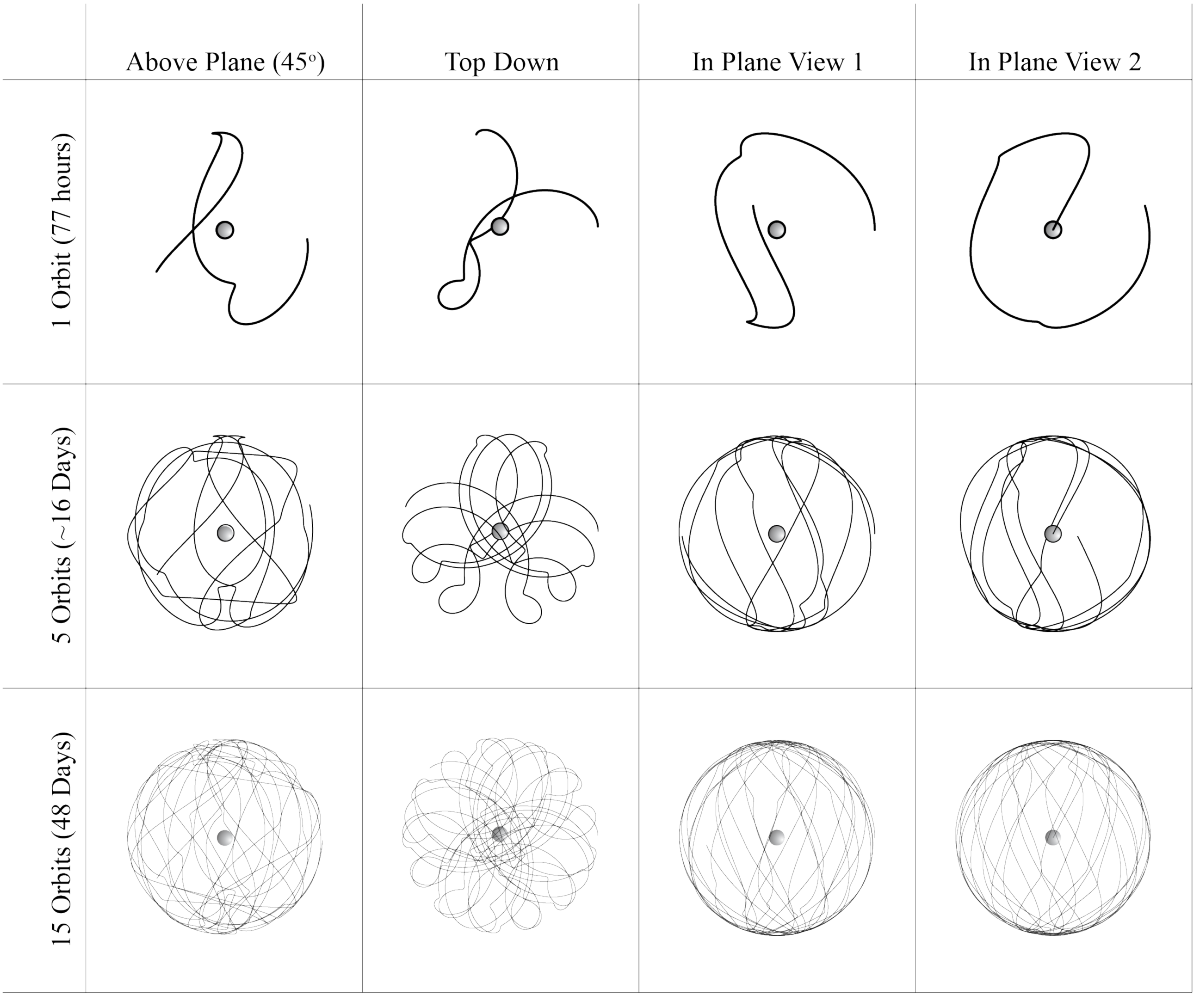

Figure E.1: At a range of $2km$ from the center, the spacecraft in a terminator orbit will take 77 hours to complete a single orbit. For the Terminator I phase, the spacecraft will complete 15 orbits in 48 days before spiralling down into the Terminator II orbit. Please note this is a fixed-body frame.

E.2 $500m$ Terminator II Orbit

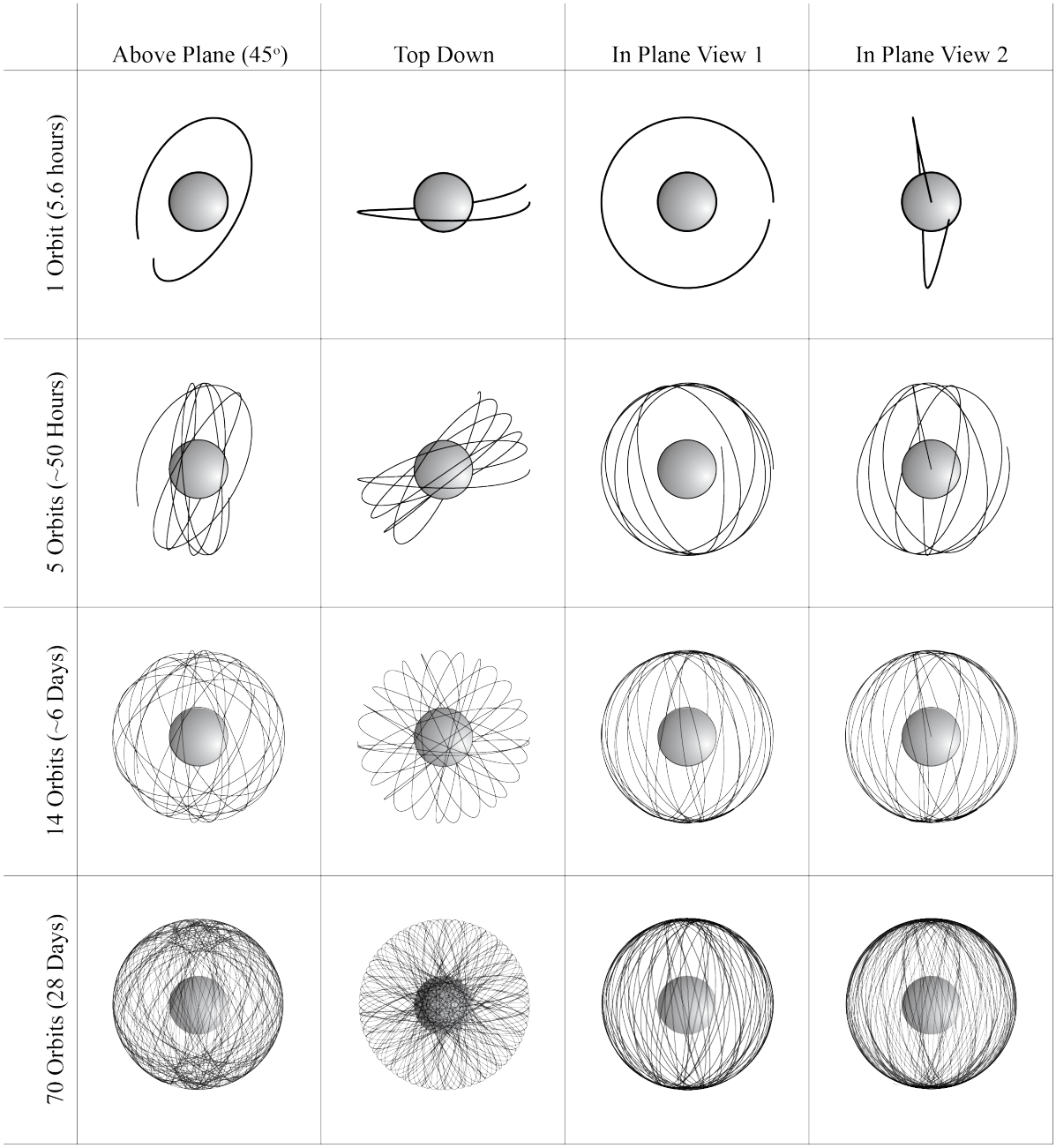

Figure E.2: At a range of $500m$ from the center, the spacecraft in a terminator orbit will take 9.6 hours to complete a single orbit. For the Terminator II phase, which is focused on RRT and is attempting to satisfy PLD.6 of $10m$ sampling distance, the spacecraft will complete 70 orbits in 30 days before spiralling down into the Terminator II orbit. This gives an average distance between samples of just over $7m$. Please note this is a fixed-body frame.

Appendix F

Mission Architecture Landscape

This section concisely shows some of the alternate ideas for mission architecture we downselected from.

F.1 Feasible Mission Options Considered

The following options were considered mature enough to be evaluated for selection as instrument options for the SET Mission. Eventually they were ruled out due to cost, complexity, or risk.

F.1.1 RTT, Radio Transmission Tomography, Twin Spacecraft

Mission/Technology Precedent: Rosetta/Philae Mission

Description: In this mission architecture, two spacecraft transmit radio waves through an object to resolve the interior of the body. This functionality has been shown with the Rosetta spacecraft receiving radio signals from the Philae lander allowing for partial understanding of the porosity of comet 67P's interior. The two spacecraft would be nearly identical and vary only in operation during measurements.

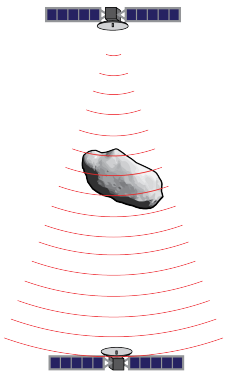

Pros: The two spacecraft have the capacity to both transmit and receive radio signals allowing for complete redundancy as the RTT equipment is the same as the RRT (Radio Reflective Tomography). This allows redundancy in the event of one spacecraft failing. The cost of this option over the chosen RRT is also minimal in respect to design as the two spacecraft are virtually the same.

Cons: The complexity of two spacecraft is greater when they must be located directly opposite the asteroid from one-and-other. The cost of two spacecraft is also substantially higher, by about 300 million dollars (assuming identical orbiter spacecraft).

F.1.2 RTT, Radio Transmission Tomography, Different Sender/Receiver Spacecraft

Mission/Technology Precedent: Rosetta/Philae Mission

Description: This mission architecture is similar to the one mentioned previously, but instead of two nearly identical spacecrafts, there would be one larger spacecraft which would fly the full imaging suite and a smaller transmitter spacecraft which would be solely for RTT purposes. This smaller transmitter spacecraft would likely be deployed from the larger spacecraft during the Approach I phase.

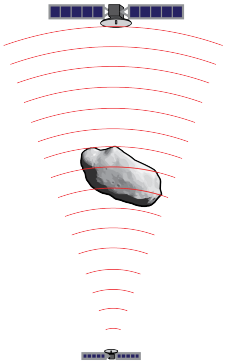

Pros: The fabrication cost of a small second spacecraft is less than the twin spacecraft option previously described and has been successfully demonstrated by the Rosetta/Philae Mission.

Cons: The risk of the transmitter spacecraft deployment failing is dramatically higher than the single spacecraft architecture currently chosen. Design costs for this mission architecture are dramatically higher due to deployment mechanisms within the larger spacecraft and a second spacecraft which includes communications, instrumentation, and control systems.

F.1.3 RTT + Seismometers, Landing Vehicle

Mission/Technology Precedent: Rosetta/Philae Mission

Description: In this mission architecture, a single lander will be coupled with the asteroid to measure seismic activity during the Earth flyby event and perform RTT measurements of the interior in conjunction with a main spacecraft. The main spacecraft would perform the operations similar to our outlined mission in respect to imaging, but instead of the RRT measurements, the lander would transmit the signals through the asteroid to the orbiting spacecraft. Alternatively the spacecraft could perform RRT making the lander's functionality solely seismic and surface based experimentation.

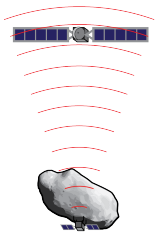

Pros: With a lander package coupled with the surface, vibrations of the surface during the Earth flyby event could be measured with higher precision providing a more in depth understanding of the seismic vibration modes and interior structure. Surface experiments from a lander could provide more insight into asteroid geology than a remote spacecraft.

Cons: The political ramifications of touching and possibly influencing a Potentially Hazardous Asteroid are still being debated. Landing packages are notoriously high risk as is exemplified by the mission precedent. Unlike 67P, Apophis has a very complex and rapid precession and rotation meaning the RTT measurements which go in a line from the lander to the spacecraft would mean uniform coverage of the interior structure is impossible.

F.1.4 Earth Based Radio Experimentation

Mission/Technology Precedent:

Description: The 2029 Apophis Earth Flyby event will potentially have every possible radio telescope pointed directly at it for the entire duration. A spacecraft would be placed to measure the Earth-transmitted waves going into and coming out of the asteroid essentially using Earth based radio sources for our own purposes. The primary reasoning for this option was the uncertainty behind the power necessary for RRT/RTT operations at an early stage and asking the question of how existing ground-based operations can aid the mission objectives.

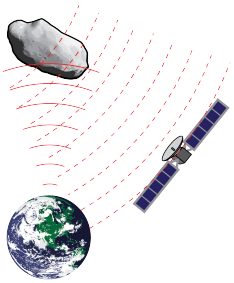

Pros: This option can utilize a far wider range of radio waves than the single spacecraft RRT and utilizes an as of yet untapped resource of Earth's radio waves. This could be an investigation implemented as part of another mission architecture.

Cons: The information gathered from the short amount of time within reasonable range of Earth is far more limited than the other mission options. There is no guarantee on what waves will be reaching the asteroid, and as such there is a high risk in how much internal characterization can be achieved.

F.1.5 Surface Coupled Seismometers

Mission/Technology Precedent:

Description: In addition to an observing spacecraft, seismometer landing packages would be distributed and coupled to the asteroid surface. During the Earth flyby event, the seismometers will measure the seismic activity caused by the tidal forces. This seismic activity would allow for deduction of the interior structure to be made in addition to understanding the tidal forces more fully. For these seismometers to function correctly surface coupling will be achieved which sets it apart from the later mentioned smart marbles and adds a layer of complexity.

Pros: This option measures the behaviors of the asteroid structure during the event better than all previously mentioned remote sensing options.

Cons: This option involves technologically challenging landers. In order for seismometers to work most effectively, they need to be anchored to the deep structure of the asteroid rather than regolith. Significant uncertainties remain over the method to achieve this coupling. The political ramifications of touching and possibly influencing a Potentially Hazardous Asteroid are still being debated.

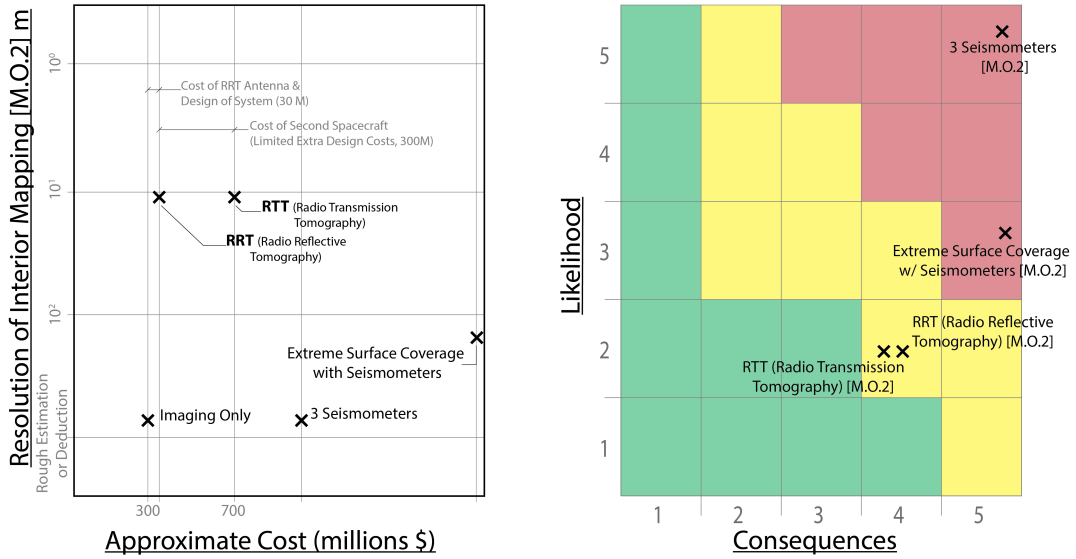

Figure F.1: The above figures compared the risks, costs, and satisfaction of M.O.2 allowing for a clear and simple decision process. It is clear in the left figure that RRT is by far one of the least expensive mission architectures and achieves the highest internal resolution. The right figure displays how even with the increased risk to the Mission Objectives, the RRT is a relatively moderate risk option. These factors were key in deciding upon the final mission architecture.

F.2 'Stretch' Mission Options for Possible Future Development

F.2.1 Spacecraft-Based Laser Vibrometer

In this section mission elements that show potential for an Apophis mission are outlined, but are not currently at a level of technological advancement to be selected for flight. In some cases, the described instruments are brainstorm concepts that may find merit with further evaluation beyond the time constraints of this study.

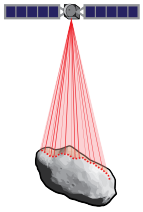

Technology Precedent: Laser Doppler Vibrometer; No Space Heritage

Description: Instead of using seismometers, this mission architecture requires the use of a Laser Doppler Vibrometer (LDV) to measure the propagation of seismic waves through the side of Apophis facing the laser during the near Earth flyby event. Using the doppler effect, seismic disturbances can be detected and measured on Apophis's surface. Subsequently, this data can be used to determine the asteroid's internal structure.

Pros: Does not require landing multiple seismometers on the surface of Apophis, thus reducing the mission's overall risk and complexity. Additionally, the LDV could have the capability to record seismic data at multiple points across the asteroid's surface.

Cons: Lacks widespread implementation on Earth, and has never been used in space. Additionally, the sensitivity of the LDV instrument is so high that it would be difficult to take accurate measurements during the near Earth flyby event due to how the asteroid's precise orbital behavior and trajectory change during the event is mostly unknown.

F.2.2 Surface Hopper

Mission/Technology Precedent: MASCOT (Hayabusa II)

Description: A non-surface-coupling lander would be used to gather surface information and seismic activity. The surface hopper MASCOT as designed for use on the Hayabusa II mission 'throws' itself off the surface and to another location using an internal moment arm. Through this relocation, the surface hopper can get a more extensive understanding of the surface conditions of the asteroid.

Pros: This option allows more surface exploration than a simple lander due to mobility. The non-coupling aspect of this mission architecture also reduces complexity of the landing package as well.

Cons: The cost and complexity of a landing package even with the reduced risks and challenges of coupling is still far greater than the mission architecture chosen. The lifespan of a MASCOT-like package is likely not long enough to characterize the entire asteroid. The political ramifications of touching and possibly influencing a Potentially Hazardous Asteroid are still being debated.

F.2.3 'Dumb' Marbles

Mission/Technology Precedent:

Description: The Hayabusa I mission investigating Itokawa showed images of small scale surface changes such as landslides which are hypothesized to be due to tidal forces. From these small scale surface changes, a rough understanding of tidal forces can be gained. In this mission architecture, small objects of known properties would be distributed across the surface. During the event these masses will be shifted, vibrated, and thrown. By knowing the motion of the objects and the properties of the object, the forces can be thoroughly analyzed. The objects being distributed could be radio reflectors of known mass with an embedded chip which uses the radio waves to 'chirp' back their identity.

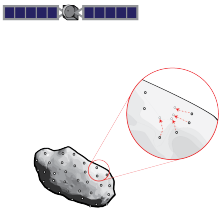

Pros: This option can be scaled up to cover larger amounts of the surface depending on the mission operations. This option allows for a more controlled exploration of the tidal forces than solely observing surface changes.

Cons: The distribution of the objects would become complex to ensure even coverage. The political ramifications of touching and possibly influencing a Potentially Hazardous Asteroid are still being debated.

F.2.4 'Smart' Marbles

Mission/Technology Precedent:

Description: The 'Smart' Marbles option is similar to the 'Dumb' Marbles option above with the addition of sensing functionality within the marble. Embedded within the marbles would be accelerometers to measure both the seismic activity of the asteroid and the coarse movement of the marbles across the surface.

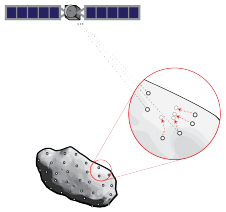

Pros: This option provides the surface seismic activity data that the lander would provide while drastically reducing the risk of lander failure.

Cons: Distribution, like above, would be complex. Power and communications for each small element would be a challenge.

F.2.5 Cubesat Swarm, 'Paparazzi'

Mission/Technology Precedent:

Description: Nature is performing a once in a thousand year experiment, the cubesat swarm uses this close proximity to Earth to its fullest with a swarm of small spacecrafts positioned strategically along the path of Apophis' Earth flyby. These spacecrafts will be imaging the entire event from multiple positions and angles to gain complete coverage. This 'paparazzi' swarm is the only option which eliminates a spacecraft rendezvousing with the asteroid prior to the event.

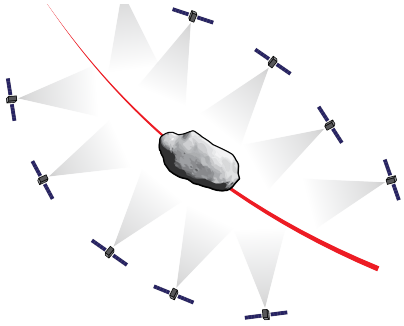

Pros: Of all the options, this one has the potential to be the least expensive and uses the most established technology, if even for unconventional means.

Cons: Apophis' high relative velocity through the swarm may render this concept ineffective.

F.2.6 Gravity Sensing using Quantum Inertial Navigation

Mission/Technology Precedent:

Description: This option uses an orbiting spacecraft to measure the gravity field of the asteroid in high resolution. The complete understanding of the gravity field allows for highly reliable deductions of the interior distribution of mass. With this information and the overall geometric knowledge of the asteroid porosity and composition are possible as well. This measurement could be done with an atomic gravimeter which uses single falling atoms as the test masses.

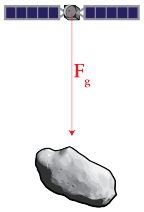

Pros: This method gives a high accuracy model of the mass distribution for the asteroid. The concept of gravity measurement for understanding material distribution is already tested and flown with the GRACE and GRAIL missions.

Cons: The atomic gravimeter technology is not mission ready in its current state, although the issue of scale has been solved.

F.2.7 Gravity Tractor

Mission/Technology Precedent:

Description: Using a large mass, possibly a boulder captured from the asteroid itself, the spacecraft will remain proximal to the asteroid and observe how the path of the asteroid varies and the orbital characteristics change. Knowing how the asteroid is affected by this gravitational force, an understanding of mass distribution can be achieved.

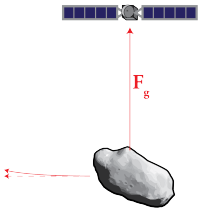

Pros: This mission architecture has very few pros in relation to the Apophis event, but the operations involving capturing a piece of an asteroid has been discussed, and thus has some heritage for future evaluation.

Cons: The possibility of no suitable boulders or masses is non-negligible and the mass of a spacecraft alone is likely to make too small of a difference for this event. The complexity of this mission is extremely high and as such the cost and the risk are high as well. The political ramifications of touching and possibly influencing a Potentially Hazardous Asteroid are still being debated.

F.2.8 Magnetic Tractor

Mission/Technology Precedent:

Description: Similar to the Gravity Tractor above, this option would use powerful electromagnets to apply a force to the asteroid. Observing how the asteroid's behavior changes as this force is applied, the makeup of the asteroid could be deduced. In addition to simply knowing mass distribution, this method would be able to begin deductions on the metal content variations throughout the body.

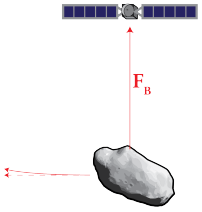

Pros: This option, over the gravity tractor, would not involve contacting the asteroid which would bring with it highly complex maneuvers.

Cons: The introduction of a high power magnet aboard the spacecraft will introduce complexity in terms of interference with other instruments and spacecraft components. The large force of the magnet would have to be offset by thrusters, increasing the fuel budget dramatically. The political ramifications of touching and possibly influencing a Potentially Hazardous Asteroid are still being debated.

F.2.9 Sample Return

Mission/Technology Precedent: Hayabusa I, Hayabusa II OSIRIS-REx

Description: A sample return is an additional aspect of a larger mission. This aspect would give a more complete understanding of the asteroid surface composition because far more experimentation can be accomplished in a lab setting than on the surface of an asteroid flying through space. If we know how the asteroid appears from earth and we know what the surface is composed of, a better remote estimation of asteroid properties could be possible.

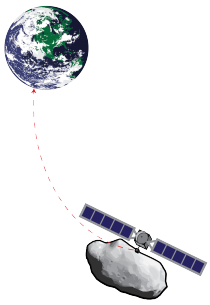

Pros: This option provides the most in depth understanding of surface composition and allows for the greatest level of experimentation on it.

Cons: This mission is one of the most complex and expensive involving a sample capture device, Earth return travel, and re-entry. The political ramifications of touching and possibly influencing a Potentially Hazardous Asteroid are still being debated.

F.2.10 Surface Rover

Mission/Technology Precedent: Hayabusa I: Muses-CN

Description: A lander alone can only measure the local region around it even if it can hop from place to place, but a rover could explore a far larger region in greater depth. The rover would be combined with the existing mission architecture to improve upon the surface characterization components. This rover would be deployed from the main spacecraft and descend to the surface. Once upon the surface, the rover could measure various properties and hypothetically place the smart or dumb marbles as previously described in a far more controlled manner.

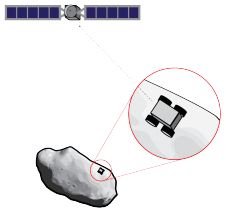

Pros: This option could increase the feasibility of various other options mentioned earlier. This option allows for a high level of surface characterization over a large portion of the asteroid.

Cons: The deployment and landing of the rover is both high risk and high cost. The design of a rover and the associated deployment device would likely require greater time than is available before the event. The political ramifications of touching and possibly influencing a Potentially Hazardous Asteroid are still being debated.